8-2016

A Bioresponsive and Multifunctional Polymer Based Nanodevice for Cancer Nanotheranostics

Ragini Jenkins
Clemson University

A BIORESPONSIVE AND MULTIFUNCTIONAL POLYMER BASED NANODEVICE FOR CANCER NANOTHERANOSTICS

A Dissertation
Presented to
the Graduate School of
Clemson University

In Partial Fulfillment
of the Requirements for the Degree
Doctor of Philosophy
Materials Science and Engineering

---

by
Ragini Jenkins
December 2015

Accepted by:
Dr. Stephen H. Foulger, Committee Chair
Dr. Igor A. Luzinov
Dr. O. Thompson Mefford
Dr. Michael G. Sehorn

Abstract

The main objective of this project is to develop a polymer based near infrared (NIR) particle that can serve as both, diagnostic and therapeutic agents, for fighting cancer. Specifically these particles will be designed to have high-contrast, high signal to noise ratios, long *in vivo* circulation lifetimes, and facilitate easy attachment of functional and target components.

Cancer is a disease where the growth of abnormal cells is uncontrollable and is one of the leading causes of death worldwide. Malignant cancer cells are more effectively treated when identified early in the disease. Identification of tumors using fluorophores, small molecules that emit visible light when excited, is gaining clinical interest. Specific interest is in near-infrared emission due to the lack of absorption of this radiation in human tissue, which facilitates deep tissue imaging. During imaging with small molecule fluorophores, the fluorophores clear from the body quickly reducing imaging effectiveness. The effectiveness of imaging can be enhanced by attaching the fluorophores to a particle. Nanometer sized particles do not clear from the body rapidly and allows the material designer to attach other "payloads" to the particle. This multifunctional "nano-device" can be used to deliver diagnostic (fluorophores) and therapeutic (drugs) agents to the afflicted tissue.

In this current project sub-100 nm poly(propargyl acrylate) (PA) particles are surface-functionalized with fluorophores or targeting molecules through a copper(I) catalyzed azide-alkyne Huisgen 1,3-Dipolar cycloaddition, and used for the following applications:

(1) *Switching fluorescence of surface modified colloids with near-infrared emitters via protein interaction for contrast-enhanced imaging:* The colloidal particles surface-functionalized with fluorophores exhibit a protein triggered activation/deactivation of the emission. Dispersing the particles into an aqueous solution, such as phosphate buffered saline (PBS), results in an aggregation of the hydrophobic fluorophores and a cessation of emission. The emission can be reinstated, or

activated, by the conversion of the surface-attached fluorophores from an aggregate to a monomeric species with the addition of an albumin. This activated probe can be deactivated and returned to a quenched state by a simple tryptic digestion of the albumin. The methodology for emission switching offers a path to maximize the signal from the typically weak quantum yield inherent in NIR fluorophores. Preliminary fluorescence imaging studies indicate that the brightness of the functionalized polymer based nanoparticles improved considerably.

(2) *Surface modified colloids with targeting molecules to disrupt Survivin activity and enhance apoptosis in cancer cells:* Survivin belongs to the family of inhibitor of apoptosis proteins (IAP) and is present in most cancers while being below detection limits in most terminally differentiated adult tissues, making it an attractive protein to target for diagnostic and, potentially, therapeutic roles. Sub-100 nm poly(propargyl acrylate) (PA) particles which are surface-functionalized with an azide terminated Survivin ligand derivative (azTM), originally proposed by Abbott Labs and speculated to bind directly to Survivin (protein) at its dimer interface. Using affinity pull-down studies, it was determined that the PA/azTM nanoparticles selectively bind Survivin and the particles can enhance apoptotic cell death in glioblastomas and other Survivin over-expressing cell lines such as A549 and MCF7 relative to cells incubated with the original Abbott-derived small molecule inhibitor.

(3) *A bioresponsive and versatile particle-protein-dye system for small molecule delivery and FRET based imaging:* Colloidal particles are surface-functionalized with small molecules such as fluorophores and ligands through an environmentally-sensitive linker. The linker used is an azide modified bovine serum albumin (azBSA) which prevents opsonization and releases the small molecule upon digestion. Attachment of the fluorophore to the particle through the azide modified bovine serum albumin (BSA) quenches the emission and is specifically activated upon the denature or digestion of the azBSA. This resulted in an enhanced tumor to background signal ratio. A fluorescence resonance energy transfer (FRET) pair of dyes can be attached to the particle and the azBSA, and the FRET efficiency can be increased by unfolding the protein. These dye modified particles gave promising results in photodynamic therapy studies performed in human head and neck squamous carcinoma cells (UMSCC22A). Further, a targeting ligand can also be attached to the particles using the same strategy to achieve higher accumulations of the desired small molecule inside the tumor. In addition, preliminary imaging and toxicity studies were carried out in human lung carcinoma cells (A549) using a Survivin targeting ligand attached to PA-azBSA particles and

an enhanced cell death relative to free molecule treatment was observed.

Dedication

To my loving parents, Shanti and Sivaram Prasad Jetty, whose unconditional love, affection, and encouragement, provided me the strength to chase my dreams. To my sister, Shalini V. Jetty, and brother-in-law, Venkat Annam, for always believing in me, even when I didn't and cheering me on until the end. To my incredibly wonderful husband, Greg Jenkins, whose support, help and enthusiasm during this long process, helped me accomplish all I set out to do.

Acknowledgments

The research included in this dissertation could not have been performed if not for the assistance, patience, and support of many individuals. Foremost, I would like to truly thank my advisor Dr. Stephen H. Foulger for mentoring me over the course of my graduate study. His continuous guidance, immense support and encouragement through extremely difficult times over the course of the analysis and the writing of the dissertation, has enabled me to develop an understanding of the subject and complete my thesis. Besides my advisor, I would like to thank the rest of my thesis committee members: Dr. Igor A. Luzinov, Dr. O. Thompson Mefford and Dr. Michael G. Sehorn, for their time and critical inputs.

I would like to acknowledge the Department of Materials Science and Engineering, Department of Bioengineering and Center for Optical Materials Science and Engineering Technologies, for allowing me to conduct this research and providing assistance. I am thankful to the faculty and staff of these departments, particularly, Dr. Gary Lickfield, Mr. Robert Bowen, Ms. Tonya Bledsoe, Ms. Cassie Gregory, Ms. Sam Bradberry, Ms. Sheryl Gonzales, Ms. Wendy Baldwin and Mr. Rob Hammett. I thank you all for your patience and kindness when helping me out with anything I needed.

I am indebted to Dr. Yuriy Bandera for his extensive help in the synthesis of various compounds without which this research work would not have been possible. I would like to thank all my colleagues over the past five years particularly, Dr. Bogdan Zdyrko, Dr. Chris Huebner, Dr. Parul Rungta, Dr. Michael Daniele, Mr. Ryan Roeder, Ms. Ali Foguth, Mr. Oleksandr Klep, Ms. Maggie Shaughnessy, Ms. Katie Burdette, Mr. Tucker McFarlane, Ms. Yangchun Li, Ms. LeAnna Ledford, Ms. Shivani Shah, Ms. Ashlee Tietje and Mr. Andrew Kelso for their invaluable camaraderie which got me through this tedious process.

I would also like to thank the faculty and my colleagues at the Medical University of South

Carolina and the University of South Carolina for use of their facilities, their guidance throughout the project, and their collaboration. I would like to acknowledge the Gregg-Graniteville Foundation for their continued financial support.

I cannot thank my husband Greg enough and without his everlasting love and constant support, this would have never been possible. In spite of the numerous adjustments and sacrifices he had to make for me to pursue this work, he wholeheartedly encouraged me. I also owe a lot to my parents, Shanti and Sivaram Prasad Jetty, for their unconditional love, support, and motivation. I thank my parents for teaching me to be persistent, hardworking and patient. I want to thank my sister, Shalini V. Jetty, and brother-in-law, Venkat Annam, for always being there for me and believing in me. I would also like to thank my grandparents for instilling good values and faith in me. I am fortunate to have a close-knit extended family and in-laws and would like to thank each and everyone of them for their support over the years. I would also like to thank my friends over the years from Clemson, University of Illinois, Vellore Institute of Technology, St. Jude's and Nasr for being there when I needed them the most. Particularly, I am very grateful to my friends, Anna Paola Soliani, Ryan McBath, Katie Davis, Akeem Cruickshank, Nicole Hoffman, Tugba Demir, Indumathi Raghu, Yuan Li, Guancheng Gu, Deepthi Kommaraju, Praveen Reddy Nalla, Dhyuti Gondi, Kartheeka Raavi, and Vamsi Gondi, who made my time at Clemson so wonderful. Finally, I would like to thank God for blessing me with the incredible family and friends I have and providing me with the opportunities I had.

Table of Contents

Title Page . . . . . **i**

Abstract . . . . . **ii**

Dedication . . . . . **v**

Acknowledgments . . . . . **vi**

List of Tables . . . . . **x**

List of Figures . . . . . **xi**

1 Introduction **1**
1.1 Small molecule imaging 4
1.2 Imaging with polymer based nanoparticles 7
1.3 Targeting 15
1.4 Activation 19
1.5 Overview 20

2 Switching fluorescence of surface modified colloids with near-infrared emitters via protein interaction for contrast-enhanced imaging **23**
2.1 Attributions 23
2.2 Introduction 24
2.3 Results & Discussion 26
2.4 Experimental 40
2.5 Conclusion 46
2.6 Supplementary Information 47

3 Surface modified colloids with targeting molecules to disrupt Survivin activity and enhance apoptosis in cancer cells **53**
3.1 Attributions 53
3.2 Introduction 54
3.3 Results & Discussion 56
3.4 Experimental 69
3.5 Conclusion 75

4 A bioresponsive and versatile particle-protein-dye system for small molecule delivery and FRET based imaging **79**
4.1 Attributions 79
4.2 Introduction 80
4.3 Results & Discussion 81
4.4 Experimental 101

4.5 Conclusion 107

5 Conclusions 110
5.1 Summary 110
5.2 Recommendations for future research 112

Appendix 115
A Copyright Permissions 116

Bibliography 128

List of Tables

2.1 Fluorophore grafting density and fluorescence quantum yield (ϕ) of surface functionalized PA particles; Fluorophore and particles dispersed in methanol 26

List of Figures

1.1 Typical molecular imaging instruments and images representative of each modality.**(a)** magnetic resonance imaging (MRI) **(b)** computed tomography (CT) **(c)** positron emission tomography (PET) **(d)** single-photon emission computed tomography (SPECT) **(e)** optical imaging **(f)** ultrasound (Reprinted with permission from Ref. [7] Copyright 2010 Elsevier B. V.) 2

1.2 Schematic structures of **(a)** polymer cross-linked micelles, **(b)** polymersomes, and **(c)** polymer-core nanoparticles (Adapted from Ref. [25]) 3

1.3 Structures of **(a)** cyanine, **(b)** squaraine, **(c)** phthalocyanine, and **(d)** boron dipyrromethane dyes 4

1.4 **(a)** Fluorescence, **(b)** transmission, and **(c)** overlapping fluorescence/ transmission images of Hela cells observed by confocal laser scanning microscopy. The cells were incubated with BODIPY conjugated surface crosslinked micelles at a concentration of 1 mM for 30 min at 37 ^{o}C under a humidified atmosphere containing 5 % CO_2. The excitation wavelength was fixed at 561 nm and the fluorescence signals were collected between 570 620 nm. (Reprinted with permission from Ref. [57] Copyright 2013 The Royal Society of Chemistry) 9

1.5 Temperature triggered self-assembly of an ELP$_{BC}$ to form multivalent spherical micelles. An N-terminal ELP[$V_1A_8G_{7-n}$] gene (hydrophilic, high T_t) and C-terminal ELP[V_{5-n}] gene (hydrophobic, low T_t) are seamlessly fused together to create a gene that encodes an ELP$_{BC}$. When the size and ratio of the blocks are correctly selected, the ELPBC self-assembles into a spherical micelle at ca. 40 ^{o}C. In the cartoon shown, upon self-assembly the spherical micelles present multiple copies of an affinity targeting moiety (green triangle) and sequester a drug or imaging agent (lightning bolt) within the core of the micelle. (Reprinted with permission from Ref. [61] Copyright 2008 American Chemical Society) 9

1.6 Schematic depiction of the incorporation of various oligo(porphyrin)-based NIRFs within polymersomes. **(a)** The NIRFs vary with respect to the number of porphyrin subunits (N), the linkage topology between porphyrin monomers, and the nature and position of ancillary aryl-group substituents (R). **(b)** Various diblock copolymer compositions have been utilized to form NIR-emissive polymersomes. **(c)** Membranous interactions between polymers and specific ancillary aryl group substituents vary the conformational populations assumed by the NIRF and can be used to tune its emission wavelengths. **(d)** Engineering the chemical composition and thickness of the polymersome membrane and helps to drive individual NIRFs into dielectric environments of matching polarity. **(e)** a family of nanoscale NIR emissive polymersomes. (Reprinted with permission from Ref. [65] Copyright 2009 John Wiley & Sons Inc.) 11

1.7 In vivo biodistribution of intravenously administered Cy5-PLA nanoparticles. Visceral organ biodistribution of Cy5-PLA nanoparticles following lateral tail vein injection using the LI-COR Odyssey scanner. Accumulation of Cy5-PLA nanoparticles within visceral organs allows for greater than 10-fold increase in fluorescent intensity in comparison with background autofluorescence. Splenic accumulation of Cy5-PLA nanoparticles is the greatest for all visceral organs examined (spleen, liver, kidney, lung, and heart); Bar 5 5 mm. (Reprinted with permission from Ref. [85] Copyright 2010 WILEY-LISS INC.) 14

1.8 Real-time fluorescence imaging of BF_2 chelated tetraarylazadipyrromethenes (near infrared dye) conjugated poly(styrene-co-methacrylic acid) particles uptake into HEK293T cells (scale bar 10 m). (Reprinted with permission from Ref. [88] Copyright 2011 American Chemical Society) 15

1.9 Schematic representation of different mechanisms by which nanocarriers can deliver drugs to tumors. Polymeric nanoparticles are shown as representative nanocarriers (circles). Passive tissue targeting is achieved by extravasation of nanoparticles through increased permeability of the tumor vasculature and ineffective lymphatic drainage (EPR effect). Active cellular targeting (inset) can be achieved by functionalizing the surface of nanoparticles with ligands that promote cell-specific recognition and binding. The nanoparticles can **(i)** release their contents in close proximity to the target cells; **(ii)** attach to the membrane of the cell and act as an extracellular sustained-release drug depot; or **(iii)** internalize into the cell. (Reprinted with permission from Ref. [49] Copyright 2007 Nature Publishing Group) 17

1.10 **(a)** Design of lactoferrin-conjugated biodegradable polymersome for glioma targeting. Polymersomes are simultaneously loaded with doxorubicin (Dox) as a model antitumor drug and tetrandrine (Tet) as an multi drug resistance (MDR) inhibitor. Lactoferrin (Lf) was conjugated on the surface of polymersomes, as glioma targeting ligand and to help overcome the obstruction of the BBB. **(b)** Accumulation of targeted polymersomes in glioma (EPR effect and overcoming BBB) was evidenced by fluorescence imaging. **(c)** The specific interaction of Lf-conjugated polymersomes with glioma cells enhanced drug delivery into these cells, improving the chemotherapy of glioma as showed by the improved survival in rats. (Reprinted with permission from Ref. [67] Copyright 2012 Wiley Periodicals Inc.) 18

1.11 Internalization of rhodamine B-labeled NPs. Fluorescence microscopy images of MCF7 cells showing the cellular uptake of nonfunctionalized (N0) and biotin-functionalized (N1) NPs (red) after 5 h of incubation. The nuclei were stained with DAPI (blue), phalloidin-fluorescein isothiocyanate (Ph-FITC, green) was used to label F-actin, and the last column represents the overlay of all types of staining. (Reprinted with permission from Ref. [22] Copyright 2012 American Chemical Society) . 19

1.12 **(a)** Increase in photoluminescence intensity ratio of PA-azICG-azPEG1K particles dispersed in a phosphate buffered solution (PBS) with the addition of 0.014 mM BSA; time evolution of the intensity at 819 nm relative to the initial intensity. Inset presents photoluminescence of particles after 2 min (○), 37 min (●), and 1174 min (▽) . Excitation energy at a wavelength of 710 nm; particle density of 1.259 x 10^{12} cm^{-3}. **(b)** Optical image of fluorescence intensity of PA-azICG-azPEG1K particles in deionized water (far left), PBS (center), and 2 h after the addition of 0.014 mM BSA to the PBS solution (far right); images taken with a Caliper Xenogen IVIS Lumina II XR Instrument with 745nm excitation filter and ICG emission filter; particle density of 1.259 x 10^{12} cm^{-3} (Reprinted with permission from Ref. [31] Copyright 2011 WILEY-VCH Verlag GmbH & Co. KGaA) 21

2.1 Schematic of 50 nm poly(propargyl acrylate) (PA) particles surface modified with an azide-terminated squaraine (azSQ) and polyethylene glycol (azPEG) through an aqueous-phase "click" transformation in the **(a)** aggregated & nonfluorescent state and in the **(b)** albumin activated fluorescent state. Particles could be deactivated and returned to the quenched state through a trypsin digestion of the albumin. 25

2.2 **(a)** Molar extinction coefficient (green) and photoluminescence (red) of azide functionalized squaraine derivative chromophore (azSQ; 6.98 μM in methanol); **(b)** Absorbance (green) and photoluminescence (red) of PA/azSQ/azPEG (FP_7) particles in methanol. Excitation energy at a wavelength of 630 nm. 28

2.3 Quantum yield of azide functionalized squaraine derivative chromophore (azSQ) with variation in grafting density to PA particles (methanol). Excitation energy at a wavelength of 650 nm. 29

2.4 **(a)** Photoluminescence of FP_7 particles dispersed in: PBS (—), PBS and 0.05mM BSA (green), PBS and 0.05mM HSA (red). Particles were incubated with serum albumin for ca. 4 days to insure increase was invariant with time, though 25% of the increase occurred within the first 30 minutes. **(b)** Photoluminescence spectra of FP_5 particles in PBS with 15 mg BSA initially at 20 °C (○), at 70 °C (●), after 70 °C anneal then cooled to 20 °C (△), after 70 °C, cool to 20 °C, heated to 70 °C (▽), and after 70 °C, cool to 20 °C, heated to 70 °C, then cooled to 20 °C (—). Inset presents the intensity ratio at 682 nm (red) for the thermal cycles relative to the initial emission and the intensity ratio (green) of the J-aggregates (745 nm) to the monomeric emission (682 nm). Excitation energy at a wavelength of 630 nm. 30

2.5 Change in fluorescence intensity at wavelength of 671 nm with exposure to hydrogen peroxide of free azSQ dye (●) and FP_7 particles incubated with BSA (○). Aqueous solution with excitation energy at a wavelength of 630 nm. 32

2.6 Variation of photoluminescence spectrum of FP_5 particles in PBS incubated with BSA (**sequence 0**), with four annealing cycles (**sequence 1-5**), with introduction & incubation of trypsin (**sequence 6-10**), reintroduction & incubation of BSA (**sequence 11-13**) and with four annealing cycles (**sequence 14-17**). Excitation energy at a wavelength of 630 nm. An annealing cycle consists of raising the sample temperature to 65 °C for 20 min and then returning the temperature to 20 °C. 34

2.7 Confocal images of FP_7 particles (1 μM) incubated with UMSCC22A cells for 1, 8, and 17 hours. One hour before imaging, cells were loaded with LysoTracker Green (LTG) to image lysosomes. LTG (green, 473 nm) is left image, PA/azSQ/azPEG particles (red, FP_7) is the center image, and the right image is their overlay. 36

2.8 Confocal images of FP_7 particles (1 μM) incubated with A549 cancer cells depicting the activation of fluorescence with incubation time (0.5 h - 1 h) and subsequent reduction in fluorescence with incubation time (2 h - 24 h) as particles enter lysosomes. Media did not contain FBS and excitation laser power was constant between images. 37

2.9 Manders' co-localization coefficient M_1 (green channel) and M_2 (red channel) from Figure 2.7 of FP_7 particles incubated with UMSCC22A cells. 38

2.10 **(a)** Confocal images of FP_7 particles (1 μM) incubated with UMSCC22A cells for 2 hours (left image) and with the addition of the raft/caveolae endocytosis pathway inhibitor filipin (FIL) (right image) and corresponding **(b)** Pearsons' co-localization coefficient between LTG and FP_7 particles. An asterisk indicates statistical significance from the control by ANOVA followed by Tukeys multiple comparisons test ($p<0.01$). 40

2.11 Reaction scheme for synthesis of azSQ. 42

2.12 Fluorescence spectra of FP_5 nanoparticles (6.53 μM) in water before (-) and 18 hours after addition of 50 mg of SDS (○). Excitation at 630 nm. 47

2.13 Fluorescence spectra of FP_7 nanoparticles (4.97 μM) in water before (-) and 18 hours after addition of 50 mg of SDS (○). Excitation at 630 nm. 48

2.14 Changes in photoluminescence intensity of FP_5 nanoparticles (0.03 mM) in phosphate buffered solution (PBS) with the addition of the four different proteins (0.04 mM) [Bovine serum albumin (○), human serum albumin (●), lysozyme (△), and trypsin (▲)]. The HSA and BSA curves typically merge after 4 days of incubation, though the lysozyme and trypsin never significantly increase the particles emission. Excitation at 630 nm. 48

2.15 Changes in absorbance spectra of FP_5 nanoparticles in phosphate buffered solution (PBS) with 15 mg of BSA. [Initially at 20 ^{o}C (●), at 70 ^{o}C (○), after 70 ^{o}C anneal then cooled to 20 ^{o}C (▼), after 70 ^{o}C, cool to 20 ^{o}C, heated to 70 ^{o}C (△) and after 70 ^{o}C, cool to 20 ^{o}C, heated to 70 ^{o}C, then cooled to 20 ^{o}C (■)] 49

2.16 Changes in photoluminescence of FP_7 nanoparticles in phosphate buffered solution (PBS) with 5 mg of BSA. [Initially at 20 ^{o}C (●), after heat and cool cycle 1 (○), after heat and cool cycle 2 ((▼), after heat and cool cycle 3 (△) and after heat and cool cycle 4 (■)]. Excitation at 630 nm. 50

2.17 Proliferation of HepG2 cells after 2 days of incubation with neat PA and PA/ azSQ (FP_5) nanoparticles at concentrations of ca. 2 x 10^{13}, 2 x 10^{11} and 2 x 10^9 particles/ mL. Each condition was tested in six replicates. Cell viability was determined via 3-[4,5-dimethylthiazol-2-yl]-2,5-diphenyl tetrazolium inner salt (MTS) assay. 2 x 10^{13} particles/ mL is about 63 μM for PA/ azSQ (FP_5). . 51
2.18 Proliferation of HepG2 cells after 2 days of incubation with PA/ azSQ/ azPEG (FP_7) nanoparticles at concentrations of ca. 2 x 10^9, 2 x 10^{11} and 2 x 10^{13} particles/ mL. Each condition was tested in six replicates. Cell viability was determined via 3-[4,5-dimethylthiazol-2-yl]-2,5-diphenyl tetrazolium inner salt (MTS) assay. 2 x 10^{13} particles/ mL is about 37 μM for PA/ azSQ/ azPEG (FP_7). . . 51
2.19 Proliferation of A549 cells after 2 days of incubation with neat PA and PA/ azSQ (FP_5) nanoparticles at concentrations of ca. 2 x 10^9, 2 x 10^{11} and 2 x 10^{13} particles/ mL. Each condition was tested in six replicates. Cell viability was determined via 3-[4,5-dimethylthiazol-2-yl]-2,5-diphenyl tetrazolium inner salt (MTS) assay. 2 x 10^{13} particles/ mL is about 98 μM for PA/ azSQ (FP_5). 52
2.20 Proliferation of A549 cells after 2 days of incubation with PA/ azSQ/ azPEG (FP_7) nanoparticles at concentrations of ca. 2 x 10^9, 2 x 10^{11} and 2 x 10^{13} particles/ mL. Each condition was tested in six replicates. Cell viability was determined via 3-[4,5-dimethylthiazol-2-yl]-2,5-diphenyl tetrazolium inner salt (MTS) assay. 2 x 10^{13} particles/ mL is about 75 μM for PA/ azSQ/ azPEG (FP_7). . . 52

3.1 **(a)** Structures of Survivin ligands, Abbott8 and Abbott17 (targeting molecule TM) proposed by Abbott Labs and an azide modified targeting molecule (azTM). **(b)** Schematic of 50 nm poly(propargyl acrylate) (PA) particles surface modified with an azide-terminated Survivin ligand (azTM) through an aqueous-phase "click" transformation sequestering anti-apoptotic protein Survivin. 56
3.2 Preliminary cell viability data in glioblastoma cells, U251MG and U118MG, using MTT assay. Untreated cells were used as the control (ctl). Cells were treated with the small molecule ligands at the indicated concentrations for 24 hours. Cell viability is presented as a percentage of viable cells in the total population. Significant difference from control value was indicated by *p<0.05. **(a)** TM and **(b)** azTM treatment of the glioblastomas. 58
3.3 Increased apoptosis in glioblastoma cells, U251MG and U118MG, with azTM small molecule ligand when compared to TM. Untreated cells were used as the control (ctl). Cells were treated with TM or azTM ligand at indicated concentrations for 24 hours. **(a)** In situ Wright staining for detection of morphological features of apoptosis. Bar diagram shows percent apoptosis based on Wright staining for **(b)** TM and **(c)** azTM treatments. Cell death is presented as percentage of apoptosis in total population. Significant difference from control value was indicated by *p < 0.05 or **p < 0.01. . . 59
3.4 Purification of Survivin and affinity pull-down of Survivin by surface-functionalized particles. **(a)** SDS-PAGE of purified recombinant Survivin (ca. 0.8 μg); **(b)** Poly(propargyl acrylate) (PA) particles were surface modified with azTM (cf. Figure 3.1) and azPEG. Control particles lacked the presence of ligand. Both sets of particles were incubated with Survivin or BSA protein. The supernatant was removed and the particles were washed with buffer. Proteins retained on the particles were eluted. The supernatant (S), wash (W) and elution (E) were separated on a 15 % polyacrylamide gel and stained with Coomassie blue. **(c)** Percentage of bound proteins on functionalized and control particles (data taken from SDS-PAGE in Part **(b)** as well as two other pull-down experiments). . 61
3.5 **(a)** Survivin conjugate azTM disrupted the activity of Survivin to promote Caspase mediated apoptosis. Both glioblastoma cell lines were treated with Survivin conjugate azTM as a free small molecule or attached to the surface of nanoparticles (1.0 μM ligand concentration) prior to extraction of protein samples. Protein samples were resolved by 4 - 20 % SDS-PAGE and Western blotting was performed using the primary IgG antibodies against Survivin, Caspase-3, and β-Actin. Quantification of expression of Survivin and Caspase-3 after treatment with free ligand (azTM) and modified particles (PA/ azTM) in **(b)** U251MG or **(c)** U118MG cells. Significant difference from control value was indicated by *p<0.1, **p<0.01 and #p<0.001. 63

3.6 Cell viability of A549 cells treated with small molecule azTM and PA/ azTM particles with two different grafting densities (gd), 0.58 and 1.91 azTM/nm^2, at varying concentrations for 48 hours. Cell viability is presented as percentage of viable cells compared to the control and the MTS assay was employed. 65
3.7 Viability of A549 cells with PA/ azTM particles of varying ligand surface density. The cells were treated with azTM and PA/ azTM of varying different grafting densities (gd) of 0.58, 0.90, 1.71, 1.77 and 1.91 azTM/ nm^2 and at varying concentrations for 48 hours. Cell viability is presented as percentage of viable cells compared to the control and the MTS assay was employed. 66
3.8 Imaging of A549 cells treated with 15 μM PA/ azTM/ azSQ and PA/ azTM/ azC6 for 24 hours and fluorescence images were taken under RFP and GFP filters, respectively. All scale bars represent 100 μm. 67
3.9 Fluoroscope images of A549 cells after incubation with 25 μM of azTM, PA/ azTM particles with two different grafting densities, PA/ azTM/ azPEG particles and PA particles. Cells were treated with an apoptotic/necrotic/healthy cells detection kit to differentiate the status of the cells. All scale bars represent 200 μm. 77
3.10 Reaction scheme for synthesis of Survivin ligands, TM and azTM 78

4.1 Schematic of the release of fluorophores from functionalized particles through trypsin digestion of the albumin. Sub 100 nm poly(propargyl acrylate) (PA) particles were surface modified with an azide-modified bovine serum albumin (azBSA) and alkyne terminated cyanine derivate fluorophore (YB317) through an aqueous-phase click transformation. 82
4.2 Structures of **(a)** azide modified N-hydroxy succinimide derivative (azNHS), **(b)** alkyne modified cyanine derivative fluorophore (CYN), **(c)** azide modified silicon phthalocyanine fluorophore with short PEG chains (azSiPc1) and long PEG chains (azSiPc2), **(d)** alkyne modified silicon phthalocyanine fluorophore with short PEG chains (SiPc1) and long PEG chains (SiPc2), **(e)** Abbott 17, **(f)** azide modified Survivin ligand (sl01), **(g)** alkyne modified Survivin ligand (sl02), and **(h)** azide modified fluorescein derivative fluorophore (azFL). 83
4.3 Absorbance (green) and photoluminescence (pink) of alkyne functionalized cyanine derivative fluorophore (CYN; 12.21 μM in methanol). 84
4.4 **(a)** Changes in photoluminescence intensity of (-) alkyne terminated cyanine fluorophore (CYN), with addition of (○) ca. 0.05 mM bovine serum albumin, followed by addition of ca. 0.215 mM trypsin, and incubated for (●) 2 hours and (△) 7203 hours. **(b)** Changes in photoluminescence intensity of (-) alkyne terminated cyanine fluorophore (CYN), with the addition of ca. 0.215 mM trypsin, and incubated for (●) 2 hours and (△) 7203 hours. 85
4.5 TEM micrographs of **(a)** unmodified PA particles, **(b)** and **(c)** particles surface modified with albumin/ cyanine 3 derivative fluorophore (PA-azBSA-CYN). All scale bars represent ca. 100 nm. 85
4.6 **(a)** Increase in photoluminescence intensity of PA-azBSA-CYN nanoparticles with addition of trypsin and incubation for 1 hour (○) and 48 hours (●) at 37 ^{o}C when dispersed in PBS. The inset presents the change in the integrated peak area of emission with the addition of trypsin. **(b)** Photoluminescence of the supernates of the PA-azBSA-CYN nanoparticles stored at 4 ^{o}C (-), incubated at 37 ^{o}C (○), and trypsin digested (●). 86
4.7 nanoDSC runs of **(a)** BSA and **(b)** azBSA. Undigested proteins (pink) and trypsin digested proteins (green) 87
4.8 **(a)** The cells were treated with 200 nM of azSiPc1 or Pc4 for 18 hours. **(b)** The cells were treated with varying concentrations of PA-azBSA-SiPc2 for 18 hours. Cell viability is presented as percentage of viable cells in total population. 90
4.9 Cell viability data using the MTS assay with A549 cells The cells were treated with sl01 and PA-azBSA-sl02 at varying concentrations for 48 hours. Cell viability is presented as percentage of viable cells in total population. 92
4.10 *in vitro* fluorescence imaging in A549 cells (after 11 hours of treatment with modified particles) . 93

4.11 Schematic of the FRET response of functionalized particles through trypsin digestion of the albumin. Sub 100 nm poly(propargyl acrylate) (PA) particles were surface modified with (1) an azide modified fluorescein fluorophore and (2) an azide-modified bovine serum albumin (azBSA) that is conjugated to alkyne terminated cyanine derivate fluorophore (YB317), through multiple aqueous-phase click transformations. 95
4.12 Absorbance and photoluminescence spectra of azFL (donor, UV - light green and PL - dark red) and CYN (acceptor, UV - dark green and PL - pink). 96
4.13 Changes in photoluminescence of PA-azFL-azBSA-CYN particles with addition of trypsin and incubation at 37 ^{o}C. Emission of the particles was measured (-) initially, after incubation for (○) 60 mins and (●) 2400 mins. The particles were dispersed in PBS and excited at 440 nm (donor). . . 97
4.14 Changes in photoluminescence of PA-azFL-azBSA-CYN particles with addition of DTT and incubation at 37 ^{o}C. Emission of the particles was measured (-) initially, after incubation for (○) 30 mins, (●) 90 mins and (△) 210 mins. The particles were dispersed in PBS and excited at 440 nm (donor). 98
4.15 Changes in photoluminescence of PA-azFL-azBSA-CYN particles with addition of l-glutathione and incubation at 4 ^{o}C. Emission of the particles was measured (-) initially, after incubation for (○) 40 mins and (●) 1230 mins. The particles were dispersed in PBS and excited at 440 nm (donor). . . 99
4.16 Reaction scheme for synthesis of azNHS. 102
4.17 Reaction scheme for synthesis of CYN. 103
4.18 Reaction scheme for synthesis of sl02. 108
4.19 Reaction scheme for synthesis of azFL. 109

Chapter 1

Introduction

Cancer is a disease where the growth of abnormal cells is uncontrollable and is one of the leading causes of death worldwide, accounting for 13 % of all deaths[1]. Malignant cancer cells are more effectively treated when identified early in the disease. Identification of tumors using nanoparticle technologies is significantly impacting molecular imaging methods[2]. Molecular imaging plays a vital role in the healthcare sector. Abnormal conditions and diseases are often diagnosed through imaging. In addition, therapeutic methods used for the treatment of abnormalities is also guided by imaging. At present, there are various forms of imaging techniques employed: tomography, magnetic resonance imaging (MRI), gamma scintigraphy, ultrasound, and optical imaging (cf. Figure 1.1). Computed tomography gives high resolution images and has the ability to differentiate between tissues, but has several drawbacks such as high cost and exposure to radiation, and also require a contrast agent for enhanced tissue contrast[3, 4]. Magnetic resonance imaging gives high resolution images with better contrast and there is no exposure to radiation, but the issues of the high cost and low sensitivity compared to radionuclide and optical techniques are still present[3, 5, 6]. In addition, MRI cannot be used in patients with metallic devices such as pacemakers[7]. Gamma scintigraphy, which includes positron emission tomography (PET) and single-photon emission computed tomography (SPECT), suffers from all the three major drawbacks: exposure to radiation, low resolution and high cost[7, 8, 9]. Ultrasound is a low cost, non-invasive and simple procedure with no radiation but the images obtained are low in resolution[3, 5, 7]. Optical imaging is a highly sensitive and low cost procedure[7, 10, 11]. The main advantages of optical imaging are: (1) can be used as an imaging agent in both live and fixed cells and tissues; (2) no additional substrate is required for visu-

alization; and (3) multiple probes with different spectral characteristics could potentially be used for multichannel imaging[3, 12, 13]. The setbacks for optical imaging is that images obtained are low in resolution and has a limited tissue penetration[7]. Some of the other general drawbacks, which are not specific to any one imaging technique, are long lasting side effects on patients, time-consuming, complex in nature and often prove to be expensive and tedious for the patient even with medical insurance. In most situations, due to the issues mentioned, the abnormalities are not detected until later stages of the disease when treatments are less effective. To this end, a better imaging system is required to overcome the limitations. In this current project, the developments in the field of optical imaging with near-infrared (NIR) fluorophores is of interest.

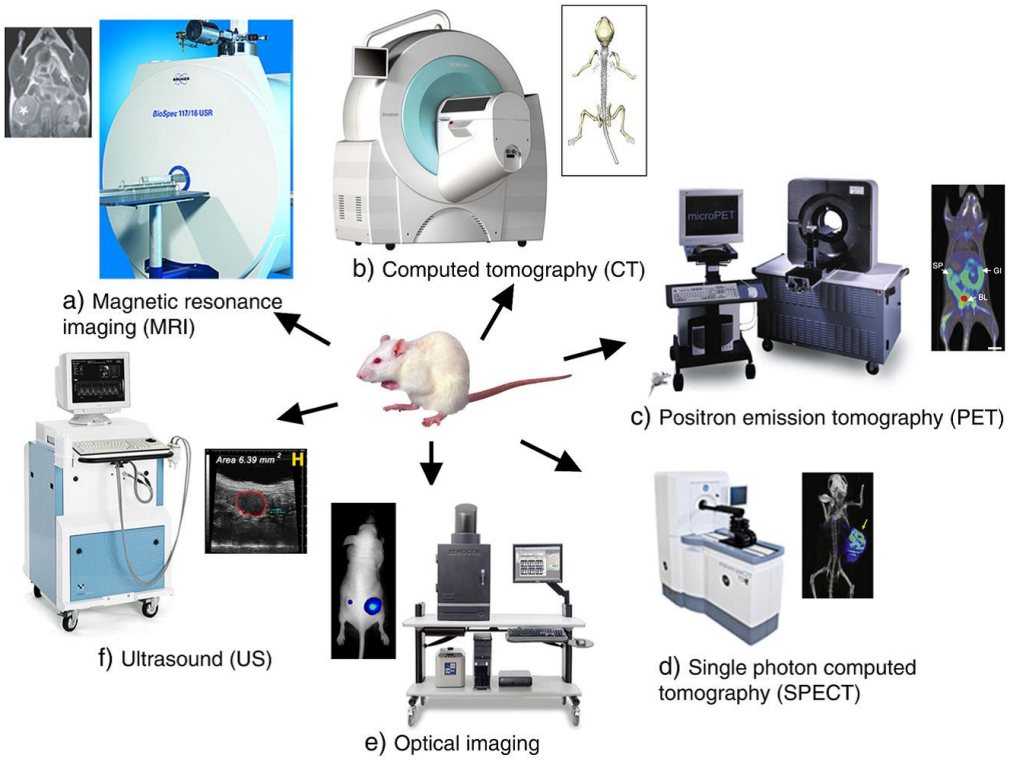

Figure 1.1: Typical molecular imaging instruments and images representative of each modality.**(a)** magnetic resonance imaging (MRI) **(b)** computed tomography (CT) **(c)** positron emission tomography (PET) **(d)** single-photon emission computed tomography (SPECT) **(e)** optical imaging **(f)** ultrasound (Reprinted with permission from Ref. [7] Copyright 2010 Elsevier B. V.)

In recent times, the use of NIR fluorophores in imaging has gained popularity. Fluorophores are small molecules with specific functional groups, which absorb light at a defined wavelength and re-emit light at a longer wavelength. These fluorophores overcome drawbacks such as background noise and facilitate for deeper imaging in human body[14]. Unfortunately, small molecule fluorophores have

four major limitations: (1) limited aqueous solubility, (2) short *in vivo* circulation lifetimes, (3) low quantum efficiencies, and (4) low signal to noise ratios. The mentioned drawbacks can be overcome by either encapsulating the fluorophore inside a nanoparticle or attaching it to the surface of the nanoparticle. In addition, targeting agents and drugs can be loaded onto the nanoparticles along with the fluorophore to create a single and multifunctional "nanodevice" for tumor theranostics. Over the years, there has been development of fluorescent nanocarriers such as surface cross-linked micelles,[15, 16], dendrimers,[17] biodegradable polymeric nanoparticles,[18, 19] magnetic and other metal particles,[20, 21] and liposomes,[20] for tumor diagnosis. Among these technologies, platforms based on polymeric materials, especially biodegradable nanoparticles, are of particular interest due to the flexibility offered by macromolecular synthesis methods, high drug loading capacities, improved drug solubility and their ease of multifunctionalization[22, 23, 24].

In this chapter, the commonly used NIR fluorophores will be discussed. That discussion will be followed up with the developments in fluorescence imaging with three polymer based platforms: cross-linked micelles, polymersomes and polymer-core nanoparticle (cf. Figure 1.2). At the end strategies such as targeting and activation for the nanoprobes will be presented.

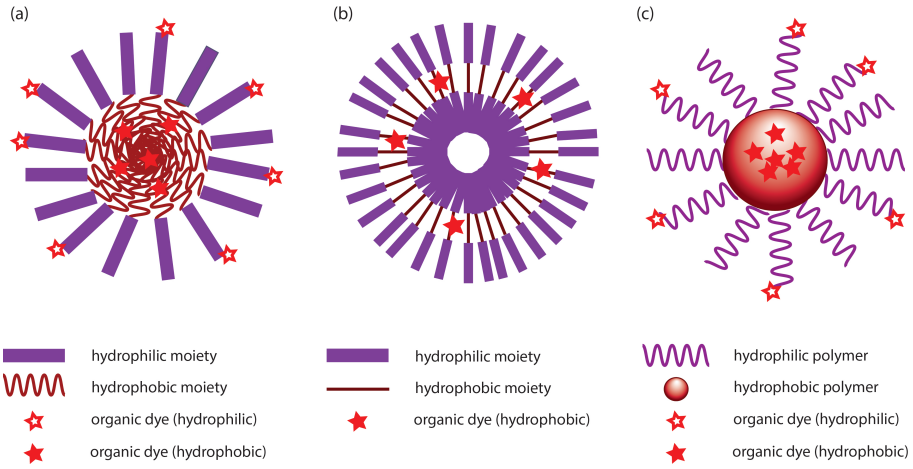

Figure 1.2: Schematic structures of **(a)** polymer cross-linked micelles, **(b)** polymersomes, and **(c)** polymer-core nanoparticles (Adapted from Ref. [25])

1.1 Small molecule imaging

Small molecule organic fluorophores have always been in demand at biomedical communities for imaging and image guided surgery or therapy. Imaging with far-red and near-infrared dyes such as cyanine, squaraine, thiazine, oxazine, porphyrins and phthalocyanines, is very common and most of them have been approved for clinical trials. Recently, a new class of dyes borondipyrromethane (BODIPY) derivatives have emerged and are gaining popularity. Despite the widespread utilization of these dyes, there is still a need for better systems due to the limitations of small molecules. Imaging with small molecules have shortcomings such as water insolubility, aggregation, low quantum yield, insufficient photostability, low tumor to background ratio, and short *in vivo* circulation lifetimes. Recently, Luo and colleagues published an overview of near-infrared (NIR) dyes and their potential applications in cancer imaging[26]. Based on that review, the following sub-sections will highlight the main points of some of the popular classes of dyes.

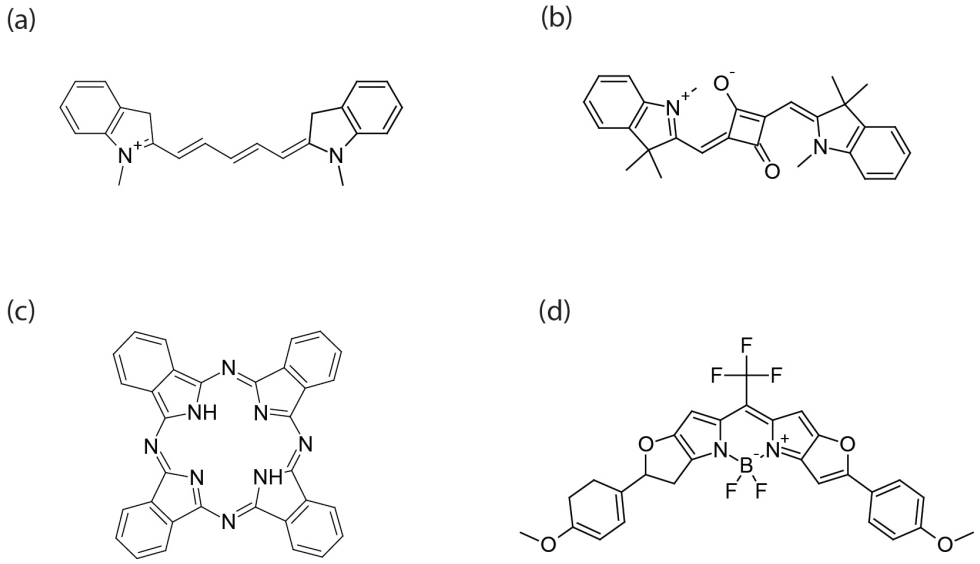

Figure 1.3: Structures of **(a)** cyanine, **(b)** squaraine, **(c)** phthalocyanine, and **(d)** boron dipyrromethane dyes

1.1.1 Cyanine dyes

The general structure of the cyanine dyes consists of two aromatic nitrogen-containing heterocycles, acting as both electron donors and acceptors. The two aromatic rings are joined by a single or odd number of methine groups in which (n + 1) bi-electrons are distributed over *n* atoms

that produce a delocalized cation across the methine chain (cf. Figure 1.3a)[26, 27, 28]. Depending on the methine chain length the cyanine dyes absorb between the visible and infrared regions of the electromagnetic spectrum[29]. In 1856, C. H. G. Williams synthesized the first cyanine dye[29, 30]. Since then many analogs with varying lengths of methine chain were used to demonstrate the application in various biomedical applications ranging from angiography to photodynamic therapy[26]. Cyanine dyes make up the majority of commercial fluorescent probes for *in vivo* imaging. Of all the cyanine dyes, indocyanine green (ICG) is the most popular and was approved by the FDA 50 years ago for evaluating blood flow and clearance[26, 27]. ICG and many other dyes generally exhibit high molar extinction coefficients but low quantum yields, poor photostability, high plasma protein binding rate and undesired aggregation[31]. To overcome some of the limitations, new analogs that have a cyclohexenyl in the middle of the methine chain and moieties such as carboxylic and sulfonate were introduced[32, 33]. These improved water solubility, photostability and quantum yields but the improvement was not sufficient.

1.1.2 Squaraine dyes

Squaraine dyes are 1, 3 - zwitter ionic donor-acceptor-donor (D-A-D) structures with the central acceptor four membered squaryl ring flanked by donor aromatic/ heterocyclic rings on either side (cf. Figure 1.3b)[34]. In 1965, Treibs and colleagues first reported the synthesis of squaraine dyes, which have extremely intense absorption bands, high molar absorption and good photoconductivity[26, 35, 36]. Despite these molecules having excellent physical-chemical properties, they gained importance only in late 2000s due to their limitations such as water solubility, aggregation, chemical stability and only few analogs of the dye emit at wavelengths higher than 800 nm[26]. Most importantly, the squarate bridge was susceptible to chemical attack by nucleophiles. Around 2005, Gassensmith and colleagues synthesized a rotaxane molecule encapsulating a squaraine dye. The rotaxane cage protected the squaraine ring and inhibited aggregation, which improved the chemical and photo stability of the dye[37]. In 2007, Umezawa and colleagues developed another alternative squaraine derivative dye of improved hydrophilicity due to the four water-solubilizing sulfonate moieties added to the general structure[38]. All these solutions to squaraine made the dye very promising for protein detection and *in vivo* imaging.

1.1.3 Porphyrin and phthalocyanine dyes

Porphyrins are tetrapyrrolic molecules that consist of four pyrrolic sub-units linked on opposing sides through four methine (CH) bridges. Phthalocyanine molecules are an extension of porphyrins where each pyrrolic ring of porphyrin is extended by a benzene ring (cf. Figure 1.3c)[39]. The central cavity of the phthalocyanine contains two hydrogen atoms and these atoms can be replaced by more than 70 metal atoms. In addition, a variety of substituents can be added to the periphery of the macrocycle or to the axial positions of the central atom[26]. These blue or greenish color dyes absorb strongly in the red and near-infrared part of the visible spectrum. In 1907, Braun and Tcherniac synthesized the first metal-free and copper phthalocyanines[40]. *In vitro* fluorescence imaging with phthalocyanines and porphyrins dates back to late 1980s and early 1990s[41]. In 1993, photofrin was the first chromophore in this class of dyes to be approved for clinical use in 1993 for the treatment of bladder cancer[39]. Since then there have been several analogs of the dyes synthesized and used. The low water solubility set back the popularity of these dyes for imaging. In 2012, a new phthalocyanine chemistry was used to create a series of PEGylated cationic molecules, which has promising *in vitro* behavior against cancer cells[42]. In the field of tumor theranostics, these dyes are more successful than the other classes of dyes due to their ability of being used as fluorophores in imaging and photosensitizers in photodynamic therapy. Recently, Yumita and colleagues synthesized a novel porphyrin derivative and demonstrated a mechanism that is related to generation of singlet oxygen to achieve destruction of cancer cells through sound rather than light[43].

1.1.4 Borondipyrromethane dyes

Borondipyrromethanes (BODIPY) have a general structure of 4, 4' - difluoro - 4 - bora - 3a, 4a - diaza - s - indacene (cf. Figure 1.3d). In 1968, Treibs and Kreuzer first reported the synthesis of BODIPY dyes[44]. These molecules typically have the following characteristics: sharp fluorescence with high quantum yield, excellent thermal and photochemical stability, and extinction coefficients around 80000 M^{-1} cm^{-1}[45]. Despite having such attractive properties, BODIPYs were not preferred as they emit in the yellow to deep-red region and the extinction coefficients were considered to be relatively low[26]. To overcome this disadvantage there were two effective solutions put forth. First, polymeric and copolymeric BODIPY dyes were synthesized to shift the emission to the near-infrared region[46]. Second, modification of pyrrole core shifts the emission to the red end

of the spectrum. The most significant modification includes aryl groups to the BODIPY. Using this modification, BODIPYS of molar extinction coefficients of 253,000 M^{-1} cm^{-1} and emitting in the near-infrared region can be obtained[47, 48].

1.2 Imaging with polymer based nanoparticles

Nanosized objects accumulate more efficiently in tumors and increase tumor to background ratio (TBR) due to enhanced permeability and retention (EPR) effect. EPR effect results in passive targeting of nanoparticles to tumor sites. Blood vessels supplying tumor tissues have larger pore sizes compared to those in healthy tissue and tumor tissues have poor lymphatic drainage, which allows preferential tumor accumulation of nanoparticles and this phenomenon is called the EPR effect[49, 50, 51, 52]. Small animal studies indicate that a 50 fold increase in accumulation of nanoparticles within tumor tissues due to EPR effect and an increase in *in vivo* circulation lifetimes can be obtained[52]. Apart from the increased accumulation and lifetimes, the nanoparticles have another advantage, which is that they provide an increased surface area per volume for increased loading of the fluorophore and other moieties[51]. To this end, conjugating the small molecule fluorophore to nanoparticles is preferred over using the fluorophore by itself for optical imaging. In addition to the EPR effect, the particle characteristics such as size distribution, surface charge, biocompatibility, biodegradation behavior and availability of functional groups for conjugation play an important role in determining circulation lifetimes and accumulation in tumor tissues[25, 51]. It is established that biodegradable microparticles made of starch, albumin or poly lactic acid, are rapidly cleared by the reticuloendothelial system (RES) and are unable to enter capillaries, making them less attractive for imaging applications[51]. As mentioned previously, polymeric nanocarriers are of particular interest due to the flexibility offered by macromolecular synthesis methods, high drug loading capacities, improved drug solubility and their ease of multifunctionalization[22, 23, 24]. The first preparation and characterization of polymeric nanoparticles was reported in 1976 and since then the research in this area has grown significantly[51, 53]. It has been established in literature that neutrally charged particles, with an average diameter of 10 - 100 nm, and molecular weights up to 800 kDa were required to obtain longer circulation lifetimes[51, 54]. In addition, choosing the right parent polymer is an important step in the design of the systems because polymer type can determine the ultimate behavior of the system in different environments[51]. Based on the above

mentioned requirements for the nanocarrier, some of the successful organic fluorescent carriers used in fluorescence imaging will be discussed in detail in the following sections (cf. Figure 1.2).

1.2.1 Crosslinked micelles

A crosslinked micelle (CM) is a nanocarrier that is based on self-assembled aggregation of amphiphilic molecules or surfactants with the fluorescent probes conjugated to it. Micelles have a dynamic structure in equilibrium and at critical micellar concentration (CMC) they exist as free monomers, so care should be taken to ensure that the concentration is below the CMC to avoid fast and undesired release of the probe upon administration[25]. Typically, CMs usually range in 5 - 150 nm in size[55], which allows extravasation and permeation into tissues and avoids clearance by the RES[56]. The CMs are simple aqueous based preparations with highly tunable emission wavelengths and an expanded stokes shift of the dye from 20 nm to about 160 nm[57], which make them an attractive carrier for fluorescence imaging. In addition, most CMs are not toxic and biologically compatible. The exceptions are surfactant based micelles as the large amounts of surfactant used might lyse the cell membrane and denature proteins, so they have a low preference[56]. In polymer based micelles, the hydrophobic units of the block copolymers form the hydrophobic core of the micelle and hydrophilic units surround the core forming a hydrophilic shell and thus making the micelle sterically stable along with protecting it from mononuclear phagocytic system (MPS) uptake[55, 56]. Using this strategy a number of block co-polymer micelles that encapsulate near infrared chromophores have been synthesized over the years and applied for imaging purposes[25, 58, 59]. Recently, in 2013, Chen and colleagues synthesized PEGylated tripropargyl amine micelles conjugated to BODIPY fluorophores, which had excellent water solubility and membrane permeability, and increased stokes shift without any covalent structure modification of the fluorophore[57, 60]. In addition, they observed that these BODIPY conjugated PEGylated tripropargyl amine micelles readily penetrate cell membranes and preferentially accumulate in the cytoplasm instead of the nucleus of the cell (cf. Figure 1.4)[60]. It was noticed that in most of the micelles, Poly(ethylene glycol) (PEG) remained as the choice of the hydrophilic unit as they are widely accepted and easily available[55]. It was also noticed that the recent advances in the crosslinked micelles were in making "smart" micelles that respond to various biological stimuli and pH of the environment, and target specific tissues (cf. Figure 1.5)[55, 61]. In addition to synthesizing stimuli responsive micelles, there has been development of micelles based on recombinant proteins. Kim and colleagues developed a 50 nm recombinant

protein micelle for targeted *in vivo* imaging. In these micelles, the multiple fluorescent probes were covalently conjugated to surface amines of crosslinked amphiphilic elastic-mimetic protein micelles using N-hydroxysuccinimide ester chemistry [62].

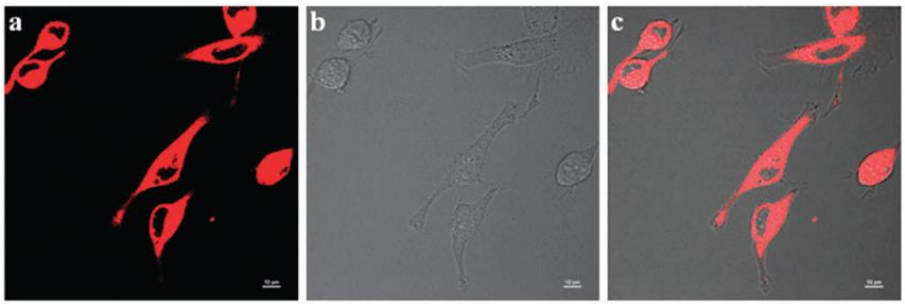

Figure 1.4: **(a)** Fluorescence, **(b)** transmission, and **(c)** overlapping fluorescence/ transmission images of Hela cells observed by confocal laser scanning microscopy. The cells were incubated with BODIPY conjugated surface crosslinked micelles at a concentration of 1 mM for 30 min at 37 ^{o}C under a humidified atmosphere containing 5 % CO_2. The excitation wavelength was fixed at 561 nm and the fluorescence signals were collected between 570 620 nm. (Reprinted with permission from Ref. [57] Copyright 2013 The Royal Society of Chemistry)

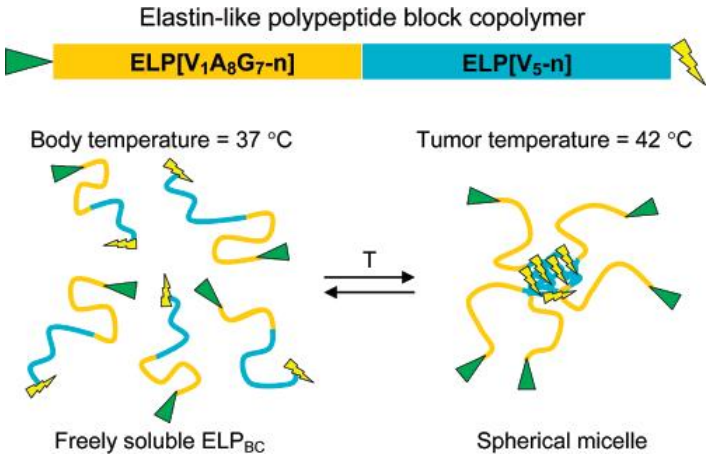

Figure 1.5: Temperature triggered self-assembly of an ELP$_{BC}$ to form multivalent spherical micelles. An N-terminal ELP[$V_1A_8G_{7-n}$] gene (hydrophilic, high T_t) and C-terminal ELP[V_{5-n}] gene (hydrophobic, low T_t) are seamlessly fused together to create a gene that encodes an ELP$_{BC}$. When the size and ratio of the blocks are correctly selected, the ELPBC self-assembles into a spherical micelle at ca. 40 ^{o}C. In the cartoon shown, upon self-assembly the spherical micelles present multiple copies of an affinity targeting moiety (green triangle) and sequester a drug or imaging agent (lightning bolt) within the core of the micelle. (Reprinted with permission from Ref. [61] Copyright 2008 American Chemical Society)

1.2.2 Polymersomes

Polymersomes are artificial vesicles or tiny hollow spheres that enclose a solution and have radii ranging from 50 nm to 50 μm[63]. They have a large hydrophilic reservoir and a thick hydropho-

bic lamellar membrane that supports the storage of a large quantity (i.e. more than 10 mol/ wt %) of hydrophobic fluorescent dyes and can protect the dyes from quenching and degradation[64, 65]. The long polymer chains regulate the mean fluorophore - fluorophore interspatial separation as well as the fluorophore - localized electronic environment[63]. Greater fluorescence was obtained for more hydrophobic fluorophores when relatively apolar membranes such as poly(γ-methyl ε-caprolactone) was used and the more amphiphilic fluorophores were better dissolved when bilayers of poly(ε-caprolactone) was used[65]. For most polymersomes, the outer shell is a layer of dense polyethylene oxide (PEO), which confers the stealth like character and results in increased biocompatibility, structural integrity in plasma, and circulation lifetimes[63, 64, 66]. In addition, the surface has terminal groups like -OH, which can be used to covalently conjugate targeting molecules, drugs and biomolecules to create a multifunctional unit[64]. There has been extensive work and investigation into developing the polymersomes as stimuli responsive multimodality agents but it is beyond the scope of this project and we will focus on the polymersomes that contributed significantly for fluorescence imaging[65, 66, 67]. Initially, Hammer and colleagues synthesized poly(ethylene oxide)-block-poly(ethylethylene) (PEO-b-PEE) diblock copolymers based polymersomes and expanded that technique to generate a number of biocompatible PEO-based amphiphilic block copolymers such as poly(ethylene oxide)-block-poly(butadiene) (PEO-b-PBD)[66]. They loaded these polymersomes with hydrophobic dyes such as Nile Red and also hydrophilic dyes such as Calcein and demonstrated its use in deep-tissue fluorescence based imaging[66, 68]. PEO-b-PBD polymersomes encapsulating porphyrin based fluorophores generated a fluorescence signal that was penetrable through 1 cm of solid tumor[66]. However, the problem with these systems were that they were not biodegradable and not fully biocompatible. To this end, around 2006, Ghoroghchian and colleagues developed the first set of self-assembled polymersome that was composed entirely of United States Food and Drug Administration (FDA) approved biodegradable diblock copolymers. They were a fully bioresorbable diblock copolymers of poly(ethylene oxide)-block-poly(ε-caprolactone) (PEO-b-PCL) and the diblock copolymer poly(ethylene oxide)-block-poly((γ-methyl ε-caprolactone) (PEO-b-PMCL) (cf. Figure 1.6)[65]. In 2012, Massignani and colleagues developed poly(2-(methacryloyloxy)ethyl phosphorylcholine)-poly(2-diisopropylaminoethyl methacrylate) (PMPC-PDPA) diblock copolymers based polymersomes and loaded it with a Rhodamine fluorophore, which had enhanced emission compared to free Rhodamine and CellTracker dye[69]. This increase was attributed to the effective dye delivery when the polymersome was used. Recently, in 2014, Quan and colleagues synthe-

sized a fluorescent polymersome that could encapsulate hydrophobic or hydrophilic drugs instead of the traditional polymersome encapsulating fluorophores. It was prepared by self-assembly of block copolymer hydrophilic poly(ethylene glycol) boron-dipyrromethenes (MPEG-BODIPY) in aqueous solution. These ca. 57 nm particles exhibited low toxicity and high accumulation in the tumor site through passive targeting[70].

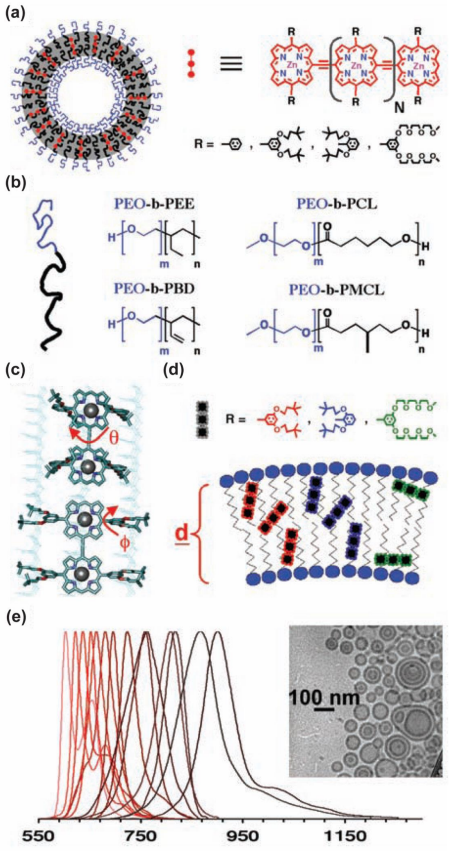

Figure 1.6: Schematic depiction of the incorporation of various oligo(porphyrin)-based NIRFs within polymersomes. **(a)** The NIRFs vary with respect to the number of porphyrin subunits (N), the linkage topology between porphyrin monomers, and the nature and position of ancillary aryl-group substituents (R). **(b)** Various diblock copolymer compositions have been utilized to form NIR-emissive polymersomes. **(c)** Membranous interactions between polymers and specific ancillary aryl group substituents vary the conformational populations assumed by the NIRF and can be used to tune its emission wavelengths. **(d)** Engineering the chemical composition and thickness of the polymersome membrane and helps to drive individual NIRFs into dielectric environments of matching polarity. **(e)** a family of nanoscale NIR emissive polymersomes. (Reprinted with permission from Ref. [65] Copyright 2009 John Wiley & Sons Inc.)

1.2.3 Polymer-core nanoparticles

The polymer-core nanoparticles can be divided into two categories: natural and synthetic. As the category name's suggest, particles made from natural polymers such as dextran, albumin, gelatin, chitosan, heparin, bacteriophages or lipoproteins fall under the natural category and the particles synthesized from synthetic or artificially produced polymers such as poly(amino acids), poly(alkyl-cyano acrylates), poly(esters), poly(orthoesters), poly(urethanes), and poly(acrylamides) are considered synthetic[25, 51]. In this current project the focus is on the synthetic polymer-core nanoparticles. The polymer-core nanoparticles are particles that have an inner core made up of cross-linked polymer and the fluorophore is either encapsulated within the core or covalently conjugated to the polymer. Encapsulation protects the fluorophore from direct interactions that could decrease its emission but at the same time cannot form beneficial host/guest assemblies or complex with biomacromolecules. Further, encapsulating the fluorophore suffers from leakage and non-specific release of the fluorophore. These drawbacks are overcome easily when the fluorophore is covalently conjugated to the outside of the particle[25, 71]. For the inner core, hydrophobic polymers such as poly(lactic-co-glycolic acid) (PLGA), poly(3-caprolactone) (PCL) and poly(methyl methacrylate) (PMMA) are preferred, as the hydrophobic matrix provides a strong affinity for the entrapment of poorly water-soluble fluorophores and drugs[72, 73]. Typical nanoparticle size varies from 50 - 500 nm and the optimum nanoparticle size for tumor accumulation is between about 70 and 200 nm as the nanoparticle uptake by the RES in the size range between 150 and 300 nm.[74, 75]. In addition, it has been well established in literature that a coating of PEG on the hydrophobic particle is necessary to render the nanoparticles biocompatible, avoid rapid clearance by the RES and also increase the circulation lifetime, which increases accumulation and allows their distribution in different tissues[25, 71, 76, 77, 78]. The following paragraph briefly summarizes some of the biodegradable polymer-core nanoparticle systems that have been developed.

As mentioned previously poly(lactic acid) (PLA) based systems are the most popular choices for the nanoparticles. PLA and its copolymers are one of the most extensively investigated matrix material for nanoparticles based diagnostic and drug delivery applications as they offer excellent biocompatibility, biodegradability into metabolizable moieties, and good manufacturing abilities[72, 79]. In addition, PLGA is approved by the FDA and is a component of many biodegradable market products for parenteral application[73, 80]. Initially, in 2004, Saxena and colleagues prepared 300410 nm

PLGA nanoparticles entrapping ICG by a modified spontaneous emulsification solvent diffusion method and were able to achieve over 74 % loading of the fluorophore in the particles[81, 82]. Later in 2006, they demonstrated the use of these particles for tumor diagnosis and photodynamic therapy and also determined the biodistribution of ICG loaded PLGA nanoparticles in healthy C57BL/6 mice (female,10-week old)[83]. In 2011, Schadlich and colleagues encapsulated different fluorophores, Nile Red and DiR (a carbocyanine based fluorophore), in PEGylated PLA nanoparticles and carried out *in vivo* and *ex vivo* imaging studies to study the impact of particle size in tumor accumulation, distribution and elimination[73, 84]. Apart from the encapsulated systems, there were other covalently conjugated fluorophore-PLA or PLGA nanoparticles. In 2010, Tong and colleagues developed Cy5-conjugated polylactide (Cy5-PLA) nanoparticles. They found these particles to have excellent signals with low tumor to background ratio fluorescence in various organs when administered intravenously to balb/c mice (cf. Figure 1.7)[85]. In 2012, Reul and colleagues, evaluated the concept of covalently labeling poly(lactide-co-glycolide) (PLGA) with a near-infrared (NIR) dye to obtain stable NIR fluorescent nanoparticles. For their studies, they coupled PLGA with DY-700 (a near infrared fluorophore) and injected intravenously into mice. According to their results, these particles had very good stability and preferentially accumulated in the liver where the free fluorophore wouldn't earlier, and could be developed further into a finely traceable PLGA nanosystem for fluorescence imaging[80].

Apart from PLA based nanosystems there have been particles based on other polymers such as poly(propargyl acrylate) (PA), poly(styrene-co-methacrylic acid), and poly(acrylic acid) (PAA). In 2011 Rungta and colleagues prepared sub-100 nm PA nanoparticles which had azide-terminated indocyanine green (azICG) covalently conjugated to the surface. The azICG was attached to the particles via azide/alkyne Huisgen cycloaddition using a copper catalyst[31]. Recently, it was reported that since the inception of "click" cycloaddition reaction in the field of drug discovery in 2001 by Sharpless and coworkers[86], it has been used by numerous researchers to prepare nanosized particles including polymeric micelles and nanoparticles, liposomes and polymersomes, capsules, metal and silica nanoparticles, carbon nanotubes and fullerenes, or bionanoparticles for tumor diagnostic and drug delivery applications[87]. In addition, significant growth and interest is seen in developing new processes for the "click" reaction to achieve high reaction kinetics, excellent biocompatibility, selective labeling of specific targets, easily accessible reactive tags and long shelf-life[87], and in future it can be expected that a majority of the nanosystems for tumor theranostics

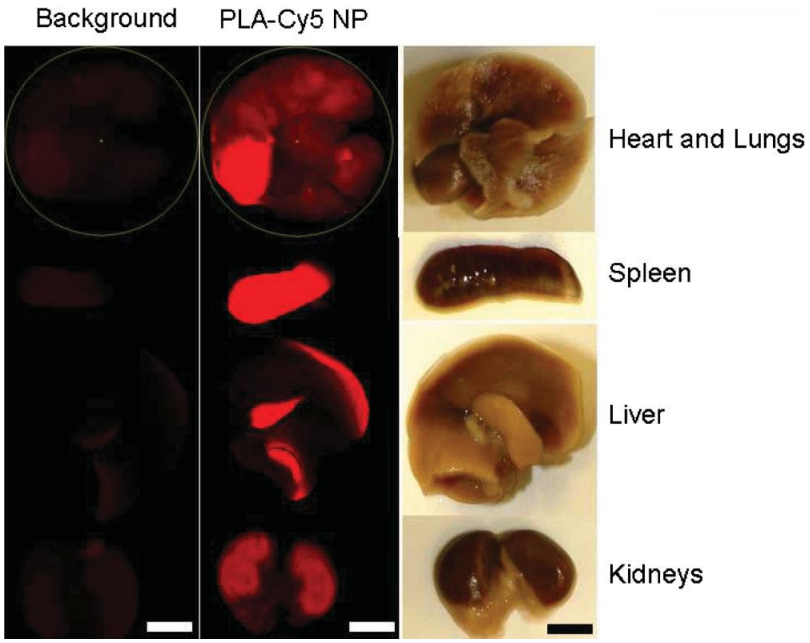

Figure 1.7: In vivo biodistribution of intravenously administered Cy5-PLA nanoparticles. Visceral organ biodistribution of Cy5-PLA nanoparticles following lateral tail vein injection using the LI-COR Odyssey scanner. Accumulation of Cy5-PLA nanoparticles within visceral organs allows for greater than 10-fold increase in fluorescent intensity in comparison with background autofluorescence. Splenic accumulation of Cy5-PLA nanoparticles is the greatest for all visceral organs examined (spleen, liver, kidney, lung, and heart); Bar 5 5 mm. (Reprinted with permission from Ref. [85] Copyright 2010 WILEY-LISS INC.)

will utilize the "click" reaction. In 2011, Palma and colleagues, prepared BF_2 chelated tetraarylazadipyrromethenes (near infrared dye) conjugated poly(styrene-co-methacrylic acid) particles. The dye was attached to the nanoparticles via a standard N-hydroxysuccinimide (NHS) and 1-ethyl-3-(3-dimethylaminopropyl)carbodiimide (EDCI) coupling reaction. Using those particles, they were able to obtain promising results for real time *in vitro* imaging in MDAMB-231 (breast cancer), HEK293T (kidney), and CAKI-1 (renal cancer) cell lines (cf. Figure 1.8)[88]. In 2013, Tao and colleagues reported the synthesis of the first biocompatible NIR-II agent nanoparticles, for *in vivo* imaging. These particles had the IR-1061, a commercially available water insoluble polymethine dye, embedded in an amphiphilic polymer poly(acrylic acid) (PAA) matrix. These nanoparticles also had a coating of the surfactant DSPE-mPEG (a polyethylene glycol-conjugated phospholipid, ca. 5 kDa) for improved biocompatibility and longer circulation lifetimes. Using these IR-1061 nanoparticles, the inner organs and blood vessels of mice were imaged and the results matched with the images previously obtained with inorganic carbon nanotubes and quantum dots[89]. Most of the recent literature published on nanoparticle systems not only are biocompatible, fully biodegradable

and exhibit high signals but also designed to target particular cells or tumors and avoid healthy cells. Specific details of these systems and examples will be discussed in the next section.

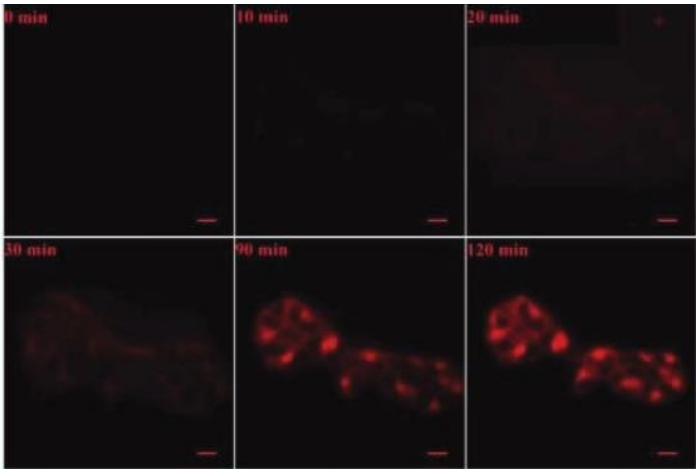

Figure 1.8: Real-time fluorescence imaging of BF_2 chelated tetraarylazadipyrromethenes (near infrared dye) conjugated poly(styrene-co-methacrylic acid) particles uptake into HEK293T cells (scale bar 10 m). (Reprinted with permission from Ref. [88] Copyright 2011 American Chemical Society)

1.3 Targeting

Up to this point we have seen examples of passive targeting of tumors in fluorescence imaging. Encapsulating or conjugating small molecule fluorophores to nanoparticles allow the particles to preferentially accumulate in tumors due to EPR effect (cf. Figure 1.9)[49, 50]. In this case, the size is used to passively target tumors. Apart from size, modifying the surface charge of the nanoparticles is the other way to passively target the tumors. The surface charge of tumors is highly negative when compared to normal cells[90], so if the surface of the nanoparticles is modified to be more cationic then the nanoparticles bind electrostatically to the negatively charged phospholipid head groups expressed on tumors and in turn preferentially accumulate in tumors[91, 92, 93, 94]. However, passive targeting is not always successful as the EPR effect, the phenomenon utilized in passive targeting for increased accumulation, is not commonly observed in some types of tumors such as gastric and pancreatic, and also in some other tumors the core might not be well perfused[52]. To this end, it is necessary to add an active targeting component to the nanoparticles so that they affect tumors and avoid healthy cells (cf. Figure 1.9). The characteristics required for an ideal target are that they should be universally and uniquely expressed by the tumors. In most cases the target is an

overexpression of a particular cell surface marker in tumors. The overexpression of the target group facilitates increased binding of the targeting agent, which in turn increases the cellular uptake of the targeting agent[55]. Recently, Prabhu and colleagues studied the different targeting approaches for polymeric nanoparticles[91]. According to them, the targeting agents can be divided into three categories: ligand - based, tumor cell and tumor endothelium targeting. In ligand - based targeting, the ligand binds specifically to a receptor this is dominantly overexpressed by tumor cells, and the ligands used vary from small molecules, vitamins, carbohydrates, peptides, antibodies, proteins and nucleic acids[49, 91, 95, 96]. In tumor cell targeting, the cell surface receptors that are overexpressed by tumors are targeted, and some of the commonly targeted receptors are transferrin, folate, and epidermal growth factor receptors (EGFRs), and glycoproteins[91, 97, 98, 99, 100, 101, 102]. In tumor endothelium targeting, the endothelial cells are targeted to prevent angiogenesis, as it plays an important role in regulating cancer growth. Targeting vascular endothelial growth factors (VEGF) receptor, $\alpha v\beta 3$ integrin, vascular cell adhesion molecule - 1 (VCAM - 1), and matrix metalloproteinases (MMP) are some examples of tumor endothelium targeting[91, 103, 104, 105, 106, 107]. In the majority of the applications, the targeting agent is not used by itself but is attached to the fluorophore or a nanocarrier to improve the accumulation and most of these targeting agents are attached via a simple covalent conjugation technique or electrostatic interactions. Attaching the targeting agent directly to the small molecule fluorophore compromises the emission and other properties of the probe so attaching the targeting agents to nanocarriers which doesn't alter the fluorophore's properties is preferred[56]. In addition, conjugating the targeting agent to the polymeric nanocarrier overcomes the hurdles such as weak reproducibility and poor control of tuning the number of targeting agents attached to the particle[72]. Once the polymeric particle is conjugated with the desired amount of the targeting agent, they can be utilized to accumulate in a specific tumor for imaging applications. Some examples of fluorescence imaging with polymeric nanoparticles are reviewed below.

Zheng and colleagues developed a novel ICG containing phospholipid-polyethylene glycol (ICG-PL-PEG) based micelle. They attached two targeting agents, a small molecule called folic acid (FA) and a large protein called integrin $\alpha_v\beta_3$ monoclonal antibody (mAb), to the ICG-PL-PEG micelles and displayed their target specificity using three different cell lines. The three cell lines used were EMT6 (murine mammary tumor cells), U87-MG (human glioblastoma cancer cells) and MCF-7 (human breast cancer cells). Laser scanning confocal microscopy, flow cytometry and other *in vitro*

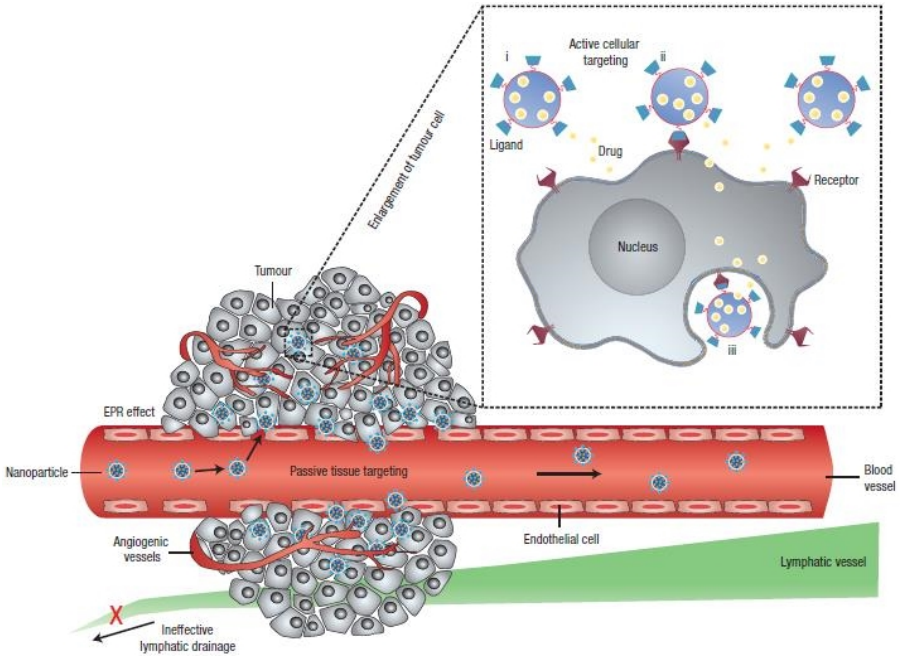

Figure 1.9: Schematic representation of different mechanisms by which nanocarriers can deliver drugs to tumors. Polymeric nanoparticles are shown as representative nanocarriers (circles). Passive tissue targeting is achieved by extravasation of nanoparticles through increased permeability of the tumor vasculature and ineffective lymphatic drainage (EPR effect). Active cellular targeting (inset) can be achieved by functionalizing the surface of nanoparticles with ligands that promote cell-specific recognition and binding. The nanoparticles can **(i)** release their contents in close proximity to the target cells; **(ii)** attach to the membrane of the cell and act as an extracellular sustained-release drug depot; or **(iii)** internalize into the cell. (Reprinted with permission from Ref. [49] Copyright 2007 Nature Publishing Group)

experiments were employed to confirm that the targeting probe was mainly internalized into cells via ligand-receptor or antigen-antibody mediated endocytosis pathway. In addition, according to their data the amount of targeting agent conjugated to the ICG-PL-PEG micelle doesn't affect the integrity and properties of the nanoprobe[56].

Pang and colleagues developed a 1,1'-Dioctadecyl-3,3,3',3'-Tetramethylindotricarbocyanine Iodide (DiR) (fluorophore) loaded methoxy poly(ethylene glycol)-poly(σ-caprolactone) based polymersome. Apart from the fluorophore the polymersome was loaded with drugs, doxorubicin (Dox) and tetrandrine (Tet), to give a therapeutic functionality to the system. These multifunctional polymersomes were conjugated with a targeting agent called Lactoferrin (Lf) and this polymersome was referred as Lf-PO-Dox/Tet-DiR. Lf is a novel brain targeting ligand, which enables drug-loaded polymersome to transport across the blood-brain barrier (BBB) with higher efficiency when compared to another targeting agent called transferrin. *In vitro* studies in C6 cells (rat glial tumor cells) were utilized to show that Lf-PO-Dox/Tet-DiR polymersomes were uptaken through receptor-mediated

endocytosis while the free Dox accumulated mainly through a diffusion mechanism. Moreover, *in vivo* studies carried out in glioma model rats further confirmed that the Lf-PO-DiR crossed the BBB and had an increased accumulated at the tumor site, which is indicated by the strong increase in fluorescence at the site of the tumor (cf. Figure 1.10). Overall, they constructed a promising targeted nanoprobe for diagnosis and therapy of gliomas[67, 108].

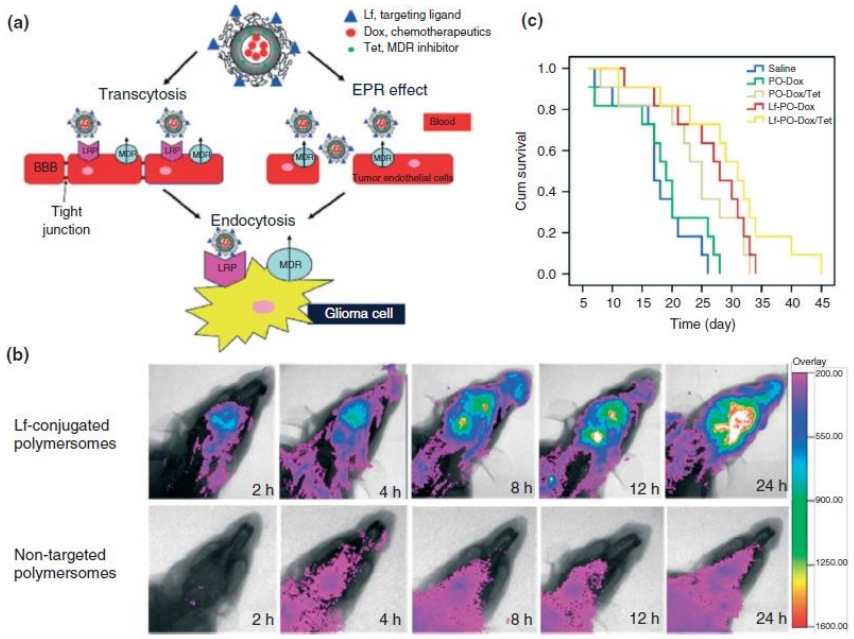

Figure 1.10: **(a)** Design of lactoferrin-conjugated biodegradable polymersome for glioma targeting. Polymersomes are simultaneously loaded with doxorubicin (Dox) as a model antitumor drug and tetrandrine (Tet) as an multi drug resistance (MDR) inhibitor. Lactoferrin (Lf) was conjugated on the surface of polymersomes, as glioma targeting ligand and to help overcome the obstruction of the BBB. **(b)** Accumulation of targeted polymersomes in glioma (EPR effect and overcoming BBB) was evidenced by fluorescence imaging. **(c)** The specific interaction of Lf-conjugated polymersomes with glioma cells enhanced drug delivery into these cells, improving the chemotherapy of glioma as showed by the improved survival in rats. (Reprinted with permission from Ref. [67] Copyright 2012 Wiley Periodicals Inc.)

Le Droumaguet and colleagues developed a Rhodamine B (fluorophore) functionalized poly (alkyl cyanoacrylate) (RhB-PACA) nanoparticles for fluorescence imaging. The RhB-PACA nanoparticles were surface functionalized with biologically active targeting ligands such as biotin, curcumin derivatives, and a monoclonal anti-Aβ_{1-42} antibody. *In vitro* studies were carried out in two cancer cell lines, MCF7 (human breast adenocarcinoma cells) and M109 (murine lung cancer cells), which both overexpress biotin receptors on their surfaces (cf. Figure 1.11). The results obtained confirmed that the biotin conjugated RhB-PACA nanoparticles were uptaken by the cells through a specific receptor mediated endocytic pathway as the fluorescence seen was mainly around the vesi-

cles surrounding the nuclei. Moreover the fluorescence signal of covalently conjugated Rhodamine B to PACA nanoparticles was fine and strong in comparison to the typical diffuse signal obtained when hydrophobic dyes are encapsulated. The specificity of biotin targeting strategy was further supported by *in vitro* studies carried out in L1210 cells that do not overexpress biotin. The biotin-RhB-PACA nanoparticles did not show the same strong fluorescence in L1210 cells as shown in MCF7 and M109 cells[22].

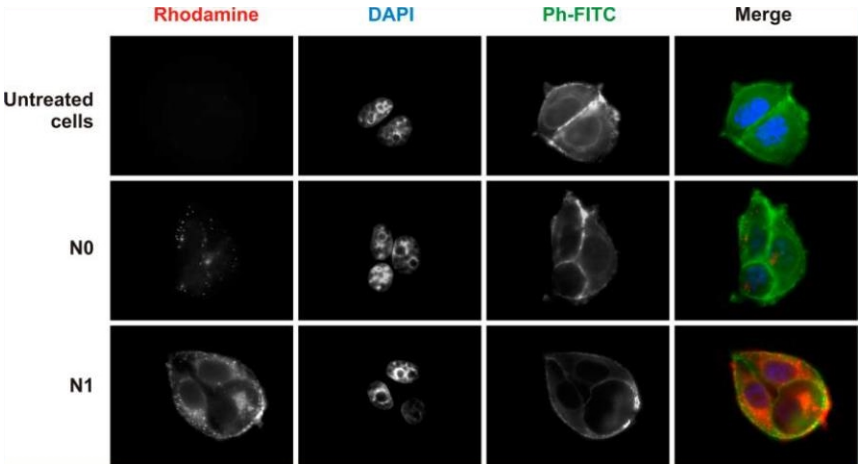

Figure 1.11: Internalization of rhodamine B-labeled NPs. Fluorescence microscopy images of MCF7 cells showing the cellular uptake of nonfunctionalized (N0) and biotin-functionalized (N1) NPs (red) after 5 h of incubation. The nuclei were stained with DAPI (blue), phalloidin-fluorescein isothiocyanate (Ph-FITC, green) was used to label F-actin, and the last column represents the overlay of all types of staining. (Reprinted with permission from Ref. [22] Copyright 2012 American Chemical Society)

1.4 Activation

One of the issues noticed with the polymer-core nanoparticles was that the emission of the probe was initially quenched, when dispersed in aqueous solutions due to aggregation of the fluorophore on the surface of the particles[31]. This drawback turned out to be an advantage to the nanoparticulate system because the probes are in "turned off" state under normal conditions and "turned on" only under specific diseased conditions, which results in enhanced tumor to background ratio[109]. To this end, identifying different activation techniques for the nanoprobes is necessary to develop activatable NIR nanoprobes. To date, various general activatable small molecule probes have been developed to image tumors and in most of these systems, the emission is "turned on" upon binding to a specific protein, enzyme or receptor[109]. Pham and colleagues reported a probe

that is activated upon binding to matrix metalloproteinase 7 (MMP), a protease overexpressed in tumors[110]. Tung and colleagues developed a NIR probe that activates when interacted with Cathepsin D, which is another protease overexpressed in tumors[111]. Urano and colleagues developed pH-activatable probes based on BODIPY fluorophore that had a cancer-targeting monoclonal antibody conjugated to it[112]. These activatable probes mentioned so far are small molecule probes and not particulate based. There are only a handful of systems reported for activatable NIR polymeric nanoparticles. In 2011, Rungta and colleagues, used PA particles modified with an azide terminated ICG to demonstrate the activation of fluorescence when mixed with bovine serum albumin (BSA) (cf. Figure 1.12)[31]. It is well established in literature that the albumins can "turn on" the emission of aggregated fluorophores[113]. Albumins bind to the hydrophobically aggregated fluorophore via a combination of hydrophobic, hydrogen bonding, and electrostatic interactions, which deaggregates the fluorophores and turns on the emission[113]. Later in 2011, Palma and colleagues demonstrated that the emission of BF_2 chelated tetraarylazadipyrromethenes (near infrared dye) conjugated poly(styrene-co-methacrylic acid) particles can be activated by sodium dodecylsulfate (SDS), a surfactant. In addition, they demonstrated the activation *in vitro* in MDAMB-231 (breast cancer), HEK293T (kidney), and CAKI-1 (renal cancer) cell lines. According to them, the phospholipids in the cell membrane, specifically lecithin is responsible for the activation and the mechanism is similar to that of SDS[88]. These two strategies of activation work but they are not specific enough like the MMP7 sensitive small molecule probe. There has been advancement in the development of nanoparticle systems which respond to various stimuli and environments to "turn on" emission (cf. Figure 1.5)[55, 61, 114], but not particles which activate emission upon binding to specific proteins or receptors that are overexpressed in tumors. It is expected that future endeavors in the field of tumor nanotheranostics will be in the direction of developing "smart" activatable NIR nanoparticles.

1.5 Overview

Although there has been significant advancement in developing polymer based nanoparticles for optical imaging, it still has several drawbacks and not one system addresses all the issues completely. To this end, it is necessary to improve a current nanoprobe and add multifunctionality so that a single "nanodevice" can be used to target, image and treat tumors effectively. **The main objective of this project is to develop a polymer based near infrared (NIR) particle that**

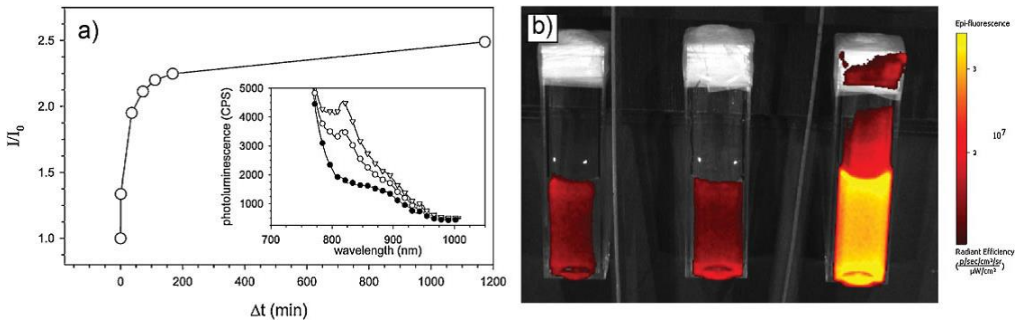

Figure 1.12: **(a)** Increase in photoluminescence intensity ratio of PA-azICG-azPEG1K particles dispersed in a phosphate buffered solution (PBS) with the addition of 0.014 mM BSA; time evolution of the intensity at 819 nm relative to the initial intensity. Inset presents photoluminescence of particles after 2 min (○), 37 min (●), and 1174 min (▽) . Excitation energy at a wavelength of 710 nm; particle density of 1.259 x 10^{12} cm^{-3}. **(b)** Optical image of fluorescence intensity of PA-azICG-azPEG1K particles in deionized water (far left), PBS (center), and 2 h after the addition of 0.014 mM BSA to the PBS solution (far right); images taken with a Caliper Xenogen IVIS Lumina II XR Instrument with 745nm excitation filter and ICG emission filter; particle density of 1.259 x 10^{12} cm^{-3} (Reprinted with permission from Ref. [31] Copyright 2011 WILEY-VCH Verlag GmbH & Co. KGaA)

can serve as both, diagnostic and therapeutic agents, for fighting cancer. Specifically these particles will be designed to have high-contrast, high signal to noise ratios, long *in vivo* circulation lifetimes, and facilitate easy attachment of functional and target components.

The chapters of this dissertation can be summarized as follows:

Chapter 2 presents sub-100 nm colloidal particles which are surface-functionalized with fluorophores that operate in the near-infrared (NIR) spectrum, through a copper(I) catalyzed azide-alkyne Huisgen 1,3-Dipolar cycloaddition. These functionalized nanoparticles exhibit a protein triggered activation/deactivation of the emission. The methodology for emission switching offers a path to maximize the signal from the typically weak quantum yield inherent in NIR fluorophores. Preliminary fluorescence imaging studies indicated that the brightness of the functionalized polymer based nanoparticles improved considerably.

Chapter 3 presents sub-100 nm colloidal particles which are surface-functionalized with an azide terminated Survivin ligand derivative (azTM) originally proposed by Abbott Labs and speculated to bind directly to Survivin (protein) at its dimer interface. Using affinity pull-down studies, it was determined that the PA/azTM nanoparticles selectively bind Survivin and the particles can enhance apoptotic cell death in glioblastomas and other Survivin over-expressing cell lines such as A549 and MCF7 relative to cells incubated with the original Abbott-derived small molecule inhibitor.

Chapter 4 presents sub-100 nm colloidal particles which are surface-functionalized with small

molecules such as drugs or fluorophores through an environmentally-sensitive linker. The linker used is an azide modified bovine serum albumin (azBSA) which prevents opsonization and releases the small molecule upon digestion. This strategy offers a delivery functionality to the colloidal particles. Additionally, the particles can be used for fluorescence resonance energy transfer (FRET) based imaging application. A FRET pair of dyes were attached to the particle and the azBSA, and the FRET efficiency was increased by unfolding the protein via heating and addition of denaturants.

Chapter 2

Switching fluorescence of surface modified colloids with near-infrared emitters via protein interaction for contrast-enhanced imaging

2.1 Attributions

The synthesis of the azide modified chromophores was conducted or aided by Dr. Yuriy P. Bandera at Clemson University. The confocal imaging studies were carried out with the aid of Dr. Hsin-I Hung, Dr. Venkat Ramshesh, Megan F. Duperreault, and Dr. Anna-Liisa Nieminen at Medical University of South Carolina. The results presented in this chapter have been published as Jetty et al., Protein triggered fluorescence switching of near-infrared emitting nanoparticles for contrast-enhanced imaging. Journal of Materials Chemistry B, 2013. Content has been reproduced with permission from Royal Society of Chemistry.

2.2 Introduction

Optical imaging in medical applications is especially attractive due to its noninvasive nature, though it can be hindered by limitations of resolution and penetration depth which are a result of the high absorption, auto fluorescence, and scattering found in biological tissues. To circumvent some of these issues, there is an interest in developing near-infrared (NIR) fluorophores since there is a region of reduced absorption for this wavelength range, providing maximum penetration of light and facilitating deep tissue imaging[115]. Unfortunately, the quantum yield of organic NIR fluorophores is typically low (< 0.2) in physiological conditions[116, 117] and routes to achieve a higher tumor to background signal ratio (TBR) are desirable. Achieving a higher TBR can be accomplished by both preferentially accumulating the probe in a targeted tissue and, once sequestered, activating the probe's fluorescence only in this region[118, 119, 120].

A myriad of activation schemes have been proposed[119, 121], though the approach was initially demonstrated with polymeric agents that emitted a signal after an enzymatic attack[13, 120]. The underlying mechanism for activation is a conversion of an aggregated quenched fluorophore back to its emissive monomeric state. To that end, the significant variations in the emission spectra of photoluminescent dyes which are routinely observed when they form supramolecular host/guest assemblies or complex with biomacromolecules[122, 123, 124, 125] and have been exploited in designing activatable contrast agents by this group[31] as well as others[88]. As indicated earlier, in addition to activating the emission only in the tissue of interest, to achieve maximum TBR, the contrast agent must accumulate in the targeted tissue while clearing rapidly from non-target organs and tissues. Small molecule fluorophores are rapidly cleared because of a short *in vivo* circulation life due to non-specific binding to proteins[116], thus improving the tumor to background ratio, but this also reduces the absolute amount of accumulation at the target. This weak accumulation is in addition to a limited aqueous solubility which frustrates parenteral administration[126].

Compared with conventional molecular scale fluorophores, dye-doped particles have demonstrated improved *in vivo* detection and enhanced targeting efficiencies through longer circulation times, designed clearance pathways, and multimeric binding capacities[77]. Since the initial report on isolating fluorophores through their encapsulation in a particle was presented[127], a multitude of efforts have been described, using both polymeric[128, 129] and inorganic[130, 131, 132, 133, 134, 135, 136] colloids. Sub-100 nm sized colloidal particles that are functionalized with multiple

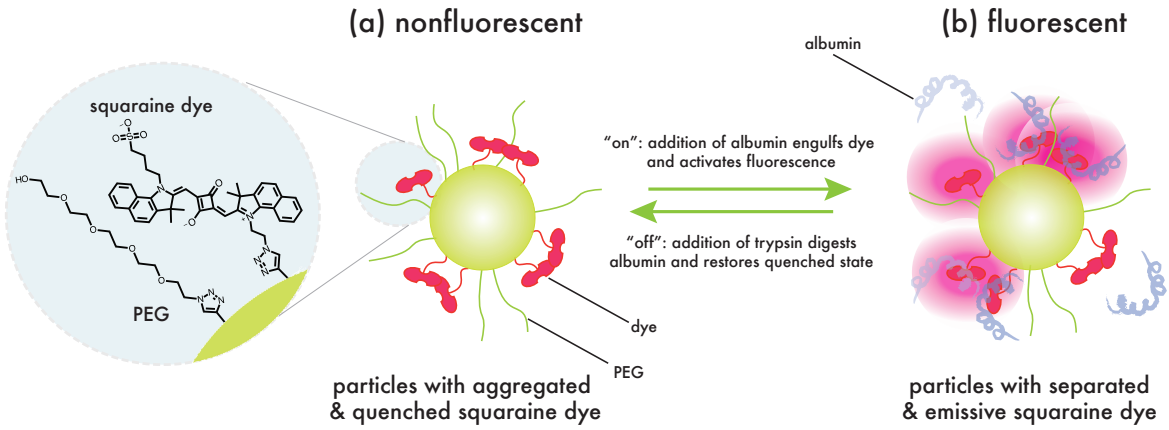

Figure 2.1: Schematic of 50 nm poly(propargyl acrylate) (PA) particles surface modified with an azide-terminated squaraine (azSQ) and polyethylene glycol (azPEG) through an aqueous-phase "click" transformation in the **(a)** aggregated & nonfluorescent state and in the **(b)** albumin activated fluorescent state. Particles could be deactivated and returned to the quenched state through a trypsin digestion of the albumin.

moieties have the potential to combine imaging, early detection, prevention, and the treatment of cancer with a single type of colloidal "nanodevice"[78, 137, 138, 139, 140]. Within the nanodevice conceptualization, the design of a sub-100 nm particle that exhibits NIR fluorescence that can be modulated on or off by specific proteins within a cancer cell is of particular interest[31, 88].

In the current effort, poly(propargyl acrylate) (PA) colloids were surface modified with an azide terminated squaraine-based dye, a NIR emitting fluorophore, and polyethylene glycol through a copper-catalyzed azide/alkyne cycloaddition performed in water[86]. The placement of the fluorophore onto the surface of the particles allows for the dye to form a guest/host complex with available proteins and this feature was exploited in achieving a fluorescence activation of the particles when in a quenching aqueous medium. In addition, the removal of the bound proteins from the particle was achieved through their enzymatic digestion, resulting in a deactivation of the emission. Reversibility may be a crucial feature if these probes are intended for real-time monitoring of *in vivo* events. These particles described a "fluorescent switch" that can be modulated *on or off* through the incorporation of simple proteins and/or enzymes and are a promising platform for developing protein or multi-protein complex sensitive contrast agents for biotechnology and biomedical applications.

Table 2.1: Fluorophore grafting density and fluorescence quantum yield (ϕ) of surface functionalized PA particles; Fluorophore and particles dispersed in methanol

	compound	fluorophore grafting density (azSQ/nm^2)	quantum yield (ϕ)
	azSQ	—	0.101
FP_0	PA/azSQ	0.05	0.051
FP_1	PA/azSQ	0.09	0.033
FP_2	PA/azSQ	0.12	0.039
FP_3	PA/azSQ	0.17	0.039
FP_4	PA/azSQ	0.28	0.034
FP_5	PA/azSQ	0.49	0.024
FP_6	PA/azSQ /azPEG	0.09	0.031
FP_7	PA/azSQ /azPEG	0.49	0.012

2.3 Results & Discussion

A schematic of the particles studied in this effort is presented in Figure 2.1. The poly(proparg-

yl acrylate) (PA) colloids were prepared using a standard aqueous emulsion polymerization technique resulting in spheres with a diameter of 49.9 ± 0.58 nm (mean and standard deviation). To functionalize the surface of the particles, a multiple step copper-catalyzed azide/alkyne cycloaddition ("click" transformation) was performed in water[86] to produce PA particles that had both squaraine and polyethylene glycol (PEG) attached to their surface. Initially, an azide-modified squaraine derivative (azSQ) was attached to the PA particles through a "click" transformation. Squaraine dyes are typically classified as a NIR dye though technically their emission is in the far-red regime[141, 142, 143, 144]. Due to their high fluorescent quantum yields compared to other NIR organic fluorophores like indocyanine green[31, 145], squaraine dyes have found a broad range of applications[141, 146, 147], with the biomedical community expressing an especially strong interest in this class of dyes[142, 143, 144, 148, 149].

To attach the fluorophores to the particles, the azSQ was initially clicked onto the particles for 15 mins and then the reaction was stopped by the removal of unreacted azSQ, sodium ascorbate, and Cu(II)SO_4 through a repeated particle washing procedure consisting of centrifugation and redispersement in methanol. To reduce the grafting density of dye, the initial amount of azide-modified dye used in the reaction was decreased. The cleaned PA/azSQ (FP_5) particles were subsequently utilized in a secondary click transformation with azide-modified polyethylene glycol

chains with molecular weight of 5k (azPEG) that was allowed to run for 48 hours and then washed to remove unreacted species; these particles are referred to as PA/azSQ/azPEG (FP_7) particles. The use of PEG to infer a hydrophilicity to the particles has been found to be important for directing protein absorption on the particles and achieving long circulation times[77]. The characteristics of the particles synthesized for this study are presented in Table 2.1.

2.3.1 Emission Spectrum

Figure 2.2a presents the molar extinction coefficient and photoluminescence of the free azide-functionalized squaraine (azSQ) dispersed in methanol. In this solvent, azSQ has a peak absorption maximum at 663 nm, while the corresponding emission peak is at 672 nm, for a relatively small Stokes shift of 9 nm. The symmetry for the absorption and emission spectra is evident, though the absorption exhibits a small peak at 626 nm. This lower energy absorption is often seen in concentrated aqueous solutions of squaraine due to the formation of H-aggregates[149, 150]; the appearance of this peak in the freshly prepared dilute methanol solution of azSQ is due to the sulfonate group which causes higher self-affinity[151].

A structurally similar squaraine dye has been recently presented[152] that was characterized by an absorption and emission peak maximum of 672 nm and 678 nm, respectively, when dispersed in toluene. In this solvent, this dye gave a fluorescence quantum yield of 0.51. In comparison, the relative fluorescence quantum yield for azSQ in toluene differed by 0.1% when measured in methanol ($\phi = 0.101$; cf. Table 2.1). Despite the minor solvent-dependent changes in the spectra between this latter squaraine dye and azSQ, the fluorescence quantum yield of the azSQ is significantly lower at 0.101. The reduction in quantum yield was speculated to be due to the substitution of an azide to the chromophore and its ability to better facilitate non-radiative deactivation to the ground state[151].

In comparison, Figure 2.2b presents the absorption and photoluminescence spectra of PA particles after they have been surface modified with the attachment of azSQ chromophores and azPEG chains (FP_7) and dispersed in methanol. The absorption spectra of the FP_7 particles indicate an absorption peak maximum that is at a wavelength of ca. 672 nm, a 9 nm bathochromic shift from the free dye. Utilizing the molar extinction coefficient in the dilute regime for the free azSQ particles in methanol (cf. Figure 2.2a) allows for the estimation of the number of chromophores attached to the particles. Following this approach, the FP_7 particles had a grafting density of 0.49 azSQ/nm^2 when analyzed over the wavelength range of 615 nm to 685 nm. The grafting density of the azPEG

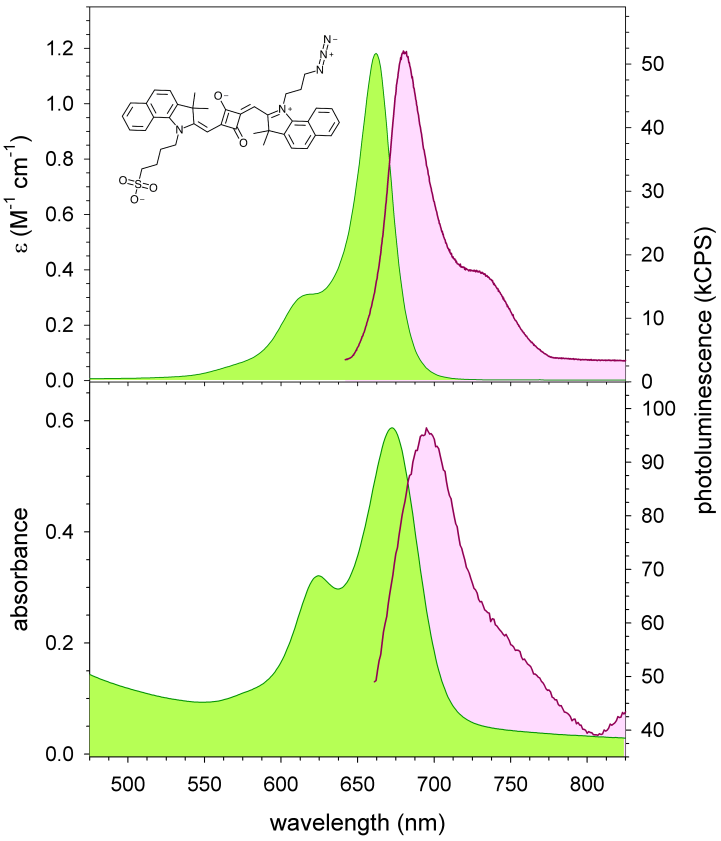

Figure 2.2: **(a)** Molar extinction coefficient (green) and photoluminescence (red) of azide functionalized squaraine derivative chromophore (azSQ; 6.98 μM in methanol); **(b)** Absorbance (green) and photoluminescence (red) of PA/azSQ/azPEG (FP_7) particles in methanol. Excitation energy at a wavelength of 630 nm.

to the particles was not assessed but the contact angle of the PA particles to water changed from $\theta >$ 70 ° to $\theta <$ 10 ° after the attachment of the azPEG indicating that their surface was hydrophilic.

2.3.2 Quantum Yield

It is well known that when fluorophores are dispersed in a solvent that a limiting concentration can be found where the dye–dye separation becomes small and statistical closely spaced pairs and larger aggregates are formed[153]. Once excited, these aggregates can find non-radiative routes to lower their energy, thereby reducing the observed luminescence quantum yield. Once the chromophores are attached to the surface of particles, the "local" concentration of the emitters is elevated due to the two-dimensional nature of the attachment. This elevated concentration of

emitters results in an enhanced propensity for aggregate formation and non-radiative routes for the excited emitters to return to their ground state. Therefore, the counter intuitive speculation is that a *reduced* number of chromophores grafted to a particle's surface will result in a higher quantum yield. Table 2.1 and Figure 2.3 presents the quantum yield for the "free" azide-functionalized squaraine derivative dye and the modified particles with varying fluorophore grafting densities. In addition, Table 2.1 presents a subset of the PA/azSQ particles clicked with an azide-modified PEG.

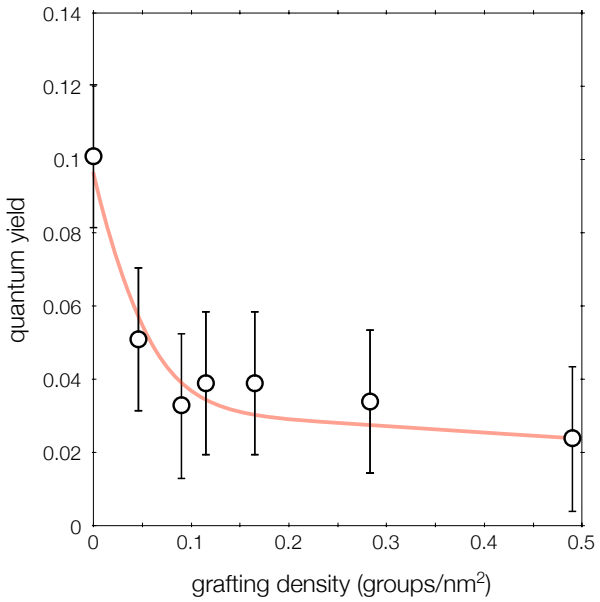

Figure 2.3: Quantum yield of azide functionalized squaraine derivative chromophore (azSQ) with variation in grafting density to PA particles (methanol). Excitation energy at a wavelength of 650 nm.

As indicated earlier, the free azSQ dye exhibited a quantum yield of $\phi = 0.101$. Once the chromophores are attached to a particle, the observed quantum yield was significantly diminished relative to the free dye's value (cf. Figure 2.3). The PA/azSQ particles (FP_5; cf. Table 2.1) with a dye grafting density of 0.49 groups/nm^2 exhibits a 76 % drop in quantum yield relative to the free dye, while the PA/azSQ particles (FP_1; cf. Table 2.1) with a grafting density of 0.09 groups/nm^2 exhibits a 67 % drop in quantum yield. The particles may act as quenching centers of fluorescence for chromophores that are adsorbed onto their surface since (1) the planar surface offers a constrained 2-dimensional region on which the chromophores can dimerize[154] and (2) a non-radiative energy transfer can occur from the excited molecules to the particle[153].

As speculated earlier, the reduction of the number of fluorophores grafted onto the particle's surface results in an increase in quantum yield (cf. Table 2.1). For the PA/azSQ particles, a 37 %

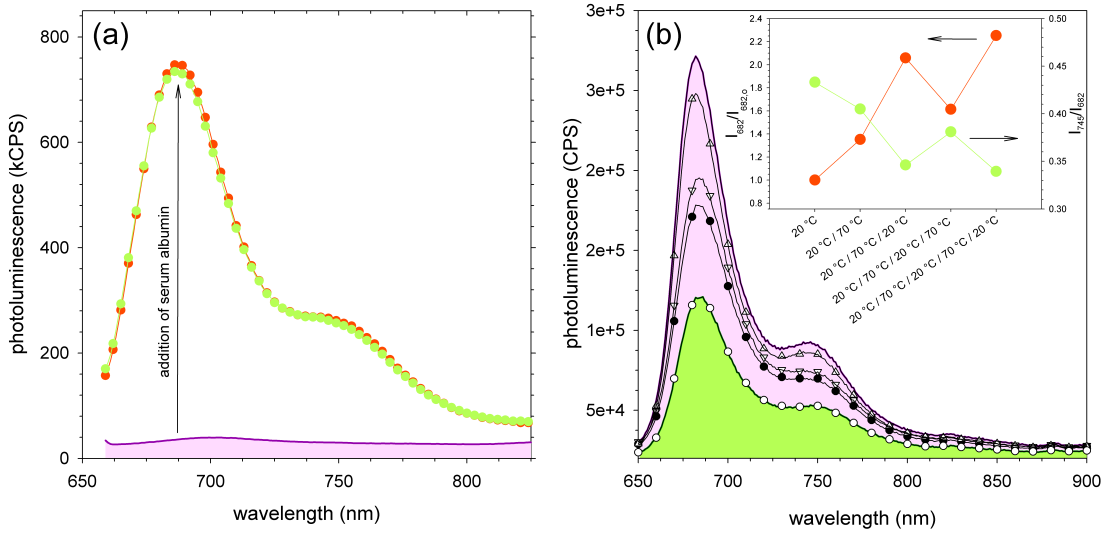

Figure 2.4: **(a)** Photoluminescence of FP_7 particles dispersed in: PBS (—), PBS and 0.05mM BSA (green), PBS and 0.05mM HSA (red). Particles were incubated with serum albumin for ca. 4 days to insure increase was invariant with time, though 25% of the increase occurred within the first 30 minutes. **(b)** Photoluminescence spectra of FP_5 particles in PBS with 15 mg BSA initially at 20 °C (○), at 70 °C (●), after 70 °C anneal then cooled to 20 °C (△), after 70 °C, cool to 20 °C, heated to 70 °C (▽), and after 70 °C, cool to 20 °C, heated to 70 °C, then cooled to 20 °C (—). Inset presents the intensity ratio at 682 nm (red) for the thermal cycles relative to the initial emission and the intensity ratio (green) of the J-aggregates (745 nm) to the monomeric emission (682 nm). Excitation energy at a wavelength of 630 nm.

reduction in grafting density, from 0.49 to 0.09 groups/nm^2, results in a 38 % increase in quantum yield. The azSQ dye can be roughly approximated as an ellipsoid with a long axis of 21 Å and a cross section of 10 Å x 5 Å. At a grafting density of 0.49 groups/nm^2, the inter-dye separation distance on the surface of the particle would be statistically 16 Å. This distance is sufficiently close that two dyes could approach one another to partially dimerize and reduce the quantum yield of emission. In contrast, a grafting density of 0.09 groups/nm^2 gives a separation distance of ca. 38 Å, a distance sufficiently large enough to frustrate dye-dye aggregation.

It is well established that PEG polymers, when attached to the surface of particles, provide steric stabilization and reduces protein absorption in biomedical applications[155]. Protein absorption promotes opsonization, which can lead to aggregation and clearance from the bloodstream. The resultant rapid removal is due to phagocytosis by the mononuclear phagocyte system (MPS) in the liver and splenic filtration[156]. Nonetheless, the addition of PEG chains to the surface of the particles reduces the quantum yield of the particles. Table 2.1 presents the fluorescence quantum yield of the particle with varying grafting densities and PEGylation. At higher grafting densities, the quantum yield of the FP_7 particles was half of the PEG-free FP_5 particles, while at the lower

grafting densities (FP_1 & FP_6), the PEGylation did not effect the yield significantly. This suggests that the attachment of the PEG chains increases the non-radiative transfer of energy when excited, and hence influences the emission characteristics of the attached squaraine.

2.3.3 Squaraine/Protein Complexation.

The utilization of an azSQ-modified particle for any *in vivo* or *in vitro* imaging application will require the particles to be dispersed in an aqueous environment. The replacement of methanol for a PBS solution in the FP_7 particles resulted in a total quenching of fluorescence (cf. Figure 2.4a). Due to the hydrophobic nature of the dye, the employment of PBS is speculated to force the bound azSQ to sequester to the particle surface and dimerize[37, 153].

It has been established that the fluorescence quantum yield of squaraine dyes can change when the dye is adsorbed onto macromolecules such as proteins and enzymes[113, 149], and this response can be employed as a fluorescent diagnostic probe in medical and biological applications. Previous studies have established that squaraine adsorption occurs on the ca. 10 nm sized human albumin protein and that dye adsorption will dominate over dye dimerization when the dye number density is less than a few times the protein number density[113]. In the current system, the FP_7 particles in water were mixed with bovine serum albumin (BSA) at concentration of 0.05 mM. The emission intensity in Figure 2.4a exhibited an immediate increase within the first 30 minutes that accounted for ca. 25% of the total increase in intensity followed by a long-term gradual increase. Even though the emission turn-on occurred in just a few minutes, the change in intensity was monitored over a 4-day incubation period to insure it had plateaued. At BSA concentration of ca. 0.05 mM, the number of BSA molecules is approximately equal to 15.4 times the total number of azSQ in the system. There was a 1991 % increase in output intensity at the peak wavelength of 687 nm, while the total integrated intensity was ca. 10 times greater. As indicated in Figure 2.4a, the study was also performed with human serum albumin (HSA) instead of BSA and the fluorescence enhancement with the human variant was identical to the bovine version. A similar study was performed with the enzymes, lysozyme and trypsin, and with the surfactant, sodium dodecyl sulfate (SDS). The surfactant was successful in breaking up the aggregation of the fluorophores and activating the fluorescence of the particles[88], while the lysozyme and trypsin were not (cf. Supplementary Information (SI)). Serum albumin is a major protein constituent of blood plasma and this protein facilitates the disposition and transport of a variety of exogenous and endogenous ligands to specific

regions. The delivery of ligands originates from two (BSA) and one (HSA) structurally selective binding site(s) where the binding affinity originates from a combination of hydrophobic, hydrogen bonding, and electrostatic interactions. The observed increase in fluorescence intensity with BSA and HSA binding likely results from the ability of the protein to "dissolve" hydrophobically aggregated azSQ on the surface of the particles[113, 143]. In addition, tight binding to the protein environment, possibly at the hydrophobic pockets, may increase the molecular rigidity of the dye, which reduces the vibrational modes and further raises the fluorescence signal[116].

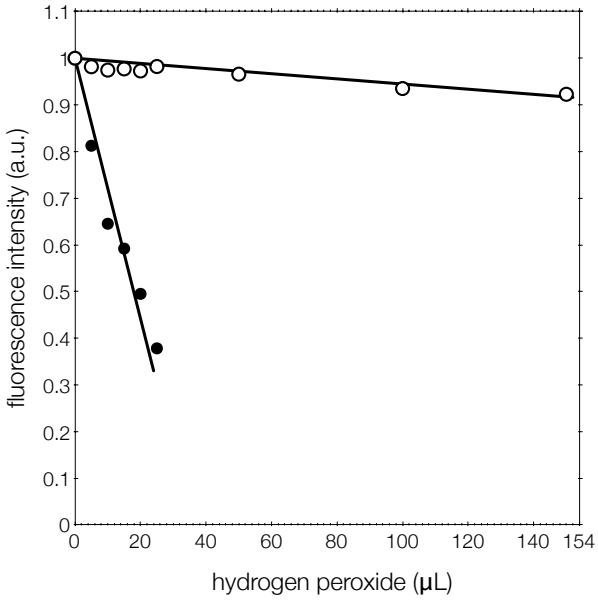

Figure 2.5: Change in fluorescence intensity at wavelength of 671 nm with exposure to hydrogen peroxide of free azSQ dye (•) and FP_7 particles incubated with BSA (○). Aqueous solution with excitation energy at a wavelength of 630 nm.

The most commonly used NIR probes, organic fluorescent dyes, are often chemically unstable and susceptible to bleaching by the attack of nucleophiles that are abundant in biological environments[29]. An approach to overcome this deficiency is through steric protection of the fluorophore by forming a rotaxane with the dye[141, 148, 157] or encapsulation inside a particle[127, 128, 129, 130, 131]. The former approach requires sophisticated chemistry to thread the dye through the macrocyclic cavity, usually resulting in a low yield, while the latter approach negates the prospect of forming beneficial guest/host assemblies with the fluorophore. The simpler and more versatile approach is the physical entrapment of the hydrophobic fluorophore inside the hydrophobic pockets of an aqueous dispersible protein or vesicle[144]. Figure 2.5 presents the normalized change in

fluorescence intensity of the free azSQ dye and FP_7 particles incubated with BSA, all dispersed in water, with exposure to hydrogen peroxide, an effective nucleophile. The drop in observed fluorescence intensity of the free dye is due to the degradation of the fluorophore by the hydrogen peroxide, while the fluorophores that are within the hydrophobic pocket of the BSA (or merely engulfed) continue to fluoresce even at much higher concentrations of hydrogen peroxide. It appears that the fluorophore/protein complex that activates the fluorophore's emission is possibly preventing the ingress of the hydrogen peroxide to the dye or acting as a scavenger for the peroxide[158, 159].

BSA has been indicated to initiate irreversible unfolding at temperatures greater than 60 - 70 °C[160]. Below this temperature, in the folded state, the protein exhibits global translational and rotational diffusion, but when above this temperature, the protein undergoes structural changes which are accompanied by changes in the protein dynamics[161, 162]. Figure 2.4b presents the increase in fluorescence when the FP_5 particles that are dispersed in PBS, have been incubated with BSA and undergo thermal cycling at temperatures above the irreversible unfolding temperature of BSA. At temperatures in the denaturation regime, the proteins initially unfold and extend, and if the proximity to one another is sufficiently high, the unfolded protein chains can entangle and potentially partially cross-link[161]. As indicated earlier, the incubation of the aqueous-phase particles with BSA results in a dramatic turn-on in emission intensity of 1.2×10^5 counts/second at 682 nm (cf. Figure 2.4a). Raising the temperature to 70 °C results in a 35 % enhancement of the emission, though once the particles are cooled to 20 °C, the emission increases by 105 % (at 682 nm). An addition annealing cycle results in a total increase in emission intensity of 125 % (cf. Figure 2.4b inset). The absolute increase in emission with annealing is dependent on both the ratio of azSQ to BSA as well as their thermal history. Nonetheless, there is a significant change in the emission characteristics with annealing.

In comparison to the "monomeric" absorbance, squaraine dyes that are dispersed in aqueous solutions tend to form aggregates that exhibit an absorbance that has a bathochromic (J-aggregates) or hypsochromic (H-aggregates) shift. These aggregates also affect the emission properties, with H-aggregates usually being poor emitters and J-aggregates often giving efficient fluorescence[149]. The inset in Figure 2.4b presents the intensity ratio of the J-aggregates (745 nm) to the monomeric emission (682 nm) and suggests a conversion of the aggregates to the monomeric form with thermal cycling; a conclusion that is corroborated with the absorption characteristics (cf. SI). Due to the steric limitations of the azSQ being tethered to the surface of the particle, J-aggregates are characterized

structurally as having only one end of the azSQ aligned with the end ring of the other azSQ. The large fluorescence turn-on associated with the conversion of the surface-attached azSQ fluorophores from "aggregate to monomeric species" may be attributed to the inclusion of the dye into the hydrophobic pocket of BSA when in its native folded form. The fluorescent enhancement of the particles when they are thermally cycled above the denaturing temperature of BSA suggests that other factors than just a pocket-based complexation is operative in converting the dye molecules from their non-emissive aggregate states to the fluorescent monomeric form. The unfolded state may offer opportunities of the protein to bind to additional fluorophores on the surface of the particle, reducing the non-radiative decay rate of the fluorescent molecules and raising the fluorescence signal[163, 164]. The PEGylated particles, FP_6 & FP_7, did not exhibit such a dramatic increase in photoluminescence with annealing. The FP_7 particles exhibited a modest 13 % increase in integrated intensity with annealing and it is speculated that the PEG chains are effective in preventing the unfolded BSA from finding, adhering to, and destroying fluorophore aggregates.

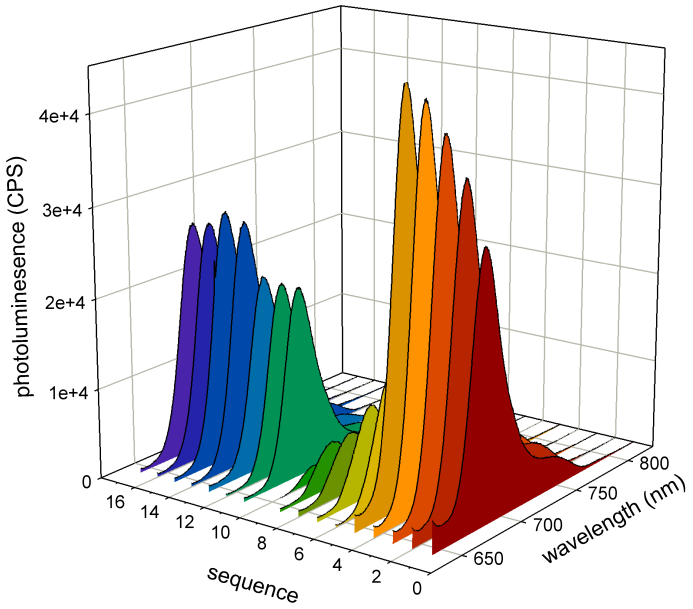

Figure 2.6: Variation of photoluminescence spectrum of FP_5 particles in PBS incubated with BSA (**sequence 0**), with four annealing cycles (**sequence 1-5**), with introduction & incubation of trypsin (**sequence 6-10**), reintroduction & incubation of BSA (**sequence 11-13**) and with four annealing cycles (**sequence 14-17**). Excitation energy at a wavelength of 630 nm. An annealing cycle consists of raising the sample temperature to 65 °C for 20 min and then returning the temperature to 20 °C.

A number of reports have demonstrated the "activation" of NIR particles through the em-

bodiment of a guest/host complexation on the surface of the particles[31, 88]. Recently, particles surface functionalized with azadipyrromethenes had their emission turned-on when mixed with either an anionic or nonionic surfactant, as well as a phospholipid[88]. Our laboratory has recently demonstrated the BSA activation of indocyanine green (ICG) functionalized particles[31]. These studies both accomplished the activation of emission through the formation of a guest/host complex, yet there has been no methodology to deactivate the emission. To this end, the use of a protein in our studies allows for its digestion once on the particle and a route to deactivate the fluorescence. Figure 2.6 presents the fluorescence activation/deactivation of FP_5. These particles were equilibrated with 0.025 mM BSA in a Tris-HCl buffer of pH 8, then annealed at 65 °C and cooled to 20 °C. The annealing step was repeated four times. As demonstrated previously (cf. Figure 2.4b), the annealing resulted in a significant enhancement in the emission intensity. Mixing the particles with trypsin (0.143 mM), a standard enzyme used for the digestion of albumin, and incubating the mixture at 37 °C for 15 hours resulted in a 71 % drop in emission, while after 64 hours the decrease was 85 % complete. With 184 hours of incubation there was an almost complete cessation of emission. The majority of the emission turn-off was complete in a few minutes, the reaction was monitored over a substantial incubation period (ca. 7.6 days) to insure a plateau was reached. Trypsin catalyses the hydrolysis of peptide bonds so that albumin is broken into smaller peptides and its speculated that the fragments from BSA are unable to effectively "coat" the azSQ and these chromophores again coalesce and quench on the surface of the particles. Performing the same digestion study with particles that had not been annealed resulted in a similar response, though the fluorescence deactivation was not as complete. It is speculated that the BSA is more structurally open after annealing and trypsin is more effective in digesting the denatured protein[165, 166]. Once again adding an excess of BSA to the FP_5 particles after the trypsin digestion results in a return to the approximate initial emission intensity after 48 hours of incubation, though the trypsin was not removed from the system and would continue to digest the BSA, preventing a full return to the initial emission characteristics. In addition, an UV/Vis absorption study confirmed that the particles could not recover all of their initial emission intensity after an annealing & digestion study due to a slight degradation of the fluorophores (cf. SI)[141]. The repeated turn-on and turn-off of the fluorescence is demonstrated in Figure 2.6, which presents the change in the photoluminescence spectrum with annealing of the FP_5 particles with BSA to activate and enhance the emission, exposure to trypsin to deactivate the emission, and a subsequent introduction of BSA again to reactivate the emission. The annealing

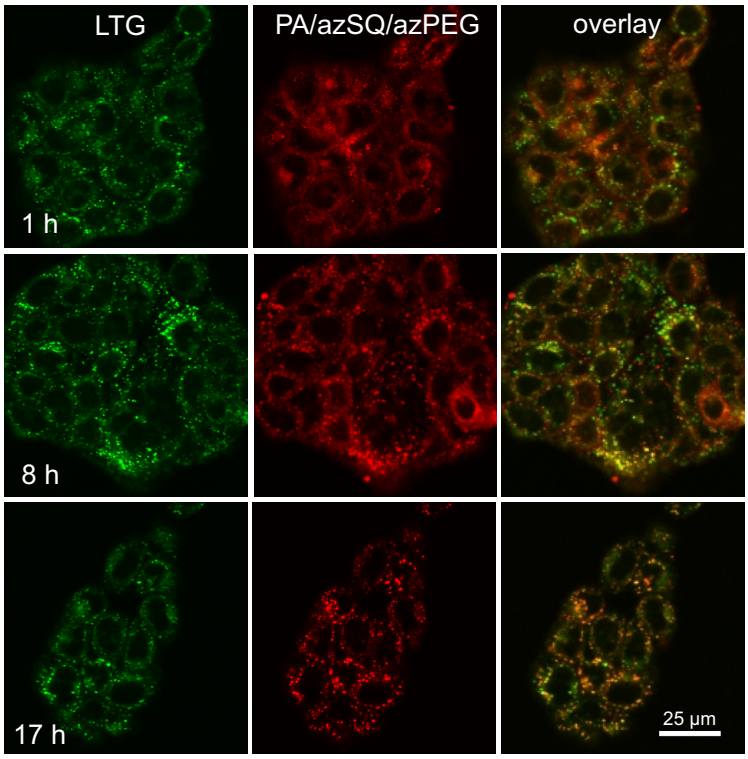

Figure 2.7: Confocal images of FP_7 particles (1 μM) incubated with UMSCC22A cells for 1, 8, and 17 hours. One hour before imaging, cells were loaded with LysoTracker Green (LTG) to image lysosomes. LTG (green, 473 nm) is left image, PA/azSQ/azPEG particles (red, FP_7) is the center image, and the right image is their overlay.

resulted in a 48 % increase in the number of active emitters and an increase in the relative quantum yield to 0.036 from 0.024, while the trypsin digestion turned-off 97 % of the emitters and dropped the relative quantum yield to $7.2\text{x}10^{-4}$. Similarly, the PEGylated particles, FP_5 & FP_7, exhibited an almost complete cessation of emission with tryptic digestion of the BSA. The FP_7 particles exhibited an eleven-fold increase integrated intensity with BSA activation, that was improved 13 % with annealing. The introduction of trypsin returned the particles to a quenched state within just a few hours of the enzyme addition.

2.3.4 *In Vitro* Co-localization.

In medical diagnostics, one of the problems limiting the use of many small molecule fluorophores is the difficulty in preparing pharmaceutical formulations that are amenable to parenteral administration[126].

The majority of organic chromophores that are of interest are not soluble in water and cannot

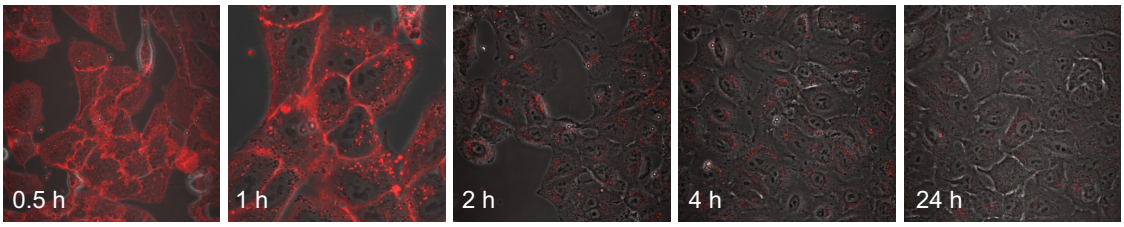

Figure 2.8: Confocal images of FP_7 particles (1 μM) incubated with A549 cancer cells depicting the activation of fluorescence with incubation time (0.5 h - 1 h) and subsequent reduction in fluorescence with incubation time (2 h - 24 h) as particles enter lysosomes. Media did not contain FBS and excitation laser power was constant between images.

be simply injected. To remedy this, a number of different approaches, including encapsulation of the fluorophore in colloidal carriers such as oil-dispersions, liposomes, and polymeric particles, have been investigated[148, 157, 167, 168]. The encapsulation in an aqueous dispersible particle allows for the straightforward insertion of the fluorophore into the patient but prevents the formation of any advantageous guest/host complexes with the chromophore and a target protein.

The surface-attachment of the fluorophore onto the particle insures its accessibility to proteins but may alter the ability of the particles to penetrate cells of interest. To that end, the cellular uptake and intracellular trafficking of the FP_7 particles (cf. Table 2.1) were studied by live cell confocal laser scanning microscopy. In addition, cell viability studies were carried out with the A549 and HepG2 cell lines and the FP_7 particles were deemed not cytotoxic at the concentrations used in this study (cf. SI).

The particles were incubated with UMSCC22A head and neck cancer cells and confocal images of the cells were collected after 1, 8, and 17 h of incubation with particles (cf. Figure 2.7); the particles' fluorescence was activated by fetal bovine serum (FBS) in the culture medium. We labeled the lysosomes with LysoTracker Green (LTG), which stains acidic compartments such as late endosomes and lysosomes, to study the co-localization between the lysosomes and particles. The fluorescence of the particles co-localized with the LTG (Figure 2.7), indicating that the particles were taken up by the cells through endocytosis and accumulated into the lysosomes. The FP_7 particles were also incubated with A549 cells which are a human alveolar adenocarcinoma cell line. These cells synthesize lecithin with a high percentage of disaturated fatty acids and are believed to be responsible for pulmonary surfactant synthesis[169]. Figure 2.8 presents a confocal image of the FP_7 emission channel overlayed on the transmitted image of the A549 cancer cells. The particles were incubated with the cells without FBS and were initially nonfluorescent, but after 30 minutes of

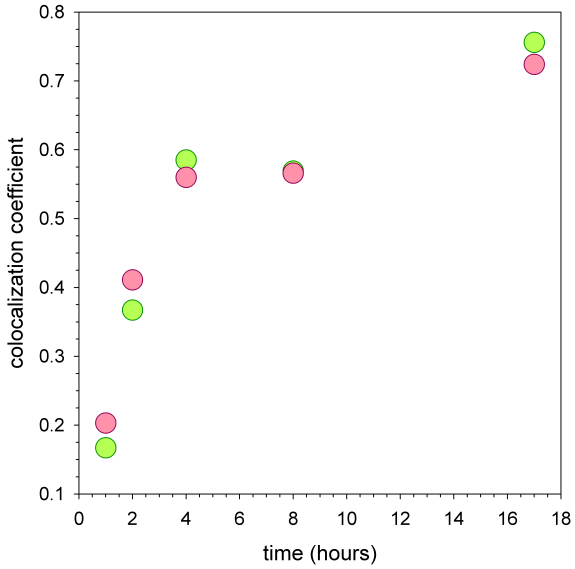

Figure 2.9: Manders' co-localization coefficient M_1 (green channel) and M_2 (red channel) from Figure 2.7 of FP_7 particles incubated with UMSCC22A cells.

incubation the particles were fluorescent as they collected onto the cell membranes (cf. Figure 2.8); the fluorescence is clearly evident by 1 hour of incubation as the particle begin to be engulfed by the cells. In this study, no FBS was utilized in the medium and the fluorescence was activated by constituents of the cells. This fluorescence turn-on is speculated to be due to the phospholipids in the cell membrane, specifically lecithin, and is mechanistically similar to the use of the surfactant SDS to activate the fluorophores[88].

For the co-localization study with the UMSCC22A cancer cells, the Manders' co-localization coefficient M_1 and M_2[170] for the FP_7 particles and LTG increased in a time-dependent manner and after 17 hours, the co-localization coefficient has risen to ca. 0.75 (cf. Figure 2.9). The relative equivalence of the coefficients (M_1 or M_2) at any sampled time suggests that the particle/LTG emitter ratio is not changing significantly, though the slight increase (0.07) in M_2 (red channel) relative to M_1 (green channel) at longer times could indicate a reduction in the number of emitting FP_7 particles. Since the lysosomes constitute the intracellular digestion compartment, the observed co-localization between the lysosomes and the FP_7 particles should result in the degradation of the fluorescence activating FBS that is absorbed on the particles and result in a return of the particles to a quenched state. Figure 2.8 presents confocal images of the FP_7 emission channel overlayed on the transmitted image of the A549 cells. As discussed earlier, since no FBS was added to the cell's

media, the fluorescence activation of the particles was accomplished by the phospholipids in the cell membrane, specifically lecithin production of the cells binding to the fluorophores and reducing their aggregate-based quenching. At 2 hours of incubation (cf. Figure 2.8), the FP_7 particles have migrated into the lysosomes and there is a high density of FP_7 emitters in the cells. Over the course of an additional 22 hours of incubation (cf. Figure 2.8), the number of FP_7 emitters appears to be diminishing, consistent with the trypsin digestion study of Figure 2.6. In order to estimate the number of emitters per cancer cell, images of the cells at 17 and 24 hours had a common threshold applied to the red channel and the number of pixels above the threshold were counted. Following this procedure, the cells incubated for 17 hours had 691 pixels per cell above the threshold, while the cells incubated for 24 hours had only 167 pixels per cell, a 75 % reduction. All *in vitro* studies with the particles indicate that the rapid emission turn-off is not due to merely dye degradation. Similarly to the previously described tryptic digestion study, we speculate that the phospholipids which are sequestered on the particles are being removed once the particles localize in the lysosomes and the adherent can no longer prevent the chromophores from aggregating and quenching their emission.

There are multiple mechanisms of endocytosis that can be utilized for penetration of nanoparticles into cells. A pharmacologic approach was used to determine which mechanism of endocytosis was involved in cellular uptake of the FP_7 particles in UMSCC22A cells. A number of compounds, when incubated with mammalian cells, disrupt specific routes of endocytosis. For example, cytochalasin D inhibits macropinocytosis, chlorpromazine inhibits clathrin-mediated endocytosis by inhibiting disassembly of clathrin-coated pits and inhibiting receptor recycling to the plasma membrane, nocodazole inhibits clathrin- and caveolae-independent endocytosis by disrupting microtubules, and filipin III inhibits caveolae-mediated endocytosis by sequestering cholesterol available for lipid rafts. When cytochalasin D, chlorpromazine, and nocodazole were initially added to the UMSCC22A cells 30 min before the addition of the FP_7 particles, no change in the final Pearsons' co-localization coefficient between LTG and the FP_7 particles were seen. In contrast, filipin (FIL) had a significant influence on the coefficient. Figure 2.10a presents confocal images of the cells incubated with the FP_7 particles without the inhibitor of the raft/caveolae endocytosis pathway and with the compound (FIL). Confocal images revealed patches of nanoparticles bound to the plasma membrane in filipin-treated cells (arrows), indicating that filipin prevented FP_7 particles from entering cells. The inclusion of the filipin decreased the Pearsons' co-localization coefficient by ca. 50% (cf. Figure 2.10b).

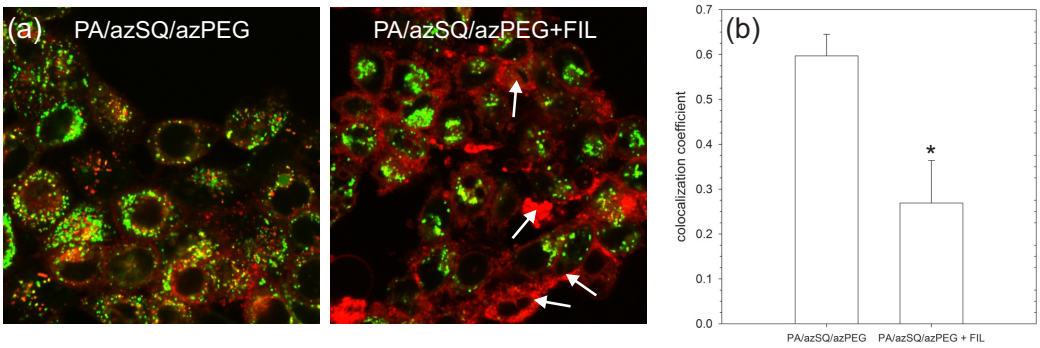

Figure 2.10: **(a)** Confocal images of FP_7 particles (1 μM) incubated with UMSCC22A cells for 2 hours (left image) and with the addition of the raft/caveolae endocytosis pathway inhibitor filipin (FIL) (right image) and corresponding **(b)** Pearsons' co-localization coefficient between LTG and FP_7 particles. An asterisk indicates statistical significance from the control by ANOVA followed by Tukeys multiple comparisons test ($p<0.01$).

The results indicate that the nanoparticles are taken up by the cells through caveolae-mediated endocytosis for a final intracellular destination at the lysosomes. A number of studies have found that nontargeted particles follow a caveolae-mediated endocytosis route from early endosomes to late endosomes and lysosomes[171, 172, 173].

2.4 Experimental

2.4.1 Reagents and solvents

All the commercial reagents were purchased from TCI America and used without further purification. All the solvents were dried according to standard methods. Deionized water was obtained from a Thermo Scientific Barnstead NANOpure Water Purification System and exhibited a resistivity of ca. 10^{18} ohm^{-1}cm^{-1}.

2.4.2 Chemical characterization methods

^{1}H and ^{13}C NMR spectra were recorded on JEOL ECX-300 spectrometers (300MHz for proton and 76MHz for carbon). Chemical shifts for protons are reported in parts per million downfield from tetramethylsilane and are referenced to residual protium in the NMR solvent ($CDCl_3$: δ 7.26 ppm, DMSO-d6: δ 2.50 ppm). Chemical shifts for carbons are reported in parts per million downfield from tetramethylsilane and are referenced to the carbon resonances of the solvent ($CDCl_3$: δ 77.16, DMSO-d6: δ 39.52 ppm). Coupling constants are reported in Hertz (Hz). LC/MS mass

spectra were obtained using Finnigan LCQ spectrometer and HP 1100 (HPLC). The IR spectra were recorded at room temperature in the wavenumber range of 400-4000 cm^{-1} and referenced against air with a Nicolet 6700 FTIR instrument. A total of 32 scans were averaged for each sample at 2 cm^{-1} resolution.

2.4.3 Preparation of azide-modified squaraine derivative chromophore (azSQ)

The reaction scheme for synthesis of azSQ is presented in Figure 2.11

3-(3-azidopropyl)-1,1,2-trimethyl-1H-benzo[e]indolium iodide (1) The solution containing 2,3,3-trimethyl-4,5-benzo-3H-indole (1 g, 4.78 mmol) and 1-azido-3-Iodopropane (2 g, 9.56 mmol) in acetonitrile (50 ml) was refluxed for 72 hours. The solvent was evaporated under vacuum and the residue was dissolved in dichloromethane (10 ml). This solution was added drop-wise to diethyl ether solution (80 ml) to precipitate the product. This purification step with diethyl ether solution was performed 3 times and the solid obtained was filtered and dried under vacuum (hygroscopic). Compound 1 was obtained as a dark-brown solid (1.61 g, yield 80 %). ^{1}H NMR ($CDCl_3$) δ 1.87 (s, 6H), 2.37 (m, 2H, J=5.9 and 6.9), 3.25 (s, 3H), 3.76 (t, 2H, J=5.9), 5.00 (t, 2H, J=6.9), 7.70 (m, 3H, J=8.6 and 1.4), 7.96 (d, 1H, J=8.9), 8.10 (m, 2H, J=8.6 and 8.9).

4-(1,1,2-trimethyl-1H-benzo[e]indolium-3-yl)butane-1-sulfonate (2) The mixture containing 2,3,3-trimethyl-4,5-benzo-3H-indole (0.6 g, 2.87 mmol) and 1,4-butanesultone (1.17 g, 8.59 mmol) was heated at 120 °C for 2 hours. After cooling, the crystallized product was washed with acetone, filtered and dried to give the compound (2). White solid (0.92 g, yield 93 %). ^{1}H NMR (DMSO-d6) δ 1.75 (s, 6H), 1.78 (m, 2H, J=7.2), 2.03 (m, 2H J=7.6), 2.52 (t, 2H, J=7.2), 2.95 (s, 3H), 4.61 (t, 2H, J=7.6), 7.69-7.80 (m, 2H, J=8.3), 8.20 (d, 2H, J=8.9), 8.27 (d, 1H, J=8.9), 8.36 (d, 1H, J=8.3).

3,4-diethoxy-3-cyclobutene-1,2-dione (3) was prepared according to the method published[147].

3-{[(2E)-3-(3-azidopropyl)-1,1-dimethyl-1H,2H,3H-benzo[e]indol-2-ylidene]methyl}-4-hydroxycyclobut-3-ene-1,2-dione (4) Pyridine (2ml) was added to the solution containing compound (1) (0.3 g, 0.71 mmol) and 3,4-diethoxy-cyclobut-3-ene-1,2-dione (1 g, 5.9 mmol) in

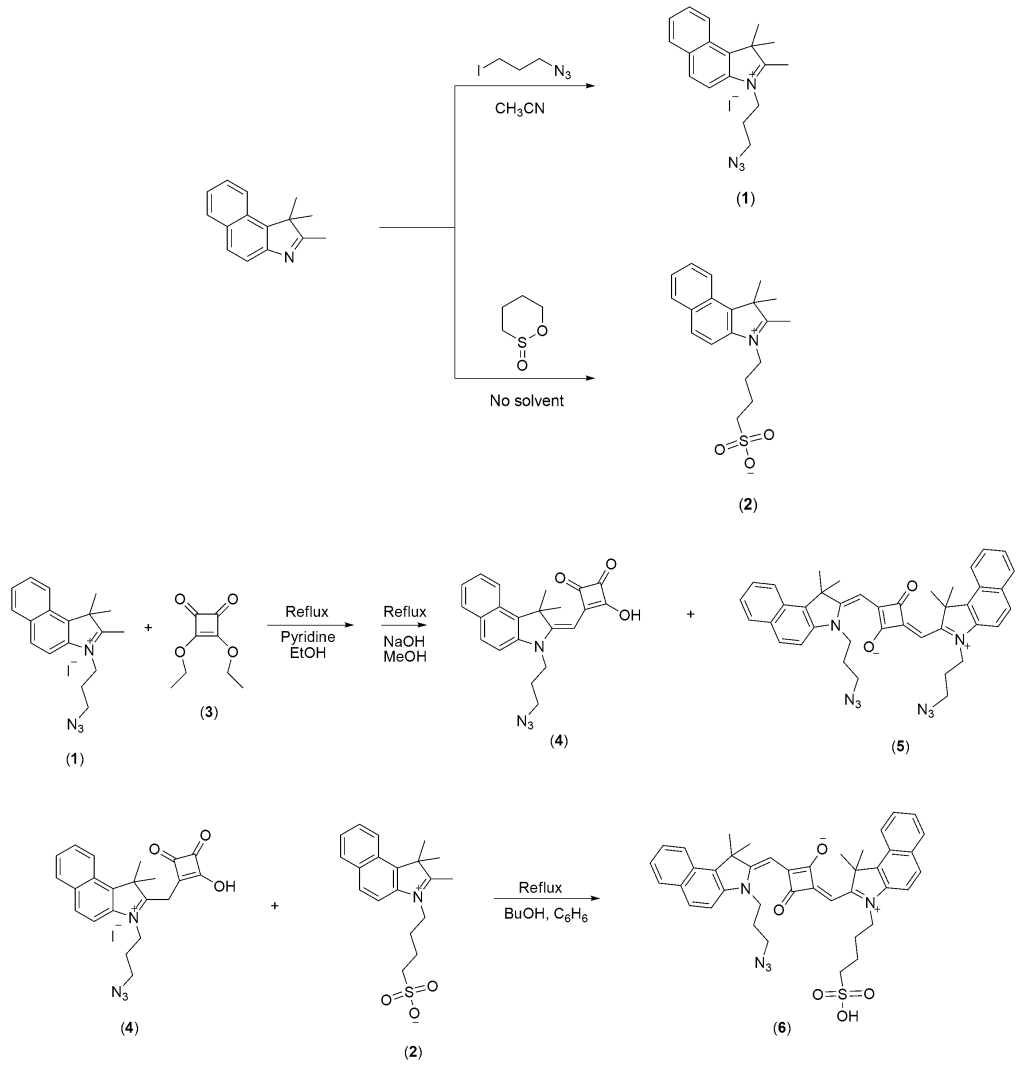

Figure 2.11: Reaction scheme for synthesis of azSQ.

ethanol (10 ml) and refluxed for 4 hours. After cooling, the green solution was evaporated and the residue was dissolved in a mixture of methanol (20 ml) and water solution of NaOH (3 ml, 0.9 mol). This mixture was refluxed for 30 min. After cooling, the mixture was filtered and evaporated. The residue was extracted with dichloromethane and washed with water 2 times. The organic layer was separated, dried with Na_2SO_4 and filtered. The filtrate was evaporated and the residue was dissolved in dichloromethane (2 ml) and added dropwise to diethyl ether solution (20 ml) to precipitate a green solid. This solid was separated by centrifugation and dried on air to give a mix of compounds (4) and (5) with molar ratio 1:2. This mixture (225 mg) was used in next step without further purification. ^{1}H NMR ($CDCl_3$) δ 1.93 (s, 6H), 2.14 (m, 2H), 3.40 (t, 2H, J=6.0), 3.98 (t,

2H, J=6.0), 5.72 (s, 1H), 7.20 (d, 1H, J=8.5), 7.47 (m, 1H), 7.82 (m, 2H), 8.07 (d, 1H, J=8.5).

2-{[(1E)-3-{[(2Z)-3-(3-azidopropyl)-1,1-dimethyl-1H,2H,3H-benzo[e]indol-2-ylidene]methyl}-2-hydroxy-4-oxocyclobut-2-en-1-ylidene]methyl}-1,1-dimethyl-3-(4-sulfonatobutyl)-1H-benzo[e]indol-3-ium (6) The mixture of compounds (4) and (5) (225 mg) (see synthesis of compound (4)) and compound (2) (140 mg, 0.4 mmol) was dissolved in butanol (15 ml) and benzene (15 ml). This solution was refluxed with Dean-Stark apparatus for 18 hours. After cooling, the solvent was evaporated under vacuum and the residue was purified by flash column chromatography (dichloromethane : methanol 9:1, silicagel). 120 mg of compound (7) (a deep blue solid) was obtained. Rf=0.2, yield 24 % (recalculated to compound (1)). ^{1}H NMR (DMSO-d6) δ 1.80 (m, 4H), 1.96 (s, 6H), 1.97 (s, 6H), 2.02 (m, 2H, J=6.6), 2.55 (t, 2H), 3.55 (t, 2H, J=6.6), 4.26 (b.t, 2H), 5.89 (s, 1H), 5.90 (s, 1H), 7.45 (m, 2H), 7.62 (m, 2H), 7.69 (d, 1H, J=9.0), 7.75 (d, 1H, J=9.0), 8.02 (m, 4H), 8.23 (d, 2H, J=8.4). ^{13}C NMR ($CDCl_3$) δ 22.45, 26.36, 26.60, 26.80, 29.81, 40.71, 43.77, 48.63, 51.22, 51.28, 86.12, 87.10, 109.88, 110.64, 122.45, 124.20, 124.36, 127.19, 127.34, 128.33, 128.61, 129.69, 129.97, 131.17, 131.44, 133.94, 134.59, 139.17, 139.55, 170.81, 172.53. ESI-Mass (LC/MS) (m/z; rel. intensity): 715.3 (M^+; 100), 987.2 (8) 632.2 (8), 330.2 (17).

2.4.4 Preparation of azide-modified polyethylene glycol (azPEG).

The azPEG was prepared according to the method published[31].

Mono-methoxy-PEG5000-methansulfonate Methylsulfonyl chloride (0.92 g, 8 mmol) in dichloromethane (5 mL) was added dropwise at room temperature to the stirring solution of triethylamine (0.89 g, 8.8 mmol) and mono-methoxy-PEG5000 (20 g, 4 mmol) in dichloromethane (70 mL). The solution was stirred at 20 °C for 4 hours, then washed with water and the organic layer was dried with Na_2SO_4 with further filtration. The solvent was evaporated under vacuum to give the product as a white solid. Yield: 20.3 g (97 %). ^{1}H NMR ($CDCl_3$) 3.07 (s, 3H), 3.36 (s, 3H), 3.48 (t, 2H), 3.53 (m, 2H), 3.62 (m, ca. 400H), 3.75 (m, 4H), 4.36 (m, 2H).

Mono-methoxy-PEG5000-azide The mixture of mono-methoxy-PEG5000-methansulfonate (20.3 g, 4 mmol) and sodium azide (1.1 g, 17 mmol) in acetonitrile (80 mL) was refluxed and stirred for 15 hours. After cooling, the mixture was filtered and the solvent was evaporated. The residue was dissolved in dichloromethane and washed with water, organic layer was separated, dried with Na_2SO_4 and filtered. The solvent was evaporated, the crystalline residue was washed with

hexane, filtered and dried in air to give the product as a white solid. Yield: 19 g (94 %). ^{1}H NMR ($CDCl_3$) 3.35 (s, 3H), 3.38 (t, 2H), 3.62 (m, ca. 400H), 3.85 (m, 2H). FTIR (cm^{-1}): 1095 (s, C-O-C); 1340, 1465 (CH2); 2100 (N3); 2880 (s, CH2).

2.4.5 Preparation of the particles

Propargyl acrylate (PA) particles were prepared according to a standard emulsion polymerization method published[31].

For a typical surface modification of the particles, for example, the grafting of azSQ and azide-modified PEG chains with molecular weight of 5000 (azPEG) onto the particles, 1 mL PA particles and 3.94 mg azSQ were added to 2 mL of deionized water. Solutions of 0.07624 g copper(II) sulfate (99.999 % Aldrich) in 10 mL deionized water and 0.3024 g sodium ascorbate (99 % Aldrich) in 10 mL deionized water were made. Initially, 0.5 mL of the $CuSO_4$ solution was added to the PA/azSQ solution, followed by 0.5 mL of the sodium ascorbate solution. The resulting mixture was maintained at a temperature of ca. 28 °C for 15 minutes and then the reaction was stopped by the removal of unreacted azSQ, sodium ascorbate, and $Cu(II)SO_4$ through a repeated particle washing procedure consisting of centrifugation and redispersement in methanol. The cleaned PA/azSQ (FP_5) particles in water were subsequently utilized in a secondary click transformation with 54.99 mg azPEG, and previously presented $CuSO_4$ and sodium ascorbate solutions. The reaction was allowed to run for 48 hours and then washed to remove unreacted species as determined by photoluminescence measurements; these particles are referred to as PA/azSQ/azPEG (FP_7) particles.

2.4.6 Cell analysis

Human HepG2 and A549 cell lines were obtained from ATCC (Rockville, MD). Human UM-SCC22A head and neck squamous carcinoma cell line was a gift from Dr. Besim Ogretmen (Medical University of South Carolina). Hep G2 cells were cultured in phenol red-free Dulbeccos modified Eagles media (DMEM) containing 5 % fetal bovine serum (FBS), 1 % Penicillin-Streptomycin, and supplemented with glutamine (Invitrogen, Carlsbad, CA). A549 cells were cultured in F-12K media (Kaighn's Modification of Ham's F-12 medium) containing 10 % fetal bovine serum (FBS) and 1 % Penicillin-Streptomycin. UMSCC22A cells were cultured in Dulbeccos modified Eagles media (DMEM) supplemented with L-glutamine containing 10 % FBS and 1 % Penicillin-Streptomycin.

Cells were cultured at 37 °C in a humidified atmosphere of 95 % air 5 % CO_2.

2.4.7 Cytotoxicity assay

HepG2 cells & A549 (20,000 cells per well) were cultured on 96 well plates for 24 hours. Subsequently, cells were, exposed to $2x10^9$, $2x10^{11}$, and $2x10^{13}$ particles/mL. After 96 hours, cell death was assessed with a MTS assay according to the manufacturer's instructions (Promega, Madison, WI). Briefly, medium was aspirated and a solution of 100 μL of DMEM containing 10 % FBS and 20 μL 3-(4,5-dimethylthiazol-2-yl)-5-(3-carboxymethoxyphenyl)-2-(4-sulfophenyl)-2H-tetrazolium, salt (MTS) and phenazine methosulfate (PMS) was added onto each well. After 60 minutes, wells were scanned colorimetrically at 490 nm on a VersaMax spectrophotometer (Molecular Devices, Sunnyvale, CA). The conversion of MTS into an aqueous soluble formazan product is achieved only by dehydrogenase enzymes which are present in metabolically active cells; the absorbance at 490 nm from the formazan product is directly proportional to the number of living cells in culture.

2.4.8 Confocal microscopy

UMSCC22A cells were cultured onto 35 mm glass-bottomed Petri dishes (MatTek Corporation, Ashland, MA) at 150,000 cells/dish and incubated for 24 hours. Subsequently, cells were incubated with 1 μM PA/ azSQ/ azPEG (FP_7) particles for different time periods of 1, 2, 4, 8, 17, and 24 hours. At the end of the incubation, the medium was aspirated and the cells were incubated with 500 nM LysoTracker Green (LTG) for 1 hour. Before imaging the concentration of the LTG dye was lowered to 100 nM. Dishes were placed in an environmental chamber at 37 °C on the stage of Olympus FV10i LIV laser scanning confocal microscope. The images of LTG (473 nm excitation and 490-540 nm emission) and FP_7 particles (635 nm excitation and 660 - 760 nm emission) were collected using a 63 X N.A. 1.4 oil immersion planapochromat objective. ImageJ software was used to post-process the images and calculate the co-localization coefficients.

2.4.9 Optical characterization methods

Absorption spectra were taken using a Perkin-Elmer Lambda 900 UV/VIS/NIR spectrophotometer. Photoluminescence (PL) spectra were collected using a Photon Technology International QuantaMaster 60 NIR with PMT spectrofluorometer and a Thermo Oriel xenon arc lamp (Thermo

Oriel 66902) mated with a Thermo Oriel Cornerstone 7400 1/8 m monochromator (Thermo Oriel 7400) and a Horiba Jobin-Yvon MicroHR spectrometer coupled to a Synapse CCD detector. Quantum yields (ϕ) of the dyes and modified particles were determined relative to the reference dye 1,1',3,3,3',3'-hexamethylindotricarbocyanine iodide (HITCI) in methanol, which has a fluorescence quantum yield of $\phi_{ref} = 0.12$[153, 174], employing established procedures[175]. It is to be noted that the diameter of the particles used through out the paper was 49.9 nm except for quantum yield measurement where a couple of particles of diameter 88.5 nm were used.

2.5 Conclusion

The 50 nm poly(propargyl acrylate) particles which were surface modified through the copper-catalyzed azide/alkyne cycloaddition of an azide-terminated squaraine derivative, a near-infrared emitter, and polyethylene glycol exhibited a protein triggered activation/deactivation of the emission. When dispersed in PBS, the initially nonfluorescent particles exhibited an albumin-based activation which resulted in an eleven-fold enhancement in integrated intensity. Deactivation with the addition of trypsin to cleave the albumin resulted in a complete return to the initial quenched state. Quenched NIR emitting particles which can have their emission activated by their exposure to a specific protein, then deactivated by exposure to another protein, are a potentially valuable nanodevice for the fight against cancer. A new generation of photonic imaging systems will be created from adaptive & responsive contrast mechanisms using highly specific fluorescent agents, such as activated fluorescent probes described in this effort, when these probes are leveraged with the recent advances in illumination & detection schemes, tomographic principles, and mathematical models that describe photon propagation in tissues[176].

Acknowledgments

The authors thank the Gregg-Graniteville Foundation for financial support. The research was supported by grants from the US National Cancer Institute, R01 CA119079 (ALN), P30 CA138313 (Hollings Cancer Center Cell and Molecular Imaging Shared Resource) and Abney Cancer Foundation (H-I H).

2.6 Supplementary Information

2.6.1 Results & Discussion

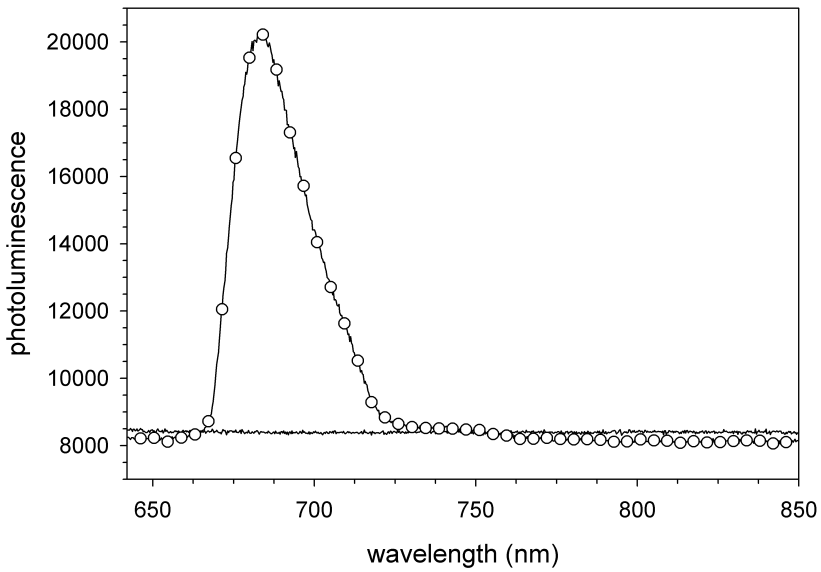

Figure 2.12: Fluorescence spectra of FP_5 nanoparticles (6.53 μM) in water before (-) and 18 hours after addition of 50 mg of SDS (○). Excitation at 630 nm.

2.6.2 Experimental

Calculation of grafting densities The molar extinction coefficient of the free dye in the dilute regime and wavelength range of 615 nm to 685 nm is used to estimate the number of fluorophores attached to the particles. First, the molar extinction coefficient for the dye in the dilute regime is measured. The concentration of the modified particles solution is estimated using Beers law (A = εbc where A is absorbance, ε is molar extinction coefficient, in $M^{-1}cm^{-1}$, b is path length in cm, and c is concentration in M). 500 μL of the modified particles solution is dried out to measure the mass. The diameter of the unmodified particle is measured using the DLS (Dynamic Light Scattering) and the surface area, mass and volume of a particle are calculated. Using the mass of a particle and the mass of 500 μL of solution, the number of modified particles per mL is calculated by assuming that the mass of the dye is negligible compared to the mass of the particle. Finally, the concentration and number of particles is used to determine the grafting density and distance between two chromophores.

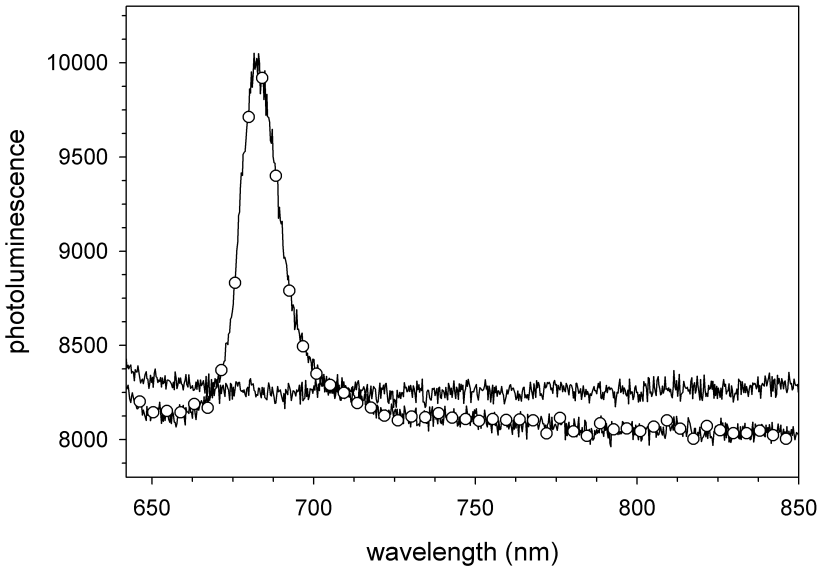

Figure 2.13: Fluorescence spectra of FP_7 nanoparticles (4.97 μM) in water before (-) and 18 hours after addition of 50 mg of SDS (○). Excitation at 630 nm.

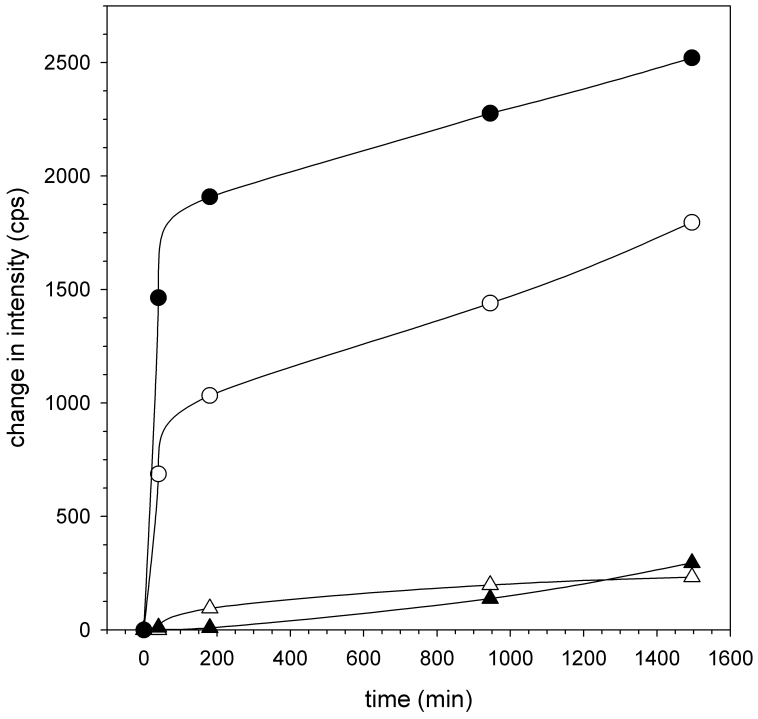

Figure 2.14: Changes in photoluminescence intensity of FP_5 nanoparticles (0.03 mM) in phosphate buffered solution (PBS) with the addition of the four different proteins (0.04 mM) [Bovine serum albumin (○), human serum albumin (●), lysozyme (△), and trypsin (▲)]. The HSA and BSA curves typically merge after 4 days of incubation, though the lysozyme and trypsin never significantly increase the particles emission. Excitation at 630 nm.

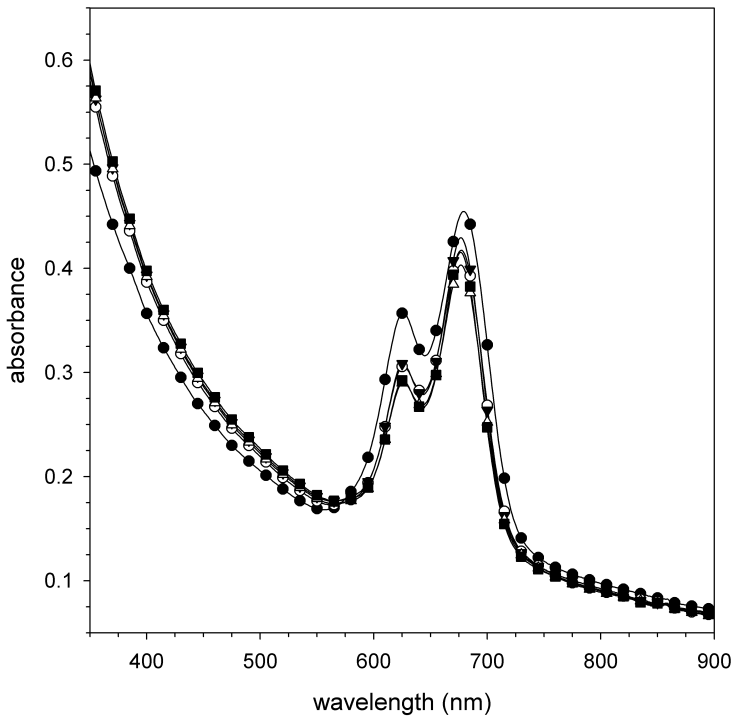

Figure 2.15: Changes in absorbance spectra of FP_5 nanoparticles in phosphate buffered solution (PBS) with 15 mg of BSA. [Initially at 20 ^{o}C (•), at 70 ^{o}C (○), after 70 ^{o}C anneal then cooled to 20 ^{o}C (▼), after 70 ^{o}C, cool to 20 ^{o}C, heated to 70 ^{o}C (△) and after 70 ^{o}C, cool to 20 ^{o}C, heated to 70 ^{o}C, then cooled to 20 ^{o}C (■)]

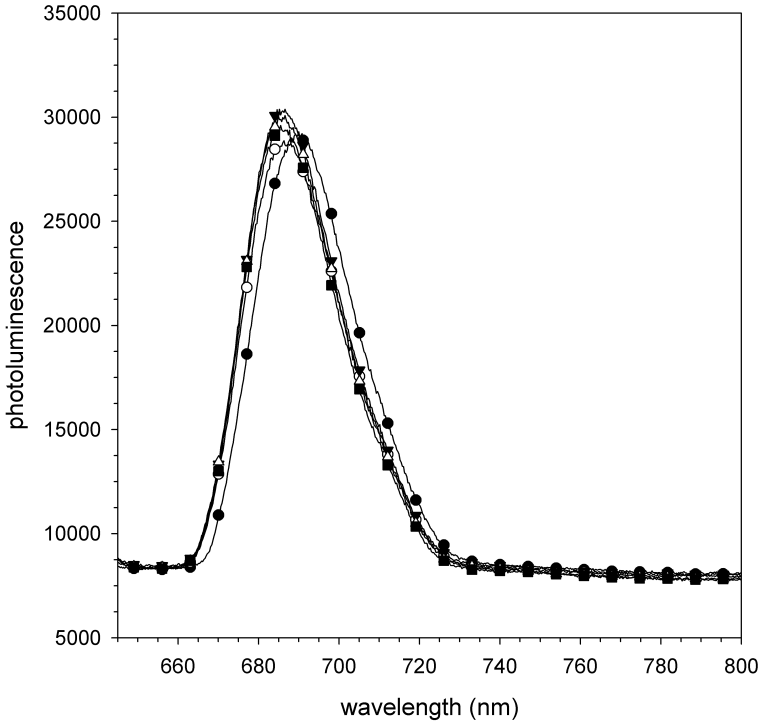

Figure 2.16: Changes in photoluminescence of FP_7 nanoparticles in phosphate buffered solution (PBS) with 5 mg of BSA. [Initially at 20 ^oC (●), after heat and cool cycle 1 (○), after heat and cool cycle 2 ((▼), after heat and cool cycle 3 (△) and after heat and cool cycle 4 (■)]. Excitation at 630 nm.

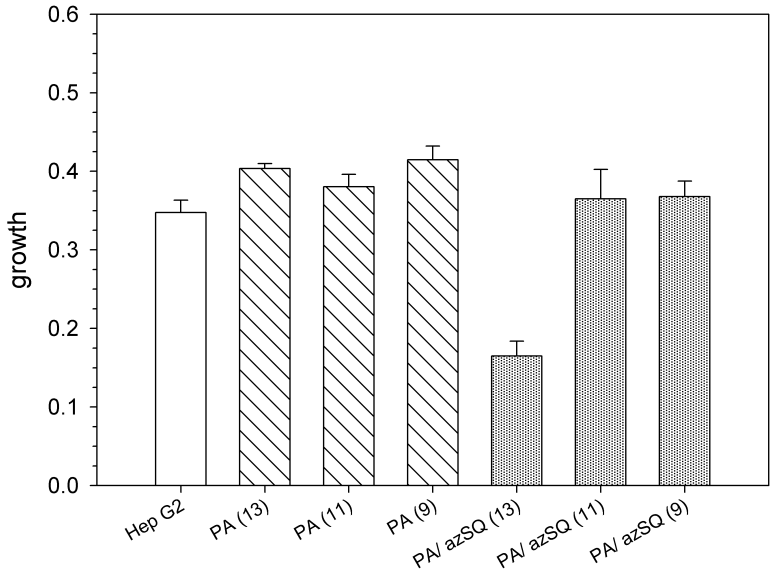

Figure 2.17: Proliferation of HepG2 cells after 2 days of incubation with neat PA and PA/ azSQ (FP_5) nanoparticles at concentrations of ca. 2 x 10^{13}, 2 x 10^{11} and 2 x 10^9 particles/ mL. Each condition was tested in six replicates. Cell viability was determined via 3-[4,5-dimethylthiazol-2-yl]-2,5-diphenyl tetrazolium inner salt (MTS) assay. 2 x 10^{13} particles/ mL is about 63 μM for PA/ azSQ (FP_5).

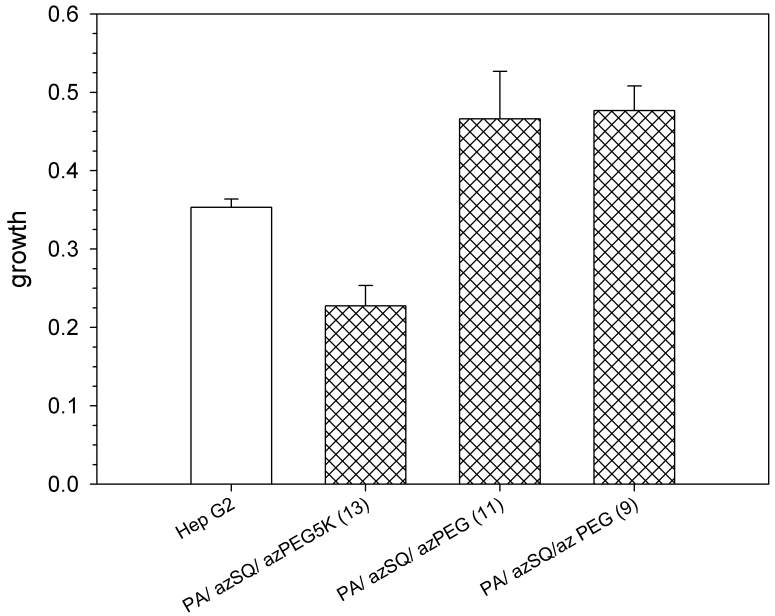

Figure 2.18: Proliferation of HepG2 cells after 2 days of incubation with PA/ azSQ/ azPEG (FP_7) nanoparticles at concentrations of ca. 2 x 10^9, 2 x 10^{11} and 2 x 10^{13} particles/ mL. Each condition was tested in six replicates. Cell viability was determined via 3-[4,5-dimethylthiazol-2-yl]-2,5-diphenyl tetrazolium inner salt (MTS) assay. 2 x 10^{13} particles/ mL is about 37 μM for PA/ azSQ/ azPEG (FP_7).

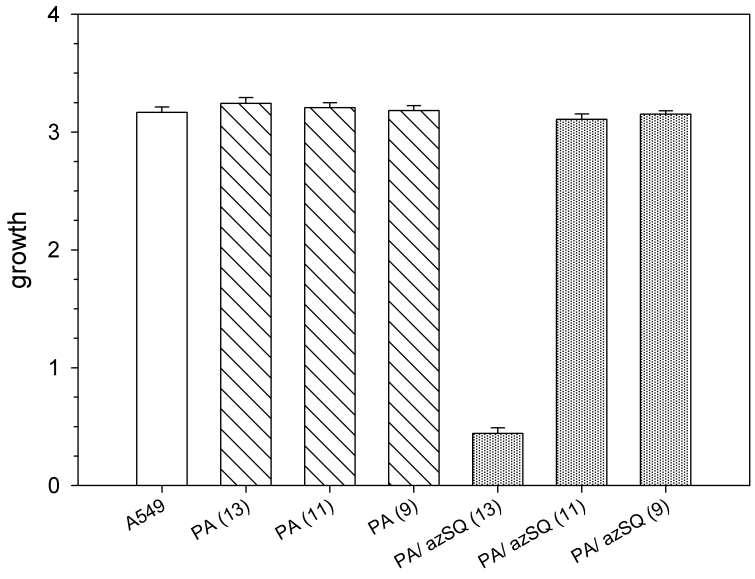

Figure 2.19: Proliferation of A549 cells after 2 days of incubation with neat PA and PA/ azSQ (FP_5) nanoparticles at concentrations of ca. 2 x 10^9, 2 x 10^{11} and 2 x 10^{13} particles/ mL. Each condition was tested in six replicates. Cell viability was determined via 3-[4,5-dimethylthiazol-2-yl]-2,5-diphenyl tetrazolium inner salt (MTS) assay. 2 x 10^{13} particles/ mL is about 98 μM for PA/ azSQ (FP_5).

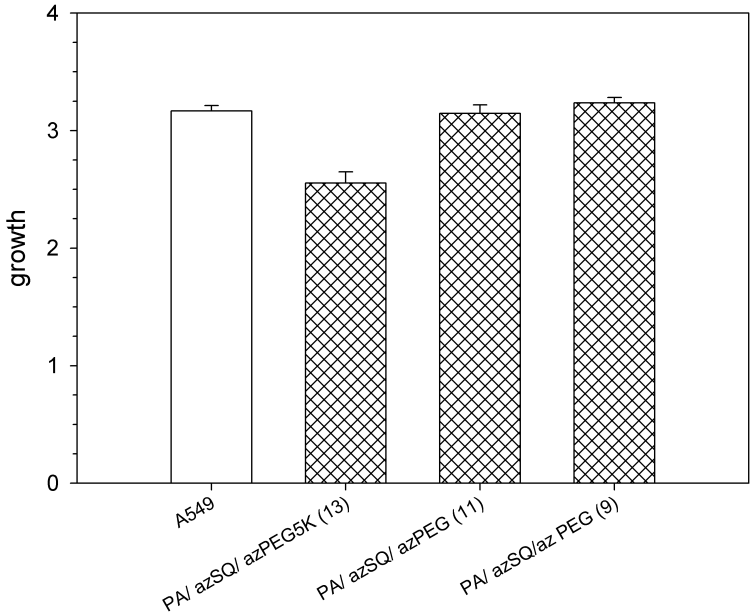

Figure 2.20: Proliferation of A549 cells after 2 days of incubation with PA/ azSQ/ azPEG (FP_7) nanoparticles at concentrations of ca. 2 x 10^9, 2 x 10^{11} and 2 x 10^{13} particles/ mL. Each condition was tested in six replicates. Cell viability was determined via 3-[4,5-dimethylthiazol-2-yl]-2,5-diphenyl tetrazolium inner salt (MTS) assay. 2 x 10^{13} particles/ mL is about 75 μM for PA/ azSQ/ azPEG (FP_7).

Chapter 3

Surface modified colloids with targeting molecules to disrupt Survivin activity and enhance apoptosis in cancer cells

3.1 Attributions

The synthesis of the unmodified and azide modified small molecules was conducted or aided by Dr. Yuriy P. Bandera at Clemson University. The preparation of Survivin and gel affinity pull down studies were carried out by Andrew A. Kelso, Dr. LeAnna L. Ledford and Dr. Michael G. Sehorn at Clemson University. The cellular studies in glioblastoma cells were carried out with the aid of Dr. Mrinmay Chakrabarti and Dr. Swapan K. Ray at University of South Carolina. Cell growth and viability assessments in A549 cells were conducted with the aid of Ashlee Tietje and Dr. Yanzhang Wei at Clemson University. The results in this chapter are in preparation for publication as Jenkins et al., Sequestring Survivin to functionalized nanoparticles: A strategy to enhance apoptosis in cancer cells, 2015.

3.2 Introduction

A prophetic indicator of cancerous cells is their circumvention of programmed cell death (apoptosis). The maintenance of tumors has been speculated to be achieved through nodal proteins that are involved in multiple signaling mechanisms[177]. One such protein *Survivin* (BIRC5), a member of the inhibitors of apoptosis (IAP) family, is vital for cellular homeostasis, playing a role in cell division and cell death[178], This protein is abundant in embryonic and fetal development[179], but is below detection limits in most terminally differentiated adult tissues[180, 181, 182], though it has been detected in primitive hematopoietic cells, T lymphocytes, polymorphonuclear neutrophils, and vascular endothelial cells[183]. A number of studies have shown that Survivin is overexpressed in human cancers and its appearance in a patient results in an increased risk factor for cancer progression and a poor prognosis[180, 184, 185, 186, 187, 188]. Survivin appears to bestow on tumor cells an enhanced adaptability, capacity to proliferate, and aversion to cell death[189, 190, 191]. Achieving apoptosis is integral to the cytotoxic activity of most chemotherapeutic drugs and radiation therapies and their reduced potency stems from antiapoptotic proteins[192]. In an effort to enhance the potency of cancer therapies, the targeting of antiapoptotic proteins expressed by cancer cells has become an important approach to cancer treatment[193].

The focus on Survivin as a means to combat cancer through a mitigation of its antiapoptotic functions has resulted in a number of inhibition or sequestration strategies, with only three inhibitors reaching clinical trials by 2013[194]. These inhibition or sequestering strategies can be divided into four broad categories: (1) molecular antagonists (antisense oligonucleotides, siRNA, and transfection of a plasmid encoding the dominant-negative Survivin) based inhibition[195, 196, 197, 198, 199, 200, 201, 202]; (2) gene therapy with small molecules such as YM155 or FL118[203, 204, 205, 206]; (3) immunotherapy, where the immune cells such as natural killer cells, dendritic cells, and cytotoxic T lymphocytes, are isolated from the patient, activated *in vitro* and transfused back to the patient to target cancer cells[194, 207, 208]; and (4) Survivin binding small molecules which attach to the protein to disrupt its antiapoptotic function[209, 210]. The antisense or siRNA approaches may result in undesirable broad phenotypic consequences, effecting normal cells and exhibit varying anti-cancer potency *in vitro*, *in vivo*, and in humans[194, 198, 211]. There is also a lack of appreciation in how these antisense oligonucleotides distribute to tissues and are taken up by cells in the human body[212]. The dominant-negative Survivin method in treating cancers is still clinically impractical,

as the mutant protein is unstable in the blood stream[194]. Phase II clinical trials of YM155, a small molecule Survivin gene suppressant, failed as adverse effects were reported and the objective tumor response rate (ORR) of patients to the treatment was only 3 - 6 %[213, 214]. Immunotherapy is a relatively new strategy compared to the other methods, and investigations are being carried out to find the epitopes that generate the strongest immunodominant, immunoprevalent T-cell reaction against Survivin[215]. Finally, the use of small molecule ligand that simply binds to the protein and disrupts Survivin's activity may present a more focused and less destructive therapeutic approach if the binding can be designed to only occur in a tumor of interest[206, 216]. Unfortunately, the widespread development of new binding ligands for Survivin is frustrated by the perceived lack of structural pockets of the appropriate geometry and hydrophilicity on the protein that act as a druggable site[209]. Survivin forms a bow-tie shaped symmetrical homodimer and contains a single baculoviral IAP repeat (BIR) domain, which is common in the IAP family[217]. A newly discovered small molecule binding site at the dimer interface on Survivin, which is distinct from the BIR site, has been recently reported[209]. This second potential binding site appears to possess a higher propensity for small-molecule binding than the BIR site, though the functional role of this site is currently unknown. Nonetheless, it is speculated that the interface site may be involved in binding to other proteins that regulate Survivin function of inhibiting apoptosis[209, 218]. Recently, high-affinity small molecule "Survivin ligands" have been proposed by Abbott Laboratories for binding to the site[209] and, based on their structural variability, this site may be a biologically relevant protein binding site that can be targeted with small molecule drugs. The small molecule ligand binds at the dimer interface and frustrates the binding of other proteins to the site, leading to the activation of apoptosis. A recent effort[218] has focused on a modified Abbott ligand[209] that was designed to disrupt the Survivin-Ran protein complex, a complex identified to promote spindle formation in tumor cells[219].

All the strategies mentioned previously exhibit varying degrees of success for disrupting the function of Survivin, but all suffer from inherent problems such as systemic toxicity, reduced bioavailability, and ineffective delivery[194]. These setbacks can be overcome by employing different delivery platforms such as liposomes, dendrimers, and polymeric nanocarriers that can enhance a drug's protection, availability, and tissue distribution[194], resulting in an improved effectiveness[194, 220, 221, 222, 223, 224, 225]. To this end, a small molecule drug that binds to Survivin was modified to allow its attachment to the surface of sub-100 nm polymer particles to assess its propensity to bind

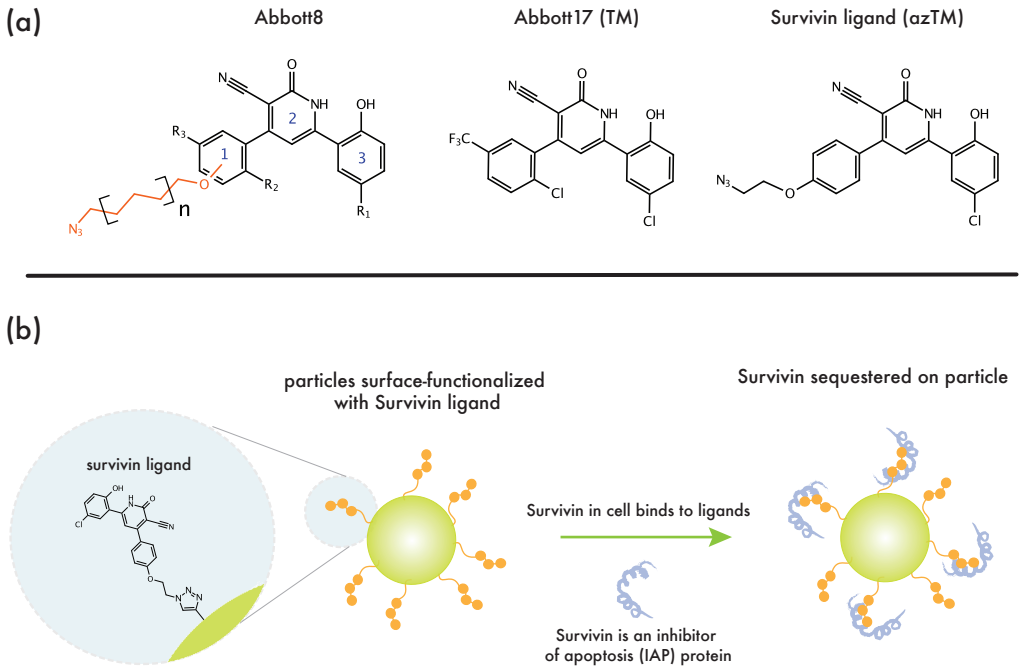

Figure 3.1: **(a)** Structures of Survivin ligands, Abbott8 and Abbott17 (targeting molecule TM) proposed by Abbott Labs and an azide modified targeting molecule (azTM). **(b)** Schematic of 50 nm poly(propargyl acrylate) (PA) particles surface modified with an azide-terminated Survivin ligand (azTM) through an aqueous-phase "click" transformation sequestering anti-apoptotic protein Survivin.

with Survivin and its effectiveness in inducing apoptosis relative to the "free" drug. Specifically, the "Survivin ligand" developed by Abbott labs was selected for this comparison[209]. In this current effort, the ligand was modified to include an azide group and attached to poly(propargyl acrylate) nanoparticles through an azide/alkyne Huisgen cycloaddition using a copper catalyst. These surface-modified particles were incubated with various cancer cell lines that are known to overexpress Survivin. The extent of Survivin sequestration and resulting enhancement in apoptosis was assessed.

3.3 Results & Discussion

Figure 3.1 presents the structures of the Survivin-binding ligands and the proposed route for "capturing" free Survivin with nanoparticles surface modified with ligands. As indicated earlier, prior art has focused on several Survivin inhibition approaches, such as, antisense oligonucleotides targeting mRNA, immunotherapeutic strategies, and small molecule binding to the BIR (Baculoviral

IAP repeat) domain. A new binding site at the dimer interface of Survivin, distinct from the BIR site, has been recently identified and appears to have an increased binding to small molecules and maybe useful for targeting & inhibition. Recently, high-affinity small molecule "Survivin ligands" have been proposed for binding to the site by Abbott Labs with binding constants (K_D) ranging from 0.037 μM to 0.88 μM and were obtained by monitoring the chemical shift changes as a function of ligand concentration[209]. According to their studies, a favorable binding of a small molecule to the dimer interface is indicated by a small value binding dissociation constant, K_D. A K_D value of sub-5 μM suggests a relative strong affinity. In their studies, it was speculated that the dimer interface plays an important role in binding to other proteins which serve a role in apoptosis. This was subsequently proven with a variant (LLP3) of an Abbott Labs compound which also binds to the dimer interface of Survivin and was utilized to prevent Ran from binding to Survivin and forming a Survivin-Ran protein complex. This disruption allowed the native apoptosis pathway to continue[219].

Figure 3.1a presents the Abbott8 compound (with labeled rings) employed by Abbott to establish the structure-activity relationship (SAR) of the Survivin ligand. In these original studies, ligands that bind to Survivin shared in a number of structural characteristics. Through high temperature superconductor (HTS) NMR studies[209], it was determined that Ring-2 must be a central pyridone, while Ring-3 must be a phenol, so that a hydrogen bonding network can form, via the 2-hydroxypyridine central ring tautomer, forcing the two rings into a coplanar arrangement. In addition, a cyano group must be on the center ring (Ring-2)[209, 226] for binding, though NMR structures provided no indication of a specific interaction with Survivin. Replacing this latter group with carboxamide, methyl, halogen, or hydrogen all greatly diminished binding[209]. In addition, only hydrophobic groups were preferred when substituted into Ring-1. On this latter ring, substitutions on 2,4 and, particularly, 2,5 with chlorine and methyl groups at the 2 position, with chlorine, methyl, and CF_3 substitution at the 4 and 5 positions resulted in energetically acceptable structures[209]. In the current effort, azide terminated methoxyalkanes with $(CH_2)_n$ of n=2 at position 4 of Ring-1 (Figure 3.1a; azTM) was employed to covalently attach the ligand to a poly(propargyl acrylate) (PA) particle through a copper-catalyzed click transformation (cf. Figure 3.1b).

***in vitro* viability and apoptosis studies of Survivin ligands in glioblastomas.** Currently, there are not many *in vitro* cytotoxicity studies in the literature that demonstrate that the Abbott-

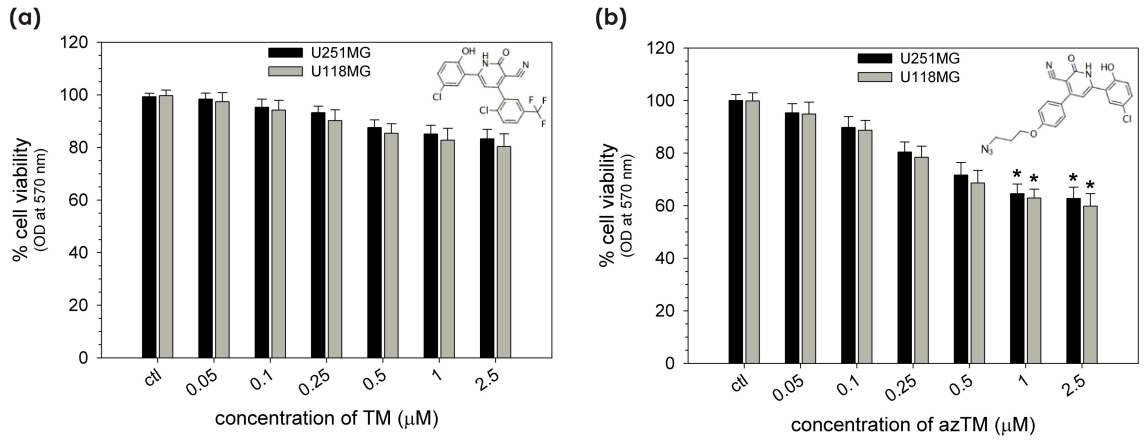

Figure 3.2: Preliminary cell viability data in glioblastoma cells, U251MG and U118MG, using MTT assay. Untreated cells were used as the control (ctl). Cells were treated with the small molecule ligands at the indicated concentrations for 24 hours. Cell viability is presented as a percentage of viable cells in the total population. Significant difference from control value was indicated by *p<0.05. **(a)** TM and **(b)** azTM treatment of the glioblastomas.

derived Survivin ligands can disrupt Survivin activity and induce apoptosis[216, 218, 227, 228]. To that end, the Survivin ligand originally proposed by Abbott Labs (6-(5-Chloro-2-hydroxyphenyl)-4-[2-chloro-5-(trifluoromethyl)phenyl]-2-oxo-1H-pyridine-3-carbonitrile; TM) and its structural analog modified with an azide linker (4-[m-(2-Azidoethoxy)
phenyl]-6-(5-chloro-2-hydroxyphenyl)-2-oxo-1H-pyridine-3-carbonitrile; azTM) (cf. Figure 3.1a) were synthesized and tested to verify their potential for Survivin activity disruption in two human glioblastoma cell lines, specifically U251MG and U118MG, which exhibit Survivin overexpression[184]. Glioblastomas are the most common form of malignant primary brain tumors and they have a propensity to encroach quickly into the surrounding tissues, frustrating surgical routes to their removal[184, 191]. These tumors were chosen for study as they exhibit an increased resistance to apoptosis and are relatively resistant to radiation and chemotherapy[184, 191].

Figure 3.2 presents the determination of cell viability of targeting molecules, TM or azTM, using the 3-(4, 5-dimethylthiazol-2-yl)-2, 5-diphenyl tetrazolium bromide (MTT) assay. Cell viability is presented as a percentage of viable cells in the total population and a significant difference from the control value was indicated by a p-level with $^*p<0.05$[184, 229]. The original Abbott-developed drug TM exhibited a ca. 10% reduction in cell viability for both cell lines that was not statistically significant, while the azide-modified version azTM resulted in a statistically significant reduction of ca. 30 % in viability for both cell lines at a dosage of 2.5 μM. A cell death of over 30 % at a dosage of

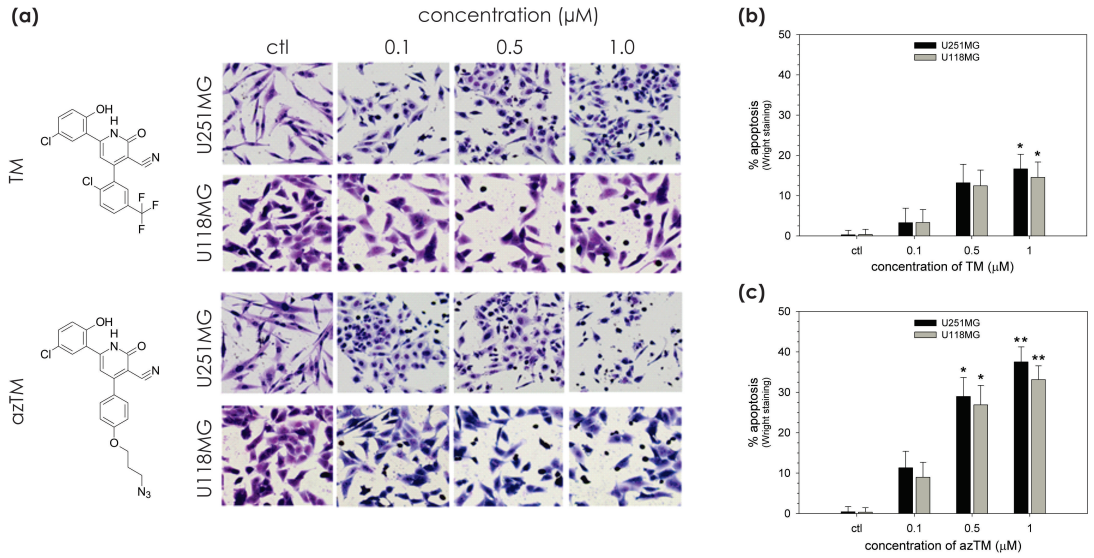

Figure 3.3: Increased apoptosis in glioblastoma cells, U251MG and U118MG, with azTM small molecule ligand when compared to TM. Untreated cells were used as the control (ctl). Cells were treated with TM or azTM ligand at indicated concentrations for 24 hours. **(a)** In situ Wright staining for detection of morphological features of apoptosis. Bar diagram shows percent apoptosis based on Wright staining for **(b)** TM and **(c)** azTM treatments. Cell death is presented as percentage of apoptosis in total population. Significant difference from control value was indicated by *p < 0.05 or **p < 0.01.

2.5 μM indicates a high ratio in comparison to other Survivin activity disruption studies; a study on the cytotoxicity in glioblastomas of a number of small molecules derived from 6-(*o*-Hydroxyphenyl)-2-oxo-4-phenyl-1H-pyridine-3-carbonitrile (i.e. Abbott8)[209] was recently presented[218]. In this study, the IC_{50} value for the lead compound (LLP3), a variant of Abbott8, was determined to be 31.2 μM, which is an order of magnitude greater than that of azTM for a similar efficacy. Assuming that the enhancement is due to an increased Survivin binding to azTM, the structural difference between TM and azTM is localized to Ring-1 (cf. Figure 3.1). The substitution of the trifluoromethyl group and chlorine on Ring-1 with the azidoethoxy group is speculated to enhance the binding of the drug to the dimer interface of Survivin[209]. The occupancy of the dimer interface has been theorized to interfere with Survivin's binding to other proteins which are required to activate its IAP functions. Specifically, LLP-3 was designed from Abbott8, the targeting molecule used in this project, by adding 2 phenyl rings to displace the Leu98 and Leu102 interactions in Survivin dimerization and weaken the protein-protein interface and results in blocking the binding of Survivin to Ran[218, 230]. GTP-binding nuclear protein Ran is a protein that is encoded by the RAN gene in humans and is a regulator of bipolar mitotic spindle assembly.

The observed efficacy of azTM in promoting cellular death in the U251MG and U118MG cell lines could be through an enhanced apoptosis (desired programmed cell death) or simply toxicity of the drug. In order to differentiate these routes to cell death, a standard *in situ* Wright staining study was employed (cf. Figure 3.3a). Typical morphologic changes in cells undergoing apoptosis include cell shrinkage, enhanced round shape, chromatin condensation, blebbing of cell membrane, and enhanced refractivity of cells under phase-contrast imaging[231]. Utilizing these visual descriptors, the cells treated with TM and azTM at a concentration of 0.1, 0.5, and 1.0 μM were compared to the untreated control cells and observed the morphological features of apoptotic cells (cf. Figure 3.3). Figure 3.3b presents the number of cells undergoing apoptosis relative to the control, and while both drugs resulted in enhanced apoptosis in both cells lines, azTM resulted in a greater proportion of cells exhibiting these feature at a set concentration relative to cells incubated with TM. The azTM treatment with 1 μM induced more than 35 % apoptosis in both cell lines and corresponds to the cell death observed in the viability study (cf. Figure 3.2). This data is presented in a bar graph in Figure 3.3b. These results confirm that azTM induces apoptosis and disrupts Survivin activity more effectively than the original TM small molecule ligand.

Surface-functionalized particles. The previous studies are promising and indicate that the Abbott derived Survivin targeting ligands are a potential tool for Survivin activity disruption as a small molecule. However, small molecules have a short *in vivo* circulation lifetime, which limits the feasibility of Survivin ligands for use in therapies. To circumvent this issue, the small molecule azTM can be attached to poly(propargyl acrylate) (PA) nanoparticles to increase circulation times and at the same time allowing the ligands to form beneficial host/ guest assemblies. A schematic of the particles studied in this effort is presented in Figure 3.1b. The PA colloids were prepared using a standard aqueous emulsion polymerization technique resulting in spheres with a diameter of 66.1 $\pm$ 0.26 nm. To functionalize the surface of the particles, a multiple step copper-catalyzed azide/alkyne cycloaddition ("click" transformation) was performed in water to produce PA particles that had Survivin ligand and polyethylene glycol (PEG) attached to their surface. To attach the azide modified Survivin ligand to the particles, the azTM was initially clicked onto the particles for 15 minutes and then the reaction was stopped by the removal of unreacted azTM, sodium ascorbate, and Cu(II)SO_4 through a repeated particle washing procedure consisting of centrifugation and redispersement in tetrahydrofuran(THF) and methanol. The cleaned PA/ azTM particles were

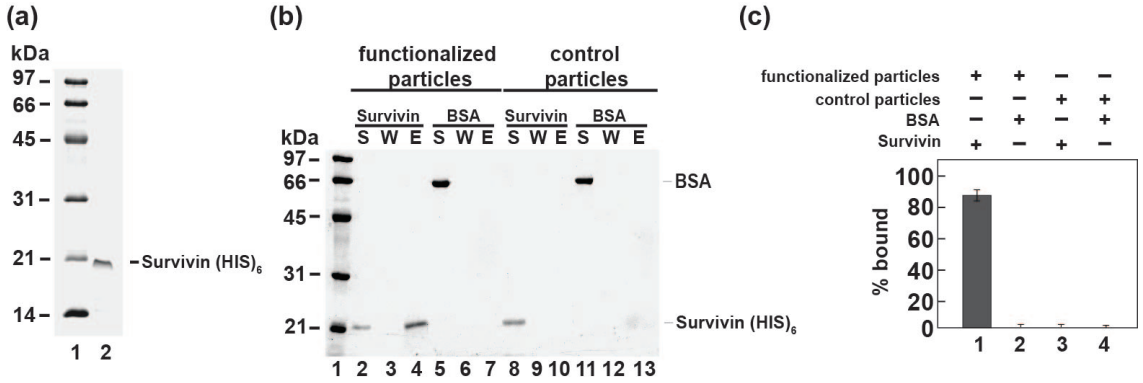

Figure 3.4: Purification of Survivin and affinity pull-down of Survivin by surface-functionalized particles. **(a)** SDS-PAGE of purified recombinant Survivin (ca. 0.8 μg); **(b)** Poly(propargyl acrylate) (PA) particles were surface modified with azTM (cf. Figure 3.1) and azPEG. Control particles lacked the presence of ligand. Both sets of particles were incubated with Survivin or BSA protein. The supernatant was removed and the particles were washed with buffer. Proteins retained on the particles were eluted. The supernatant (S), wash (W) and elution (E) were separated on a 15 % polyacrylamide gel and stained with Coomassie blue. **(c)** Percentage of bound proteins on functionalized and control particles (data taken from SDS-PAGE in Part **(b)** as well as two other pull-down experiments).

subsequently utilized in a secondary click transformation with azide-modified polyethylene glycol chains with molecular weight of 5k (azPEG) that was allowed to run for 24 hours and then washed to remove unreacted species; these particles are referred to as PA/ azTM/ azPEG particles. We have demonstrated previously that this method of cleaning was sufficient to remove all the copper from the system and these cleaned particles are not toxic to cells[31, 71]. In addition cytotoxicity tests were carried out using PA/ azPEG particles (data not shown) to verify that these particles are not toxic. The use of PEG to infer a hydrophilicity to the particles has been found to be important for directing protein absorption in the particles and achieving long circulation times[77].

Selective binding of functionalized particles. As stated earlier, prior art suggests that the ligand directly binds at the dimer interface of Survivin. Computational modeling of the molecular interactions along the dimerization interface[209, 230], affinity screening studies[209], cytotoxicity studies[218, 227, 228] and fluorescence binding studies of several modified analogs of TM with the wild-type protein and the mutant form of Survivin$^{F101A/L102A}$[218], have been explored to establish the direct binding between the small molecule "free" ligand and Survivin, but no studies have been performed to establish the efficacy of the ligands when attached to the surface of nanoparticles. To this end, affinity pull-down experiments were employed. A purification protocol that utilized both affinity and conventional chromatography to purify Survivin to near homogeneity was developed

(Figure 3.4a). About 0.4 mg of Survivin was obtained from 60 g of bacterial cell pellet. The particles were surface modified with an azide-terminated (azTM) conjugate and poly(ethylene glycol) (azPEG) chains of 5k molecular weight attached to their surface while control particles only had the azPEG modification. After incubation of the particles with purified Survivin, the supernatant was removed and the particles were washed with buffer. Any Survivin retained on the particles was eluted and subjected to SDS-PAGE analysis. As indicated in Figure 3.4b, Survivin bound the functionalized particles evidenced by its presence in the elution (cf. Figure 3.4b, lane 4). The interaction with the azTM conjugate is specific since Survivin is only present in the supernatant with the control azPEG particles (cf. Figure 3.4b, lane 10). As expected, bovine serum albumin (BSA) failed to interact with either the azTM or the azPEG.

Figure 3.4c quantifies the results presented in Figure 3.4b, as well as two other pull-down experiments. In this figure, the columns of + or - above the graph indicate what combination of particle and protein was employed. For example, in lane 1, the amount of bound Survivin on the functionalized particles was quantified while in lane 2, the amount of BSA on the functionalized particles was assessed. Lane 3 & 4 are the control lanes and present the amount of bound protein with Survivin & control particles (lane 3) and BSA & control particles (lane 4). These results suggest that the binding specificity of the Survivin ligand is not altered when attached to particles and over 85 % of the Survivin bound to the functionalized particles.

Enhanced apoptosis with functionalized particles. It's clear that the functionalized particles are capable of selectively binding Survivin, but the question remains, will this binding of the protein result in any enhancement of apoptosis of cancer cells. The precise mechanism by which Survivin suppresses apoptosis is still in debate, but it is speculated that Survivin directly suppresses Caspase-3, a protein which is believed to play a central role in the execution-phase of cell apoptosis[190]. To this end, Western blotting for Survivin and other proteins involved in Caspase-mediated apoptosis was employed to determine how effectively the modified particles restrain Survivin activity in comparison to the "free" drug. Both glioblastoma cell lines were treated with azTM or PA/ azTM nanoparticles (1.0 μM ligand concentration) prior to extraction of protein samples. Protein samples were separated by SDS-PAGE and Western blotting was performed using the primary IgG antibodies against Survivin, Caspase-3, and β-Actin. The horseradish peroxidase conjugated anti-rabbit IgG was used as secondary antibody. Western blots were incubated with ECL detection reagents,

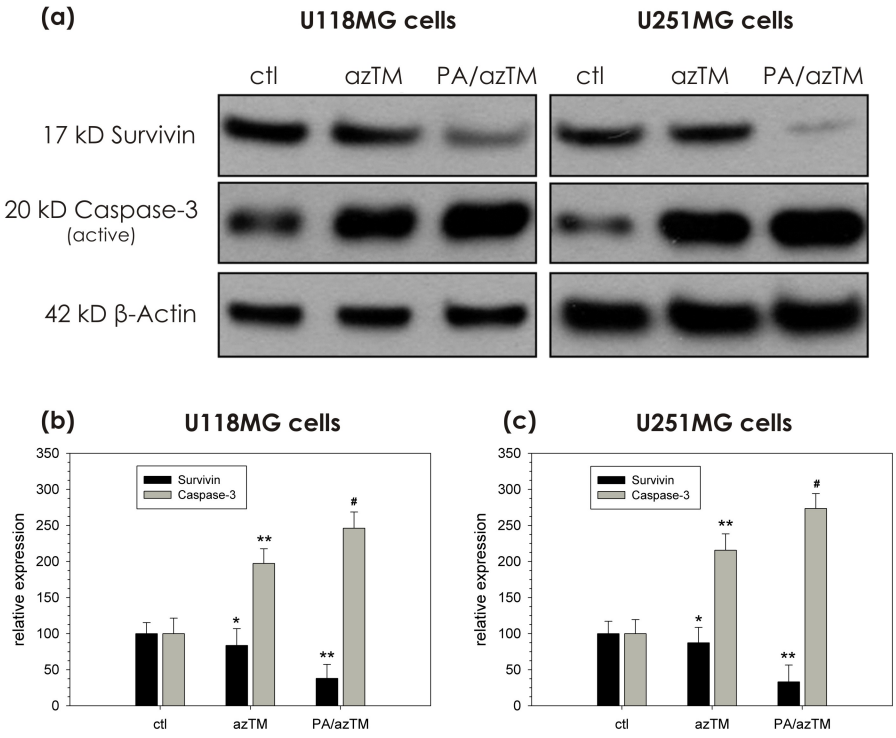

Figure 3.5: **(a)** Survivin conjugate azTM disrupted the activity of Survivin to promote Caspase mediated apoptosis. Both glioblastoma cell lines were treated with Survivin conjugate azTM as a free small molecule or attached to the surface of nanoparticles (1.0 μM ligand concentration) prior to extraction of protein samples. Protein samples were resolved by 4 - 20 % SDS-PAGE and Western blotting was performed using the primary IgG antibodies against Survivin, Caspase-3, and β-Actin. Quantification of expression of Survivin and Caspase-3 after treatment with free ligand (azTM) and modified particles (PA/ azTM) in **(b)** U251MG or **(c)** U118MG cells. Significant difference from control value was indicated by *p<0.1, **p<0.01 and #p<0.001.

exposed to X-OMAT AR films, and photographed (cf. Figure 3.5). The Western blot indicated that both azTM and PA/ azTM nanoparticles increased the activation of Caspase-3, the final executioner of apoptosis, in these glioblastoma cell lines. Importantly, PA/ azTM nanoparticles exhibited a pronounced Survivin sequestration relative to the "free" azTM for activation of Caspase-3 for apoptosis in both glioblastoma cell lines. Figure 3.5 presents the quantification of the Western blot data. For both the cell lines, the quantification demonstrated that the Caspase-3 expression was increased by 95 % and 140 % for azTM and PA/ azTM, respectively, when compared to the untreated control cells. In addition, it was noticed that for the PA/ azTM treatment, the expression of Survivin was decreased by 60 %. This decrease might not be an actual reduction in expression of Survivin as it is speculated that the sequestered Survivin could have still been bound to the nanoparticles and couldn't be extracted completely for SDS-PAGE and Western blotting studies.

Viability studies in other cell lines. To further support and validate the results obtained in the glioblastoma cells, cell viability studies were carried out in the A549 line, cell line known to overexpress Survivin[232]. Figure 3.6 presents the cell viability data with A549 cells using the MTS assay. A549 cells are a human alveolar adenocarcinoma cell line which can synthesize lecithin with a high percentage of disaturated fatty acids and are believed to be responsible for pulmonary surfactant synthesis[169]. The cells were treated with azTM and PA/ azTM with two different grafting densities (gd), 0.58 and 1.91 azTM/nm^2, at varying concentrations for 48 hours. In A549 cells, the small molecule and modified particles exhibited the same behavior as exhibited in the glioblastomas cells, though there was an observed dependence on cell reduction with the particle's azTM grafting density. In this A549 line, the "free" molecule exhibited an IC_{50} of 25 μM, while particles with a grafting density of 0.58 gave an IC_{50} between 1 and 6.5 μM. Surprisingly, particles with a higher grafting density of 1.91 gave an IC_{50} that was greater than 25 μM. Similarly, PA/ azTM particles with a low grafting density of 0.77 azTM/nm^2 gave an IC_{50} between 6.5 and 25 μM in MCF7 cells, a human breast adenocarcinoma cell line. Clearly, the dosage of the small molecule azTM when attached to the particles is a combination of particles administered and the grafting density of the ligand to the particle, so a range of particles with grafting densities were investigated. Figure 3.7 presents the A549 cell viability with particles of varying grafting densities. As a reference point, 1 μM concentration the free ligand (azTM) indicated cell death of ca. 15%, which is lower than the 35 % obtained from glioblastomas (cf. Figure 3.6). For the "free" molecule, this lower efficiency in the A549 cell line could be due to the fact that the over-expression of Survivin in A549 might be higher than in Glioblastomas; it is commonly observed that the efficiency of drugs or targeting molecules varies with different cell lines due to the differing expression levels[232]. From Figure 3.7, particles with the lowest grafting density (e.g., 0.58 azTM/nm^2) exhibited the greatest impact in cell viability with a 60 % reduction at an azTM concentration of 6.5 μM. Subsequent increases in dosage with the 0.58 azTM/nm^2 particles result in a reduction in efficacy that converge on the cell viability exhibited with particles of higher grafting density. Particles with grafting densities between 0.90 and 1.91 azTM/nm^2 exhibited similar efficacies with a IC_{50} which is greater than 25 μM.

It is speculated that the enhanced IC_{50} values for particles with higher grafting densities was due to an inability of the protein to bind to the particles because of steric concerns. The surface grafting density of 1.91 azTM groups/nm^2 corresponds to a 91 % coverage (on a 67 nm diameter particle) if the distance of an azTM at its widest point (ca. 7.8 Å) can be assumed to define the

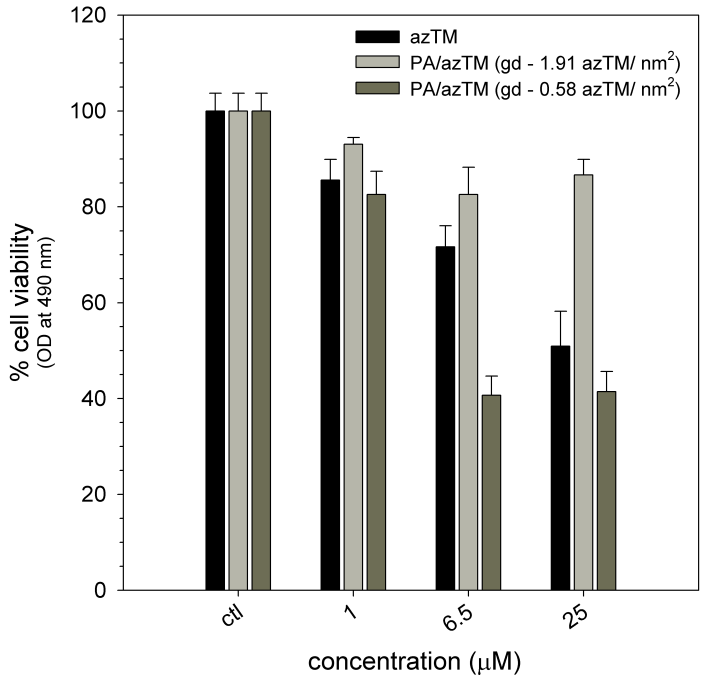

Figure 3.6: Cell viability of A549 cells treated with small molecule azTM and PA/ azTM particles with two different grafting densities (gd), 0.58 and 1.91 azTM/nm^2, at varying concentrations for 48 hours. Cell viability is presented as percentage of viable cells compared to the control and the MTS assay was employed.

diameter of a cylinder enclosing the moiety and attached to the PA surface; each particle would then have ca. 29.5k azTM moieties. Similarly, it was noticed that particles modified with both azTM and long azPEG chain (5k) exhibited a decreased percentage of cell death (data not presented). This decrease could be due to the fact that the long PEG chains physically hinder the binding of the ligand with a Survivin protein or that a higher dosage is required because the transport of the particles into the cells is reduced with the large hydration shell when the PEGs are attached to the particles[233, 234, 235, 236].

Functionalized particles localized in cells. Survivin has been found to only operate within the cell, and to verify that these particles are taken up by the cells and not just located on the surface of cell, particles were modified with the Survivin ligand (azTM) and a near infrared fluorophore squaraine (azSQ). A549 cells were treated with 15 μM PA/ azTM/ azSQ for 24 hours and washed with PBS before imaging. The fluorescence from the squaraine dye was used to identify that the particles were taken up by the cells (cf. Figure 3.8). In methanol, azSQ has a peak absorption

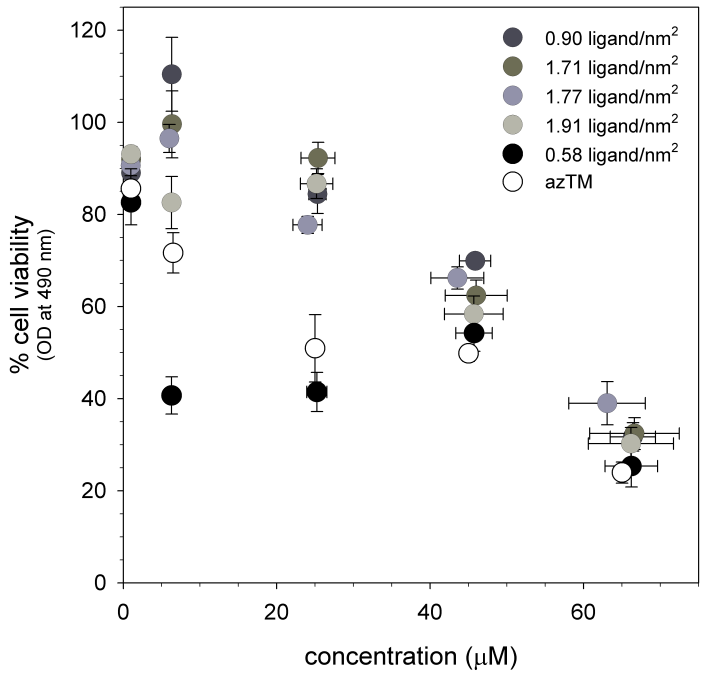

Figure 3.7: Viability of A549 cells with PA/ azTM particles of varying ligand surface density. The cells were treated with azTM and PA/ azTM of varying different grafting densities (gd) of 0.58, 0.90, 1.71, 1.77 and 1.91 azTM/ nm^2 and at varying concentrations for 48 hours. Cell viability is presented as percentage of viable cells compared to the control and the MTS assay was employed.

maximum at 663 nm, while the corresponding emission peak is at 672 nm, for a relatively small Stokes shift of 9 nm. Previous efforts from this laboratory have indicated that PA/ azSQ particles are activated by the phospholipids in cells and typically taken up through endocytosis and localize in the late endosomes and lysosomes of UMSCC22A head and neck cancer cells[71]. Based on these previous studies, we speculate that the PA/ azTM/ azSQ particles would also be taken up by the A549 cells through endocytosis and localize in the endosomes and lysosomes of the cells after a 24 hour treatment. This is confirmed in Figure 3.8 where, due to the low quantum yield of the azSQ, the brightness and contrast of the image obtained was increased to enhance the emission of the PA/ azTM/ azSQ particles. In addition, the imaging study was carried out with an azide terminated Coumarin-6 (zC6). The azC6 is attached to the PA/ azTM particles through a secondary click reaction and referred as PA/ azTM/ azC6. The A549 cells were treated with the PA/ azTM/ azC6 particles for 24 hours and then washed with PBS. This fluorophore has a higher quantum yield than azSQ and is easier to visualize; the fluoroscope images of the localization of modified particles with

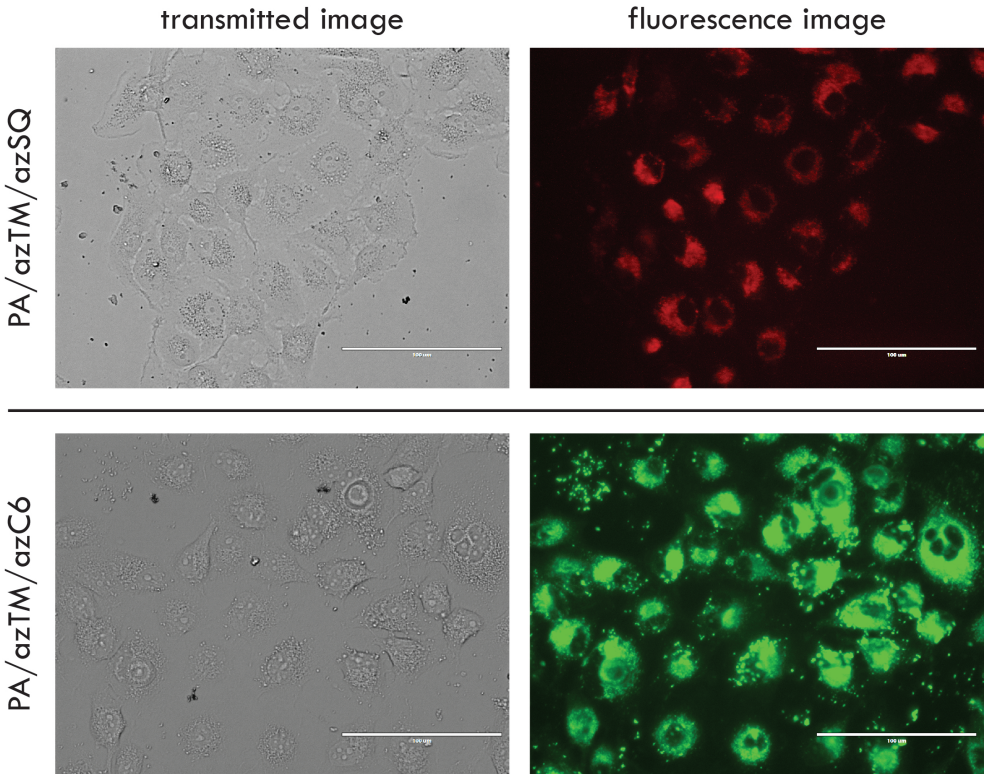

Figure 3.8: Imaging of A549 cells treated with 15 μM PA/ azTM/ azSQ and PA/ azTM/ azC6 for 24 hours and fluorescence images were taken under RFP and GFP filters, respectively. All scale bars represent 100 μm.

azC6 in the A549 cells can be clearly seen (cf. Figure 3.8). In THF, azC6 has a peak absorption maximum at 437 nm, while the corresponding emission peak is at 485 nm, which gives a large Stokes shift of 48 nm and also couples in well with the properties of the GFP filter of the fluoroscope.

In addition, an apoptotic/necrotic/healthy cells detection kit that contains three stains: Hoechst 33342, Annexin V labeled fluorescein, and Ethidium homodimer III, was employed to establish the state of the A549 cells when incubated with PA/ azTM particles. Hoechst 33342 (λ_{abs}/ λ_{em} = 350/461 nm) is a membrane permeable dye, which stains the nuclei of the cells as it binds specifically to the DNA[237]. Upon binding to the DNA, the Hoechst dye emits a blue fluorescence that can be seen under a DAPI filter of the fluoroscope[238]. For healthy cells where the DNA is intact, the emission is bright, while for apoptotic or necrotic cells the emission is dimmer if the treatment damages the DNA of the cell[237, 239, 240]. Annexin V labeled fluorescein (FITC - Annexin V) (λ_{abs}/ λ_{em} = 492/514 nm) is used to detect apoptotic cells. In apoptosis, the disassembly of the cell takes place with changes in the phospholipid content of the outer leaflet of the cytoplasmic

membrane and the Phosphatidylserine (PS) is translocated from the inner to the outer surface of the cell for phagocytic cell recognition[241]. Annexin V (35 kD) is a phospholipid protein that binds to the translocated PS with a high binding affinity and upon binding to the PS, the FITC-Annexin V emits a bright green fluorescence that can be seen with a GFP filter of the fluoroscope[242, 243]. For the detection of necrotic cells, an Ethidium homodimer III (EthD-III) (λ_{abs}/ λ_{em} = 528/617 nm) stain is used. EthD-III is a highly positively charged nucleic acid probe, which is impermeant to live or apoptotic cells, but stains necrotic cells intensively with red and can be seen under a RFP filter of the fluoroscope[244, 245].

In the current study, A549 cells were treated for 24 hours with 25 μM of azTM, unmodified PA particles, PA/ azTM particles of two different grafting densities of 0.63 and 1.77 azTM/ nm^2, and PA/ azTM/ azPEG particles. After the treatment, the cells were stained with the Hoechst 33342, FITC-Annexin V, and EthD-III stains as per the manufacturer's instructions and imaged with a standard fluoroscope and Figure 3.9 presents the images obtained. As expected, for the two control treatments (cf. Figure 3.9 - panels 1 to 6), only the emission from Hoechst staining (blue) was seen. This confirms that the cells are healthy and that the PA particles are not toxic. For the azTM treated cells, the Hoechst staining (cf. Figure 3.9 - panel 7) indicated that the number of healthy cells decreased by ca. 38 % which was coupled with a decrease in the intensity of the blue emission, suggesting the possibility of DNA damage. In addition, the emission was not a normal bright round spot but appeared to be shaped like clumped random strands. It was subsequently verified that this blue emission from random strand like shapes was attributed to the emission of the azTM and not the Hoechst dye. The azTM treated cells indicated ca. 43 % apoptotic cell death and the images obtained (cf. Figure 3.9 - panels 7 to 9) suggested that the cells were in the late apoptotic stage, as they were stained by all the three dyes (blue, green and red). When cells are stained with the triple colors blue, green, and red, this indicates that those cells are dead cells progressing from apoptotic cell population[246, 247]. For the treatment of PA/ azTM particles with a grafting density of 0.63 azTM/ nm^2 (cf. Figure 3.9 - panels 10 to 12), ca. 66 % reduction in healthy cells was observed and the late apoptotic cell population was ca. 18 %. In this treatment, the apoptotic cell death was lower than expected, which could be due to a loss of dead cells during the wash with buffer prior to the staining process. For treatments with particles of higher grafting density of azTM/nm^2 (cf. Figure 3.9 - panels 13 and 16), the number of healthy cells was not reduced when compared to the controls (cf. Figure 3.9 - panels 1 and 4), suggesting that the high azTM grafting density particles were not

that effective. This result is in accordance with the earlier speculation that particles with higher grafting densities of the ligands did not allow the proteins the spatial flexibility to bind (cf. Figure 3.7). In addition, there is a ca. 30 to 40 % decrease in the number of late apoptotic cells for treatment with the PEGylated particles (cf. Figure 3.9 - panel 17) when compared to non-PEGylated particles (cf. Figure 3.9 - panel 14), which also supports the previous speculation that protein transport to the surface of the particles is reduced with a large PEG hydration shell.

3.4 Experimental

Reagents and solvents. All the commercial reagents were purchased from TCI America and Alfa Aesar and used without further purification. All the solvents were dried according to standard methods. Deionized water was obtained from a Thermo Scientific Barnstead NANOpure Water Purification System and exhibited a resistivity of ca. 10^{18} ohm^{-1}cm^{-1}.

Chemical characterization methods. ^{1}H and ^{13}C NMR spectra were recorded on JEOL ECX-300 spectrometers (300MHz for proton and 76MHz for carbon). Chemical shifts for protons are reported in parts per million downfield from tetramethylsilane and are referenced to residual protium in the NMR solvent ($CDCl_3$: δ 7.26 ppm, DMSO-d6: δ 2.50 ppm). Chemical shifts for carbons are reported in parts per million downfield from tetramethylsilane and are referenced to the carbon resonances of the solvent ($CDCl_3$: δ 77.16, DMSO-d6: δ 39.52 ppm). Coupling constants are reported in Hertz (Hz). LC/MS mass spectra were obtained using Finnigan LCQ spectrometer and HP 1100 (HPLC). The IR spectra were recorded at room temperature in the wavenumber range of 400-4000 cm^{-1} and referenced against air with a Nicolet 6700 FTIR instrument. A total of 32 scans were averaged for each sample at 2 cm^{-1} resolution.

Preparation of Survivin ligands (TM and azTM) The Survivin ligand TM was prepared based on the method published[209, 248, 249]. The reaction scheme for the synthesis of TM is presented in Figure 3.10.

6-(5-chloro-2-hydroxyphenyl)-4-(2-chloro-5-(trifluoromethyl)phenyl)-2-oxo-1,2-dihydropyridine-3- carbonitrile (1) 1-(5-Chloro-2-hydroxyphenyl) ethanone (0.1 g, 0.586 mmol), 2-chloro-5-(trifluor-

omethyl) benzaldehyde (0.122 g, 0.586 mmol), ethyl cyanoacetate (0.1 g, 0.88 mmol), and ammonium

acetate (0.45 g, 5.86 mmol) were dissolved in ethanol (7 mL) and stirred under nitrogen atmosphere in sealed flask at 110 ^{o}C for 3 hours. After cooling, the precipitated yellow solid was diluted with diethyl ether (7ml), filtered, washed with diethyl ether and with water, and then dried to give the product. Yield: 0.1 g (40 %). m.p. = 330 ^{o}C with destruction. ^{1}H NMR (DMSO-d6) δ 6.69 (d, 1H, J = 8.9 Hz), 6.83 (s, 1H), 7.15 (d.d, 1H, J = 8.9 Hz, J= 2.6 Hz), 7.82 (m, 1H), 7.86 (m, 1H), 7.88 (m, 2H); 8.02 (d, 1H, J= 2.6 Hz). ^{13}C NMR (DMSO-d6) δ 95.78, 102.78, 117.52, 118.18, 120.00, 120.60, 121.86, 125.46, 127.10, 127.30 (m), 127.83, 128.26, 130.81, 131.63, 135.75, 137.77, 154.11, 155.33, 161.92, 163.50. ESI-Mass m/z (%): 426.7 (75), 423.27 ([M-H]$^{-}$; 100).

The reaction scheme for the synthesis of azTM is presented in Figure 3.10.

4-(3-azidopropoxy)benzaldehyde (2) *p*-Hydroxybenzaldehyde (0.1 g, 0.82 mmol) and 1-azido-3-iodo propane (0.19 g, 0.9 mmol) were dissolved in acetone (15 mL). Potassium carbonate (0.113 g, 0.82 mmol) was added to the solution and obtained mixture was stirred and refluxed for 5 hours. After cooling the mixture was quenched with water and extracted with dichloromethane. Organic layer was separated, dried with Na_2SO_4 and filtered. The filtrate was evaporated to give a clear oil. Yield: 0.13 g (77 %). ^{1}H NMR ($CDCl_3$) δ 2.09 (m, 2H, J = 6.3 Hz), 3.54 (t, 2H, J = 6.5 Hz), 4.14 (t, 2H, J = 6.0 Hz), 7.00 (d, 2H, J = 8.6 Hz), 7.80 (d, 2H, J = 8.6 Hz), 9.88 (s, 1H).

4-(4-(3-azidopropoxy)phenyl)-6-(5-chloro-2-hydroxyphenyl)-2-oxo-1,2-dihydropyridine-3-carbonitrile (3)1-(5-Chloro-2-hydroxyphenyl)ethanone (0.277 g, 1.62 mmol), 4-(3-azidopropoxy) benzaldehyde (0.4 g, 1.95 mmol), ethyl cyanoacetate (0.238 g, 2.11 mmol) and ammonium acetate (0.75 g, 9.72 mmol) were dissolved in ethanol (7 mL) and stirred under nitrogen atmosphere in sealed flask at 110 ^{o}C for 16 hours. After cooling, the precipitated yellow solid was filtered, washed with cold ethanol and with water, and then dried. Obtained yellow solid (0.265 g) is the mix of two compounds with same molecular weight. The mix was separated by flash column chromatography on silica, solvent ethyl acetate : hexane (1 : 1). R_F=0.8. Yield: 0.105 g (15 %). m.p. = 186 ^{o}C with decomposition. ^{1}H NMR (DMSO-d6) δ 2.02 (m, 2H, J = 6.5 Hz), 3.54 (t, 2H, J = 6.5 Hz), 4.13 (t, 2H, J = 6.0 Hz), 7.05 (d, 2H, J = 8.9 Hz), 7.36 (d, 1H, J = 8.9 Hz), 7.60 (d.d, 1H, J = 2.4 Hz, J = 8.9 Hz), 7.92 (s, 1H), 8.28 (d, 2H, J = 8.9 Hz), 8.65 (d, 1H, J = 2.4 Hz). ^{13}C NMR (DMSO-d6) δ 28.16, 47.73, 64.87, 95.28, 100.27, 114.37, 118.72, 119.0, 124.65, 129.05, 129.29, 130.05, 132.0, 143.41, 150.60, 160.18, 160.48, 160.65. ESI-Mass m/z (%): 423 (70) [M+H]$^{+}$, 418 (100).

Preparation of azide-modified polyethylene glycol (azPEG). The azPEG was prepared according to the method published[31].

Mono-methoxy-PEG5000-methansulfonate Methylsulfonyl chloride (0.92 g, 8 mmol) in dichloromethane (5 mL) was added dropwise at room temperature to the stirring solution of triethylamine (0.89 g, 8.8 mmol) and mono-methoxy-PEG5000 (20 g, 4 mmol) in dichloromethane (70 mL). The solution was stirred at 20 ^{o}C for 4 hours, then washed with water and the organic layer was dried with Na_2SO_4 with further filtration. The solvent was evaporated under vacuum to give the product as a white solid. Yield: 20.3 g (97 %). ^{1}H NMR ($CDCl_3$) δ 3.07 (s, 3H), 3.36 (s, 3H), 3.48 (t, 2H), 3.53 (m, 2H), 3.62 (m, ca. 400H), 3.75 (m, 4H), 4.36 (m, 2H).

Mono-methoxy-PEG5000-azide The mixture of mono-methoxy-PEG5000-methansulfonate (20.3 g, 4 mmol) and sodium azide (1.1 g, 17 mmol) in acetonitrile (80 mL) was refluxed and stirred for 15 hours. After cooling, the mixture was filtered and the solvent was evaporated. The residue was dissolved in dichloromethane and washed with water, organic layer was separated, dried with Na_2SO_4 and filtered. The solvent was evaporated, the crystalline residue was washed with hexane, filtered and dried in air to give the product as a white solid. Yield: 19 g (94 %). ^{1}H NMR ($CDCl_3$) δ 3.35 (s, 3H), 3.38 (t, 2H), 3.62 (m, ca. 400H), 3.85 (m, 2H). FTIR (cm^{-1}): 1095 (s, C-O-C); 1340, 1465 (CH2); 2100 (N3); 2880 (s, CH2).

Preparation of the particles. Propargyl acrylate (PA) particles were prepared according to a standard emulsion polymerization method published[31].

For a typical surface modification of the particles, for example, the grafting of azTM and azide-modified PEG chains with molecular weight of 5000 (azPEG) onto the particles, 1 mL PA particles and 5 mg azTM were added to 2 mL of deionized water. Solutions of 0.07624 g copper(II) sulfate (99.999% Aldrich) in 10 mL deionized water and 0.3024 g sodium ascorbate (99% Aldrich) in 10 mL deionized water were made. Initially, 0.5 mL of the $CuSO_4$ solution was added to the PA/ azTM solution, followed by 0.5 mL of the sodium ascorbate solution. The resulting mixture was maintained at a temperature of ca. 28 ^{o}C for 15 minutes and then the reaction was stopped by the removal of unreacted azTM, sodium ascorbate, and Cu(II)SO_4 through a repeated particle washing procedure consisting of centrifugation and redispersement in methanol. The cleaned PA/ azTM particles in water were subsequently utilized in a secondary click transformation with 54.99 mg azPEG, and previously presented $CuSO_4$ and sodium ascorbate solutions. The reaction was allowed

to run for 24 hours and then washed to remove unreacted species as determined by absorbance measurements; these particles are referred to as PA/ azTM/ azPEG particles.

Affinity pull-down assay. The particles (conjugated or control) were washed 3 times with Buffer A (20 mM KH_2PO_4 pH 7.5, 10 % glycerol, 0.5 mM EDTA, 0.01 % Igepal, and 1 % Triton) before the addition of Survivin-$HIS_{(6)}$ or BSA (6 μg each). The reactions were agitated at 4 ^{o}C for 30 min in Buffer B containing 150 mM KCl (final volume of 30 μL). The supernatant was removed from the beads followed by 3 washes of the beads with Buffer A containing 300 mM KCl. Equal volumes of 2x SDS dye was added to the supernatant and wash fractions, while 30 μL of 2xSDS loading dye was added to the bead fraction. The fractions were subjected to SDS-PAGE analysis on 15 % gels followed by Coomassie Blue staining.

Cell analysis. Human A549, MCF7, and U118MG cell lines were obtained from ATCC (Rockville, MD). Human glioblastoma U251MG cell line was obtained from National Cancer Institute (Frederick, MD). A549 cells were cultured in F-12K media (Kaighn's Modification of Ham's F-12 medium) containing 10 % fetal bovine serum (FBS) and 1 % antibiotic. MCF7 cells were cultured in phenol red-free Dulbeccos modified Eagles media (DMEM) containing 10 % fetal bovine serum (FBS) and 1 % Penicillin-Streptomycin. U118MG cells were cultured in Dulbeccos modified Eagles media (DMEM) containing 10 % fetal bovine serum (FBS) and antibiotics. U251MG cells were cultured in Roswell Park Memorial Institute (RPMI) 1640 containing 10 % fetal bovine serum (FBS) and antibiotics. Cells were cultured at 37 °C in a humidified atmosphere of 95 % air 5 % CO_2.

Cytotoxicity assay. A549 cells (5,000 cells per well) were cultured on 96 well plates for 24 hours. Subsequently, cells were, exposed to 15 and 20 μM of PA, 15 and 20 μM of PA/ azPEG, 1, 6.5, 25, 45, and 65 μM of azTM, 1, 6.5, 25, 45, and 65 μM of PA/ azTM and 1, 6.5, 25, 45, and 65 μM of PA/ azTM/ azPEG. After 48 hours, cell death was assessed with a MTS assay according to the manufacturer's instructions (Promega, Madison, WI). Briefly, medium was aspirated and a solution of 100 μL of F-12K containing 10% FBS and 3-(4,5-dimethylthiazol-2-yl)-5-(3-carboxymethoxyphenyl)-2-(4-sulfophenyl)-2H-tetrazolium, salt (MTS) and phenazine methosulfate (PMS) was added onto each well. After 150 minutes, wells were scanned colorimetrically at 490 nm on a spectrophotometer. The conversion of MTS into an aqueous soluble formazan product is achieved only by dehydrogenase enzymes, which are present in metabolically active cells; the absorbance at 490 nm from the formazan

product is directly proportional to the number of living cells in culture. MCF7 cells (20,000 cells per well) were cultured on 96 well plates for 24 hours. Subsequently, cells were, exposed to 1, 6.5, 25, 45, and 65 μM of azTM, 1, 6.5, 25, 45, and 65 μM of PA/ azTM and 6.5, 25, 45, and 65 μM of PA/ azTM/ azPEG. After 72 hours, cell death was assessed with a MTS assay according to the manufacturer's instructions (Promega, Madison, WI). Briefly, medium was aspirated and a solution of 100 μL of DMEM containing 10% FBS and 3-(4,5-dimethylthiazol-2-yl)-5-(3-carboxymethoxyphenyl)-2-(4-sulfophenyl)-2H-tetrazolium, salt (MTS) and phenazine methosulfate (PMS) was added onto each well. After 180 minutes, wells were scanned colorimetrically at 490 nm on a spectrophotometer. Human glioblastoma U118MG and U251MG cells were cultured on 96 well plates for 24 hours. Subsequently, cells were, exposed to 0.05, 0.1, 0.25, 0.5, 1.0, and 2.5 μM of TM and 0.05, 0.1, 0.25, 0.5, 1.0, and 2.5 μM of azTM. The growth medium was supplemented with 2 % FBS and treated with TM or azTM. After 24 hours, cell death was assessed with a MTT assay according to the manufacturer's instructions. Briefly, medium was aspirated and a solution of DMEM containing 10 % FBS and 0.2 mg/ mL MTT was added onto each well. After 180 minutes, DMSO (200 μL) was added to each well to dissolve the formazan crystals and absorbance was measured at 570 nm with background subtraction at 630 nm. Cell viability was presented as percentage of viable cells in total population. Significant difference from control value was indicated by $^{*}p < 0.05$.

In situ Wright staining for the detection of morphological features of apoptosis. The U118MG and U251MG cells were grown in 6 - well plates and treated with TM (0.1, 0.5, or 1.0 μM) or azTM (0.1, 0.5, or 1.0 μM) for 24 hours. At the end of treatments, both adherent and floating cells were centrifuged at a low rpm to sediment them. The cells were then washed twice with PBS, pH 7.4, before being fixed and subjected to in situ Wright staining. The 6 - well plates were then allowed to dry and cells (n = 300) were examined under the light microscope. The morphology of the apoptotic cells as examined under light microscopy included such characteristic features as chromatin condensation, cell-volume shrinkage, and membrane-bound apoptotic bodies. Four randomly selected fields were counted for at least 300 cells. The percentage of apoptotic cells was calculated from three separate experiments.

Western blotting using specific antibodies. Both glioblastoma cell lines (U118MG and U251MG) were treated with azTM or PA/ azTM (1.0 μM Survivin ligand concentration) prior to

extraction of protein samples. The protein samples (10 μg) were mixed with Laemmli composition of buffer and boiled in water for 5 min. The boiled protein samples were loaded onto precast 4 - 20 % polyacrylamide gradient gels (Bio-Rad Laboratories, Hercules, CA) and electroblotted to the polyvinylidene fluoride (PVDF) membranes (Millipore, Bedford, MA). The non-specific binding sites in the membrane were blocked with 5 % non-fat dry milk for 1 hour at room temperature. The membranes were then incubated overnight at 4 ^{o}C on a rocker with appropriate dilution of primary IgG antibody followed by three times washing in washing buffer (20 mM TrisHCl, pH 7.6, 137 mM NaCl, 0.1 % Tween 20). After washing, the membranes were incubated with the appropriate alkaline horseradish peroxidase (HRP)-conjugated secondary IgG antibody for 1 hour followed by three times washing in washing buffer. Specific protein bands were detected by incubation for 5 min at room temperature with Immun-StarTM HRP Lumino/Enhancer (Bio-Rad Laboratories, Hercules, CA) and exposing to BIOMAX XAR films (Kodak, Rochester, NY) for autoradiography. The antibody against β-Actin (clone AC-15) was purchased from Sigma (St. Louis, MO), and antibodies against Survivin and Caspase-3, were from Santa Cruz Biotechnology (Santa Cruz, CA). The alkaline HRP-conjugated anti-rabbit and anti-mouse secondary IgG antibodies were purchased from Biomeda (Foster City, CA) and anti-goat secondary IgG antibody was from Santa Cruz Biotechnology (Santa Cruz, CA). The autoradiograms were scanned on an EPSON Scanner using Photoshop software (Adobe Systems, Seattle, WA, USA) and optical density (OD) of each band was determined using the NIH Image software. The OD of bands in the control treatment was designated as 100. All experiments were performed in triplicates and results were analyzed for statistical significance.

Determination of apoptotic,necrotic and healthy cells A549 cells (5,000 cells per well) were cultured on 96 well plates for 24 hours. Subsequently, cells were exposed to 25 μM of azTM, unmodified PA particles, PA/ azTM particles of two different grafting densities of 0.63 and 1.77 azTM/ nm^2, and PA/ azTM/ azPEG particles. After 24 hours of treatment, the apoptotic, necrotic and healthy cells quantification kit purchased from Biotium, Inc. (Hayward, CA, USA) was used according to the manufacturer's instruction. The stained cells were observed under a Life Technologies EVOS® FL Cell Imaging System using filter sets of DAPI, GFP and RFP. Healthy cells were stained with Hoechst 33342 and had only blue emission. Necrotic cells were stained with Hoechst 33342 and Ethidium homodimer III, and had both blue and red emissions. Apoptotic cells had blue, red and green emissions as those cells were stained by all the three stains: Hoechst 33342, Ethidium

homodimer III and fluorescein labeled Annexin-V. Cells stained by the triple colors indicate dead cells progressing from apoptotic cell population[246, 247]. All the three types of cells were counted and expressed as percentage of total cells.

3.5 Conclusion

Disrupting the activity of anti-apoptotic proteins that are over-expressed by cancer cells is a potentially attractive route to combating this disease. Survivin belongs to the family of inhibitor of apoptosis proteins (IAP) and is present in most cancers while being below detection limits in most terminally differentiated adult tissues, making it an attractive protein to target for diagnostic and, potentially, therapeutic roles. To this end, sub-100 nm poly(propargyl acrylate) particles were surface modified through the copper-catalyzed azide/alkyne cycloaddition of an azide-terminated Survivin ligand derivative (azTM) originally proposed by Abbott Labs and speculated to bind directly to Survivin (protein) at its dimer interface. Using affinity pull-down studies, it was determined that the PA/azTM nanoparticles selectively bind Survivin. Incubating the modified particles with glioblastomas and other Survivin over-expressing cell lines such as A549 and MCF7 resulted in a higher percentage of cell death relative to cells incubated with the original Abbott-derived small molecule. In situ Wright staining and selective dyes were used to confirm that the cell death observed was through apoptosis. In addition, a Western blot assay indicated that there was an significant increase in the expression of Caspase-3, the final executioner of apoptosis, during the treatment with the PA/azTM particles. Overall, the results obtained validate the statement mentioned in the introduction that the nanocarriers increase circulation lifetimes and enhance the effectiveness of the drug/ligand for Survivin inhibition or sequestration. This nanocarrier technique can be expanded to the other Survivin inhibition approaches, such as attaching a plasmid or siRNA, as well as a targeting group that will single-out specific tumors and avoid healthy cells. These particles offer a flexible platform that can be easily surface modified to recursively attach a range of moieties such as near infrared fluorophores, antibodies, and drugs to one particle, creating a multifunctional nanodevice for use against cancer.

Acknowledgments

The authors thank the Gregg-Graniteville Foundation and the National Institutes of Health (GM098510) for financial support.

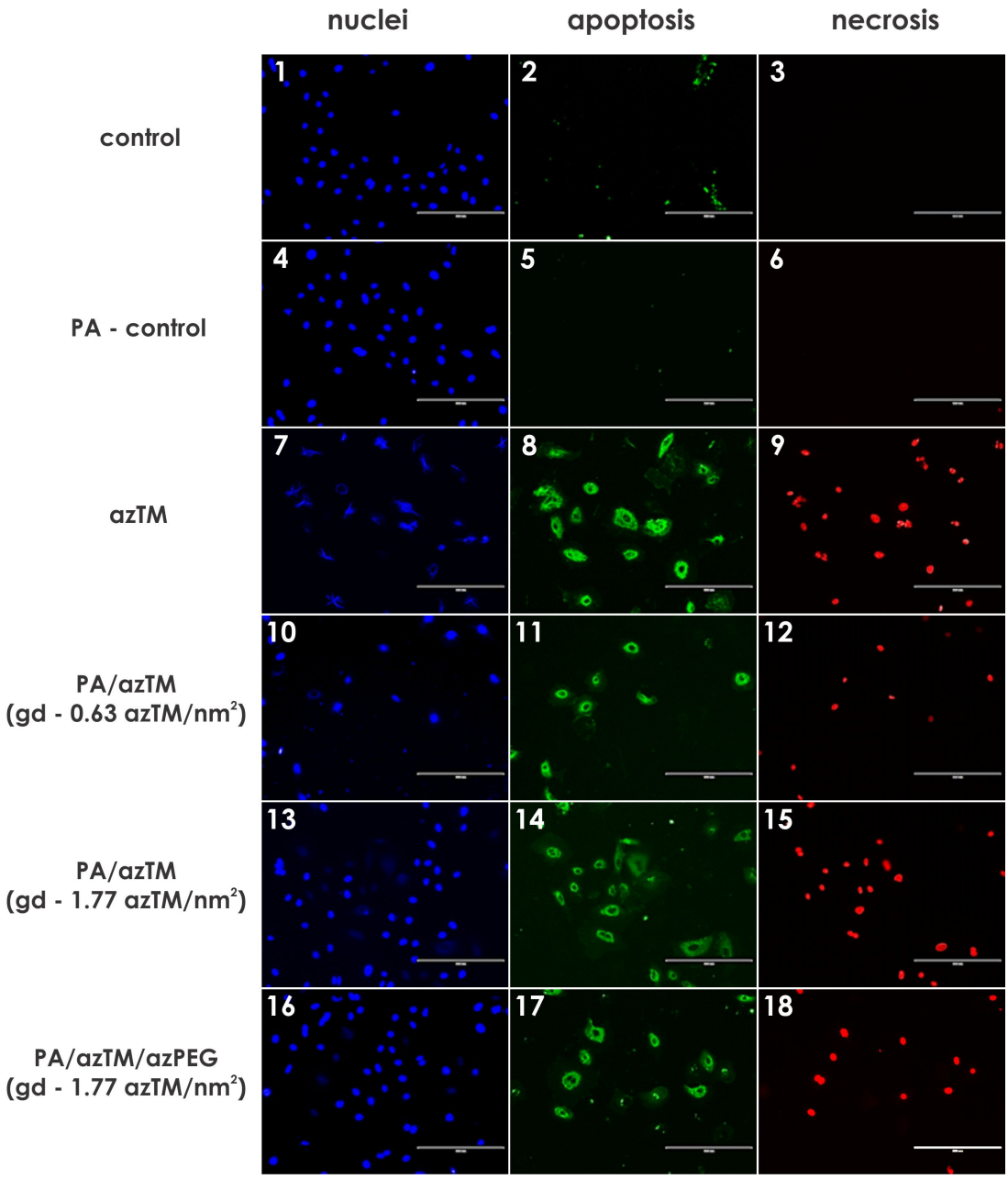

Figure 3.9: Fluoroscope images of A549 cells after incubation with 25 μM of azTM, PA/ azTM particles with two different grafting densities, PA/ azTM/ azPEG particles and PA particles. Cells were treated with an apoptotic/necrotic/healthy cells detection kit to differentiate the status of the cells. All scale bars represent 200 μm.

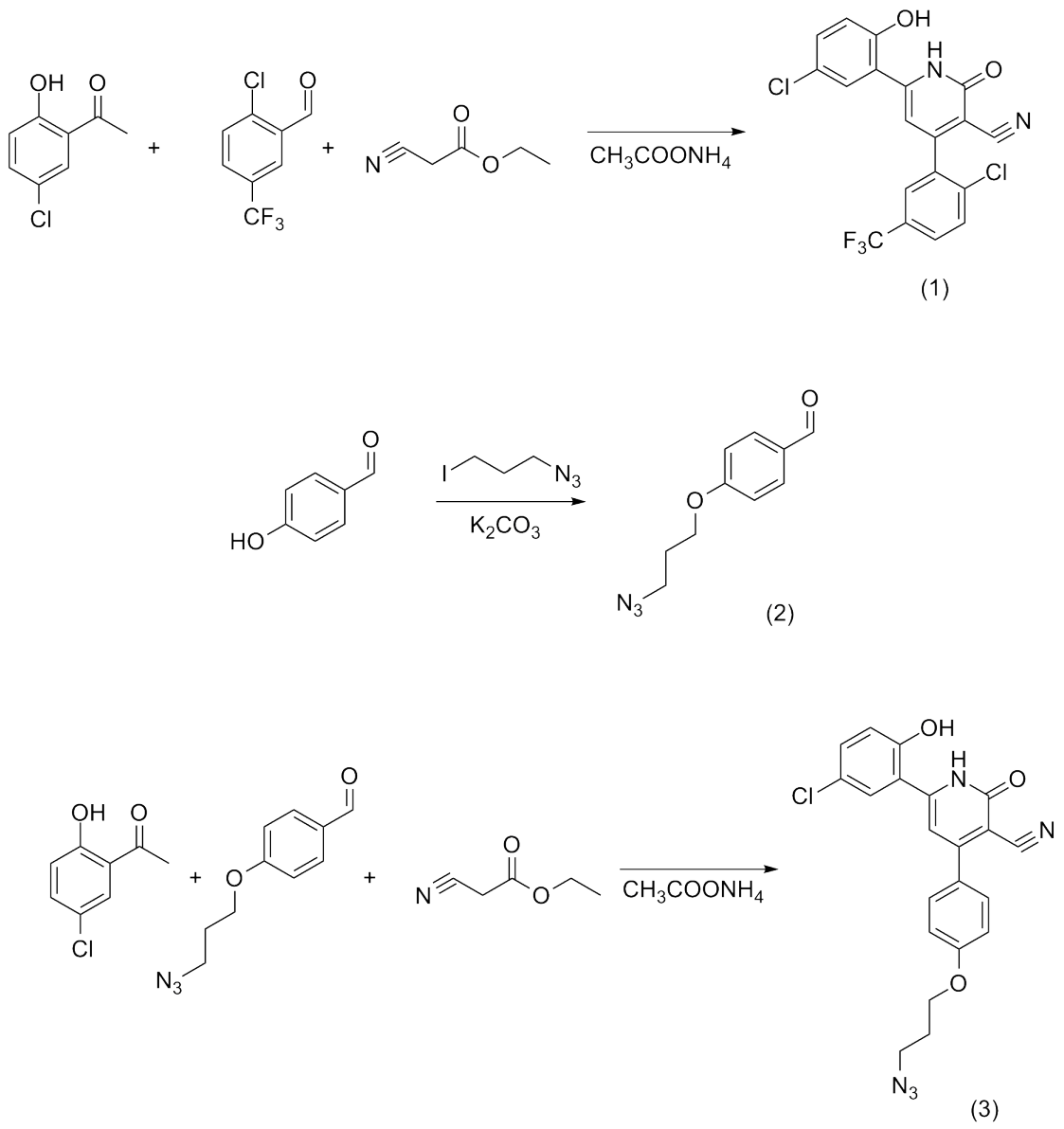

Figure 3.10: Reaction scheme for synthesis of Survivin ligands, TM and azTM

Chapter 4

A bioresponsive and versatile particle-protein-dye system for small molecule delivery and FRET based imaging

4.1 Attributions

The synthesis of the azide and alkyne modified small molecules was conducted or aided by Dr. Yuriy P. Bandera at Clemson University. Cell growth and viability assessments in A549 cells were conducted with the aid of Ashlee Tietje and Dr. Yanzhang Wei at Clemson University. Photodynamic therapy study was carried out with the aid of Dr. Anna-Liisa Nieminen at Medical University of South Carolina. a—e - UV-Vis-IR Spectral Software 1.2, FluorTools, was used to decompose the overlapped spectra for ratiometric FRET calculations. The results in this chapter are in preparation for publication as Jenkins et al., Click-engineered, bioresponsive and versatile particle-protein-dye system, 2015.

4.2 Introduction

In the recent years, there has been a significant growth and development of multifunctional nanocarriers such as surface cross-linked micelles[15, 16], dendrimers[17], biodegradable polymeric nanoparticles[18, 19], magnetic and other metal particles[20, 21], and liposomes[20], for cancer theranostics. Among these technologies, platforms based on polymeric materials, especially biodegradable nanoparticles, are of particular interest due to the flexibility offered by macromolecular synthesis methods, high drug loading capacities, improved drug solubility and their ease of multifunctionalization[22, 23, 24]. Combining imaging and therapeutic agents into a single formulation enables direct visualization of the theranostic pharmacokinetics and provides important insight into heterogeneities between tumors and patients, which will be helpful for the physician to decide or change the dosage, drug choice and treatment method accordingly and results in an effective 'personalized medicine' treatment of the disease[52]. In order for the 'personalized medicine' treatment to be successful, the single nanocarrier should demonstrate the following properties: (1) be biocompatible/ biodegradable; (2) prolonged circulation lifetimes; (3) ability to accumulate specifically in the required zone of interest; (4) responsiveness to local stimuli, such as pH and/ or temperature changes; (5) allow for an effective intracellular drug delivery; and (6) bear a contrast/ reporter moiety for real-time observation[22, 78]. To prepare such a smart multifunctional nanocarrier, it is necessary that the chemical moieties that are responsible for the properties should be attached on the surface of the nanocarrier to prevent opsonization, facilitate for formation of beneficial host/guest assemblies and specifically target the tumors[21, 78, 250].

A prevalent and quickly developing technique to prepare and surface functionalize the nanoparticles is through 'click' transformations because the reactions are reliable, experimentally simple, facilitate bioconjugation and yield products of high orthogonality and functionalization[18, 87, 251]. Previously, we have reported a poly(propargyl acrylate) particle surface functionalized with a near-infrared fluorophore for fluorescence imaging and photodynamic therapy applications[31, 71]. These particles exhibit a good tumor-to-background ratio and have a good circulation lifetimes but attaching the fluorophore directly to the particle decreased the quantum efficiency of the system by 60 to 70 %. In addition, the contrast agents are attached to the particles at all times, which makes it less attractive for drug delivery applications. To this end we need to design an improved system of surface modified particles, particularly, a system that attaches the drugs to the particle

through a linker that responds specifically to release the drug. After a detailed literature search, it was identified that BSA could be the potential linker for the improved system as it stable, inert to many biochemical reactions and prevents non-specific adsorption of other proteins to surfaces[252].

Recently, the quantification and digestion of bovine serum albumin (BSA) covalently conjugated to gold nanoparticles was illustrated and in these particles, the protein was conjugated to the surface of the particles using a standard NHS activation approach, where the primary amines of the protein react with carboxyl containing substrates and form a covalent amide bond[252]. This conjugation with NHS substrates is a well established strategy and is widely used to construct fluorescent oligonucleotides and proteins[253, 254]. Utilizing the NHS activation and click transformations, the improved system of modified particles can be made. In this current effort, we present a particle-protein-dye system (cf. Figure 4.1), where the particles are surface modified with the azide modified BSA (azBSA) that is conjugated to fluorophores. These fluorophore functionalized particles exhibit improved efficiencies in imaging and photodynamic therapy applications because they are activated only after the digestion of the azBSA protein. This allows the particles to be in the 'off' state till they reach their end locations, which is the lysosome and endosome. In those regions of the cell, the pH is ca. 4 - 5 and the digestive enzymes are located here, so the albumin linker is digested and results in the release and turn 'on' of the emission of the fluorophore. In this system as the fluorophore will be released as a free molecule, there will not be a significant reduction in quantum efficiency and photosensitizing activity. In addition, this system can also be prepared such that a ligand or drug is attached instead of the fluorophore to use it for targeting and other delivery applications and if desired the azBSA can be conjugated with a number of fluorophores, ligands, antibodies and drugs at the same time by adjusting the ratios of those small molecules during click transformations. These multiple functionalized particles represent a single 'nanodevice' that can be a very attractive platform for personalized medicine.

4.3 Results & Discussion

A schematic of the particle-based system studied in this effort is presented in Figure 4.1. The poly(propargyl acrylate) (PA) colloids were prepared using a standard aqueous emulsion polymerization technique with sodium dodecyl sulfate as the surfactant, potassium persulfate as the initiator, and divinyl benzene as a crosslinker, resulting in spheres with a diameter of ca. 88.5 nm.

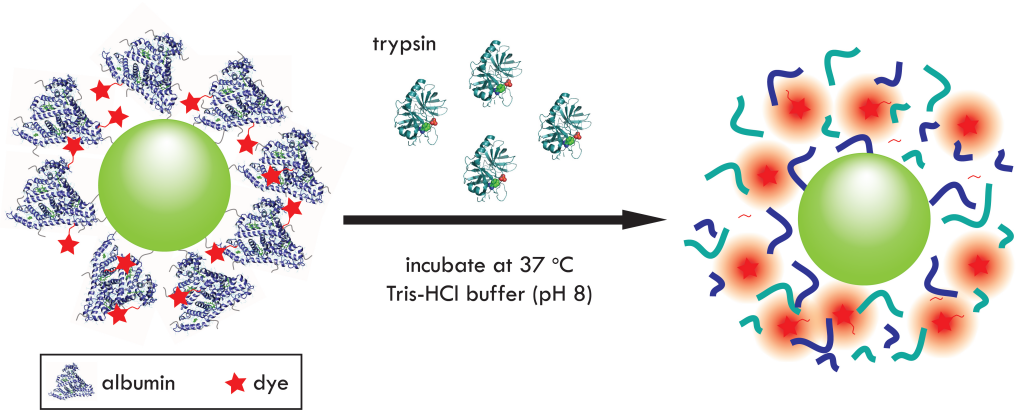

Figure 4.1: Schematic of the release of fluorophores from functionalized particles through trypsin digestion of the albumin. Sub 100 nm poly(propargyl acrylate) (PA) particles were surface modified with an azide-modified bovine serum albumin (azBSA) and alkyne terminated cyanine derivate fluorophore (YB317) through an aqueous-phase click transformation.

To functionalize the particle surface with the protein bovine serum albumin (BSA), BSA has to be modified to have terminal azide groups. Standard BSA was reacted with excess azide modified N - hydroxysuccinimide ester (azNHS) to produce azide labeled BSA (azBSA) that has several free azide terminated groups. A multiple step "click" reaction was performed to conjugate alkyne terminated cyanine derivative fluorophore (CYN) to azBSA and then functionalize the PA particles with the azBSA-CYN conjugate.

4.3.1 Emission of free fluorophore and interaction with proteins

The structure of the free alkyne terminated cyanine 3 derivative (CYN) fluorophore is presented in Figure 4.2 and its absorbance and photoluminescence when dispersed in methanol is presented in Figure 4.3. In this solvent, CYN has a peak absorption maximum at 546 nm and the corresponding emission peak is at 569 nm, which gives a stokes shift of 23 nm. CYN exhibits a reduced emission when dispersed in aqueous solutions due to quenching, (cf. Figure 4.4a) and for biological applications, the fluorophore needs to be dispersed in aqueous solutions. The quenching of the emission of fluorophores is a well-known phenomenon where the dye-dye separation becomes small at a limiting concentration and the fluorophore forms aggregates. These aggregates, upon excitation, transfer energy through a non-radiative pathway, which results in a decreased or zero emission of the fluorophore[143, 255]. The emission of these large aggregates is typically activated by albumins which solubilize the fluorophore by breaking up the aggregates and binding the fluo-

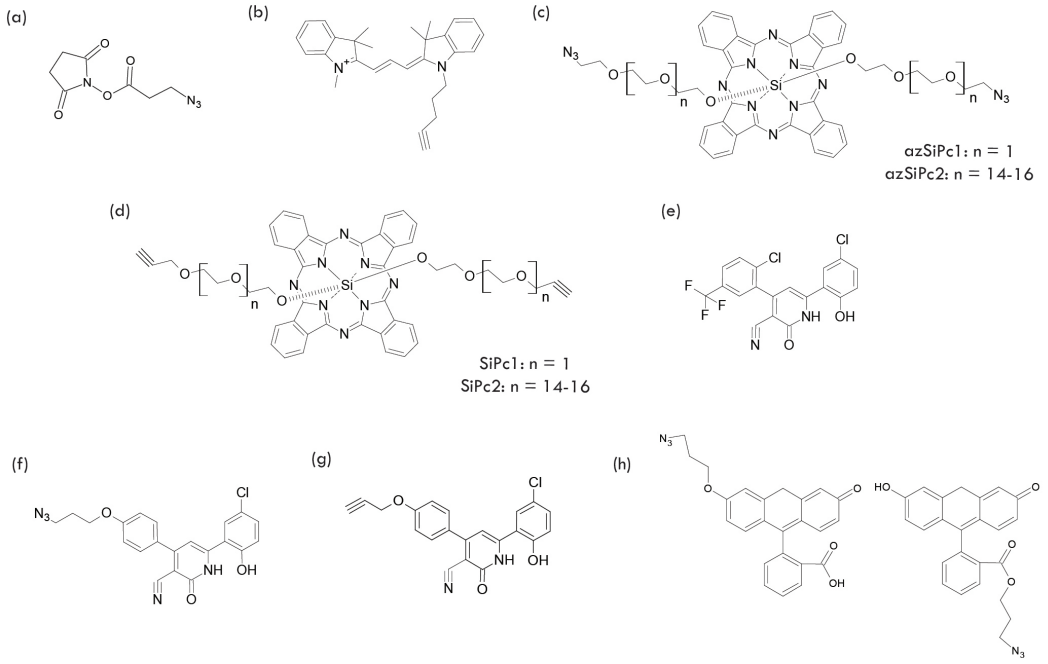

Figure 4.2: Structures of **(a)** azide modified N-hydroxy succinimide derivative (azNHS), **(b)** alkyne modified cyanine derivative fluorophore (CYN), **(c)** azide modified silicon phthalocyanine fluorophore with short PEG chains (azSiPc1) and long PEG chains (azSiPc2), **(d)** alkyne modified silicon phthalocyanine fluorophore with short PEG chains (SiPc1) and long PEG chains (SiPc2), **(e)** Abbott 17, **(f)** azide modified Survivin ligand (sl01), **(g)** alkyne modified Survivin ligand (sl02), and **(h)** azide modified fluorescein derivative fluorophore (azFL).

rophore non-specifically[143, 255]. The activation of CYN in a Tris-HCL buffer of pH 8 is presented in Figure 4.4a. Upon addition of 0.05 mM BSA to CYN, a dramatic increase in photoluminescence was observed in 1 hour. There was a 4742 % increase in the integrated peak area of emission. The activated emission can be deactivated using trypsin. It is well known that trypsin digests BSA when incubated at high temperatures and at a pH of 7 - 8[166, 256]. When ca. 0.215 mM trypsin was added to the BSA-CYN complex and incubated at 37 ^{o}C, BSA was broken down into smaller peptides which can no longer bind to CYN. This leads the CYN to form aggregates and quench the emission once again. At longer periods of incubation of the albumin activated CYN with trypsin, the emission returned to the initial intensity as the BSA is completely digested. In addition to the activation/ deactivation study of the CYN, it is necessary to study the changes in emission of CYN with trypsin to eliminate the possibility of trypsin activating the emission of CYN. In this study, ca. 0.215 mM trypsin was added to CYN fluorophore and incubated at 37 ^{o}C. The emission of CYN is monitored during incubation and after 2 hours of incubation, the photoluminescence intensity increased by 95 % (cf. Figure 4.4b) which is much lower compared to the activation with albumin.

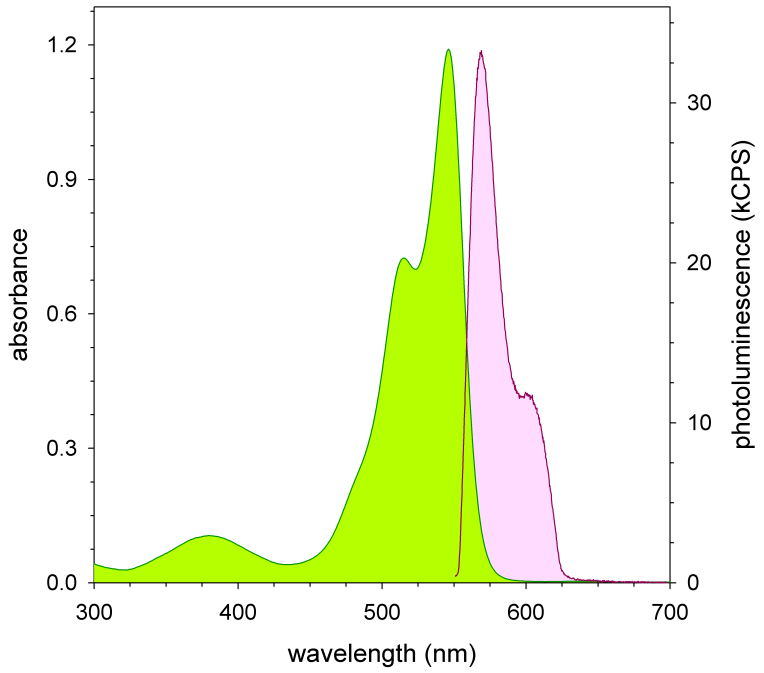

Figure 4.3: Absorbance (green) and photoluminescence (pink) of alkyne functionalized cyanine derivative fluorophore (CYN; 12.21 μM in methanol).

After incubation for longer periods of time, the emission returns to the initial intensity as trypsin digests itself too. Therefore from the activation studies of CYN, it can be concluded that CYN is selectively activated by BSA and activation by trypsin is negligible in comparison to the activation by BSA.

4.3.2 Modification of BSA and attachment of the azBSA-CYN conjugate to PA particles

To synthesize PA nanoparticles functionalized with azBSA-CYN conjugate, first BSA needs to be modified to have free azide end groups. We follow a standard NHS coupling reaction that is typically used to label oligonucleotides with azido group[253]. The BSA was reacted with excess azide modified N - hydroxysuccinimide ester (azNHS) (cf. Figure 4.2) to produce azide labeled BSA (azBSA). The product was dialyzed in a 12,000 - 14,000 MWCO dialysis bag for 2 days to remove the excess starting material. To the cleaned azBSA, alkyne modified cyanine derivative fluorophore

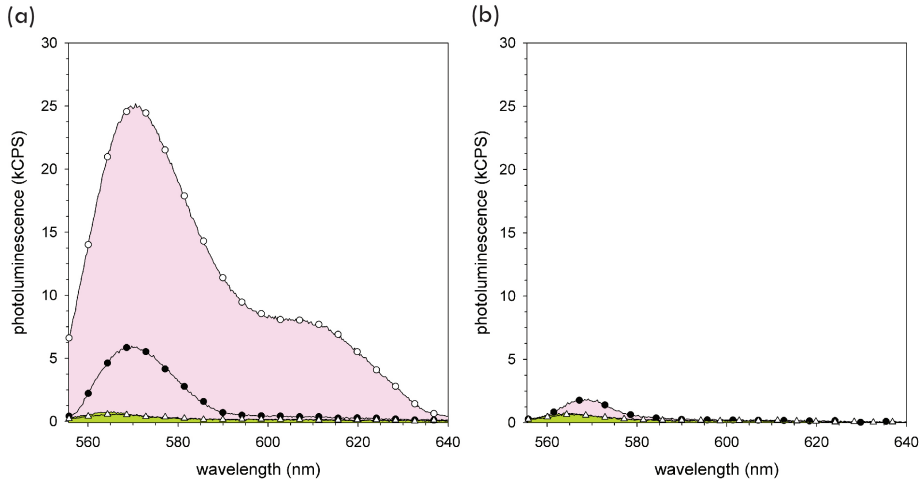

Figure 4.4: **(a)** Changes in photoluminescence intensity of (-) alkyne terminated cyanine fluorophore (CYN), with addition of (○) ca. 0.05 mM bovine serum albumin, followed by addition of ca. 0.215 mM trypsin, and incubated for (●) 2 hours and (△) 7203 hours. **(b)** Changes in photoluminescence intensity of (-) alkyne terminated cyanine fluorophore (CYN), with the addition of ca. 0.215 mM trypsin, and incubated for (●) 2 hours and (△) 7203 hours.

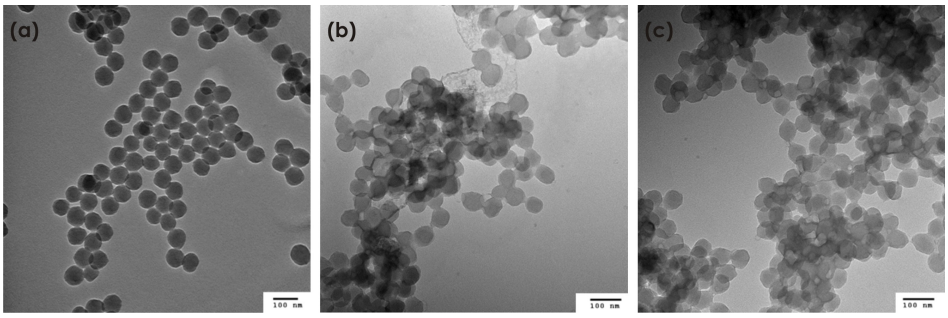

Figure 4.5: TEM micrographs of **(a)** unmodified PA particles, **(b)** and **(c)** particles surface modified with albumin/ cyanine 3 derivative fluorophore (PA-azBSA-CYN). All scale bars represent ca. 100 nm.

(CYN) (cf. Figure 4.2) was attached through a copper-catalyzed azide/ alkyne cycloaddition ('click' transformation) that is performed in water[254]. The CYN was clicked onto the azBSA for 24 hours and then the reaction was stopped by the removal unreacted sodium ascorbate and Cu(II)SO_4 through dialysis for 48 - 72 hours. The cleaned azBSA-CYN were subsequently utilized in a secondary click transformation with poly (propargyl acrylate) nanoparticles (PA). This reaction was allowed to run for 48 hours and then washed to remove unreacted species through dialyzing for 48 - 72 hours and a repeated washing procedure consisting of centrifugation and redispersement in phosphate buffered solution (PBS) that had 10 - 30 % THF. The last couple of washes were carried out using just PBS and the cleaned particles were dispersed in fresh PBS. The absorbance of the supernate

and thin layer chromatography (TLC) of the modified particles were used to confirm that all the free unbound dye was removed. The final cleaned particles are referred as PA-azBSA-CYN. TEM images were taken for particles before and after modification (cf. Figure 4.5). The initial unmodified particles are very monodisperse and surface outline can be seen neatly. After the click reaction, the PA-azBSA-CYN particles looked like they were clumped together and were held together with the azBSA. The azBSA has multiple free azide groups before the secondary click reaction, so it is possible to attach one azBSA to two or more particles. This results in a system where the particles are held together with an adhesive-like substance, which is azBSA.

4.3.3 Release of the fluorophore upon tryptic digestion of the particles functionalized with azBSA-CYN conjugate

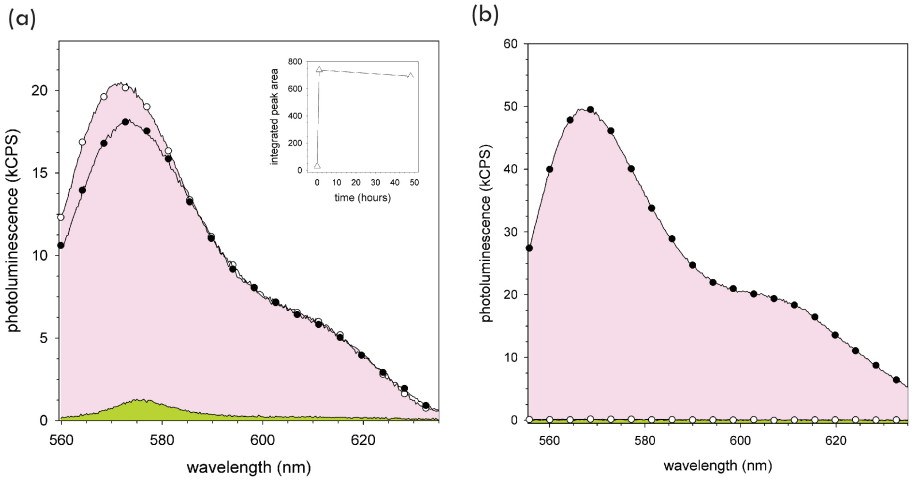

Figure 4.6: **(a)** Increase in photoluminescence intensity of PA-azBSA-CYN nanoparticles with addition of trypsin and incubation for 1 hour (○) and 48 hours (●) at 37 ^{o}C when dispersed in PBS. The inset presents the change in the integrated peak area of emission with the addition of trypsin. **(b)** Photoluminescence of the supernates of the PA-azBSA-CYN nanoparticles stored at 4 ^{o}C (-), incubated at 37 ^{o}C (○), and trypsin digested (●).

An important feature of the PA-azBSA-CYN nanoparticles is the release of the free fluorophore upon tryptic digestion. Initially, the modified particles have a lower emission and are said to be in an 'off' state because the fluorophore transfers energy non-radiatively to the protein and particles. In this scenario, the protein acts as a linker that attaches the fluorophore to the particle, and it is expected that upon digestion of the protein, it gets broken down to smaller peptide chains and results in the release of the fluorophore. As the fluorophore is free and no longer attached to

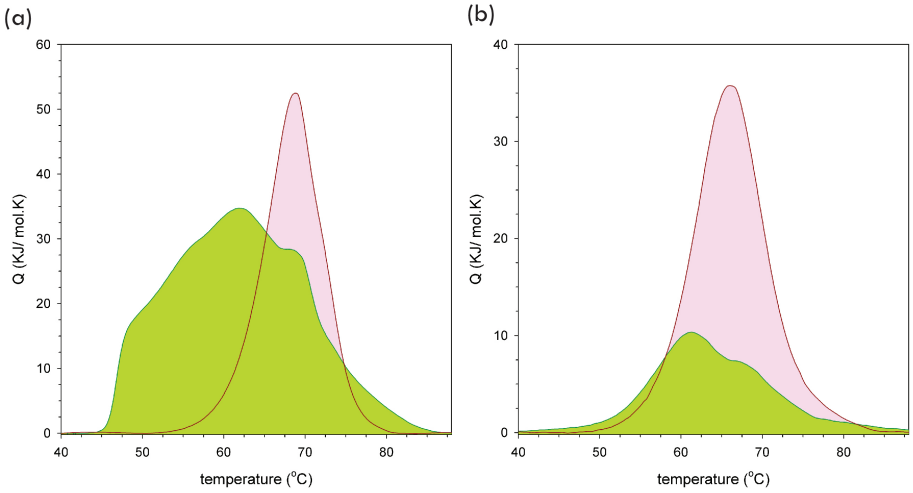

Figure 4.7: nanoDSC runs of **(a)** BSA and **(b)** azBSA. Undigested proteins (pink) and trypsin digested proteins (green)

the particles, the non-radiative transfer of energy is decreased, which leads to a significant increase in the emission of the fluorophore, and this emission activation is called the 'on' state of the system. This system of particle-protein-dye has two main advantages. First, the particles are in the 'off' state until they are taken up by the cells where eventually the protein gets digested to release the fluorophore and the emission is turned 'on'. This activation of the emission inside the cell will enhance the tumor-to-background ratio. Second, the fluorophore is initially immobilized on the particles, so it will accumulate inside the cells at a higher concentration due to the enhanced permeability and retention (EPR) effect. These advantages make the particle-protein-dye system an attractive option for fluorescence imaging applications.

To illustrate the emission 'turn on' due to the release of the fluorophore from the modified particles, clean PA-azBSA-CYN particles were incubated with 0.215 mM trypsin at 37 ^{o}C (cf. Figure 4.6a). After an hour of incubation, an increase of ca. 2360 % in integrated intensity area was observed, and that increase dropped slightly at longer incubation times. This response of the modified particles implied that the majority of the fluorophore was released within the first hour of incubation and at longer periods it is possible that the fluorophore is dropping out of solution or the emission is quenching due to aggregation of the fluorophores[143, 255]. In addition, it can be argued that the emission 'turn-on' of the modified particles could be from the denaturing of the BSA. It is speculated that during the initial unfolding stage, emission could be activated due to the

increased non-specific interaction between the BSA and CYN[71]. To disprove this speculation and confirm that the fluorophore was actually released, the PA-azBSA-CYN particles were centrifuged at 15,000 rpm for 15 minutes to separate the particles from the free fluorophore. If the fluorophore was released then it would remain in the supernate instead of still remaining attached to the crashed particles, and measuring the emission of the supernate of the trypsin digested particles would reveal if the fluorophore was released or not. Figure 4.6b presents the emission of the supernate when excited at 550 nm. The undigested particles that were stored at 4 ^{o}C and the particles incubated at 37 ^{o}C without trypsin were used as controls in this supernate study. For both controls, the supernate obtained after centrifugation had no emission and the supernate of the trypsin digested particles had a strong emission (cf. Figure 4.6b). These measurements confirm the release of the fluorophore from the modified particles, upon trypsin digestion. However, it is important to note that in some of the batches of the PA-azBSA-CYN particles, the yields of the release of the fluorophore upon tryptic digestion were low. This inconsistency in the release of the fluorophore was anticipated and can be attributed to the modification of BSA and the digestion conditions[257]. In tryptic digestion, it is well established that trypsin cleaves at the amino side of the cysteine residues. The primary amines of the BSA are all modified for conjugation to azNHS to facilitate the attachment of the CYN fluorophore, so there is a high possibility that most of the peptide bonds formed during the NHS coupling might not be cleavable by the trypsin. Usually, the extent of digestion is usually defined by measuring the amino acid sequence coverage (SQ %) but it can be a misleading parameter to use, as different mass spectrometers and different search parameters in subsequent data analysis may reveal various SQ % and is beyond the scope of this current project[258, 259]. Instead of measuring the SQ %, a calorimetric study of thermal denaturation of the proteins was performed to understand the changes in the protein during the tryptic digestion. The nanoDSC curves obtained (cf. Figure 4.7) showed the essential differences between the undigested and digested proteins. Both the undigested proteins exhibited a single endotherm peak in the nanoDSC curve. For the BSA curve, the single peak was near 69 ^{o}C, which agreed well will the data obtained from literature[260]. On the other hand, the azBSA curve showed the single peak near 66 ^{o}C, which indicated that there is slight modification in the structure when compared to the native BSA but not a major conformation change. Regarding the digested proteins, instead of the single isothermal peak, multiple smaller peaks were seen in the nanoDSC curves. In those curves, the lower intensity of the peaks compared to undigested proteins evidences that most of the protein was denatured during the digestion step and the multiple peaks

obtained indicate that the changes observed could be from multiple structurally independent or dependent parts. On comparison of the data from the two digested proteins, two main differences were noticed: (1) the onset temperature for denaturing the digested BSA was ca. 44 ^{o}C, which is much lower compared to the digested azBSA; and (2) in the case of digested azBSA there are two transitions, one at ca. 62 ^{o}C and the other at ca. 68 ^{o}C, whereas, for the digested BSA, apart from the two transitions at ca. 62 ^{o}C and ca. 68 ^{o}C, there were other additional transitions in the ca. 44 ^{o}C to 60 ^{o}C temperature range. These differences in the calorimetric study confirm that the azBSA is not being completely digested by trypsin. This drawback of partial digestion of azBSA can be overcome by using other enzymes, such as pepsin, which have a higher digestion efficiency of serums than trypsin[261]. We mentioned earlier that apart from the modification of BSA, the digestion conditions could also lead to incomplete digestion of proteins. Usually to ensure a complete digestion of the protein, it is denatured prior to the digestion step because digestive enzymes, such as trypsin, cannot gain access to the cleavage sites if the protein is folded or in the native 'globular' form and upon denaturing the protein, the sites which were once inaccessible become available for cleaving. In general, the protein can be denatured by a number of ways such as: (1) high temperatures; (2) high/ low pH (depending on the protein and enzyme); (3) change in ionic strength; and (4) addition of chaotropic agents and organic solvents[262]. In the above study, the PA-azBSA-CYN particles were digested at 37 ^{o}C, which is lower than the irreversible unfolding temperature of BSA (i.e. 60 - 70 ^{o}C)[71]. At 37 ^{o}C, there might be some unfolding which is reversible so the trypsin can sometimes gain access to the cleavage sites and this leads to low yields of the release of the CYN from the modified particles. This issue is fixable by denaturing the modified particles by one of the four methods mentioned above, prior to the tryptic digestion step. This sequential denaturation and digestion method will ensure a high release of the fluorophore, provided the right digestive enzyme is used.

4.3.4 *in vitro* photodynamic therapy studies of the particles-protein-dye system

The earlier section illustrated the use of the particle-protein-dye system for fluorescence imaging. Apart from imaging, this system can be beneficial for therapeutical applications. It is known that most of the small molecule fluorophores are used for photodynamic therapy (PDT) and

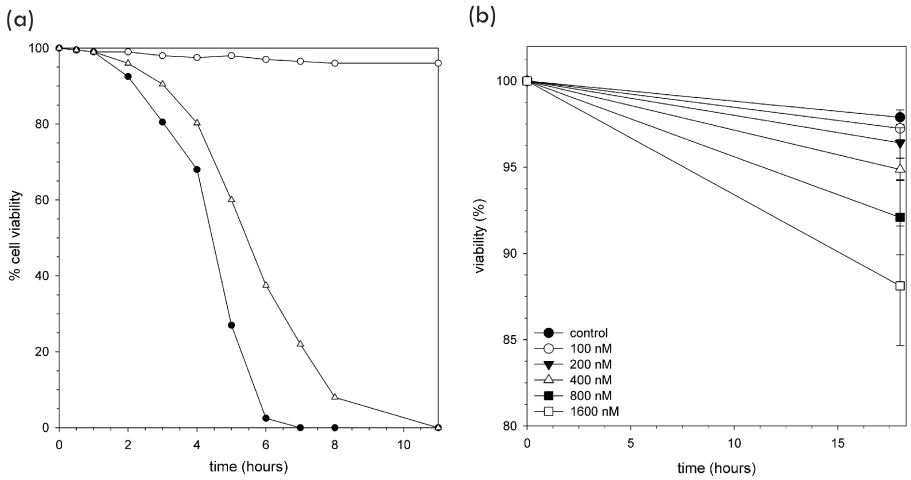

Figure 4.8: **(a)** The cells were treated with 200 nM of azSiPc1 or Pc4 for 18 hours. **(b)** The cells were treated with varying concentrations of PA-azBSA-SiPc2 for 18 hours. Cell viability is presented as percentage of viable cells in total population.

among them, porphyrins such as phthalocyanine fluorophores that emit in the near-infrared region, are the more popular and widely used photosensitizing agents in PDT[40, 263]. In PDT, upon excitation the photosensitizer undergoes inter-system crossing to longer-lived triplet states and this excited triplet energy is transferred to ground-state triplet of the oxygen in tissue and the highly cytotoxic reactive singlet oxygen ($^1O_2$) is formed. This toxic singlet oxygen can directly kill tumor cells by the induction of necrosis and/or apoptosis, can cause destruction of tumor vasculature and produces an acute inflammatory response that attracts leukocytes such as dendritic cells and neutrophils[264]. Previous efforts to localize the PDT by attaching the photosensitizer to polymeric nanoparticles were moderately successful as the immobilization of fluorophore on the particle decreased the amount of singlet oxygen yield formed as more of the energy was transferred non-radiatively to the particles compared to free molecules[31]. To this end, the particle-protein-dye system can be a good solution to the issue as the initial immobilization of the protein-dye conjugate on the particles allows for the higher accumulation[265], and upon digestion of the protein the fluorophore is released. The released fluorophore is free and no longer attached to the particles so energy is not lost through other non-radiative transfers and high yields of singlet oxygen species can be obtained.

For the demonstration of the application of modified particles in PDT, silicon phthalocyanine is chosen as the fluorophore as they have high quantum yields and excellent photostability. The structures of the azide and alkyne terminated silicon phthalocyanines that were used to functionalize

the particles are presented in Figure 4.2. Two different sets of silicon phthalocyanines were tested. The first set of fluorophores include SiPc1 and azSiPC1, which have short poly(ethylene glycol) (PEG)chains, and the second set include SiPc2 and azSiPc2, which have longer PEG chains. PEG increases the solubility of the hydrophobic fluorophores in aqueous solutions and the two sets were tested to check if the solubility has any effect on the PDT results. In the first round of PDT studies, the photosensitizing abilities of azSiPc1 and azSiPc2 were tested and compared to the efficiency of Pc4, a standard silicon phthalocyanine used in PDT[266, 267]. In this PDT experiment, UMSCC22A cells were cultured for 24 hours and then incubated with varying concentrations of 25 - 400 nM of fluorophore for 18 hours in culture medium. After 18 hours, the cells were irradiated with 670 nm light and cell death was assessed with propidium iodide exclusion over time. Of the two fluorophores tested, azSiPc1 gave results that had a similar response as the Pc4. The results from the 200 nM treatment azSiPc1 is presented in Figure 4.8a and 100 % cell death was observed after 11 hours from the irradiation, which is slightly longer compared to Pc4. Nonetheless, azSiPc1 is considered effective as complete cell death was achieved with a reasonable concentration where the fluorophore by itself was not toxic[266]. For the PDT study with azSiPc2 (data not shown) only 10 % cell death was observed. From these results, it is speculated that solubility does not affect the PDT capability of the fluorophore and for hydrophobic dyes the solutions for treatment can be made from concentrated DMSO stocks and then diluting in aqueous solutions, such that the DMSO is less than 1 %. In addition, as the azSiPc1 was more effective than azSiPc2, it can be speculated that the long PEG chains might be responsible for the decreased PDT activity in azSiPC2, as energy can be lost non-radiatively due to the long PEG groups. It is possible that the modification of the silicon phthalocyanine at the porphyrin ring will not change the singlet oxygen yields significantly but any modification at the axial position of the silicon will drastically change the yields because it is well established in literature that the central metal moiety is the vital determining group of the amount of singlet oxygen generation in phthalocyanines[268]. Moving onto the modified particles, the second round of PDT studies was carried out with particles directly functionalized with just the azide modified phthalocyanines (i.e. azSiPc1 and azSiPc2). The azSiPc1 or azSiPc2 groups were attached to the surface of the PA particles through a click reaction, and these particles are referred as PA-azSiPc1 or PA-azSiPc2. Both of these particles, failed to show any cell death and the number of cells after the treatment were equal to the untreated control cells when monitored over a period of 18 hours from the light irradiation step. This study confirms that when particles are directly

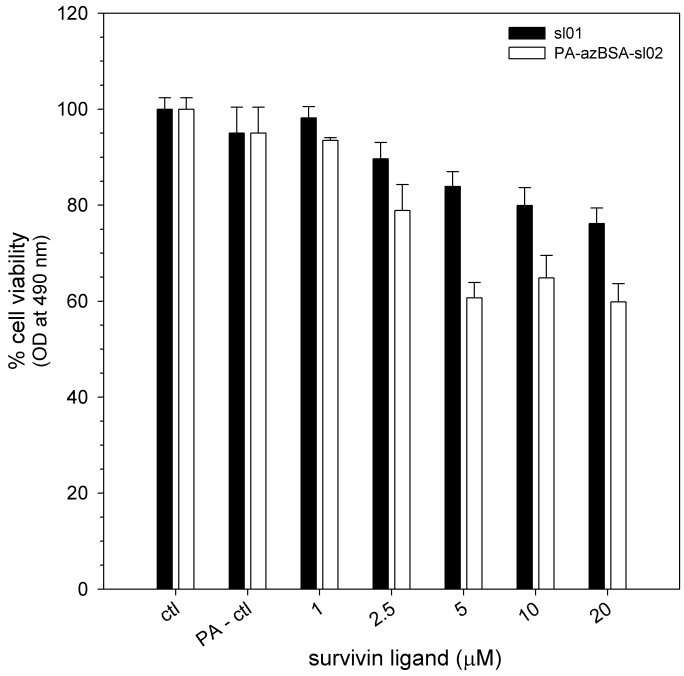

Figure 4.9: Cell viability data using the MTS assay with A549 cells The cells were treated with sl01 and PA-azBSA-sl02 at varying concentrations for 48 hours. Cell viability is presented as percentage of viable cells in total population.

surface modified with fluorophores the energy is lost, perhaps non-radiatively, and causes the singlet oxygen yields to diminish. This failure of PDT with modified particles, leads to a necessity to identify alternate systems which can increase accumulation and *in vivo* circulation lifetimes without decreasing the singlet oxygen yields. As mention earlier, the particle-protein-dye system could be a solution to this issue so the last round of PDT studies was carried out with particles modified with azBSA-SiPc2 conjugate. The preliminary results obtained (cf. Figure 4.8b) for treatment with PA-azBSA-SiPC2 are promising as 12 % cell death was obtained for 1600 nM treatment.

4.3.5 *in vitro* studies of the particles-protein-ligand system

Apart from the delivery and therapy applications of the particle-protein-dye system, this multifunctional system can be used for active targeting applications by replacing the dye in the PA-azBSA-CYN with a ligand, that binds to a specific protein, to enhance targeting capabilities of the ligand. For this enhanced targeting demonstration, the protein chosen is 'Survivin', which

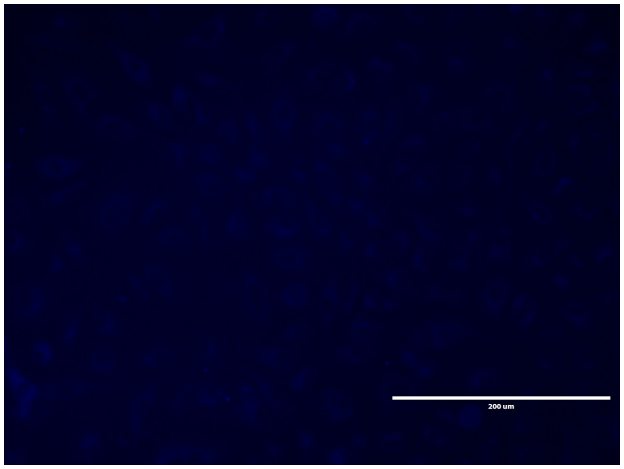

Figure 4.10: *in vitro* fluorescence imaging in A549 cells (after 11 hours of treatment with modified particles)

is a member of the inhibitor of apoptosis (IAP) proteins and regulates cell division and death[178, 230]. In addition, Survivin is abundantly expressed during fetal development in humans, but rarely present in adult tissues, which makes it an attractive target for tumor theranostics in the medical community[180, 181, 182, 183]. The ligand used in this project is sl02 (cf. Figure 4.2), which is an alkyne modified version of the original Abbott17 compound. In 2007, Abbott labs discovered a new direct binding site at the dimer interface of the Survivin and a ligand called Abbott17, which binds specifically to the dimer site using affinity-based screening methods[209]. In this current effort, the Abbott17 is modified to include an alkyne moiety (cf. Figure 4.2) to facilitate the conjugation to azBSA and this small molecule ligand is referred as sl02. The PA-azBSA-sl02 is prepared using the same method as the PA-azBSA-CYN particles. The next step is to determine the binding efficiency of the modified particles to Survivin and verify the enhancement in binding. The binding affinity between the protein and ligand is usually expressed by the binding dissociation constant, K_D, but in the case of the Survivin and Abbott17 binding, the binding efficiency is directly correlated to toxicity so toxicity studies can be used to understand the binding efficiencies between them. According to literature, the ligand binds to the dimer interface of the Survivin and blocks other proteins, such as Ran, which regulate the activity of Survivin. As these other apoptosis inhibitor proteins can no longer bind at the dimer interface, the Survivin can no longer inhibit apoptosis and cell death is observed[180, 218]. Therefore, it can be concluded that higher binding of the ligand, blocks the inhibitors binding at that site and leads to activation of apoptosis, which results in cell death, so

cell toxicity is a direct indicator of the binding of the ligand to the protein, and toxicity studies can be used to prove the enhanced targeting of the Survivin by PA-azBSA-sl02 particles. Preliminary toxicity studies were carried out in A549 cells, which are known to overexpress Survivin. The A549 cells were treated with varying concentrations of sl01, an azide modified version of the Abbott17 compound (cf. Figure 4.2), and PA-azBSA-sl02. After 48 hours, the cell viability was determined using MTS assay. From the cell viability data (cf. Figure 4.9), it is evident that the particles have a higher cell death, which indicates a higher binding affinity of the system compared to the free small molecule. This increase in cell death is as expected because immobilizing the ligand on the particle increases the accumulation of the ligand inside the cells due to enhanced permeability and retention effect and the higher accumulation leads to an increased blocking of the inhibitors that bind at the dimer interface, which results in enhanced cell death. However, one can argue that the higher accumulation is not possible as the modified particles are larger (i.e. diameter greater than 1000 nm) as the particles are held together by the protein and most of the cell death seen could be from the fact that these particles are suffocating the cell at the cell surface. To disprove that, *in vitro* fluorescence imaging study of A549 was carried out to verify the location of the PA-azBSA-sl02 particles. The sl02 has an emission maximum at ca. 424 nm, and can be seen under a DAPI filter on a fluoroscope. For the fluorescence imaging study the A549 cells were treated with 20 μM of PA-azBSA-sl02 particles and the cells were viewed under a fluoroscope with DAPI filer. After 11 hours of treatment, it can be seen that the emission is coming from the inside of the cells, which verifies the argument that the cells take up the modified particles without any issue (cf. Figure 4.10). In addition, we know from the PA-azBSA-CYN system that the modified particles by themselves do not have a strong emission and only upon denaturing or digestion of the azBSA the emission is activated. From the Figure 4.10, it can be said that these particles are being activated *in vitro* either due to the denaturing or cleavage of the peptide bonds when the particles are inside the cell.

4.3.6 Fluorescence resonance energy transfer (FRET) response of the particles-protein-dye system

The bioresponsive aspect of this particle-protein-dye system makes these modified particles attractive for fluorescence resonance energy transfer (FRET) based imaging applications. FRET is a non-radiative transfer of energy from an excited donor molecule to a suitable ground state acceptor

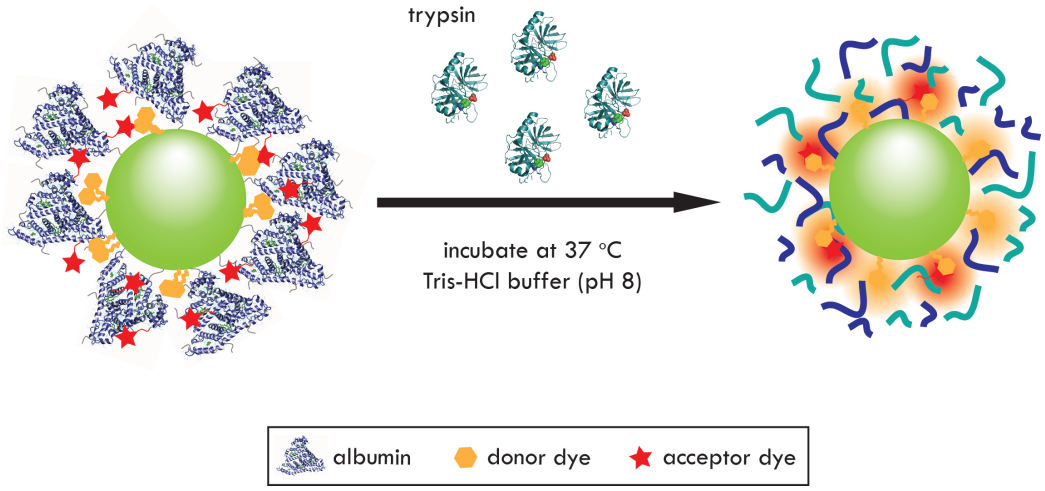

Figure 4.11: Schematic of the FRET response of functionalized particles through trypsin digestion of the albumin. Sub 100 nm poly(propargyl acrylate) (PA) particles were surface modified with (1) an azide modified fluorescein fluorophore and (2) an azide-modified bovine serum albumin (azBSA) that is conjugated to alkyne terminated cyanine derivate fluorophore (YB317), through multiple aqueous-phase click transformations.

molecule in close proximity. This results in emission from the acceptor molecule, when excited at the wavelength for donor emission. The non-radiative transfer of energy is highly dependent on: (1) the distance between the two molecules and is typically effective up to ca. 10 nm; and (2) the spectral overlap of donor's emission and acceptor's absorption. In this current effort, a suitable donor fluorophore is attached to the PA-azBSA-CYN particles and the azBSA on the particles can be digested, folded or unfolded to increase/ decrease the distance between the two fluorophores which results in changes in the FRET response of the particles (cf. Figure 4.11).

The first step in this effort is to identify a fluorophore that forms a good FRET pair with the CYN, which is a cyanine 3 derivative fluorophore. After a literature search, fluorescein is chosen as the donor molecule, as fluorescein (donor) and cyanine 3 (acceptor) fluorophores form a good FRET pair that is well documented and established[269]. The chosen fluorescein fluorophore is modified to include an azide moiety (cf. Figure 4.2), which will facilitate the fluorophore to be attached to the surface of the particles via a 'click' reaction. As mentioned earlier, the FRET response depends on the spectral overlap between the donor's emission and acceptor's absorption, so typically this spectral overlap is used as the parameter to confirm that the chosen donor-acceptor molecules form a good FRET pair. The emission of azFL has a good overlap with the absorbance of the CYN fluorophore (acceptor)(cf. Figure 4.12), which verifies that the modifications of the standard fluorophores did not alter the FRET response of the pair. After the selection and characterization of the

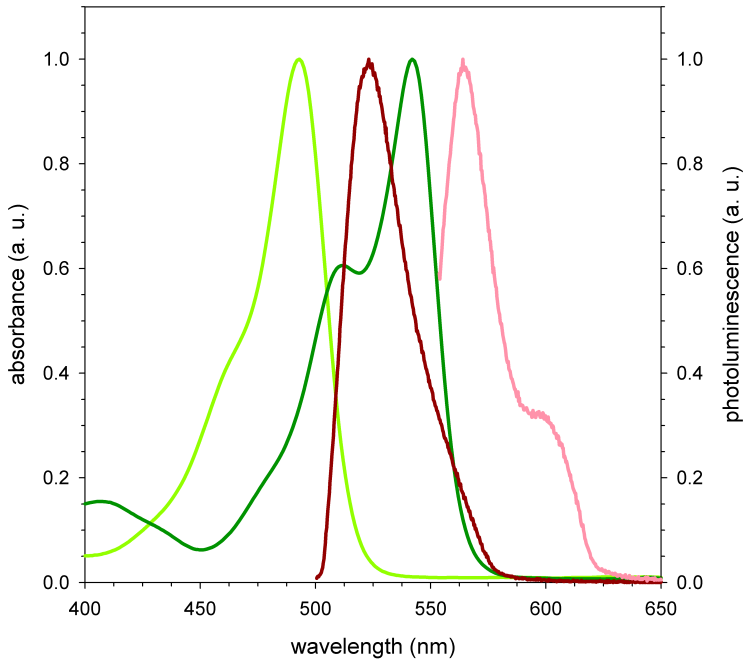

Figure 4.12: Absorbance and photoluminescence spectra of azFL (donor, UV - light green and PL - dark red) and CYN (acceptor, UV - dark green and PL - pink).

donor molecule, the PA particles are surface modified to attach azide modified fluorescein derivative fluorophore (azFL) via 'click' reaction and cleaned to remove unreacted species. Simultaneously, alkyne modified cyanine 3 derivative fluorophore (CYN) was clicked to azBSA and cleaned. Then, these two were parts were 'clicked' together to obtain particles surface modified with azFL and azBSA-CYN conjugate and these particles are referred as PA-azFL-azBSA-CYN.

The changes in the FRET response can be detected using several different methods such as donor or acceptor photobleaching, ratio imaging, sensitized emission and fluorescent lifetime measurements. For this current effort, the interest is mainly in recording the relative changes in FRET efficiency when the azBSA is altered to change the distance between the fluorophores. To this end, a simple ratiometric FRET that provides qualitative changes in FRET efficiency is sufficient. In the ratiometric FRET method the 'relative' FRET efficiency, E_{rel}, is given by equation (4.1), where I_A and I_D are the emission intensities of the acceptor and donor molecules, respectively. The emission of the donor and acceptor molecules of the PA-azFL-azBSA-CYN particles overlap slightly, so the spectra is decomposed into the isolated donor and acceptor emission components

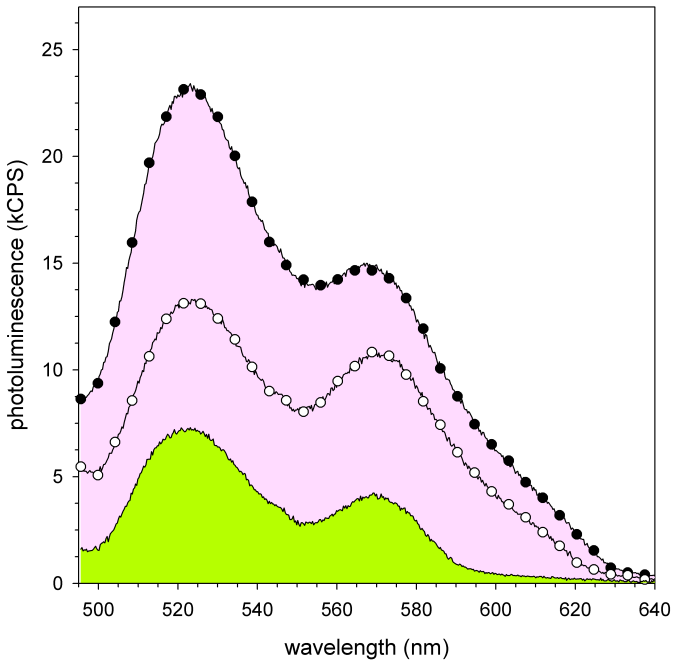

Figure 4.13: Changes in photoluminescence of PA-azFL-azBSA-CYN particles with addition of trypsin and incubation at 37 ^{o}C. Emission of the particles was measured (-) initially, after incubation for (○) 60 mins and (●) 2400 mins. The particles were dispersed in PBS and excited at 440 nm (donor).

before calculating the E_{rel} value. The E_{rel} of the cleaned particles was determined to be ca. 0.27, which indicates a low FRET response. The changes in this value of E_{rel} will give an estimate if the FRET between the two fluorophores is increased or decreased.

$$E_{rel} = \frac{I_A}{I_D + I_A} \tag{4.1}$$

In the previous section, it was established that trypsin digests the azBSA to release the free fluorophore that was attached to the surface of the particles. Upon release, it is expected that the free CYN can be in close proximity to the azFL attached to the surface of the particles and results in an increase of FRET as the distance between the two fluorophores would be lower compared to the initial particles. To verify this assumption, ca. 0.286 mM of trypsin was added to the PA-azFL-azBSA-CYN particles and incubated at 37 ^{o}C. After 60 and 2400 minutes of incubation, the particles were excited at 440 nm (the excitation wavelength of the donor molecule) and the emission was measured (cf. Figure 4.13). From the Figure 4.13, it can be seen that the emission of CYN

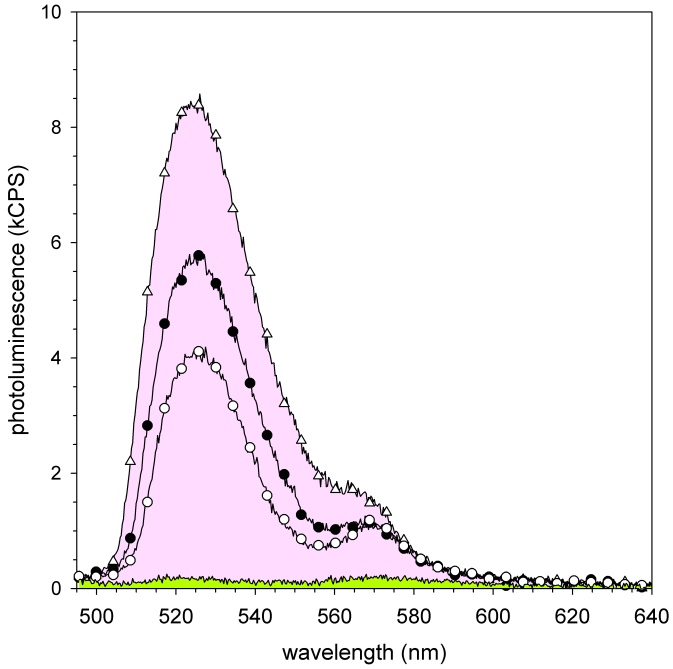

Figure 4.14: Changes in photoluminescence of PA-azFL-azBSA-CYN particles with addition of DTT and incubation at 37 ^{o}C. Emission of the particles was measured (-) initially, after incubation for (○) 30 mins, (●) 90 mins and (△) 210 mins. The particles were dispersed in PBS and excited at 440 nm (donor).

increased as expected and the E_{rel} increased from ca. 0.27 to 0.39 after the 60 minutes incubation. This ca. 46 % increase in ratiometric FRET might not seem significant but it should be noted that this increase being discussed is the ratiometric FRET and not the actual FRET. The conversion to FRET from ratiometric FRET depends on (1) the contribution of direct excitation of the acceptor and (2) the ratio of quantum yields of the donor and acceptor. The quantum yield of fluorescein is higher than that of cyanine 3 and when this difference in quantum yields is accounted for in the conversion to FRET from ratiometric FRET, the increase in FRET will be significant[270, 271, 272].

In the current study, it was noticed that after the initial increase in ratiometric FRET, it dropped to 0.33 at longer incubation times. The drop at longer times is unexpected and could be either due to the fact that at longer durations the fluorophore might be falling out of solution or FRET quenching is occurring. Another interesting change that was noticed during the tryptic digestion of PA-azFL-azBSA-CYN particles is that along with the increase in FRET, the emission of azFL (donor) also increased significantly. This increase in azFL emission indicates that the emission

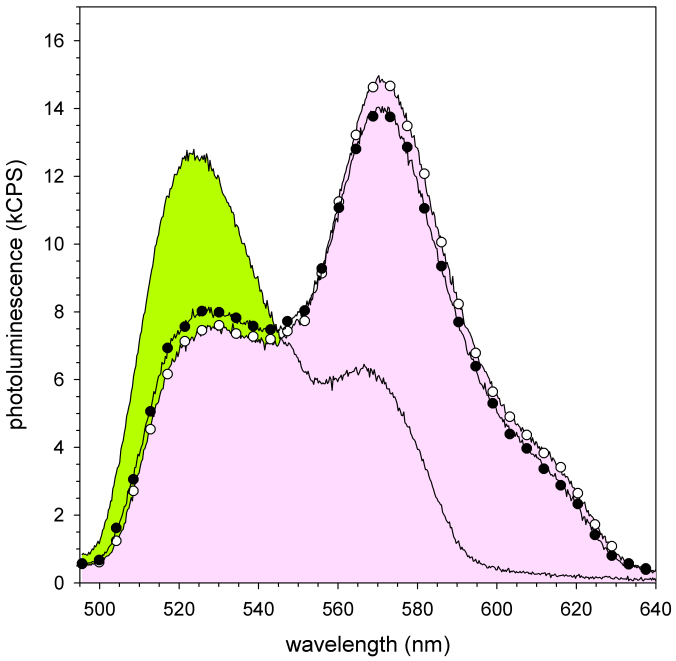

Figure 4.15: Changes in photoluminescence of PA-azFL-azBSA-CYN particles with addition of l-glutathione and incubation at 4 ^{o}C. Emission of the particles was measured (-) initially, after incubation for (○) 40 mins and (●) 1230 mins. The particles were dispersed in PBS and excited at 440 nm (donor).

of azFL was quenched initially by the azBSA-CYN conjugate. This quenching of the azFL emission is not surprising as it was demonstrated previously in literature, where attachment of azPEG molecules on the surface of the particles decreased the emission of the modified particles[71]. Further, it is stated that the emission is dependent upon the grafting density of the fluorophore and at low grafting densities, a higher emission is obtained[71]. Based on that, it can be concluded that initially the azFL on the particles transfer energy non-radiatively to the azBSA-CYN conjugate and the emission is quenched. Upon trypsin digestion the azBSA is broken down into smaller peptides and no longer available for the azFL to transfer energy non-radiatively which results in the increase in emission of azFL. In addition, this explains the drop in ratiometric FRET at longer periods of incubation time. Initially, it was speculated that the drop could be due to the fluorophore falling out of solution or FRET quenching, but that might not be the case as we know that there are two phenomena happening during tryptic digestion. First is the FRET between the two fluorophore and second is the turn on of the quenched emission of azFL by the azBSA conjugate. This implies that the initial

increase in ratiometric FRET is mainly due to increase in FRET but at longer times it is possible that the dominant change in ratiometric FRET is due to an increase in emission of azFL and the FRET might be the same or unchanged. In addition, in this system the azFL is in grafted in excess of CYN and upon digestion it is possible that not all of the azFL is in close proximity of the CYN, so the energy of those fluorophores is not transferred to CYN and emits radiatively upon excitation.

Our current effort is to demonstrate the changes in FRET with modifying or unfolding the azBSA and we have established that with trypsin digestion, a ca. 46 % increase in ratiometric FRET can be obtained for the fluorophore pair of azFL and CYN. The next step is to monitor the changes in FRET of these modified particles with the addition of strong reducing agents such as dithiothreitol (DTT) and l-glutathione. Both of these compounds are routinely and frequently used to reduce the disulfide bonds of proteins and prevent unwanted or wrong disulfide bonding between the thiol groups of proteins[273, 274, 275]. First, the changes with respect to addition of DTT are studied. DTT reduces a typical disulfide bond by two sequential thiol-disulfide exchange reactions and the reduction usually does not stop at the mixed-disulfide species because the second reaction, which forms the 6-membered ring containing the disulfide bridge, is more energetically favored[273, 276]. The reducing power of DTT is limited to pH values above 7, since only the negatively charged thiolate form -S is reactive (the protonated thiol form -SH is not)[276, 277]. In addition, DTT cannot reduce buried (solvent-inaccessible) disulfide bonds, so sometimes the reduction of disulfide bonds has to be carried out under denaturing conditions, such as high temperatures or in the presence of strong denaturants like urea or sodium dodecylsulfate[278]. In this project, the modified particles are mixed with ca. 43 mM DTT and incubated at 37 ^{o}C. After 30, 90 and 210 minutes of incubation, the particles were excited at 440 nm (the excitation wavelength of the donor molecule) and the emission was measured (cf. Figure 4.14). The calculated E_{rel} dropped significantly to 0.05. Unlike in the case of trypsin, where both an increase in ratiometric FRET and azFL emission increased, here the ratiometric FRET decreased and the azFL emission increased. This leads to the speculation that the change in actual FRET is not known as the ratiometric FRET is mainly dominated by the increase in azFL emission. Moreover, the temperatures used for the incubation were not high nor were there other denaturants used so it is possible that only some of the disulfide bonds of azBSA are reduced and the protein is partially unfolded[279, 280]. Consequently, the azBSA is no longer quenching azFL emission and as the protein is only partially unfolded the distance between the two fluorophores could either be the same or increased. It is well known that FRET is dependent on the

proximity of the two molecules so if the distance is the same or increased then FRET either does not change or decreases, respectively. It is also possible that the DTT might be oxidized as it is old so it might not be reducing the disulfide bonds effectively. Secondly, coming to changes with the addition of l-glutathione, a better FRET response was obtained (cf. Figure 4.15). L-glutathione also reduces the disulfide bonds but is stronger reducing agent than DTT. It is possible that the l-glutathione reduced the azBSA effectively, so the azBSA unfolded and collapsed on the surface of the particle where more of the azFL come in close proximity to the CYN, which subsequently results in an increase in ratiometric FRET. When ca. 21.7 mM of L-glutathione was added to the modified particles and incubated at 4 ^{o}C for 40 minutes, the ratiometric FRET increased from 0.23 to 0.62 (cf. Figure 4.15). The FRET response was measured again at longer incubation time of 1230 minutes and only a slight drop in the ratio was observed. Overall, from the entire FRET responses studied it can be concluded that the highest increase in FRET response of the PA-azFL-azBSA-CYN particles was achieved when the azBSA was reduced using L-glutathione and ca. 156 - 171 % increase in ratiometric FRET can be obtained.

4.4 Experimental

4.4.1 Reagents and solvents

All the commercial reagents were used without further purification. All the solvents were dried according to standard methods. Deionized water was obtained from a Nanopure System and exhibited a resistivity of ca. 10^{18} ohm^{-1}cm^{-1}.

4.4.2 Characterization

^{1}H and ^{13}C NMR spectra were recorded on JEOL ECX-300 spectrometers (300MHz for proton and 76MHz for carbon). Chemical shifts for protons are reported in parts per million downfield from tetramethylsilane and are referenced to residual protium in the NMR solvent ($CDCl_3$: δ 7.26 ppm, DMSO-d6: δ 2.50 ppm). Chemical shifts for carbons are reported in parts per million downfield from tetramethylsilane and are referenced to the carbon resonances of the solvent ($CDCl_3$: δ 77.16, DMSO-d6: δ 39.52 ppm). Electron impact (EI) (70 eV) ionization mass spectra were obtained using Shimadzu GC-17A mass spectrometer. LC/MS mass spectra were obtained using Finnigan

LCQ spectrometer and HP 1100 (HPLC). Thermal denaturation data of the proteins was obtained using TA instruments Nano DSC.

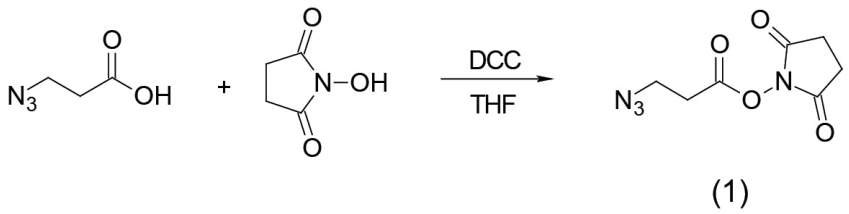

Figure 4.16: Reaction scheme for synthesis of azNHS.

The azNHS was prepared based on the method published[281]. The reaction scheme for the synthesis of azNHS is presented in Figure 4.16.

2,5-dioxopyrrolidin-1-yl 3-azidopropanoate (1) 2-azidopropyonic acid (1.8 g, 15.64 mmol) and N-hydroxysuccynimide (1.98 g, 17.2 mmol) were dissolved in THF (30 ml). Obtained solution was cooled with ice and N,N'-dicyclohexylcarbodiimide (3.54 g, 17.2 mmol) was added. Mixture was stirred at cooling for 0.5 hour, then at room temperature for 6h and filtered. Insoluble solid was washed with dichloromethane. Filtrates were combined and evaporated, the residue was dissolved in dichloromethane (15 ml), cooled in freezer and filtered to remove precipitates. The filtrate was evaporated. Product was used in the next reactions without additional purification. Yield 3.3 g (99 %), clear oil. ^{1}H NMR ($CDCl_3$) δ 2.86 (s, 4H), 2.89 (t, 2H, J = 6.5 Hz), 3.69 (t, 2H, J = 6.5 Hz).

The reaction scheme for the synthesis of CYN is presented in Figure 4.17.

5-Iodopent-1-yne (2) 5-Iodopent-1-yne was synthesized according to the literature[282].

1,2,3,3-tetramethyl-3H-indolium iodide (3) 1,2,3,3-tetramethyl-3H-indolium iodide was synthesized according to the literature[283]. 2,3,3-trimethyl-3H-indole (0.5 g, 3.14 mmol) and iodo-

methane (1.34 g, 9.42 mmol) were dissolved in acetonitrile (5 ml) and refluxed for 5 hours. After cooling, the precipitated solid was filtered and washed with acetone then dried to give white crystalline product. Yield 0.94 g (99 %), mp = 259 ^{o}C (lit). ^{1}H NMR (DMSO-d6) δ 1.53 (s, 6H), 2.76 (s, 3H), 3.97 (s, 3H), 7.60 - 7.64 (m, 2H), 7.81 - 7.84 (m, 1H), 7.90 - 7.93 (m, 1H).

2,3,3-trimethyl-1-pent-4-ynyl-3H-indolium iodide (4) The solution of 2,3,3-trimethyl-3H-indole (0.83 g, 5.21 mmol) and 5-iodo-pent-1-yne (1.5 g, 7.82 mmol) in acetonitrile (10 ml) was

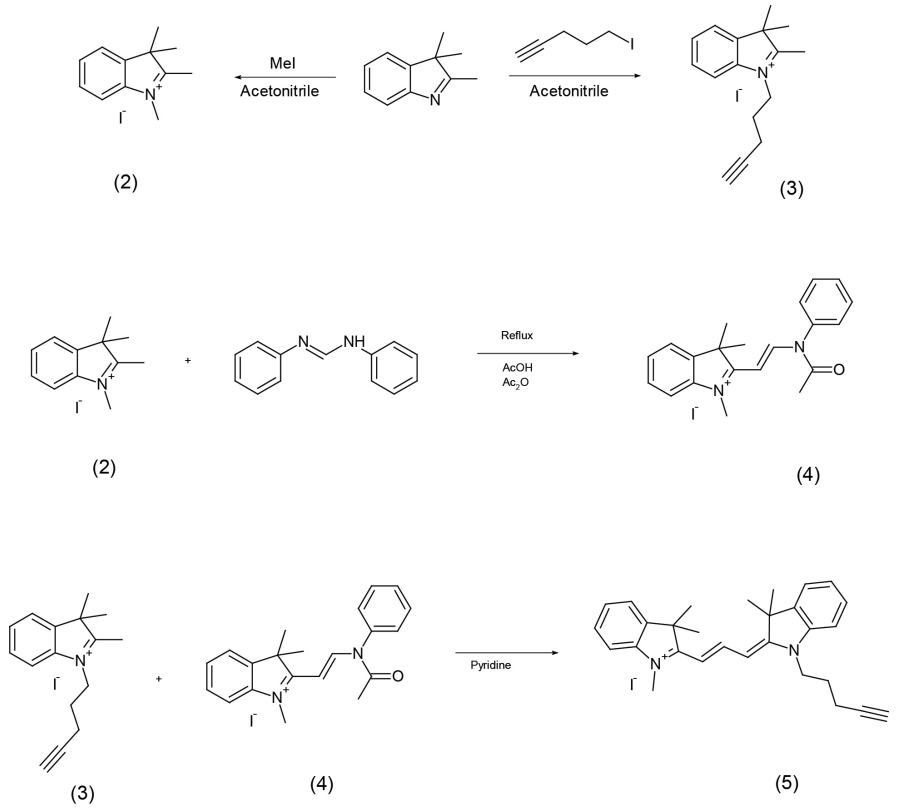

Figure 4.17: Reaction scheme for synthesis of CYN.

refluxed for 24 hours. After cooling, the solvent was evaporated and the brown residue quenched with acetone to crystallize a product. Obtained solid was filtered, washed with acetone and dried. Yield 1.05 g (57 %), mp = 190 - 191 ^{o}C. ^{1}H NMR (DMSO-d6) δ 1.54 (s, 6H), 2.06 (m, 2H, J = 7.4 Hz), 2.42 (m, 2H, J = 7.4 Hz, J = 2.6 Hz), 2.84 (s, 3H), 2.96 (t, 1H, J = 2.6 Hz), 4.92 (t, 2H, J = 7.4 Hz), 7.63 (m, 2H), 7.85 (m, 1H), 7.96 (m, 1H).

2-[2-(acetyl-phenyl-amino)-vinyl]-1,3,3-trimethyl-3H-indolium iodide (5) 1,2,3,3-tetramethyl-3H-indolium iodide (3) (0.65 g, 2.16 mmol) and N,N'-diphenyl-formamidine (0.51 g, 2.60 mmol) were mixed with acetic acid (8 ml) and acetic anhydride (4 ml). Obtained mixture was refluxed and stirred for 1 hour. After cooling, the solvent was evaporated, the residue was dissolved in dichloromethane (2 ml) and added to diethyl ether solution. Precipitated dark solid was separated by centrifugation. This crude product was dissolved in dichloromethane and washed with water. Organic layer was separated and evaporated, obtained residue was dissolved in dichloromethane and precipitated with diethyl ether once again. The dark-brown solid was filtered and dried. Yield 0.87

g (90 %), solid, mp = 228 ^{o}C. ^{1}H NMR (CDCl3) δ 1.83 (s, 6H), 2.11 (s, 3H), 3.85 (s, 3H), 5.59 (d, 1H, J = 14.3 Hz), 7.46 - 7.50 (m, 4H, J = 5.2 Hz, J = 1.4 Hz), 7.53 - 7.55 (m, 2H, J = 5.2 Hz, J = 1.4 Hz), 7.63 - 7.73 (m, 3H, J = 7.4 Hz, J = 1.4 Hz), 9.17 (d, 1H, J = 14.3 Hz).

2-[3-(3,3-dimethyl-1-pent-4-ynyl-1,3-dihydro-indol-2-ylidene)-propenyl]-1,3,3-trimethyl-3H-indolium iodide (6) Compounds (4) and (5) were dissolved in pyridine (6 ml) and stirred at 45 ^{o}C for 3 hours. After cooling, the solution was added dropwise to diethyl ether solution to precipitate a dark-brown crude product which was separated by centrifugation. Organic solution was decanted and obtained residue was dissolved in dichloromethane, washed with water. Organic layer was separated and concentrated. Product was precipitated from diethyl ether solution two more times, filtered, dried. Yield 0.12 g (50 %), brown solid, mp = 211 - 213 ^{o}C with destruction. ^{1}H NMR (CDCl3) δ 1.70 (s, 12H), 2.08 (t, 1H, J = 2.5 Hz), 2.11 (m, 2H, J = 6.6 Hz, 7.7 Hz), 2.62 (m, 2H, J = 6.6 Hz, J = 2.5 Hz), 3.80 (s, 3H), 4.40 (t, 2H, J = 7.7 Hz), 7.11 - 7.54 (m, 10H), 8.43 (t, 1H, J = 13.5 Hz); ^{1}3C NMR (CDCl3) δ 16.51, 26.22, 28.20, 28.29, 32.94, 43.67, 48.90, 69.81, 83.65, 104.96, 105.44, 110.92, 111.04, 122.13, 122.19, 125.36, 125.42, 128.98, 129.04, 140.60, 142.27, 142.79, 150.95; ESI-Mass (m/z): calculated for $C_{29}H_{33}N_2$ $[M\text{-}I]^+$ 409.26, found 409.27.

The Survivin ligands (sl01 and sl02) were synthesized according to the literature[209, 248, 249]. The reaction scheme for the synthesis of sl02 is presented in Figure 4.18.

4-(prop-2-yn-1-yloxy)benzaldehyde (7) p-hydroxybenzaldehyde (0.3 g, 2.45 mmol) and propargyl bromide (0.38 g, 3.19 mmol) were dissolved in acetone (20 ml), then potassium carbonate (0.34 g, 2.46 mmol) was added. Obtained mixture was stirred under reflux for 12 hours. After cooling, the mixture was quenched with cold water, extracted with dichloromethane. Organic solution was washed with water, separated, dried with Na_2SO_4, filtered, evaporated under reduced pressure. Yield 0.32 g (82 %). Clear crystals, mp = 73 - 74 ^{o}C. ^{1}H NMR (CDCl3) δ 2.57 (t, 1H, J = 2.4 Hz), 2.77 (d, 2H, J = 2.4 Hz), 7.08 (d, 2H, J = 8.9 Hz), 7.85 (d, 2H, J = 8.9 Hz), 9.89 (s, 1H).

6-(5-chloro-2-hydroxyphenyl)-2-oxo-4-(4-(prop-2-yn-1-yloxy)phenyl)-1,2-dihydropyridine-3-carbonitrile (8) 1-(5-chloro-2-hydroxyphenyl)ethanone (0.266 g, 1.56 mmol) and 4-(prop-2-yn-1-yloxy)benzaldehyde (7) (0.3 g, 1.87 mmol) were dissolved in dry ethanol (7 ml). Ethyl cyanoacetate (0.23 g, 2.03 mmol) and ammonium acetate (0.72 g, 9.36 mmol) were added into the solution. Mixture was stirred in sealed pressure vessel at 110 ^{o}C for 2 hours. After cooling, precipitated solid was filtered and washed with cold ethanol then with water, dried, purified by flash

column chromatography on silica. Solvent ethyl acetate, $R_f = 0.9$. Yield 0.09 g (15 %), mp = 229 ^{o}C. ^{1}H NMR (DMSO-d6) δ 3.64 (t, 1H, J = 2.2 Hz), 4.92 (d, 2H, J = 2.2 Hz), 7.13 (d, 2H, J = 8.9 Hz), 7.42 (d, 1H, J = 8.9 Hz), 7.66 (d.d, 1H, J = 8.6 Hz, J = 2.4 Hz), 7.91 (br.s, 1H), 8.01 (s, 1H), 8.33 (d, 2H, J = 8.6 Hz), 8.71 (d, 1H, J = 2.4 Hz); ^{13}C NMR (DMSO-d6) δ 55.59, 78.58, 79.05, 95.40, 100.41, 114.78, 118.72, 119.03, 124.68, 129.05, 129.18, 130.37, 130.64, 132.03, 143.48, 150.62, 158.30, 159.18, 160.18, 160.59, 160.64; ESI-Mass (m/z): calculated for $C_{21}H_{13}ClN_2O_3$ $[M+H]^+$ 377.07, found 377.07.

The reaction scheme for the synthesis of azFL is presented in Figure 4.19.

2-(3-(3-azidopropoxy)-6-hydroxy-9H-xanthen-9-yl)benzoic acid (9) and 3-azidopropyl 2-(3,6-dihydroxy-9H-xanthen-9-yl)benzoate (10) Fluorescein (0.8 g, 2.4 mmol), 1-azido-3-iodopropane (0.51 g, 2.4 mmol) and potassium carbonate (0.33 g, 2.4 mmol) were mixed with dry DMF (15 ml) and stirred at 80 ^{o}C for 14 hours. After cooling, the mixture was quenched with water. Precipitated orange solid was filtered, washed with water and dried to give 0.926 g of mix of isomers 1 and 2 with a ratio 2:1. ^{1}H NMR (DMSO-d6) (mix of two compounds) δ 1.53 (m, 2H), 2.02 (m, 1H), 3.09 (t, 2H), 3.52 (t, 2H), 3.99 (t, 2H), 4.22 (t, 1H), 6.27 (d, 0.5H), 6.42 (d.d, 0.5H), 6.61 (m, 3.5H), 6.81-6.95 (m, 3H), 7.27 (m, 1H), 7.50 (m, 1H), 7.70-7.90 (m, 3H), 8.00 (m, 0.5H), 8.22 (m, 1H).

4.4.3 Optical characterization methods

Absorption spectra were taken using a Perkin-Elmer Lambda 900 UV/VIS/NIR spectrophotometer. Photoluminescence (PL) spectra were collected using a Thermo Oriel xenon arc lamp (Thermo Oriel 66902) mated with a Thermo Oriel Cornerstone 7400 1/8m monochromator (Thermo Oriel 7400) and a Horiba Jobin-Yvon MicroHR spectrometer coupled to a Synapse CCD detector.

4.4.4 Materials

4.4.5 Preparation of the particles

Propargyl acrylate (PA) particles were prepared according to published method.

Cell analysis. Human A549 cell lines was obtained from ATCC (Rockville, MD) and were cultured in F-12K media (Kaighn's Modification of Ham's F-12 medium) containing 10 % fetal bovine serum

(FBS) and 1 % Penicillin-Streptomycin. Human UMSCC22A head and neck squamous carcinoma cell line was a gift from Dr. Besim Ogretmen (Medical University of South Carolina) and were cultured in Dulbeccos modified Eagles media (DMEM) supplemented with L-glutamine containing 10 % FBS and 1 % Penicillin-Streptomycin. Cells were cultured at 37 ^{o}C in a humidified atmosphere of 95 % air 5 % CO_2.

Photodynamic therapy. Cell cultures were incubated with 50 - 400 nm of the sample for 18 hours before exposure to 200 - 400 mJ/cm2 red light (670 nm) from an Intense-HPD 7404 diode laser (North Brunswick, NJ). After exposure to red light, cells were incubated for various periods of time prior to analysis. Cell death was assessed by propidium iodide (PI) fluorometry using a multi-well fluorescence plate reader, as previously described[284]. Before exposure to light, cells were changed to fresh medium supplemented with PI (30 m) and Insulin-Transferrin-Selenium-X (ITX) reagent [insulin (10 g/ml), transferrin (5.5 g/ml), selenium (6.7 ng/ml), ethanolamine (0.2 mg/ml)] (Gibco) but omitting FBS. PI fluorescence was measured at frequent intervals using 530 nm excitation (25 nm band pass) and 620 nm emission (40 nm band pass) filters. Between measurements, microliter plates were placed in a 37 ^{o}C incubator. At the end of the experiment, digitonin (200 m) was added to each well to permeabilize all cells and label all nuclei with PI. Cell viability determined by PI fluorometry is essentially the same as cell viability determined by trypan blue exclusion[284].

Fluorescence imaging. A549 cells (60,000 cells per well) were cultured on 12 well plates for 24 hours. Subsequently, cells were, exposed to 20 μM of PA-azBSA-sl02. The emission from the treated particles was monitored with a DAPI filter on the Life Technologies EVOS® FL Cell Imaging System.

Cytotoxicity assay. A549 cells (5,000 cells per well) were cultured on 96 well plates for 24 hours. Subsequently, cells were, exposed to 20 μM of PA, 1, 2.5, 5, 10, 15 and 20 μM of sl01, and 1, 2.5, 5, 10, 15 and 20 μM of PA-azBSA-sl02. After 48 hours, cell death was assessed with a MTS assay according to the manufacturer's instructions (Promega, Madison, WI). Briefly, medium was aspirated and a solution of 100 μL of F-12K containing 10% FBS and μL 3-(4,5-dimethylthiazol-2-yl)-5-(3-carboxymethoxyphenyl)-2-(4-sulfophenyl)-2H-tetrazolium, salt (MTS) and phenazine methosulfate (PMS) was added onto each well. After 150 minutes, wells were scanned colorimetrically at 490 nm on a spectrophotometer. The conversion of MTS into an aqueous soluble formazan product

is achieved only by dehydrogenase enzymes, which are present in metabolically active cells; the absorbance at 490 nm from the formazan product is directly proportional to the number of living cells in culture. Cell viability was presented as percentage of viable cells in total population.

4.5 Conclusion

The sub 100 nm poly(propargyl acrylate) particles were surface modified with an azide modified bovine serum albumin that is covalently conjugated to alkyne terminated fluorophore, through a multi-step copper-catalyzed azide/ alkyne cycloaddition. Initially, these particles have a quenched emission, and upon trypsin digestion they exhibited an activation of emission due to the cleavage of the protein and release of the fluorophore. This release strategy gave promising results when the silicon phthalocyanine fluorophore is used in photodynamic therapy studies. The particles can also be used for fluorescence imaging studies and when modified with a FRET pair of fluorophores, the FRET efficiency can be tuned by unfolding the protein. The particles are modified with drugs or antibodies instead of the fluorophores, and are more effective than the free small molecule in drug delivery and targeting applications. In addition, the fluorophore and drugs modifications can be combined and attached to the same particle for direct visualization of the treatment, which will enable the physician to decide and modify the treatment of the tumors easily. To conclude, the particles modified with environmentally sensitive molecules using the bovine serum albumin as the linker exhibited promising results for theranostic applications of tumors and if optimized better this strategy will become a new and valuable platform for personalized medicine. This versatile nanodevice is not just limited to the fight against cancer but has a huge potential to be expanded to treatment of several other diseases and vaccinations, due to the ease of the modification of the particles with several moieties.

Acknowledgments

The authors thank the Gregg-Graniteville Foundation for financial support and TA instruments for the loaner Nano DSC.

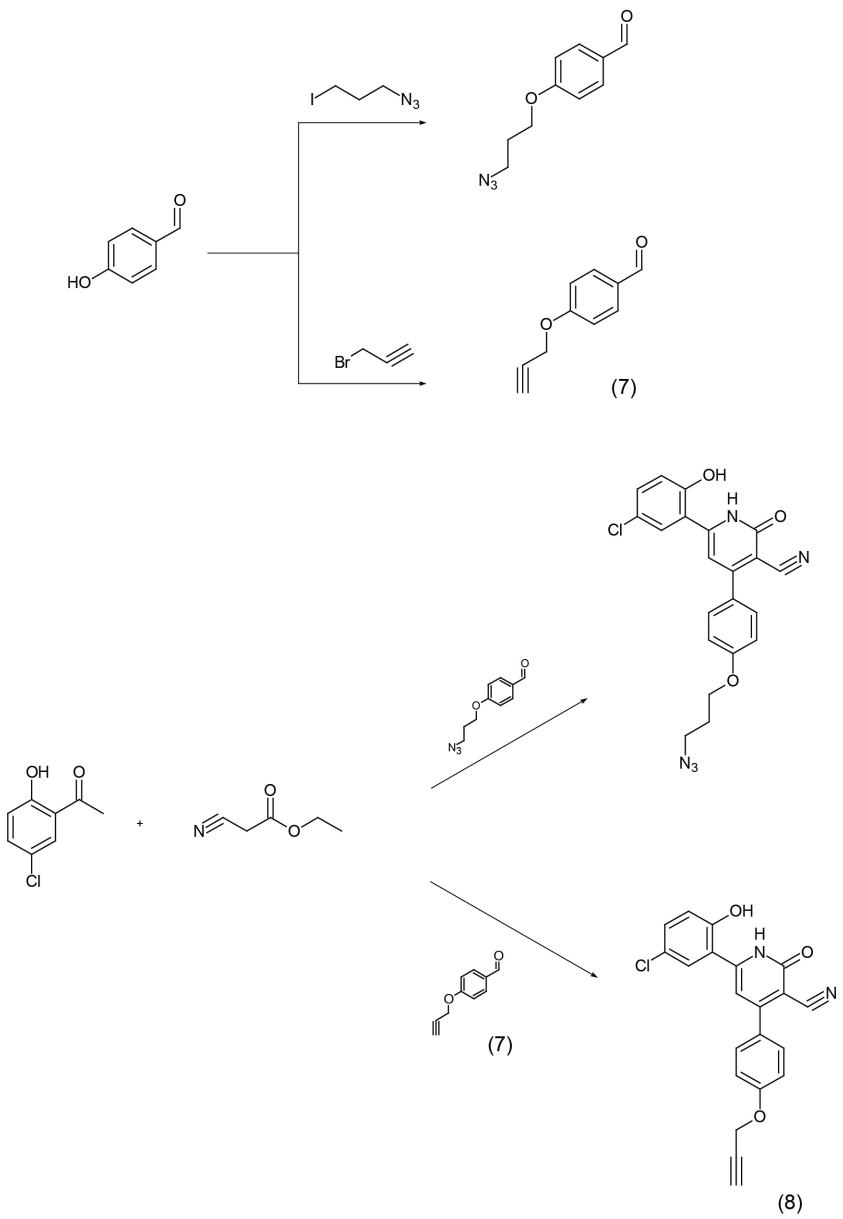

Figure 4.18: Reaction scheme for synthesis of sl02.

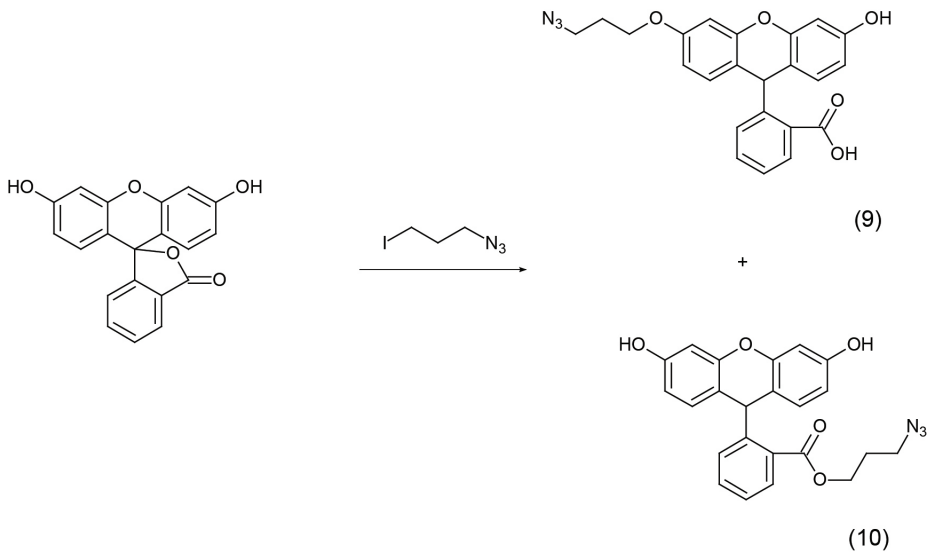

Figure 4.19: Reaction scheme for synthesis of azFL.

Chapter 5

Conclusions

5.1 Summary

The main objective of this project is to develop a polymer based near infrared (NIR) particle that can serve as both, diagnostic and therapeutic agents, for fighting cancer. Specifically these particles will be designed to have high-contrast, high signal to noise ratios, long *in vivo* circulation lifetimes, and facilitate easy attachment of functional and target components. To this end, a flexible platform of sub-100 nm poly(propargyl acrylate) (PA) particles was synthesized. These PA particles can be surface-functionalized with fluorophores or targeting molecules or drugs through a copper(I) catalyzed azide-alkyne Huisgen 1,3-Dipolar cycloaddition, and used for cancer theranostics. The results obtained are summarized below and indicate the efficiency of the PA nanoparticles in various applications:

(1) *Switching fluorescence of surface modified colloids with near-infrared emitters via protein interaction for contrast-enhanced imaging (cf. Chapter 2)*; conclusions drawn from this work include:

- PA particles were surface functionalized with an azide terminated squaraine derivative fluorophore (azSQ) and azide terminated poly(ethylene glycol) (azPEG) chains.
- Attachment of azPEG on the nanoparticle increased the nonradiative transfer of the emitters during the return to ground state.
- Lower grafting densities of azSQ on nanoparticles resulted in higher quantum efficiencies, due to lower rates of aggregation.

- The placement of azSQ onto the surface of the particles allowed for the fluorophores to complex with proteins that resulted in the enhancement of the dye emission.
- The quantum efficiency of the nanoparticles can be boosted by a simple annealing experiment.
- Tryptic digestion was used to deactivate the nanoparticles, and can be reactivated when desired.
- In human UMSCC22A head and neck squamous carcinoma cells, the non-toxic, functionalized particles are taken up by endosomes/lysosomes, and 80 % of these nanoparticles co-localized with the lysosome after 17 hours of incubation.
- The activation/ deactivation of the emission of the functionalized particles was demonstrated in human A549 alveolar adenocarcinoma cells.

(2) *Surface modified colloids with targeting molecules to disrupt Survivin activity and enhance apoptosis in cancer cells (cf. Chapter 3)*; conclusions drawn from this work include:

- PA particles were surface functionalized with an azide-terminated Survivin ligand derivative (azTM).
- azTM is a small molecule that specifically targets and binds directly to Survivin (protein) at the dimer interface of the protein, which disrupts the activity of anti-apoptotic proteins that are over-expressed by cancer cells and is a potentially attractive route to combating this disease.
- Using affinity pull studies, it was determined that the binding specificity of the Survivin ligand is not compromised when attached to particles and over 85 % of the Survivin bound to the functionalized particles.
- *In vitro* cytotoxicity studies with functionalized particles that were carried out in glioblastoma, A549 and MCF7 cells indicated a higher percentage of cell death relative to cells incubated with the original Abbott-derived small molecule.
- In situ Wright staining studies indicated that the cell death observed in glioblastomas was through apoptosis and an apoptotic/necrotic/healthy cells detection kit was used to confirm the apoptotic cell death in A549 cells.

- Western blotting studies for the proteins indicated that the functionalized particles facilitated for an enhanced increase in Caspase-3, a protein which is believed to play a central role in the execution-phase of cell apoptosis.

(3) *A bioresponsive and versatile particle-protein-dye system for small molecule delivery and FRET based imaging (cf. Chapter 4)*; conclusions drawn from this work include:

- PA particles were surface functionalized with an azide modified bovine serum albumin (BSA) that was covalently conjugated to alkyne terminated cyanine derivative fluorophore (CYN).
- The quenched emission of these functionalized particles was activated upon trypsin digestion because the fluorophores went from being in a aggregated state, which caused the quenching of emission, to free fluorophore in solution.
- The particles surface was modified with an azide terminated fluorescein fluorophore (azFL), which is a fluorescence resonance energy transfer (FRET) pair to CYN, for FRET based imaging. The FRET efficiency was tuned by altering the protein unfolding, which was through heating and addition of denaturants such as L-glutathione.
- *In vitro* cytotoxicity studies for PA particles modified with BSA conjugated to azTM were carried out in A549 cells to illustrate that they were more effective than the free small molecule, and fluorescence imaging in A549 cells showed that these particles were taken up by the cells even though the size of these were > 100 nm.
- Although the PDT study with the PA particles modified with BSA conjugated to SiPc (an alkyne terminated silicon phthalocyanine derivative fluorophore) is promising, more thorough studies with the functionalized particles are necessary and those studies are currently being pursued by other members of the Foulger group.

5.2 Recommendations for future research

The results discussed in this dissertation establish that the polymeric nanoparticles are a promising platform for cancer theranostics and lead to numerous possibilities for future work. Firstly, the particle-protein-dye system can be explored in detail for photodynamic therapy. For this study, a short alkyne PEG terminated silicon phthalocyanine can be attached to proteins and subsequently

clicked to PA particles. Cytotoxicity and colocalization studies in tumor cells with these modified particles can be carried out to better understand the uptake mechanism of the particles and improve photodynamic therapy studies. Secondly, the targeting strategy can be expanded to target the epidermal growth factor receptors (EGFR) located on cell surface and overexpressed by tumors. Small molecules such as gefitinib can be modified to include an azide group and then attached to particles via a 'click' reaction. Gefitinib is a small molecule drug that specifically binds to EGFR at the adenosine triphosphate (ATP)-binding site of the enzyme, which interrupts the signaling and activates apoptosis. Thirdly, the particulate platform can be used to improve EGFR tyrosine kinase inhibitors (TKIs) treatment for non-small cell lung cancer (NSCLC). Recently, it has been discovered that the overall response rate to EGFR TKIs is limited because the treatment with the TKIs such as erlotinib and gefitinib result in an overexpression of the Survivin, which in turn protects the cells from TKI treatment induced apoptosis. To this end, the particle platform can be beneficial for sequential application of drugs/ small molecules to enhance cell death by rewiring apoptotic signaling networks. In this scenario, a TKI such as gefitinib can be directly attached to the particle and the Survivin ligand is attached to the particles via the albumin linker. Upon treatment with the particles, initially the particles bind to EGFR and lead to the activation of the apoptosis pathway. The Survivin ligand is attached to the protein so it is released eventually after the digestion of protein and restrains the overexpressed Survivin activity. Fourthly, the drug release strategy can be improved to a specific response stimuli particles. For this scenario instead of using albumin, the linker can be switched to a desired amino acid sequence, where one end is attached to the small molecule and the other to the particle. This allows for tuning the release of the small molecule occurs during a specific desired digestion environment. Fifthly, the particles can be modified to attach DNA/ RNA strands and used as a transfection method or in DNA/ RNA based therapeutic applications. Lastly, the particle platform can be expanded to other applications apart from cancer theranostics. Sub-100 nm colloidal particles with an intrinsic radioluminescent component (core) can be synthesized and the exterior of the particle (shell) can be functionalized with multiple environmentally-sensitive moieties that have the potential to combine opsin activation and imaging with a single type of "nanodevice". The particles can be additionally surface-modified with targeting ligands that have an affinity for a protein domain engineered within the target opsin. Once tethered to the opsin, routine medical levels of radiation (or lower) will be used to activate the radioluminescent component of the particles. This light is then free to gate open the channel component of the opsin protein. The activation will

be through a judiciously chosen donor-acceptor pairing to achieve Forster resonance energy transfer (FRET), reducing or eliminating all local temperature increases normally experienced when the region around the opsin is flooded by light. In this way, RLP technology is superior to current methods because (1) it obviates the need for implanting devices into the brain tissue that can cause damage and lose effectiveness over time, (2) it can be modulated to much lower power densities to achieve opsin activation (reducing damage to tissue), and (3) the uniformity of light delivery will reduce non-specific effects of a graded response due to light absorption and scatter from a single point source.

Appendix

Appendix A Copyright Permissions

ELSEVIER LICENSE
TERMS AND CONDITIONS

Jul 13, 2015

This is a License Agreement between Ragini Jenkins ("You") and Elsevier ("Elsevier") provided by Copyright Clearance Center ("CCC"). The license consists of your order details, the terms and conditions provided by Elsevier, and the payment terms and conditions.

All payments must be made in full to CCC. For payment instructions, please see information listed at the bottom of this form.

Supplier	Elsevier Limited The Boulevard,Langford Lane Kidlington,Oxford,OX5 1GB,UK
Registered Company Number	1982084
Customer name	Ragini Jenkins
Customer address	2550 Redlich Ct DECATUR, IL 62521
License number	3667350932836
License date	Jul 13, 2015
Licensed content publisher	Elsevier
Licensed content publication	Advanced Drug Delivery Reviews
Licensed content title	Imaging and drug delivery using theranostic nanoparticles
Licensed content author	J. Andrew MacKay,Ara S. Moses,J. Andrew MacKay
Licensed content date	30 August 2010
Licensed content volume number	62
Licensed content issue number	11
Number of pages	12
Start Page	1052
End Page	1063
Type of Use	reuse in a thesis/dissertation
Portion	figures/tables/illustrations
Number of figures/tables/illustrations	1
Format	both print and electronic
Are you the author of this Elsevier article?	No

MDPI Open Access Information and Policy

All articles published by MDPI are made immediately available worldwide under an open access license. This means:

everyone has free and unlimited access to the full-text of *all* articles published in MDPI journals, and
everyone is free to re-use the published material if proper accreditation/citation of the original publication is given.
open access publication is supported by the authors' institutes or research funding agencies by payment of a comparatively low Article Processing Charge (APC) for accepted articles.

External Open Access Resources

MDPI is a RoMEO green publisher — RoMEO is a database of Publishers' copyright and self-archiving policies hosted by the University of Nottingham

Those who are new to the concept of open access might find the following websites or 'Open Access 101' video informative:

Wikipedia article on 'Open Access'
Peter Suber's 'Open Access Overview'
Information Platform Open Access [in English, in German]
SHERPA's 'Authors and Open Access'

Meaning of Open Access

In accordance with major definitions of open access in scientific literature (namely the Budapest, Berlin, and Bethesda declarations), MDPI defines *open access* by the following conditions:

- **peer-reviewed literature is freely available without subscription or price barriers,**
- **literature is immediately released in open access format (no embargo period), and**
- **published material can be re-used without obtaining permission as long as a correct citation to the original publication is given.**

Until 2008, most articles published by MDPI contained the note: "© *year* by MDPI (http://www.mdpi.org). Reproduction is permitted for noncommercial purposes". During 2008, MDPI journals started to publish articles under the Creative Commons Attribution License. All articles published by MDPI before and during 2008 should now be considered as having been released under the post-2008 Creative Commons Attribution License.

SPARC Open Access 101 Video

This means that all articles published in MDPI journals, including data, graphics, and supplements, can be linked from external sources, scanned by search engines, re-used by text mining applications or websites, blogs, etc. free of charge under the sole condition of proper accreditation of the source and original publisher. MDPI believes that open access publishing fosters the exchange of research results amongst scientists from different disciplines, thus facilitating interdisciplinary research. Open access publishing also provides access to research results to researchers worldwide, including those from developing countries, and to an interested general public. Although MDPI publishes all of its journals under the open access model, we believe that open access is an enriching part of the scholarly communication process that can and should co-exist with other forms of communication and publication, such as society-based publishing and conferencing activities.

Important Note: some articles (especially *Reviews*) may contain figures, tables or text taken from other publications, for which MDPI does not hold the copyright or the right to re-license the published material. Please note that you should inquire with the original copyright holder (usually the original publisher or authors), whether or not this material can be re-used.

ROYAL SOCIETY OF CHEMISTRY LICENSE TERMS AND CONDITIONS

Jul 13, 2015

This is a License Agreement between Ragini Jenkins ("You") and Royal Society of Chemistry ("Royal Society of Chemistry") provided by Copyright Clearance Center ("CCC"). The license consists of your order details, the terms and conditions provided by Royal Society of Chemistry, and the payment terms and conditions.

All payments must be made in full to CCC. For payment instructions, please see information listed at the bottom of this form.

License Number	3667361184886
License date	Jul 13, 2015
Licensed content publisher	Royal Society of Chemistry
Licensed content publication	Chemical Communications (Cambridge)
Licensed content title	Water-soluble, membrane-permeable organic fluorescent nanoparticles with large tunability in emission wavelengths and Stokes shifts
Licensed content author	Yu-Zhe Chen,Peng-Zhong Chen,Hui-Qing Peng,Yan Zhao,Hui-Ying Ding,Li-Zhu Wu,Chen-Ho Tung,Qing-Zheng Yang
Licensed content date	May 13, 2013
Volume number	49
Issue number	52
Type of Use	Thesis/Dissertation
Requestor type	academic/educational
Portion	figures/tables/images
Number of figures/tables/images	1
Format	print and electronic
Distribution quantity	1
Will you be translating?	no
Order reference number	None
Title of the thesis/dissertation	A bioresponsive and multifunctional polymer based nanodevice for cancer theranostics
Expected completion date	Dec 2015
Estimated size	150
Total	0.00 USD

Terms and Conditions

This License Agreement is between {Requestor Name} ("You") and The Royal Society of

JOHN WILEY AND SONS LICENSE TERMS AND CONDITIONS

Jul 13, 2015

This Agreement between Ragini Jenkins ("You") and John Wiley and Sons ("John Wiley and Sons") consists of your license details and the terms and conditions provided by John Wiley and Sons and Copyright Clearance Center.

License Number	3667371258404
License date	Jul 13, 2015
Licensed Content Publisher	John Wiley and Sons
Licensed Content Publication	Wiley Interdisciplinary Reviews - Nanomedicine and Nanobiotechnology
Licensed Content Title	In vivo fluorescence imaging: a personal perspective
Licensed Content Author	P. Peter Ghoroghchian,Michael J. Therien,Daniel A. Hammer
Licensed Content Date	Jan 13, 2009
Pages	12
Type of use	Dissertation/Thesis
Requestor type	University/Academic
Format	Print and electronic
Portion	Figure/table
Number of figures/tables	1
Original Wiley figure/table number(s)	Figure 3
Will you be translating?	No
Title of your thesis / dissertation	A bioresponsive and multifunctional polymer based nanodevice for cancer theranostics
Expected completion date	Dec 2015
Expected size (number of pages)	150
Requestor Location	Ragini Jenkins 2550 Redlich Ct DECATUR, IL 62521 United States Attn: Ragini Jenkins

JOHN WILEY AND SONS LICENSE TERMS AND CONDITIONS

Jul 13, 2015

This Agreement between Ragini Jenkins ("You") and John Wiley and Sons ("John Wiley and Sons") consists of your license details and the terms and conditions provided by John Wiley and Sons and Copyright Clearance Center.

License Number	3667371394904
License date	Jul 13, 2015
Licensed Content Publisher	John Wiley and Sons
Licensed Content Publication	Microscopy Research and Technique
Licensed Content Title	Polylactide nanoparticles containing stably incorporated cyanine dyes for in vitro and in vivo imaging applications
Licensed Content Author	Rong Tong,Virginia J. Coyle,Li Tang,Anne M. Barger,Timothy M. Fan,Jianjun Cheng
Licensed Content Date	Feb 9, 2010
Pages	9
Type of use	Dissertation/Thesis
Requestor type	University/Academic
Format	Print and electronic
Portion	Figure/table
Number of figures/tables	1
Original Wiley figure/table number(s)	Fig. 4.
Will you be translating?	No
Title of your thesis / dissertation	A bioresponsive and multifunctional polymer based nanodevice for cancer theranostics
Expected completion date	Dec 2015
Expected size (number of pages)	150
Requestor Location	Ragini Jenkins 2550 Redlich Ct DECATUR, IL 62521 United States Attn: Ragini Jenkins

NATURE PUBLISHING GROUP LICENSE
TERMS AND CONDITIONS

Jul 13, 2015

This is a License Agreement between Ragini Jenkins ("You") and Nature Publishing Group ("Nature Publishing Group") provided by Copyright Clearance Center ("CCC"). The license consists of your order details, the terms and conditions provided by Nature Publishing Group, and the payment terms and conditions.

All payments must be made in full to CCC. For payment instructions, please see information listed at the bottom of this form.

License Number	3667370414570
License date	Jul 13, 2015
Licensed content publisher	Nature Publishing Group
Licensed content publication	Nature Nanotechnology
Licensed content title	Nanocarriers as an emerging platform for cancer therapy
Licensed content author	Dan Peer, Jeffrey M. Karp, Seungpyo Hong, Omid C. Farokhzad, Rimona Margalit
Licensed content date	Dec 1, 2007
Volume number	2
Issue number	12
Type of Use	reuse in a dissertation / thesis
Requestor type	academic/educational
Format	print and electronic
Portion	figures/tables/illustrations
Number of figures/tables/illustrations	1
High-res required	no
Figures	Figure 1
Author of this NPG article	no
Your reference number	None
Title of your thesis / dissertation	A bioresponsive and multifunctional polymer based nanodevice for cancer theranostics
Expected completion date	Dec 2015
Estimated size (number of pages)	150
Total	0.00 USD
Terms and Conditions	

JOHN WILEY AND SONS LICENSE TERMS AND CONDITIONS

Jul 13, 2015

This Agreement between Ragini Jenkins ("You") and John Wiley and Sons ("John Wiley and Sons") consists of your license details and the terms and conditions provided by John Wiley and Sons and Copyright Clearance Center.

License Number	3667370585875
License date	Jul 13, 2015
Licensed Content Publisher	John Wiley and Sons
Licensed Content Publication	Wiley Interdisciplinary Reviews - Nanomedicine and Nanobiotechnology
Licensed Content Title	Smart polymersomes for therapy and diagnosis: fast progress toward multifunctional biomimetic nanomedicines
Licensed Content Author	Hugo De Oliveira,Julie Thevenot,Sébastien Lecommandoux
Licensed Content Date	Jul 3, 2012
Pages	22
Type of use	Dissertation/Thesis
Requestor type	University/Academic
Format	Print and electronic
Portion	Figure/table
Number of figures/tables	1
Original Wiley figure/table number(s)	Figure 6
Will you be translating?	No
Title of your thesis / dissertation	A bioresponsive and multifunctional polymer based nanodevice for cancer theranostics
Expected completion date	Dec 2015
Expected size (number of pages)	150
Requestor Location	Ragini Jenkins 2550 Redlich Ct DECATUR, IL 62521 United States Attn: Ragini Jenkins

JOHN WILEY AND SONS LICENSE TERMS AND CONDITIONS

Jul 13, 2015

This Agreement between Ragini Jenkins ("You") and John Wiley and Sons ("John Wiley and Sons") consists of your license details and the terms and conditions provided by John Wiley and Sons and Copyright Clearance Center.

License Number	3667370940451
License date	Jul 13, 2015
Licensed Content Publisher	John Wiley and Sons
Licensed Content Publication	Macromolecular Bioscience
Licensed Content Title	Selective Imaging and Killing of Cancer Cells with Protein-Activated Near-Infrared Fluorescing Nanoparticles
Licensed Content Author	Parul Rungta,Yuriy P. Bandera,Ryan D. Roeder,Yangchun Li,William S. Baldwin,Deepti Sharma,Michael G. Sehorn,Igor Luzinov,Stephen H. Foulger
Licensed Content Date	Apr 8, 2011
Pages	11
Type of use	Dissertation/Thesis
Requestor type	University/Academic
Format	Print and electronic
Portion	Figure/table
Number of figures/tables	1
Original Wiley figure/table number(s)	Figure 4
Will you be translating?	No
Title of your thesis / dissertation	A bioresponsive and multifunctional polymer based nanodevice for cancer theranostics
Expected completion date	Dec 2015
Expected size (number of pages)	150
Requestor Location	Ragini Jenkins 2550 Redlich Ct DECATUR, IL 62521 United States Attn: Ragini Jenkins

Protein triggered fluorescence switching of near-infrared emitting nanoparticles for contrast-enhanced imaging

R. Jetty, Y. P. Bandera, M. A. Daniele, D. Hanor, Hsin-I. Hung, V. Ramshesh, M. F. Duperreault, A. Nieminen, J. J. Lemasters and S. H. Foulger, *J. Mater. Chem. B*, 2013, **1**, 4542
DOI: 10.1039/C3TB20681E

Bibliography

[1] S. Trabulo, A. M. Cardoso, T. Santos-Ferreira, A. L. Cardoso, S. Simoes, and M. C. P. de Lima. Survivin silencing as a promising strategy to enhance the sensitivity of cancer cells to chemotherapeutic agents. *Molecular Pharmaceutics*, 8:1120–1131, 2011.

[2] Y. D. Jin, C. X. Jia, S. W. Huang, M. O'Donnell, and X. H. Gao. Multifunctional nanoparticles as coupled contrast agents. *Nature Communications*, 1, 2010.

[3] T. F. Massoud and S. S. Gambhir. Molecular imaging in living subjects: seeing fundamental biological processes in a new light. *Genes & Development*, 17:545–580, 2003.

[4] M. J. Paulus, S. S. Gleason, M. E. Easterly, and C. J. Foltz. A review of high resolution x-ray computed tomography and other imaging modalities for small animal research. *Lab Animal*, 30:36–45, 2001.

[5] V. V. Mody, M. I. Nounou, and M. Bikram. Novel nanomedicine-based mri contrast agents for gynecological malignancies. *Advanced Drug Delivery Reviews*, 61:795–807, 2009.

[6] M. E. Phelps. Pet - a biological imaging technique. *Neurochemical Research*, 16:929–940, 1991.

[7] S. M. Janib, A. S. Moses, and J. A. MacKay. Imaging and drug delivery using theranostic nanoparticles. *Advanced Drug Delivery Reviews*, 62:1052–1063, 2010.

[8] A. J. Beer and M. Schwaiger. Imaging of integrin alpha v beta 3 expression. *Cancer and Metastasis Reviews*, 27:631–644, 2008.

[9] M. R. Zalutsky, D. A. Reardon, O. R. Pozzi, G. Vaidyanathan, and D. D. Bigner. Targeted alpha-particle radiotherapy with at-211-labeled monoclonal antibodies. *Nuclear Medicine and Biology*, 34:779–785, 2007.

[10] P. Debbage and W. Jaschke. Molecular imaging with nanoparticles: giant roles for dwarf actors. *Histochemistry and Cell Biology*, 130:845–875, 2008.

[11] K. Park, S. Lee, E. Kang, K. Kim, K. Choi, and I. C. Kwon. New generation of multifunctional nanoparticles for cancer imaging and therapy. *Advanced Functional Materials*, 19:1553–1566, 2009.

[12] D. J. Spergel, U. Kruth, D. R. Shimshek, R. Sprengel, and P. H. Seeburg. Using reporter genes to label selected neuronal populations in transgenic mice for gene promoter, anatomical, and physiological studies. *Progress in Neurobiology*, 63:673–686, 2001.

[13] R. Weissleder, C. H. Tung, U. Mahmood, and A. Bogdanov. In vivo imaging of tumors with protease-activated near-infrared fluorescent probes. *Nature Biotechnology*, 17(4):375–378, 1999.

[14] J. V. Frangioni. In vivo near-infrared fluorescence imaging. *Current Opinion in Chemical Biology*, 7:626–634, 2003.

[15] V. P. Torchilin. Micellar nanocarriers: Pharmaceutical perspectives. *Pharmaceutical Research*, 24:1–16, 2007.

[16] N. Nasongkla, E. Bey, J. M. Ren, H. Ai, C. Khemtong, J. S. Guthi, S. F. Chin, A. D. Sherry, D. A. Boothman, and J. M. Gao. Multifunctional polymeric micelles as cancer-targeted, mri-ultrasensitive drug delivery systems. *Nano Letters*, 6:2427–2430, 2006.

[17] E. Lallana, F. Fernandez-Trillo, A. Sousa-Herves, R. Riguera, and E. Fernandez-Megia. Click chemistry with polymers, dendrimers, and hydrogels for drug delivery. *Pharmaceutical Research*, 29:902–921, 2012.

[18] H. P. Yap, A. P. R. Johnston, G. K. Such, Y. Yan, and F. Caruso. Click-engineered, bioresponsive, drug-loaded peg spheres. *Advanced Materials*, 21:4348–+, 2009.

[19] Z. H. Sheng, D. H. Hu, M. M. Xue, M. He, P. Gong, and L. T. Cai. Indocyanine green nanoparticles for theranostic applications. *Nano-Micro Letters*, 5:145–150, 2013.

[20] K. Riehemann, S. W. Schneider, T. A. Luger, B. Godin, M. Ferrari, and H. Fuchs. Nanomedicine-challenge and perspectives. *Angewandte Chemie-International Edition*, 48:872–897, 2009.

[21] S. K. Sahoo and V. Labhasetwar. Nanotech approaches to delivery and imaging drug. *Drug Discovery Today*, 8:1112–1120, 2003.

[22] B. Le Droumaguet, J. Nicolas, D. Brambilla, S. Mura, A. Maksimenko, L. De Kimpe, E. Salvati, C. Zona, C. Airoldi, M. Canovi, M. Gobbi, M. Noiray, B. La Ferla, F. Nicotra, W. Scheper, O. Flores, M. Masserini, K. Andrieux, and P. Couvreur. Versatile and efficient targeting using a single nanoparticulate platform: application to cancer and alzheimer's disease. *Acs Nano*, 6:5866–5879, 2012.

[23] J. K. Pokorski, K. Breitenkamp, L. O. Liepold, S. Qazi, and M. G. Finn. Functional virus-based polymer-protein nanoparticles by atom transfer radical polymerization. *Journal of the American Chemical Society*, 133:9242–9245, 2011.

[24] J. W. Cui, Y. Yan, Y. J. Wang, and F. Caruso. Templated assembly of ph-labile polymer-drug particles for intracellular drug delivery. *Advanced Functional Materials*, 22:4718–4723, 2012.

[25] J. Merian, J. Gravier, F. Navarro, and I. Texier. Fluorescent nanoprobes dedicated to in vivo imaging: From preclinical validations to clinical translation. *Molecules*, 17:5564–5591, 2012.

[26] S. L. Luo, E. L. Zhang, Y. P. Su, T. M. Cheng, and C. M. Shi. A review of nir dyes in cancer targeting and imaging. *Biomaterials*, 32:7127–7138, 2011.

[27] C. H. Quek and K. W. Leong. Near-infrared fluorescent nanoprobes for in vivo optical imaging. *Nanomaterials*, 2:92–112, 2012.

[28] J. O. Escobedo, O. Rusin, S. Lim, and R. M. Strongin. Nir dyes for bioimaging applications. *Current Opinion in Chemical Biology*, 14:64–70, 2010.

[29] A. Mishra, R. K. Behera, P. K. Behera, B. K. Mishra, and G. B. Behera. Cyanines during the 1990s: A review. *Chemical Reviews*, 100(6):1973–2011, 2000.

[30] N. Tyutyulkov, F. Dietz, A. Ivanova, and K. Mullen. Structure and properties of new classes of coupled polymethine dyes. *Dyes and Pigments*, 42:215–222, 1999.

[31] P. Rungta, Y. P. Bandera, R. D. Roeder, Y. C. Li, W. S. Baldwin, D. Sharma, M. G. Sehorn, I. Luzinov, and S. H. Foulger. Selective imaging and killing of cancer cells with protein-activated near-infrared fluorescing nanoparticles. *Macromolecular Bioscience*, 11(7):927–937, 2011.

[32] T. Gorecki, G. Patonay, L. Strekowski, R. Chin, and N. Salazar. Synthesis of novel near-infrared cyanine dyes for metal ion determination. *Journal of Heterocyclic Chemistry*, 33:1871–1876, 1996.

[33] G. Patonay, M. D. Antoine, S. Devanathan, and L. Strekowski. Near-infrared probe for determination of solvent hydrophobicity. *Applied Spectroscopy*, 45:457–461, 1991.

[34] R. R. Avirah, D. T. Jayaram, N. Adarsh, and D. Ramaiah. Squaraine dyes in pdt: from basic design to in vivo demonstration. *Organic & Biomolecular Chemistry*, 10:911–920, 2012.

[35] A. Treibs and K. Jacob. Cyclotrimethine dyes derived from squaric acid. *Angewandte Chemie-International Edition*, 4:694–, 1965.

[36] L. Hu, Z. Q. Yan, and H. Y. Xu. Advances in synthesis and application of near-infrared absorbing squaraine dyes. *Rsc Advances*, 3:7667–7676, 2013.

[37] J. J. Gassensmith, J. M. Baumes, and B. D. Smith. Discovery and early development of squaraine rotaxanes. *Chemical Communications*, (42):6329–6338, 2009.

[38] K. Umezawa, D. Cittierio, and K. Suzuki. Water-soluble nir fluorescent probes based on squaraine and their application for protein labeling. *Analytical Sciences*, 24:213–217, 2008.

[39] L. B. Josefsen and R. W. Boyle. Unique diagnostic and therapeutic roles of porphyrins and phthalocyanines in photodynamic therapy, imaging and theranostics. *Theranostics*, 2:916–966, 2012.

[40] N. Sekkat, H. van den Bergh, T. Nyokong, and N. Lange. Like a bolt from the blue: Phthalocyanines in biomedical optics. *Molecules*, 17:98–144, 2012.

[41] J. F. Lovell and P. C. Lo. Porphyrins and phthalocyanines for theranostics. *Theranostics*, 2:815–816, 2012.

[42] B. G. Ongarora, X. K. Hu, S. D. Verberne-Sutton, J. C. Garno, and M. G. H. Vicente. Syntheses and photodynamic activity of pegylated cationic zn(ii)-phthalocyanines in hep2 cells. *Theranostics*, 2:850–870, 2012.

[43] N. Yumita, Y. Iwase, K. Nishi, H. Komatsu, K. Takeda, K. Onodera, T. Fukai, T. Ikeda, S. Umemura, K. Okudaira, and Y. Momose. Involvement of reactive oxygen species in sonodynamically induced apoptosis using a novel porphyrin derivative. *Theranostics*, 2:880–888, 2012.

[44] A. Treibs and F. H. Kreuzer. Di- and tri- pyrrylmethene complexes with di-fluoro boron. *Annalen Der Chemie-Justus Liebig*, 718:208–+, 1968.

[45] Y. Ni and J. S. Wu. Far-red and near infrared bodipy dyes: synthesis and applications for fluorescent ph probes and bio-imaging. *Organic & Biomolecular Chemistry*, 12:3774–3791, 2014.

[46] V. R. Donuru, S. L. Zhu, S. Green, and H. Y. Liu. Near-infrared emissive bodipy polymeric and copolymeric dyes. *Polymer*, 51:5359–5368, 2010.

[47] K. Umezawa, A. Matsui, Y. Nakamura, D. Citterio, and K. Suzuki. Bright, color-tunable fluorescent dyes in the vis/nir region: Establishment of new "tailor-made" multicolor fluorophores based on borondipyrromethene. *Chemistry-a European Journal*, 15:1096–1106, 2009.

[48] K. Umezawa, Y. Nakamura, H. Makino, D. Citterio, and K. Suzuki. Bright, color-tunable fluorescent dyes in the visible-near-infrared region. *Journal of the American Chemical Society*, 130:1550–+, 2008.

[49] D. Peer, J. M. Karp, S. Hong, O. C. FaroKhzad, R. Margalit, and R. Langer. Nanocarriers as an emerging platform for cancer therapy. *Nature Nanotechnology*, 2:751–760, 2007.

[50] O. C. Farokhzad and R. Langer. Impact of nanotechnology on drug delivery. *Acs Nano*, 3:16–20, 2009.

[51] A. Fernandez-Fernandez, R. Manchanda, and A. J. McGoron. Theranostic applications of nanomaterials in cancer: Drug delivery, image-guided therapy, and multifunctional platforms. *Applied Biochemistry and Biotechnology*, 165:1628–1651, 2011.

[52] Z. L. Cheng, A. Al Zaki, J. Z. Hui, V. R. Muzykantov, and A. Tsourkas. Multifunctional nanoparticles: Cost versus benefit of adding targeting and imaging capabilities. *Science*, 338:903–910, 2012.

[53] G. Birrenbach and P. P. Speiser. Polymerized micelles and their use as adjuvants in immunology. *Journal of Pharmaceutical Sciences*, 65:1763–1766, 1976.

[54] L. W. Seymour, Y. Miyamoto, H. Maeda, M. Brereton, J. Strohalm, K. Ulbrich, and R. Duncan. Influence of molecular-weight on passive tumor accumulation of a soluble macromolecular drug carrier. *European Journal of Cancer*, 31A:766–770, 1995.

[55] N. Larson and H. Ghandehari. Polymeric conjugates for drug delivery. *Chemistry of Materials*, 24:840–853, 2012.

[56] X. H. Zheng, D. Xing, F. F. Zhou, B. Y. Wu, and W. R. Chen. Indocyanine green-containing nanostructure as near infrared dual-functional targeting probes for optical imaging and photothermal therapy. *Molecular Pharmaceutics*, 8:447–456, 2011.

[57] Y. Z. Chen, P. Z. Chen, H. Q. Peng, Y. Zhao, H. Y. Ding, L. Z. Wu, C. H. Tung, and Q. Z. Yang. Water-soluble, membrane-permeable organic fluorescent nanoparticles with large tunability in emission wavelengths and stokes shifts. *Chemical Communications*, 49:5877–5879, 2013.

[58] H. Tanisaka, S. Kizaka-Kondoh, A. Makino, S. Tanaka, M. Hiraoka, and S. Kimura. Near-infrared fluorescent labeled peptosome for application to cancer imaging. *Bioconjugate Chemistry*, 19:109–117, 2008.

[59] V. B. Rodriguez, S. M. Henry, A. S. Hoffman, P. S. Stayton, X. D. Li, and S. H. Pun. Encapsulation and stabilization of indocyanine green within poly(styrene-alt-maleic anhydride) block-poly(styrene) micelles for near-infrared imaging. *Journal of Biomedical Optics*, 13, 2008.

[60] S. Y. Zhang and Y. Zhao. Facile synthesis of multivalent water-soluble organic nanoparticles via "surface clicking" of alkynylated surfactant micelles. *Macromolecules*, 43:4020–4022, 2010.

[61] M. R. Dreher, A. J. Simnick, K. Fischer, R. J. Smith, A. Patel, M. Schmidt, and A. Chilkoti. Temperature triggered self-assembly of polypeptides into multivalent spherical micelles. *Journal of the American Chemical Society*, 130:687–694, 2008.

[62] W. Kim, C. Brady, and E. L. Chaikof. Amphiphilic protein micelles for targeted in vivo imaging. *Acta Biomaterialia*, 8:2476–2482, 2012.

[63] P. P. Ghoroghchian, P. R. Frail, K. Susumu, D. Blessington, A. K. Brannan, F. S. Bates, B. Chance, D. A. Hammer, and M. J. Therien. Near-infrared-emissive polymersomes: Self-assembled soft matter for in vivo optical imaging. *Proceedings of the National Academy of Sciences of the United States of America*, 102:2922–2927, 2005.

[64] Z. H. Li, L. Y. Wu, P. R. Hu, S. H. Han, T. Zhang, H. L. Fan, W. Jin, Q. H. Jin, and Y. Mu. Soft nanomaterial-based targeting polymersomes for near-infrared fluorescence multispectral in vivo imaging. *Nanoscale*, 4:7097–7105, 2012.

[65] P. P. Ghoroghchian, M. J. Therien, and D. A. Hammer. In vivo fluorescence imaging: a personal perspective. *Wiley Interdisciplinary Reviews-Nanomedicine and Nanobiotechnology*, 1:156–167, 2009.

[66] D. H. Levine, P. P. Ghoroghchian, J. Freudenberg, G. Zhang, M. J. Therien, M. I. Greene, D. A. Hammer, and R. Murali. Polymersomes: A new multi-functional tool for cancer diagnosis and therapy. *Methods*, 46:25–32, 2008.

[67] H. De Oliveira, J. Thevenot, and S. Lecommandoux. Smart polymersomes for therapy and diagnosis: fast progress toward multifunctional biomimetic nanomedicines. *Wiley Interdisciplinary Reviews-Nanomedicine and Nanobiotechnology*, 4:525–546, 2012.

[68] J. Z. Du and R. K. O'Reilly. Advances and challenges in smart and functional polymer vesicles. *Soft Matter*, 5:3544–3561, 2009.

[69] M. Massignani, I. Canton, T. Sun, V. Hearnden, S. MacNeil, A. Blanazs, S. P. Armes, A. Lewis, and G. Battaglia. Enhanced fluorescence imaging of live cells by effective cytosolic delivery of probes. *Plos One*, 5, 2010.

[70] L. Quan, S. Liu, T. T. Sun, X. G. Guan, W. H. Lin, Z. G. Xie, Y. B. Huang, Y. Q. Wang, and X. B. Jing. Near-infrared emitting fluorescent bodipy nanovesicles for in vivo molecular imaging and drug delivery. *Acs Applied Materials & Interfaces*, 6:16166–16173, 2014.

[71] R. Jetty, Y. P. Bandera, M. A. Daniele, D. Hanor, H. I. Hung, V. Ramshesh, M. F. Duperreault, A. L. Nieminen, J. J. Lemasters, and S. H. Foulger. Protein triggered fluorescence switching of near-infrared emitting nanoparticles for contrast-enhanced imaging. *Journal of Materials Chemistry B*, 1:4542–4554, 2013.

[72] A. Vollrath, S. Schubert, and U. S. Schubert. Fluorescence imaging of cancer tissue based on metal-free polymeric nanoparticles - a review. *Journal of Materials Chemistry B*, 1:1994–2007, 2013.

[73] A. Schadlich, H. Caysa, T. Mueller, F. Tenambergen, C. Rose, A. Gopferich, J. Kuntsche, and K. Mader. Tumor accumulation of nir fluorescent peg pla nanoparticles: Impact of particle size and human xenograft tumor model. *Acs Nano*, 5:8710–8720, 2011.

[74] G. Storm, S. O. Belliot, T. Daemen, and D. D. Lasic. Surface modification of nanoparticles to oppose uptake by the mononuclear phagocyte system. *Advanced Drug Delivery Reviews*, 17:31–48, 1995.

[75] S. M. Moghimi. Mechanisms of splenic clearance of blood-cells and particles - towards development of new splenotropic agents. *Advanced Drug Delivery Reviews*, 17:103–115, 1995.

[76] P. Couvreur and C. Vauthier. Nanotechnology: Intelligent design to treat complex disease. *Pharmaceutical Research*, 23:1417–1450, 2006.

[77] S. M. Moghimi, A. C. Hunter, and J. C. Murray. Long-circulating and target-specific nanoparticles: Theory to practice. *Pharmacological Reviews*, 53(2):283–318, 2001.

[78] V. P. Torchilin. Multifunctional nanocarriers. *Advanced Drug Delivery Reviews*, 58(14):1532–1555, 2006.

[79] S. Schubert, J. T. Delaney, and U. S. Schubert. Nanoprecipitation and nanoformulation of polymers: from history to powerful possibilities beyond poly(lactic acid). *Soft Matter*, 7:1581–1588, 2011.

[80] R. Reul, N. Tsapis, H. Hillaireau, L. Sancey, S. Mura, M. Recher, J. Nicolas, J. L. Coll, and E. Fattal. Near infrared labeling of plga for in vivo imaging of nanoparticles. *Polymer Chemistry*, 3:694–702, 2012.

[81] V. Saxena, M. Sadoqi, and J. Shao. Enhanced photo-stability, thermal-stability and aqueous-stability of indocyanine green in polymeric nanoparticulate systems. *Journal of Photochemistry and Photobiology B-Biology*, 74:29–38, 2004.

[82] V. Saxena, M. Sadoqi, and J. Shao. Indocyanine green-loaded biodegradable nanoparticles: preparation, physicochemical characterization and in vitro release. *International Journal of Pharmaceutics*, 278:293–301, 2004.

[83] V. Saxena, M. Sadoqi, and J. Shao. Polymeric nanoparticulate delivery system for indocyanine green: Biodistribution in healthy mice. *International Journal of Pharmaceutics*, 308:200–204, 2006.

[84] A. Schadlich, C. Rose, J. Kuntsche, H. Caysa, T. Mueller, A. Gopferich, and K. Mader. How stealthy are peg-pla nanoparticles? an nir in vivo study combined with detailed size measurements. *Pharmaceutical Research*, 28:1995–2007, 2011.

[85] R. Tong, V. J. Coyle, L. Tang, A. M. Barger, T. M. Fan, and J. J. Cheng. Polylactide nanoparticles containing stably incorporated cyanine dyes for in vitro and in vivo imaging applications. *Microscopy Research and Technique*, 73:901–909, 2010.

[86] H. C. Kolb, M. G. Finn, and K. B. Sharpless. Click chemistry: Diverse chemical function from a few good reactions. *Angewandte Chemie-International Edition*, 40(11):2004–2021, 2001.

[87] E. Lallana, A. Sousa-Herves, F. Fernandez-Trillo, R. Riguera, and E. Fernandez-Megia. Click chemistry for drug delivery nanosystems. *Pharmaceutical Research*, 29:1–34, 2012.

[88] A. Palma, L. A. Alvarez, D. Scholz, D. O. Frimannsson, M. Grossi, S. J. Quinn, and D. F. O'Shea. Cellular uptake mediated off/on responsive near-infrared fluorescent nanoparticles. *Journal of the American Chemical Society*, 133(49):19618–19621, 2011.

[89] Z. M. Tao, G. S. Hong, C. Shinji, C. X. Chen, S. Diao, A. L. Antaris, B. Zhang, Y. P. Zou, and H. J. Dai. Biological imaging using nanoparticles of small organic molecules with fluorescence emission at wavelengths longer than 1000 nm. *Angewandte Chemie-International Edition*, 52:13002–13006, 2013.

[90] A. M. James, E. J. Ambrose, and J. H. Lowick. Differences between the electrical charge carried by normal and homologous tumour cells. *Nature*, 177, 1956.

[91] R. H. Prabhu, V. B. Patravale, and M. D. Joshi. Polymeric nanoparticles for targeted treatment in oncology: current insights. *International Journal of Nanomedicine*, 10:1001–1018, 2015.

[92] S. Ran, A. Downes, and P. E. Thorpe. Increased exposure of anionic phospholipids on the surface of tumor blood vessels. *Cancer Research*, 62:6132–6140, 2002.

[93] A. Asati, S. Santra, C. Kaittanis, and J. M. Perez. Surface-charge-dependent cell localization and cytotoxicity of cerium oxide nanoparticles. *Acs Nano*, 4:5321–5331, 2010.

[94] C. W. Beh, W. Y. Seow, Y. Wang, Y. Zhang, Z. Y. Ong, P. L. R. Ee, and Y. Y. Yang. Efficient delivery of bcl-2-targeted sirna using cationic polymer nanoparticles: Downregulating mrna expression level and sensitizing cancer cells to anticancer drug. *Biomacromolecules*, 10:41–48, 2009.

[95] F. Danhier, O. Feron, and V. Preat. To exploit the tumor microenvironment: Passive and active tumor targeting of nanocarriers for anti-cancer drug delivery. *Journal of Controlled Release*, 148:135–146, 2010.

[96] D. B. Kirpotin, D. C. Drummond, Y. Shao, M. R. Shalaby, K. L. Hong, U. B. Nielsen, J. D. Marks, C. C. Benz, and J. W. Park. Antibody targeting of long-circulating lipidic nanoparticles does not increase tumor localization but does increase internalization in animal models. *Cancer Research*, 66:6732–6740, 2006.

[97] T. R. Daniels, T. Delgado, G. Helguera, and M. L. Penichet. The transferrin receptor part ii: Targeted delivery of therapeutic agents into cancer cells. *Clinical Immunology*, 121:159–176, 2006.

[98] P. S. Low and S. A. Kularatne. Folate-targeted therapeutic and imaging agents for cancer. *Current Opinion in Chemical Biology*, 13:256–262, 2009.

[99] J. Sudimack and R. J. Lee. Targeted drug delivery via the folate receptor. *Advanced Drug Delivery Reviews*, 41:147–162, 2000.

[100] J. J. Laskin and A. B. Sandier. Epidermal growth factor receptor: a promising target in solid tumours. *Cancer Treatment Reviews*, 30:1–17, 2004.

[101] M. Scaltriti and J. Baselga. The epidermal growth factor receptor pathway: A model for targeted therapy. *Clinical Cancer Research*, 12:5268–5272, 2006.

[102] T. Minko. Drug targeting to the colon with lectins and neoglycoconjugates. *Advanced Drug Delivery Reviews*, 56:491–509, 2004.

[103] T. Lammers, W. E. Hennink, and G. Storm. Tumour-targeted nanomedicines: principles and practice. *British Journal of Cancer*, 99:392–397, 2008.

[104] P. Carmeliet. Vegf as a key mediator of angiogenesis in cancer. *Oncology*, 69:4–10, 2005.

[105] J. S. Desgrosellier and D. A. Cheresh. Integrins in cancer: biological implications and therapeutic opportunities. *Nature Reviews Cancer*, 10:9–22, 2010.

[106] L. Osborn, C. Hession, R. Tizard, C. Vassallo, S. Luhowskyj, G. Chirosso, and R. Lobb. Direct expression cloning of vascular cell-adhesion molecule-1, a cytokine-induced endothelial protein that binds to lymphocytes. *Cell*, 59:1203–1211, 1989.

[107] R. Roy, J. Yang, and M. A. Moses. Matrix metalloproteinases as novel biomarkers and potential therapeutic targets in human cancer. *Journal of Clinical Oncology*, 27:5287–5297, 2009.

[108] Z. Pang, L. Feng, R. Hua, J. Chen, H. Gao, S. Pan, X. Jiang, and P. Zhang. Lactoferrin-conjugated biodegradable polymersome holding doxorubicin and tetrandrine for chemotherapy of glioma rats. *Molecular Pharmaceutics*, 7:1995–2005, 2010.

[109] A. Yuan, J. H. Wu, X. L. Tang, L. L. Zhao, F. Xu, and Y. Q. Hu. Application of near-infrared dyes for tumor imaging, photothermal, and photodynamic therapies. *Journal of Pharmaceutical Sciences*, 102:6–28, 2013.

[110] W. Pham, Y. D. Choi, R. Weissleder, and C. H. Tung. Developing a peptide-based near-infrared molecular probe for protease sensing. *Bioconjugate Chemistry*, 15:1403–1407, 2004.

[111] C. H. Tung, U. Mahmood, S. Bredow, and R. Weissleder. In vivo imaging of proteolytic enzyme activity using a novel molecular reporter. *Cancer Research*, 60:4953–4958, 2000.

[112] Y. Urano, D. Asanuma, Y. Hama, Y. Koyama, T. Barrett, M. Kamiya, T. Nagano, T. Watanabe, A. Hasegawa, P. L. Choyke, and H. Kobayashi. Selective molecular imaging of viable cancer cells with ph-activatable fluorescence probes. *Nature Medicine*, 15:104–109, 2009.

[113] V. S. Jisha, K. T. Arun, M. Hariharan, and D. Ramaiah. Site-selective interactions: Squaraine dye-serum albumin complexes with enhanced fluorescence and triplet yields. *Journal of Physical Chemistry B*, 114(17):5912–5919, 2010.

[114] K. Kim, M. Lee, H. Park, J. H. Kim, S. Kim, H. Chung, K. Choi, I. S. Kim, B. L. Seong, and I. C. Kwon. Cell-permeable and biocompatible polymeric nanoparticles for apoptosis imaging. *Journal of the American Chemical Society*, 128:3490–3491, 2006.

[115] S. A. Hilderbrand and R. Weissleder. Near-infrared fluorescence: application to in vivo molecular imaging. *Current Opinion in Chemical Biology*, 14(1):71–79, 2010.

[116] S. A. Soper and Q. L. Mattingly. Steady-state and picosecond laser fluorescence studies of nonradiative pathways in tricarbocyanine dyes - Implications to the design of near-IR fluorochromes with high fluorescence efficiencies. *Journal of the American Chemical Society*, 116(9):3744–3752, 1994.

[117] A. K. Chibisov, G. V. Zakharova, H. Gorner, Y. A. Sogulyaev, I. L. Mushkalo, and A. I. Tolmachev. Photorelaxation processes in covalently-linked indocarbocyanine and thiacarbocyanine dyes. *Journal of Physical Chemistry*, 99(3):886–893, 1995.

[118] Y. Hama, Y. Urano, Y. Koyama, P. L. Choyke, and H. Kobayashi. Activatable fluorescent molecular imaging of peritoneal metastases following pretargeting with a biotinylated monoclonal antibody. *Cancer Research*, 67(8):3809–3817, 2007.

[119] H. Kobayashi, M. R. Longmire, M. Ogawa, and P. L. Choyke. Rational chemical design of the next generation of molecular imaging probes based on physics and biology: mixing modalities, colors and signals. *Chemical Society Reviews*, 40(9):4626–4648, 2011.

[120] C. H. Tung, S. Bredow, U. Mahmood, and R. Weissleder. Preparation of a cathepsin d sensitive near-infrared fluorescence probe for imaging. *Bioconjugate Chemistry*, 10(5):892–896, 1999.

[121] H. Kobayashi and P. L. Choyke. Target-cancer-cell-specific activatable fluorescence imaging probes: Rational design and in vivo applications. *Accounts of Chemical Research*, 44(2):83–90, 2011.

[122] A. C. Bhasikuttan, J. Mohanty, W. M. Nau, and H. Pal. Efficient fluorescence enhancement and cooperative binding of an organic dye in a supra-biomolecular host-protein assembly. *Angewandte Chemie-International Edition*, 46(22):4120–4122, 2007.

[123] R. Zadmard and T. Schrader. Nanomolar protein sensing with embedded receptor molecules. *Journal of the American Chemical Society*, 127(3):904–915, 2005.

[124] S. Gadde, E. K. Batchelor, J. P. Weiss, Y. H. Ling, and A. E. Kaifer. Control of h- and j-aggregate formation via host-guest complexation using cucurbituril hosts. *Journal of the American Chemical Society*, 130(50):17114–17119, 2008.

[125] A. Toutchkine, V. Kraynov, and K. Hahn. Solvent-sensitive dyes to report protein conformational changes in living cells. *Journal of the American Chemical Society*, 125(14):4132–4145, 2003.

[126] R. G. Strickley. Solubilizing excipients in oral and injectable formulations. *Pharmaceutical Research*, 21(2):201–230, 2004.

[127] D. Avnir, D. Levy, and R. Reisfeld. The nature of the silica cage as reflected by spectral changes and enhanced photostability of trapped rhodamine-6g. *Journal of Physical Chemistry*, 88(24):5956–5959, 1984.

[128] J. M. Devoisselle, S. Soulie-Begu, S. Mordon, T. Desmettre, and H. Maillols. A preliminary study of the in vivo behaviour of an emulsion formulation of indocyanine green. *Lasers in Medical Science*, 13(4):279–282, 1998.

[129] J. Yu, M. A. Yaseen, B. Anvari, and M. S. Wong. Synthesis of near-infrared-absorbing nanoparticle-assembled capsules. *Chemistry of Materials*, 19(6):1277–1284, 2007.

[130] E. I. Altinoglu, T. J. Russin, J. M. Kaiser, B. M. Barth, P. C. Eklund, M. Kester, and J. H. Adair. Near-infrared emitting fluorophore-doped calcium phosphate nanoparticles for in vivo imaging of human breast cancer. *ACS Nano*, 2(10):2075–2084, 2008.

[131] H. S. Muddana, T. T. Morgan, J. H. Adair, and P. J. Butler. Photophysics of Cy3-encapsulated calcium phosphate nanoparticles. *Nano Letters*, 9(4):1559–1566, 2009.

[132] A. Burns, H. Ow, and U. Wiesner. Fluorescent core-shell silica nanoparticles: towards "lab on a particle" architectures for nanobiotechnology. *Chemical Society Reviews*, 35(11):1028–1042, 2006.

[133] S. Kim, T. Y. Ohulchanskyy, H. E. Pudavar, R. K. Pandey, and P. N. Prasad. Organically modified silica nanoparticles co-encapsulating photosensitizing drug and aggregation-enhanced two-photon absorbing fluorescent dye aggregates for two-photon photodynamic therapy. *Journal of the American Chemical Society*, 129(9):2669–2675, 2007.

[134] Y. Piao, A. Burns, J. Kim, U. Wiesner, and T. Hyeon. Designed fabrication of silica-based nanostructured particle systems for nanomedicine applications. *Advanced Functional Materials*, 18(23):3745–3758, 2008.

[135] Y. Ueno, J. Jose, A. Loudet, C. Perez-Bolivar, P. Anzenbacher, and K. Burgess. Encapsulated energy-transfer cassettes with extremely well resolved fluorescent outputs. *Journal of the American Chemical Society*, 133(1):51–55, 2011.

[136] J. Yu, D. Javier, M. A. Yaseen, N. Nitin, R. Richards-Kortum, B. Anvari, and M. S. Wong. Self-assembly synthesis, tumor cell targeting, and photothermal capabilities of antibody-coated indocyanine green nanocapsules. *Journal of the American Chemical Society*, 132(6):1929–1938, 2010.

[137] A. K. Gupta and M. Gupta. Synthesis and surface engineering of iron oxide nanoparticles for biomedical applications. *Biomaterials*, 26(18):3995–4021, 2005.

[138] A. H. Lu, E. L. Salabas, and F. Schuth. Magnetic nanoparticles: Synthesis, protection, functionalization, and application. *Angewandte Chemie-International Edition*, 46(8):1222–1244, 2007.

[139] C. Medina, M. J. Santos-Martinez, A. Radomski, O. I. Corrigan, and M. W. Radomski. Nanoparticles: pharmacological and toxicological significance. *British Journal of Pharmacology*, 150(5):552–558, 2007.

[140] W. H. De Jong and P. J. A. Borm. Drug delivery and nanoparticles: Applications and hazards. *International Journal of Nanomedicine*, 3(2):133–149, 2008.

[141] E. Arunkumar, C. C. Forbes, B. C. Noll, and B. D. Smith. Squaraine-derived rotaxanes: Sterically protected fluorescent near-ir dyes. *Journal of the American Chemical Society*, 127(10):3288–3289, 2005.

[142] L. Beverina, M. Crippa, M. Landenna, R. Ruffo, P. Salice, F. Silvestri, S. Versari, A. Villa, L. Ciaffoni, E. Collini, C. Ferrante, S. Bradamante, C. M. Mari, R. Bozio, and G. A. Pagani. Assessment of water-soluble pi-extended squaraines as one- and two-photon singlet oxygen photosensitizers: Design, synthesis, and characterization. *Journal of the American Chemical Society*, 130(6):1894–1902, 2008.

[143] V. S. Jisha, K. T. Arun, M. Hariharan, and D. Ramaiah. Site-selective binding and dual mode recognition of serum albumin by a squaraine dye. *Journal of the American Chemical Society*, 128(18):6024–6025, 2006.

[144] D Lee, Y, K Lim, C, S Kim, C. Kwon, I, and J. Kim. Squaraine-doped functional nanoprobes: Lipophilically protected near-infrared fluorescence for bioimaging. *Advanced Functional Materials*, 20(17):2786–2793, 2010.

[145] T. Desmettre, J. M. Devoisselle, and S. Mordon. Fluorescence properties and metabolic features of indocyanine green (ICG) as related to angiography. *Survey of Ophthalmology*, 45(1):15–27, 2000.

[146] S. Sreejith, P. Carol, P. Chithra, and A. Ajayaghosh. Squaraine dyes: a mine of molecular materials. *Journal of Materials Chemistry*, 18(3):264–274, 2008.

[147] J. H. Yum, P. Walter, S. Huber, D. Rentsch, T. Geiger, F. Nuesch, F. De Angelis, M. Gratzel, and M. K. Nazeeruddin. Efficient far red sensitization of nanocrystalline tio2 films by an unsymmetrical squaraine dye. *Journal of the American Chemical Society*, 129(34):10320–+, 2007.

[148] J. Johnson, N. Fu, E. Arunkumar, W. M. Leevy, S. Gammon, D. Piwnica-Worms, and B. Smith. Squaraine rotaxanes: Superior substitutes for cy-5 in molecular probes for near-infrared fluorescence cell imaging. *Angewandte Chemie International Edition*, 46(29):5528–5531, 2007.

[149] Y. Xu, Z. Li, A. Malkovskiy, S. Sun, and Y. Pang. Aggregation control of squaraines and their use as near-infrared fluorescent sensors for protein. *The Journal of Physical Chemistry B*, 114(25):8574–8580, 2010.

[150] K. Y. Law. Squaraine chemistry: effects of structural changes on the absorption and multiple fluorescence emission of bis[4-(dimethylamino)phenyl]squaraine and its derivatives. *The Journal of Physical Chemistry*, 91(20):5184–5193, 1987.

[151] C. L. Amiot, S. P. Xu, S. Liang, L. Y. Pan, and J. X. J. Zhao. Near-infrared fluorescent materials for sensing of biological targets. *Sensors*, 8(5):3082–3105, 2008.

[152] P. Salice, J. Arnbjerg, B. W. Pedersen, R. Toftegaard, L. Beverina, G. A. Pagani, and P. R. Ogilby. Photophysics of squaraine dyes: Role of charge-transfer in singlet oxygen production and removal. *The Journal of Physical Chemistry A*, 114(7):2518–2525.

[153] R. Philip, A. Penzkofer, W. Baumler, R. M. Szeimies, and C. Abels. Absorption and fluorescence spectroscopic investigation of indocyanine green. *Journal of Photochemistry and Photobiology A-Chemistry*, 96(1-3):137–148, 1996.

[154] E. Mubarekyan and M. Santore. Characterization of polystyrene latex surfaces by the adsorption of rhodamine 6g. *Langmuir*, 14(7):1597–1603, 1998.

[155] Konstantinos Avgoustakis. Pegylated poly(lactide) and poly(lactide-co-glycolide) nanoparticles: Preparation, properties and possible applications in drug delivery. *Current Drug Delivery*, 1:321–333, 2004.

[156] F. Alexis, E. Pridgen, L. K. Molnar, and O. C. Farokhzad. Factors affecting the clearance and biodistribution of polymeric nanoparticles. *Molecular Pharmaceutics*, 5(4):505–515, 2008.

[157] E. Arunkumar, C. C. Forbes, and B. D. Smith. Improving the properties of organic dyes by molecular encapsulation. *European Journal of Organic Chemistry*, pages 4051–4059, 2005.

[158] R. Pirisino, P. Disimplicio, G. Ignesti, G. Bianchi, and P. Barbera. Sulfhydryl-groups and peroxidase-like activity of albumin as scavenger of organic peroxides. *Pharmacological Research Communications*, 20(7):545–552, 1988.

[159] C. P. Baron, H. H. F. Refsgaard, L. H. Skibsted, and M. L. Andersen. Oxidation of bovine serum albumin initiated by the fenton reaction - effect of edta, tert-butylhydroperoxide and tetrahydrofuran. *Free Radical Research*, 40(4):409–417, 2006.

[160] P. L. SanBiagio, D. Bulone, A. Emanuele, and M. U. Palma. Self-assembly of biopolymeric structures below the threshold of random cross-link percolation. *Biophysical Journal*, 70(1):494–499, 1996.

[161] I. H. M. Vanstokkum, H. Linsdell, J. M. Hadden, P. I. Haris, D. Chapman, and M. Bloemendal. Temperature-induced changes in protein structures studied by fourier-transformed infrared-spectroscopy and global analysis. *Biochemistry*, 34(33):10508–10518, 1995.

[162] M. Hennig, F. Roosen-Runge, F. J. Zhang, S. Zorn, M. W. A. Skoda, R. M. J. Jacobs, T. Seydel, and F. Schreiber. Dynamics of highly concentrated protein solutions around the denaturing transition. *Soft Matter*, 8(5):1628–1633, 2012.

[163] R. P. Cory, R. R. Becker, Rosenblu.R, and I. Isenberg. Synthesis and fluorescent properties of some n-methyl-2-anilino-6-naphthalenesulfonyl derivatives. *Journal of the American Chemical Society*, 90(6):1643, 1968.

[164] V. H. Rees, J. E. Fildes, and D. J. Laurence. The dye-binding capacity of human plasma determined fluorimetrically and its relation to the determination of plasma albumin. *Journal of clinical pathology*, 7(4):336–40, 1954.

[165] D. Lopez-Ferrer, K. Petritis, K. K. Hixson, T. H. Heibeck, R. J. Moore, M. E. Belov, D. G. Camp, and R. D. Smith. Application of pressurized solvents for ultrafast trypsin hydrolysis in proteomics: Proteomics on the fly. *Journal of Proteome Research*, 7(8):3276–3281, 2008.

[166] J. L. Capelo, R. Carreira, M. Diniz, L. Fernandes, M. Galesio, C. Lodeiro, H. M. Santos, and G. Vale. Overview on modern approaches to speed up protein identification workflows relying on enzymatic cleavage and mass spectrometry-based techniques. *Analytica Chimica Acta*, 650(2):151–159, 2009.

[167] J. J. Gassensmith, E. Arunkumar, L. Barr, J. M. Baumes, K. M. DiVittorio, J. R. Johnson, B. C. Noll, and B. D. Smith. Self-assembly of fluorescent inclusion complexes in competitive media including the interior of living cells. *Journal of the American Chemical Society*, 129(48):15054–15059, 2007.

[168] Y. N. Konan, R. Gurny, and E. Allemann. State of the art in the delivery of photosensitizers for photodynamic therapy. *Journal of Photochemistry and Photobiology B-Biology*, 66(2):89–106, 2002.

[169] M. Lieber, B. Smith, A. Szakal, W. Nelsonrees, and G. Todaro. Continuous tumor-cell line from a human lung carcinoma with properties of type-ii alveolar epithelial cells. *International Journal of Cancer*, 17(1):62–70, 1976.

[170] V. Zinchuk and O. Zinchuk. Quantitative colocalization analysis of confocal fluorescence microscopy images. *Curr. Protoc. Cell Biol.*, 39:4.19.1–4.19.16., 2008.

[171] M. Oba, S. Fukushima, N. Kanayama, K. Aoyagi, N. Nishiyama, H. Koyama, and K. Kataoka. Cyclic rgd peptide-conjugated polyplex micelles as a targetable gene delivery system directed to cells possessing alpha(v)beta(3) and alpha(v)beta(5) integrins. *Bioconjugate Chemistry*, 18(5):1415–1423, 2007.

[172] M. Oba, K. Aoyagi, K. Miyata, Y. Matsumoto, K. Itaka, N. Nishiyama, Y. Yarnasaki, H. Koyama, and K. Kataoka. Polyplex micelles with cyclic rgd peptide ligands and disulfide cross-links directing to the enhanced transfection via controlled intracellular trafficking. *Molecular Pharmaceutics*, 5(6):1080–1092, 2008.

[173] S. Hak, E. Helgesen, H. H. Hektoen, E. M. Huuse, P. A. Jarzyna, W. J. M. Mulder, O. Haraldseth, and C. D. Davies. The effect of nanoparticle polyethylene glycol surface density on ligand-directed tumor targeting studied in vivo by dual modality imaging. *Acs Nano*, 6(6):5648–5658, 2012.

[174] P. Sperber, W. Spangler, B. Meier, and A. Penzkofer. Experimental and theoretical investigation of tunable picosecond pulse generation in longitudinally pumped dye-laser generators and amplifiers. *Optical and Quantum Electronics*, 20(5):395–431, 1988.

[175] A. T. R. Williams, S. A. Winfield, and J. N. Miller. Relative fluorescence quantum yields using a computer-controlled luminescence spectrometer. *Analyst*, 108(1290):1067–1071, 1983.

[176] V. Ntziachristos, J. Ripoll, L. H. V. Wang, and R. Weissleder. Looking and listening to light: the evolution of whole-body photonic imaging. *Nature Biotechnology*, 23(3):313–320, 2005.

[177] D. C. Altieri. Opinion - survivin, cancer networks and pathway-directed drug discovery. *Nature Reviews Cancer*, 8:61–70, 2008.

[178] F. Z. Li, G. Ambrosini, E. Y. Chu, J. Plescia, S. Tognin, P. C. Marchisio, and D. C. Altieri. Control of apoptosis and mitotic spindle checkpoint by survivin. *Nature*, 396:580–584, 1998.

[179] C. Adida, P. L. Crotty, J. McGrath, D. Berrebi, J. Diebold, and D. C. Altieri. Developmentally regulated expression of the novel cancer anti-apoptosis gene survivin in human and mouse differentiation. *American Journal of Pathology*, 152:43–49, 1998.

[180] G. Ambrosini, C. Adida, and D. C. Altieri. A novel anti-apoptosis gene, survivin, expressed in cancer and lymphoma. *Nature Medicine*, 3:917–921, 1997.

[181] D. C. Altieri. Validating survivin as a cancer therapeutic target. *Nature Reviews Cancer*, 3:46–54, 2003.

[182] D. C. Altieri. Survivin, versatile modulation of cell division and apoptosis in cancer. *Oncogene*, 22:8581–8589, 2003.

[183] S. Fukuda and L. M. Pelus. Survivin, a cancer target with an emerging role in normal adult tissues. *Molecular Cancer Therapeutics*, 5:1087–1098, 2006.

[184] J. George, N. L. Banik, and S. K. Ray. Survivin knockdown and concurrent 4-hpr treatment controlled human glioblastoma in vitro and in vivo. *Neuro-Oncology*, 12:1088–1101, 2010.

[185] I. Fraunholz, C. Rodel, L. Distel, M. Rave-Frank, D. Kohler, S. Falk, and F. Rodel. High survivin expression as a risk factor in patients with anal carcinoma treated with concurrent chemoradiotherapy. *Radiation Oncology*, 7, 2012.

[186] S. M. Kennedy, L. O'Driscoll, R. Purcell, N. Fitz-simons, E. W. McDermott, A. D. Hill, N. J. O'Higgins, M. Parkinson, R. Linehan, and M. Clynes. Prognostic importance of survivin in breast cancer. *British Journal of Cancer*, 88:1077–1083, 2003.

[187] Y. G. Lv, F. Yu, Q. Yao, J. H. Chen, and L. Wang. The role of survivin in diagnosis, prognosis and treatment of breast cancer. *Journal of thoracic disease*, 2, 2010.

[188] H. Yamamoto, C. Y. Ngan, and M. Monden. Cancer cells survive with survivin. *Cancer Science*, 99:1709–1714, 2008.

[189] M. E. Johnson and E. W. Howerth. Survivin: A bifunctional inhibitor of apoptosis protein. *Veterinary Pathology*, 41:599–607, 2004.

[190] S. Shin, B. J. Sung, Y. S. Cho, H. J. Kim, N. C. Ha, J. I. Hwang, C. W. Chung, Y. K. Jung, and B. H. Oh. An anti-apoptotic protein human survivin is a direct inhibitor of caspase-3 and-7. *Biochemistry*, 40:1117–1123, 2001.

[191] J. Drappatz, A. D. Norden, and P. Y. Wen. Therapeutic strategies for inhibiting invasion in glioblastoma. *Expert review of neurotherapeutics*, 9, 2009.

[192] S. Fulda and K. M. Debatin. Extrinsic versus intrinsic apoptosis pathways in anticancer chemotherapy. *Oncogene*, 25:4798–4811, 2006.

[193] C. S. Straub. Targeting iaps as an approach to anti-cancer therapy. *Current Topics in Medicinal Chemistry*, 11:291–316, 2011.

[194] M. S. Coumar, F. Y. Tsai, J. R. Kanwar, S. Sarvagalla, and C. H. A. Cheung. Treat cancers by targeting survivin: Just a dream or future reality? *Cancer Treatment Reviews*, 39:802–811.

[195] D. C. Talbot, M. Ranson, J. Davies, M. Lahn, S. Callies, V. Andre, S. Kadam, M. Burgess, C. Slapak, A. L. Olsen, P. J. McHugh, J. S. de Bono, J. Matthews, A. Saleem, and P. Price. Tumor survivin is downregulated by the antisense oligonucleotide ly2181308: A proof-of-concept, first-in-human dose study. *Clinical Cancer Research*, 16:6150–6158, 2010.

[196] P. Sapra, M. L. Wang, R. Bandaru, H. Zhao, L. M. Greenberger, and I. D. Horak. Down-modulation of survivin expression and inhibition of tumor growth in vivo by ezn-3042, a locked nucleic acid antisense oligonucleotide. *Nucleosides Nucleotides & Nucleic Acids*, 29:97–112, 2010.

[197] D. Mahalingam, E. C. Medina, J. A. Esquivel, C. M. Espitia, S. Smith, K. Oberheu, R. Swords, K. R. Kelly, M. M. Mita, A. C. Mita, J. S. Carew, F. J. Giles, and S. T. Nawrocki. Vorinostat enhances the activity of temsirolimus in renal cell carcinoma through suppression of survivin levels. *Clinical Cancer Research*, 16:141–153, 2010.

[198] R. A. Olie, A. P. Simoes-Wust, B. Baumann, S. H. Leech, D. Fabbro, R. A. Stahel, and U. Zangemeister-Wittke. A novel antisense oligonucleotide targeting survivin expression induces apoptosis and sensitizes lung cancer cells to chemotherapy. *Cancer Research*, 60:2805–2809, 2000.

[199] D. J. Dai, C. D. Lu, R. Y. Lai, J. M. Guo, H. Meng, W. S. Chen, and J. Gu. Survivin antisense compound inhibits proliferation and promotes apoptosis in liver cancer cells. *World Journal of Gastroenterology*, 11:193–199, 2005.

[200] R. A. Carrasco, N. B. Stamm, E. Marcusson, G. Sandusky, P. Iversen, and B. K. R. Patel. Antisense inhibition of survivin expression as a cancer therapeutic. *Molecular Cancer Therapeutics*, 10:221–232, 2011.

[201] S. Callies, V. Andre, B. Patel, D. Waters, P. Francis, M. Burgess, and M. Lahn. Integrated analysis of preclinical data to support the design of the first in man study of ly2181308, a second generation antisense oligonucleotide. *British Journal of Clinical Pharmacology*, 71:416–428, 2011.

[202] J. B. Hansen, N. Fisker, M. Westergaard, L. S. Kjaerulff, H. F. Hansen, C. A. Thrue, C. Rosenbohm, M. Wissenbach, H. Orum, and T. Koch. Spc3042: a proapoptotic survivin inhibitor. *Molecular Cancer Therapeutics*, 7:2736–2745, 2008.

[203] K. Yamanaka, T. Nakahara, T. Yamauchi, A. Kita, M. Takeuchi, F. Kiyonaga, N. Kaneko, and M. Sasamata. Antitumor activity of ym155, a selective small-molecule survivin suppressant, alone and in combination with docetaxel in human malignant melanoma models. *Clinical Cancer Research*, 17:5423–5431, 2011.

[204] T. Nakahara, M. Takeuchi, I. Kinoyama, T. Minematsu, K. Shirasuna, A. Matsuhisa, A. Kita, F. Tominaga, K. Yamanaka, M. Kudoh, and M. Sasamata. Ym155, a novel small-molecule survivin suppressant, induces regression of established human hormone-refractory prostate tumor xenografts. *Cancer Research*, 67:8014–8021, 2007.

[205] Q. Cheng, X. Ling, A. Haller, T. Nakahara, K. Yamanaka, A. Kita, H. Koutoku, M. Takeuchi, M. G. Brattain, and F. Li. Suppression of survivin promoter activity by ym155 involves disruption of sp1-dna interaction in the survivin core promoter. *International journal of biochemistry and molecular biology*, 3, 2012.

[206] X. Ling, S. S. Cao, Q. Y. Cheng, J. T. Keefe, Y. M. Rustum, and F. Z. Li. A novel small molecule fl118 that selectively inhibits survivin, mcl-1, xiap and ciap2 in a p53-independent manner, shows superior antitumor activity. *Plos One*, 7:18.

[207] V. Pisarev, B. Yu, R. Salup, S. Sherman, D. C. Altieri, and D. I. Gabrilovich. Full-length dominant-negative survivin for cancer immunotherapy. *Clinical Cancer Research*, 9:6523–6533, 2003.

[208] S. Siegel, A. Wagner, N. Schmitz, and M. Zeis. Induction of antitumour immunity using survivin peptide-pulsed dendritic cells in a murine lymphoma model. *British Journal of Haematology*, 122:911–914, 2003.

[209] M. D. Wendt, C. H. Sun, A. Kunzer, D. Sauer, K. Sarris, E. Hoff, L. P. Yu, D. G. Nettesheim, J. Chen, S. Jin, K. M. Comess, Y. H. Fan, S. N. Anderson, B. Isaac, E. T. Olejniczak, P. J. Hajduk, S. H. Rosenberg, and S. W. Elmore. Discovery of a novel small molecule binding site of human survivin. *Bioorganic & Medicinal Chemistry Letters*, 17:3122–3129, 2007.

[210] T. Oikawa, Y. Unno, K. Matsuno, J. Sawada, N. Ogo, K. Tanaka, and A. Asai. Identification of a small-molecule inhibitor of the interaction between survivin and smac/diablo. *Biochemical and Biophysical Research Communications*, 393:253–258, 2010.

[211] N. Zaffaroni, M. Pennati, and M. G. Daidone. Survivin as a target for new anticancer interventions. *Journal of Cellular and Molecular Medicine*, 9:360–372, 2005.

[212] C. F. Bennett and E. E. Swayze. Rna targeting therapeutics: Molecular mechanisms of antisense oligonucleotides as a therapeutic platform. *Annual Review of Pharmacology and Toxicology*, 50:259–293, 2010.

[213] K. D. Lewis, W. Samlowski, J. Ward, J. Catlett, L. Cranmer, J. Kirkwood, D. Lawson, E. Whitman, and R. Gonzalez. A multi-center phase ii evaluation of the small molecule survivin suppressor ym155 in patients with unresectable stage iii or iv melanoma. *Investigational New Drugs*, 29:161–166, 2011.

[214] G. Giaccone, P. Zatloukal, J. Roubec, K. Floor, J. Musil, M. Kuta, R. J. van Klaveren, S. Chaudhary, A. Gunther, and S. Shamsili. Multicenter phase ii trial of ym155, a small-molecule suppressor of survivin, in patients with advanced, refractory, non-small-cell lung cancer. *Journal of Clinical Oncology*, 27:4481–4486, 2009.

[215] M. Mobahat, A. Narendran, and K. Riabowol. Survivin as a preferential target for cancer therapy. *International Journal of Molecular Sciences*, 15:2494–2516, 2014.

[216] A. Berezov, Z. Cai, J. A. Freudenberg, H. Zhang, X. Cheng, T. Thompson, R. Murali, M. I. Greene, and Q. Wang. Disabling the mitotic spindle and tumor growth by targeting a cavity-induced allosteric site of survivin. *Oncogene*, 31:1938–1948.

[217] Y. G. Shi. Survivin structure: crystal unclear. *Nature Structural Biology*, 7:620–623, 2000.

[218] H. Guvenc, M. S. Pavlyukov, K. Joshi, H. Kurt, Y. K. Banasavadi-Siddegowda, P. Mao, C. Hong, R. Yamada, C. H. Kwon, D. Bhasin, S. Chettiar, G. Kitange, I. H. Park, J. N. Sarkaria, C. L. Li, M. I. Shakhparonov, and I. Nakano. Impairment of glioma stem cell survival and growth by a novel inhibitor for survivin-ran protein complex. *Clinical Cancer Research*, 19:631–642, 2013.

[219] F. Xia, P. M. Canovas, T. M. Guadagno, and D. C. Altieri. A survivin-ran complex regulates spindle formation in tumor cells. *Molecular and Cellular Biology*, 28:5299–5311, 2008.

[220] M. K. Yu, J. Park, and S. Jon. Targeting strategies for multifunctional nanoparticles in cancer imaging and therapy. *Theranostics*, 2:3–44, 2012.

[221] R. Weissleder, K. Kelly, E. Y. Sun, T. Shtatland, and L. Josephson. Cell-specific targeting of nanoparticles by multivalent attachment of small molecules. *Nature Biotechnology*, 23:1418–1423, 2005.

[222] A. V. Ullal, T. Reiner, K. S. Yang, R. Gorbatov, C. Min, D. Issadore, H. Lee, and R. Weissleder. Nanoparticle-mediated measurement of target-drug binding in cancer cells. *Acs Nano*, 5:9216–9224, 2011.

[223] C. Tassa, J. L. Duffner, T. A. Lewis, R. Weissleder, S. L. Schreiber, A. N. Koehler, and S. Y. Shaw. Binding affinity and kinetic analysis of targeted small molecule-modified nanoparticles. *Bioconjugate Chemistry*, 21:14–19, 2009.

[224] S. Hong, P. R. Leroueil, I. J. Majoros, B. G. Orr, J. R. Baker Jr, and M. M. Banaszak Holl. The binding avidity of a nanoparticle-based multivalent targeted drug delivery platform. *Chemistry & Biology*, 14:107–115, 2007.

[225] J. B. Haun, N. K. Devaraj, S. A. Hilderbrand, H. Lee, and R. Weissleder. Bioorthogonal chemistry amplifies nanoparticle binding and enhances the sensitivity of cell detection. *Nature Nanotechnology*, 5:660–665, 2010.

[226] I. H. Park and C. L. Li. Dynamic ligand-induced-fit simulation via enhanced conformational samplings and ensemble dockings: A survivin example. *Journal of Physical Chemistry B*, 114:5144–5153, 2010.

[227] A. H. Abadi, T. M. Ibrahim, K. M. Abouzid, J. Lehmann, H. N. Tinsley, B. D. Gary, and G. A. Piazza. Design, synthesis and biological evaluation of novel pyridine derivatives as anticancer agents and phosphodiesterase 3 inhibitors. *Bioorganic & Medicinal Chemistry*, 17:5974–5982, 2009.

[228] A. H. Abadi, M. S. Hany, S. A. Elsharif, A. A. H. Eissa, B. D. Gary, H. N. Tinsley, and G. A. Piazza. Modulating the cyclic guanosine monophosphate substrate selectivity of the phosphodiesterase 3 inhibitors by pyridine, pyrido[2,3-d]pyrimidine derivatives and their effects upon the growth of ht-29 cancer cell line. *Chemical & Pharmaceutical Bulletin*, 61:405–410.

[229] R. Janardhanan, N. L. Banik, and S. K. Ray. N-myc down regulation induced differentiation, early cell cycle exit, and apoptosis in human malignant neuroblastoma cells having wild type or mutant p53. *Biochemical Pharmacology*, 78:1105–1114, 2009.

[230] S. N. Chettiar, J. V. Cooley, I. H. Park, D. Bhasin, A. Chakravarti, P. K. Li, C. L. Li, and N. K. Jacob. Design, synthesis and biological studies of survivin dimerization modulators that prolong mitotic cycle. *Bioorganic & Medicinal Chemistry Letters*, 23:5429–5433.

[231] H. N. Zhen, L. W. Li, W. Zhang, Z. Fei, C. H. Shi, T. T. Yang, W. T. Bai, and X. Zhang. Short hairpin rna targeting survivin inhibits growth and angiogenesis of glioma u251 cells. *International Journal of Oncology*, 31:1111–1117, 2007.

[232] I. Tamm, Y. Wang, E. Sausville, D. A. Scudiero, N. Vigna, T. Oltersdorf, and J. C. Reed. Iap-family protein survivin inhibits caspase activity and apoptosis induced by fas (cd95), bax, caspases, and anticancer drugs. *Cancer Research*, 58:5315–5320, 1998.

[233] A. L. Klibanov, K. Maruyama, V. P. Torchilin, and L. Huang. Amphipathic polyethyleneglycols effectively prolong the circulation time of liposomes. *Febs Letters*, 268:235–237, 1990.

[234] V. P. Torchilin, A. L. Klibanov, L. Huang, S. Odonnell, N. D. Nossiff, and B. A. Khaw. Targeted accumulation of polyethylene glycol-coated immunoliposomes in infarcted rabbit myocardium. *Faseb Journal*, 6:2716–2719, 1992.

[235] M. Vittaz, D. Bazile, G. Spenlehauer, T. Verrecchia, M. Veillard, F. Puisieux, and D. Labarre. Effect of peo surface density on long-circulating pla-peo nanoparticles which are very low complement activators. *Biomaterials*, 17:1575–1581, 1996.

[236] F. De Jaeghere, E. Allemann, J. Feijen, T. Kissel, E. Doelker, and R. Gurny. Cellular uptake of peo surface-modified nanoparticles: Evaluation of nanoparticles made of pla : Peo diblock and triblock copolymers. *Journal of Drug Targeting*, 8:143–153, 2000.

[237] F. Belloc, P. Dumain, M. R. Boisseau, C. Jalloustre, J. Reiffers, P. Bernard, and F. Lacombe. A flow cytometric method using hoechst-33342 and propidium iodide for simultaneous cell-cycle analysis and apoptosis determination in unfixed cells. *Cytometry*, 17:59–65, 1994.

[238] C. F. Brunk, K. C. Jones, and T. W. James. Assay for nanogram quantities of dna in cellular homogenates. *Analytical Biochemistry*, 92:497–500, 1979.

[239] H. A. Crissman, M. E. Wilder, and R. A. Tobey. Flow cytometric localization within the cell-cycle and isolation of viable cells following exposure to cyto-toxic agents. *Cancer Research*, 48:5742–5746, 1988.

[240] H. M. Shapiro. Flow cytometric estimation of dna and rna-content in intact-cells stained with hoechst-33342 and pyronin-y. *Cytometry*, 2:143–150, 1981.

[241] S. J. Martin, C. P. M. Reutelingsperger, A. J. McGahon, J. A. Rader, Rcaa Vanschie, D. M. Laface, and D. R. Green. Early redistribution of plasma-membrane phosphatidylserine is a general feature of apoptosis regardless of the initiating stimulus - inhibition by overexpression of bcl-2 and abl. *Journal of Experimental Medicine*, 182:1545–1556, 1995.

[242] I. Vermes, C. Haanen, H. Steffensnakken, and C. Reutelingsperger. A novel assay for apoptosis - flow cytometric detection of phosphatidylserine expression on early apoptotic cells using fluorescein-labelled annexin-v. *Journal of Immunological Methods*, 184:39–51, 1995.

[243] A. W. M. Boersma, K. Nooter, R. G. Oostrum, and G. Stoter. Quantification of apoptotic cells with fluorescein isothiocyanate-labeled annexin v in chinese hamster ovary cell cultures treated with cisplatin. *Cytometry*, 24:123–130, 1996.

[244] J. M. Laing, M. D. Gober, E. K. Golembewski, S. M. Thompson, K. A. Gyure, P. J. Yarowsky, and L. Aurelian. Intranasal administration of the growth-compromised hsv-2 vector delta rr prevents kainate-induced seizures and neuronal loss in rats and mice. *Molecular Therapy*, 13:870–881, 2006.

[245] E. Tuite and B. Norden. Intercalative interactions of ethidium dyes with triplex structures. *Bioorganic & Medicinal Chemistry*, 3:701–711, 1995.

[246] E. Szliszka, Z. P. Czuba, K. Jernas, and W. Krol. Dietary flavonoids sensitize hela cells to tumor necrosis factor-related apoptosis-inducing ligand (trail). *International Journal of Molecular Sciences*, 9:56–64, 2008.

[247] J. Bronikowska, E. Szliszka, Z. P. Czuba, D. Zwolinski, D. Szmydki, and W. Krol. The combination of trail and isoflavones enhances apoptosis in cancer cells. *Molecules*, 15:2000–2015, 2010.

[248] A. H. Abadi, D. A. Abouel-Ella, J. Lehmann, H. N. Tinsley, B. D. Gary, G. A. Piazza, and M. A. O. Abdel-Fattah. Discovery of colon tumor cell growth inhibitory agents through a combinatorial approach. *European Journal of Medicinal Chemistry*, 45:90–97, 2010.

[249] A. Abadi, O. Al-Deeb, A. Al-Afify, and H. El-Kashef. Synthesis of 4-alkyl (aryl)-6-aryl-3-cyano-2(1h)-pyridinones and their 2-imino isosteres as nonsteroidal cardiotonic agents. *Il Farmaco*, 54:195–201, 1999.

[250] M. A. Dobrovolskaia and S. E. McNeil. Immunological properties of engineered nanomaterials. *Nature Nanotechnology*, 2:469–478, 2007.

[251] E. Lallana, R. Riguera, and E. Fernandez-Megia. Reliable and efficient procedures for the conjugation of biomolecules through huisgen azide-alkyne cycloadditions. *Angewandte Chemie-International Edition*, 50:8794–8804, 2011.

[252] S. Ju and W. S. Yeo. Quantification of proteins on gold nanoparticles by combining maldi-tof ms and proteolysis. *Nanotechnology*, 23, 2012.

[253] T. S. Seo, Z. M. Li, H. Ruparel, and J. Y. Ju. Click chemistry to construct fluorescent oligonucleotides for dna sequencing. *Journal of Organic Chemistry*, 68:609–612, 2003.

[254] A. J. T. Dirks, S. S. van Berkel, N. S. Hatzakis, J. A. Opsteen, F. L. van Delft, Jjlm Cornelissen, A. E. Rowan, J. C. M. van Hest, Fpjt Rutjes, and R. J. M. Nolte. Preparation of biohybrid amphiphiles via the copper catalysed huisgen [3+2] dipolar cycloaddition reaction. *Chemical Communications*, pages 4172–4174, 2005.

[255] H. Tong, Y. N. Hong, Y. Q. Dong, M. Haussler, J. W. Y. Lam, Z. Li, Z. F. Guo, Z. H. Guo, and B. Z. Tang. Fluorescent "light-up" bioprobes based on tetraphenylethylene derivatives with aggregation-induced emission characteristics. *Chemical Communications*, pages 3705–3707, 2006.

[256] D. Lopez-Ferrer, J. L. Capelo, and J. Vazquez. Ultra fast trypsin digestion of proteins by high intensity focused ultrasound. *Journal of Proteome Research*, 4:1569–1574, 2005.

[257] J. E. Butler. Solid supports in enzyme-linked immunosorbent assay and other solid-phase immunoassays. *Methods-a Companion to Methods in Enzymology*, 22:4–23, 2000.

[258] F. Xu, W. H. Wang, Y. J. Tan, and M. L. Bruening. Facile trypsin immobilization in polymeric membranes for rapid, efficient protein digestion. *Analytical Chemistry*, 82:10045–10051, 2010.

[259] H. K. Hustoft, H. Malerod, S. R. Wilson, L. Reubsaet, E. Lundanes, and T. Greibrokk. A critical review of trypsin digestion for lc-ms based proteomics. In H. C. Leung, editor, *Integrative Proteomics*, pages 73–92. InTech, 2012.

[260] A. Michnik. Thermal stability of bovine serum albumin dsc study. *Journal of Thermal Analysis and Calorimetry*, 71:509–519, 2003.

[261] R. G. A. Jones and J. Landon. Enhanced pepsin digestion: a novel process for purifying antibody f(ab ')(2) fragments in high yield from serum. *Journal of Immunological Methods*, 263:57–74, 2002.

[262] J. L. Proc, M. A. Kuzyk, D. B. Hardie, J. Yang, D. S. Smith, A. M. Jackson, C. E. Parker, and C. H. Borchers. A quantitative study of the effects of chaotropic agents, surfactants, and solvents on the digestion efficiency of human plasma proteins by trypsin. *Journal of Proteome Research*, 9:5422–5437, 2010.

[263] M. R. Detty, S. L. Gibson, and S. J. Wagner. Current clinical and preclinical photosensitizers for use in photodynamic therapy. *Journal of Medicinal Chemistry*, 47:3897–3915, 2004.

[264] A. P. Castano, P. Mroz, and M. R. Hamblin. Photodynamic therapy and anti-tumour immunity. *Nature Reviews Cancer*, 6:535–545, 2006.

[265] M. E. Wieder, D. C. Hone, M. J. Cook, M. M. Handsley, J. Gavrilovic, and D. A. Russell. Intracellular photodynamic therapy with photosensitizer-nanoparticle conjugates: cancer therapy using a 'trojan horse'. *Photochemical and Photobiological Sciences*, 5:727–734, 2006.

[266] M. E. Rodriguez, P. Zhang, K. Azizuddin, G. B. Delos Santos, S. M. Chiu, L. Y. Xue, J. C. Berlin, X. Z. Peng, H. Q. Wu, M. Lam, A. L. Nieminen, M. E. Kenney, and N. L. Oleinick. Structural factors and mechanisms underlying the improved photodynamic cell killing with silicon phthalocyanine photosensitizers directed to lysosomes versus mitochondria. *Photochemistry and Photobiology*, 85:1189–1200, 2009.

[267] Timothy James Kinsella, Elma D. Baron, Valdir C. Colussi, Kevin D. Cooper, Charles L. Hoppel, Stephen T. Ingalls, Malcolm E. Kenney, Xiaolin Li, Nancy L. Oleinick, Seth R. Stevens, and Scot C. Remick. Preliminary clinical and pharmacologic investigation of photodynamic therapy with the silicon phthalocyanine photosensitizer pc 4 for primary or metastatic cutaneous cancers. *Frontiers in oncology*, 1:14, 2011.

[268] H. Shinohara, O. Tsaryova, G. Schnurpfeil, and D. Wohrle. Differently substituted phthalocyanines: Comparison of calculated energy levels, singlet oxygen quantum yields, photo-oxidative stabilities, photocatalytic and catalytic activities. *Journal of Photochemistry and Photobiology a-Chemistry*, 184:50–57, 2006.

[269] D. G. Norman, R. J. Grainger, D. Uhrin, and D. M. J. Lilley. Location of cyanine-3 on double-stranded dna: Importance for fluorescence resonance energy transfer studies. *Biochemistry*, 39:6317–6324, 2000.

[270] Ratnakar B. Mujumdar, Lauren A. Ernst, Swati R. Mujumdar, Christopher J. Lewis, and Alan S. Waggoner. Cyanine dye labeling reagents: Sulfoindocyanine succinimidyl esters. *Bioconjugate Chemistry*, 4:105–111, 1993.

[271] Hari S. Muddana, Thomas T. Morgan, James H. Adair, and Peter J. Butler. Photophysics of cy3-encapsulated calcium phosphate nanoparticles. *Nano letters*, 9:1559–1566, 2009.

[272] X. F. Zhang, J. L. Zhang, and L. M. Liu. Fluorescence properties of twenty fluorescein derivatives: Lifetime, quantum yield, absorption and emission spectra. *Journal of Fluorescence*, 24:819–826, 2014.

[273] W. Konigsberg. 13 reduction of disulfide bonds in proteins with dithiothreitol. *Methods in enzymology*, 25, 1972.

[274] B. E. Davidson and F. J. R. Hird. Reactivity of disulphide bonds of purified proteins in relationship to primary structure. *Biochemical Journal*, 104:473–, 1967.

[275] R. Frater and F. J. Hird. The reaction of glutathione with serum albumin, gluten and flour proteins. *The Biochemical journal*, 88, 1963.

[276] W. W. Cleland. Dithiothreitol, a new protective reagent for sh groups. *Biochemistry*, 3:480–482, 1964.

[277] Kateina Dolekov, Martin Kan, Libor Mike, Jared Cartwright, Petr Jedelsk, Eric L. Schneider, Jan Dvok, Adrian P. Mountford, Charles S. Craik, and Petr Hork. The functional expression and characterisation of a cysteine peptidase from the invasive stage of the neuropathogenic schistosome trichobilharzia regenti. *International Journal for Parasitology*, 39:201–211, 2009.

[278] P. Alexander and L. D. Hamilton. Changes in the reactivity of disulfide bonds in bovine serum albumin on denaturation. *Archives of biochemistry and biophysics*, 88, 1960.

[279] Y. N. Kang, H. Kim, W. S. Shin, G. Woo, and T. W. Moon. Effect of disulfide bond reduction on bovine serum albumin-stabilized emulsion gel formed by microbial transglutaminase. *Journal of Food Science*, 68:2215–2220, 2003.

[280] T. A. Bewley and C. H. Li. Reduction of protein disulphide bonds in absence of denaturants. *International Journal of Protein Research*, 1:117–, 1969.

[281] X. Y. Cheng, S. B. Lowe, S. Ciampi, A. Magenau, K. Gaus, P. J. Reece, and J. J. Gooding. Versatile "click chemistry" approach to functionalizing silicon quantum dots: Applications toward fluorescent cellular imaging. *Langmuir*, 30:5209–5216, 2014.

[282] D. M. Barber, H. J. Sanganee, and D. J. Dixon. One-pot catalytic enantioselective synthesis of tetrahydropyridines via a nitro-mannich/hydroamination cascade. *Organic Letters*, 14:5290–5293, 2012.

[283] J. M. Gu, U. R. Anumala, F. Lo Monte, T. Kramer, R. H. von Haussen, J. Holzer, V. Goetschy-Meyer, G. Mall, I. Hilger, C. Czech, and B. Schmidt. 2-styrylindolium based fluorescent probes visualize neurofibrillary tangles in alzheimer's disease. *Bioorganic & Medicinal Chemistry Letters*, 22:7667–7671, 2012.

[284] Anna-Liisa Nieminen, Gregory J. Gores, John M. Bond, Roberto Imberti, Brian Herman, and John J. Lemasters. A novel cytotoxicity screening assay using a multiwell fluorescence scanner. *Toxicology and Applied Pharmacology*, 115:147–155, 1992.